Influences of copper and titanium contaminations on the photovoltaic performances of crystalline silicon solar cells

Tleuzhan Turmagambetov

UNIVERSITÉ GRENOBLE ALPES

THÈSE

Pour obtenir le grade de
DOCTEUR DE L'UNIVERSITÉ GRENOBLE ALPES
Spécialité : **Ingénierie-matériaux mécanique énergétique environnement procédés production**
Arrêté ministériel : 7 août 2006

Présentée par
Tleuzhan TURMAGAMBETOV

Thèse dirigée par **Jean-Paul GARANDET** et
codirigée par **Sébastien DUBOIS**

préparée au sein du **Laboratoire des Concepts Innovants pour le Photovoltaïque (LCIPV) – CEA/LITEN/DTS, INES**

dans **l'École Doctorale Ingénierie - Matériaux, Mécanique, Energétique, Environnement, Procédés, Production (I-MEP2)**

De l'influence de contaminations par le cuivre et le titane sur les performances photovoltaïques de cellules solaires au silicium cristallin

Thèse soutenue publiquement le **29 mai 2015**,

devant le jury composé de :

Mme Anne KAMINSKI-CACHOPO
Professeur, Université Grenoble Alpes, Présidente du jury
M. Daniel MATHIOT
Professeur, Université de Strasbourg, Rapporteur
M. Olivier PALAIS
Professeur, Université d'Aix-Marseille, Rapporteur
M. Daniel MORVAN
Professeur, Ecole Nationale Supérieure de Chimie de Paris, Examinateur
M. Jean-Paul GARANDET
Ingénieur chercheur HDR, CEA, Directeur de thèse
M. Sébastien DUBOIS
Ingénieur chercheur HDR, CEA, Encadrant

ACKNOWLEDGEMENTS

It is a great pleasure to save this page aside as a mark of gratitude to all of those who contributed to this work.

Firstly I would like to say deepest thanks to my supervisors for good advices, for teaching me and assistance with manuscript. Sébastien Dubois was my main supervisor for all three years. He always supported me and always had time for questions. He used a lot of his time helping me and guided through the writing processes. Jean-Paul GARANDET was my academic supervisor. He always gave helpful advises and always has time for re-reading correction and revising this manuscript.

Secondly I would like to acknowledge to all the people I worked with over this study, who highly contributed to the content of this manuscript.

A special thanks goes to Nicolas Enjalbert who supported me for the most part of the experiments conducted at INES. Without his help and friendship, this manuscript would never be done.

Deepest thanks also to Jordi Veirman and Benoit Martel, who often played a great role in the results presented here.

I would like to thank all the colleagues from INES I had the opportunity to work with.

I also would express my gratitude to all jury members: Anne Kaminski-Cachopo, Daniel Mathiot, Olivier Palais and Daniel Morvan.

RESUME

Ce travail s'est intéressé à l'influence de contaminations par le cuivre (Cu) et le titane (Ti) sur les performances des cellules solaires photovoltaiques (PV) au silicium (Si) cristallin. Le Cu et le Ti sont des impuretés souvent présentes dans les plaquettes à l'issue de l'étape de croissance des lingots, et peuvent être considérées comme des impuretés modèles respectivement pour les difuseurs rapides et les diffuseurs lents. Des lingots monocristallins Czochralski (Cz) et multicristallins (mc), certains volontairement contaminés et d'autres sans contaminations volontaires ont été cristallisés. Leurs propriétés électriques et compositionnelles ont été caractérisées, et des cellules ont été fabriquées. Les influences du Cu et du Ti sur le rendement de conversion PV (η), sa stabilité sous éclairement, et la tension de claquage (V_{bd}) de la jonction, ont pu être évaluées. La contamination par le Ti, même à une concentration de 6 ppm pds ajoutée à la charge de Si, affecte significativement le η. Cela est lié au fort pouvoir recombinant des atomes de Ti (malgré un traitement d'hydrogénation) et au faible coefficient de diffusion du Ti, qui ne permet pas son extraction du volume par l'effet getter externe développé par la diffusion P. La contamination par le Ti cependant n'a pas d'influence significative sur la V_{bd} et est compatible avec des η stables sous éclairement. D'un autre côté, nous avons montré que la contamination par le Cu, pourtant importante (concentration de 90 ppm pds ajoutée au Si charge), n'affecte pas le η des cellules mc. Cela s'explique par le faible pouvoir recombinant des atomes de Cu, par ailleurs efficacement extraits du volume au cours de la diffusion P, en raison du coefficient de diffusion élevé du Cu. Par contre la contamination par le Cu influencerait de façon négative le claquage des jonctions. Un point important est que le η des cellules contaminées Cu diminue sous éclairement. Nous avons montré que cette dégradation est activée par l'étape de recuit rapide des métallisations. Cela confirme de façon indirecte que ces effets de dégradation sont liés à des mécanismes de précipitation du Cu sous éclairement.

Mots clés : silicium, photovoltaïque, impureté, cuivre, titane, recombinaison.

ABSTRACT

This thesis focuses on the influence of copper (Cu) and titanium (Ti) contaminations on the photovoltaic (PV) performances of *p*-type crystalline silicon (Si) solar cells. These impurities are common in Si and can be considered as model elements since they behave differently and their properties are similar to those of other transition metals. For these studies, deliberately contaminated and uncontaminated single-crystalline Czochralski (Cz) and multicrystalline (mc) ingots were grown. The compositional and electrical properties of these ingots were extensively characterized. Then wafers from these ingots were transformed into solar cells in order to assess the impact of Cu and Ti on the PV conversion efficiency (η), its evolution under illumination, and the *p*-*n* junction breakdown voltage (V_{bd}). We showed that Ti strongly affects the η, for both Cz and mc Si solar cells (even if only 6 ppm wt of Ti were added into the feedstock). This is due to the high recombination strength of interstitial Ti atoms (even after an hydrogenation step), which are not efficiently extracted by the external gettering effect developped by the phosphorus (P) diffusion, due to their low diffusivity. However, the Ti contamination did not significantly influence the V_{bd} and was compatible with stable η under illumination. On the other hand, we unexpectedly showed that a strong contamination of the Si feedstock by Cu (90 ppm wt of Cu added to the feedstock) do not affect the η of the mc cells. This is essentially due to the lower recombination strength of Cu atoms, which are in addition efficiently extracted by external gettering effects due to their high diffusivity. Nevertheless, we showed that Cu could slighty enhance the junction breakdown. Above all, the mc Cu contaminated cells were affected by light-induced degradation (LID) effects. We showed that these Cu-related LID were activated by the metallization firing step (rapid annealing), which indirectely confirmed that these LID effects would be due to the precipitation of Cu atoms under illumination.

Keywords: silicon, photovoltaic, impurity, copper, titanium, recombination.

CONTENTS

INTRODUCTION

The photovoltaic (PV) market, in strong monotonic growth for several decades, is nowadays still largely dominated by crystalline silicon (c-Si) based solar modules, with a share historically oscillating from 80 to 90 %. In 2014, 60 % and 40 % of the wafers used by the c-Si based PV industry are multicrystalline (mc) and single-crystalline Czochralski (Cz)-grown wafers, respectively. The growth of the PV market is associated with a continuous and significant decrease of the cost of PV energy (Figure 1), with a price of the PV module approaching 0.7 $/W in 2014 [1].

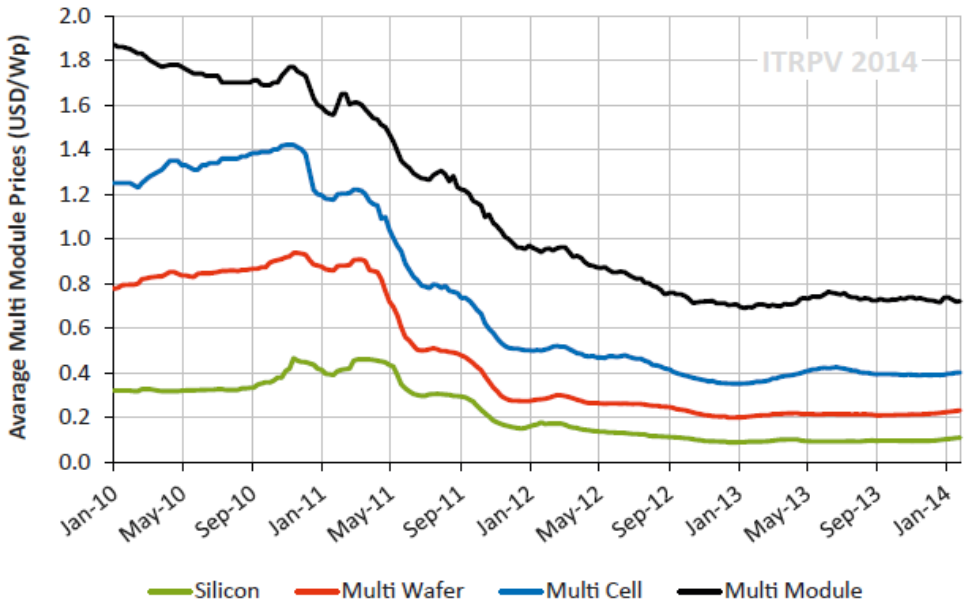

Figure 1 – Price trends for poly-Si (feedstock), multicrystalline Si wafers, solar cells and modules (reprinted from [1]).

In order to sustain such a growth, the PV conversion efficiencies (η) have to keep increasing, and in parallel, the cost of the solar module fabrication process has to keep decreasing.

The forecasts regarding the future η of the industrial solar cells fabricated from such wafers are ambitious. Indeed in 2018 for homo-junction (*diffused* junctions) solar cells, η of 20.0 % and 25.0 % are expected for industrial mc and Cz solar cells respectively. These forecasts are ambitious but realistic, since a record efficiency on a large size mc-solar cell of 20.5 % was recently announced, even though the fabrication process is not detailed enough to assess the industrial viability of the technology [2]. Such high η can be obtained only if both the base material and the *p-n* junction exhibit an excellent quality. Regarding the material, this means that the carrier lifetime should be very high, or equivalently that the quantity of

electrically active metal impurities has to be drastically reduced, since these are known for introducing harmful charge carrier recombination centers [3,4]. Regarding the *p-n* junction, the point on the metal content is equally valid, since metals are among the main causes of localized shunts of the *p-n* junctions [5].

In parallel of these improvements of the η, the cost of PV energy could be reduced by developing metallurgical processes for the Si purification, which would replace the conventional chemical purification (Siemens-type processes). Low cost refinement processes by metallurgical routes (the material remains either in solid or liquid states but never enters the gas phase) limit the energy consumption (reduction of the module energy pay-back time) and limit the use of harmful chloride compounds. However one of the drawbacks of these new processes is that the produced materials generally contain higher amount of metal impurities which can significantly alter the PV properties.

Therefore, the presence of metal impurities in Si is a major issue that both main challenges for the PV industry (η improvements and cost reductions) have to overcome. Thus the goal of this PhD thesis is to bring new insights into the role of metal impurities in Si-based PV. The developed knowledge will be essential for the development of innovative defect engineering processes, for the neutralization or the extraction of the more deleterious elements.

Numerous studies were devoted to the influence of iron (Fe) and chromium (Cr) on the PV performances of crystalline Si solar cells, and nowadays their effects can be considered as rather well known [4]. Thus this PhD thesis focuses on two relatively less studied elements, namely copper (Cu) and titanium (Ti). These impurities were selected both for their relevance to the PV industry, and due to the fact that their physical properties in Si are rather well known in order to simplify the experimental and interpretation work.

Cu is one of the most abundant metal impurities in cast mc-Si for solar cells fabrication. Cu concentrations ([Cu]) as high as 10^{13} cm^{-3} have been reported in commercial mc-Si wafers [6]. Cu essentially comes from the silica crucible and its silicon nitride coating [7]. In addition, owing to a large diffusion coefficient, Cu contamination may easily occur during Si PV solar sell manufacturing [8]. Furthermore Cu is used as a catalyst for the production of fluidized bed reactor polysilicon. In the future, the replacement of expensive screen-printed silver front contacts with Cu-plated contacts might further increase the probability of Cu contamination.

Ti on the other hand is one of the most common metal impurities in metallurgical grade Si. The Ti concentrations ([Ti]) in metallurgical grade Si are usually in the range 160 – 200

ppm wt [9]. Therefore, large [Ti] are likely to be found in low cost Si feedstock purified by metallurgical routes.

Consequently studies about the properties of Cu- and Ti- contaminated Si solar cells are of paramount importance. Notice also that we chose these two elements because they behave differently in Si. Particularly, Cu is a fast diffusing element, whereas Ti has a low diffusivity in Si [8]. In addition, dissolved Cu atoms have a benign electrical activity [10], whereas dissolved Ti strongly affects the charge carrier lifetime [11]. Last but not least, these elements have properties in Si representative of those of other impurities (cobalt and nickel for Cu, vanadium for Ti), in order to transpose our conclusions to a wide range of metal impurities found in Si.

Another study focusing on the influences of both Cu and Ti on the PV performances of crystalline solar cells was recently published [12]. However, we believe this PhD thesis brings original and complementary approaches regarding the effects of both elements. Firstly, we studied the effects of Cu and Ti for both single- and multi-crystalline Si. Secondly we used specific experimental protocols in order to highlight the efficiency of the external gettering and bulk hydrogenation steps, associated with a conventional solar cell process. Furthermore, we evaluated the forward but also reverse current-voltage (I-V) characteristics of the fabricated cells. Finally, we systematically assessed the stability under illumination of the PV parameters.

The first chapter of this PhD thesis summarizes some important fundamentals of the physics of semiconductors and solar cells, which are needed for the understanding of the following chapters. In addition, it gives a concise description of the Si feedstock production via conventional and alternatives routes, followed by a short account of the ingot crystallization and solar cell fabrication processes.

Chapter 2 presents the main properties of Cu and Ti in Si, and summarizes the previous studies regarding their influences on the PV performances of crystalline Si solar cells. Chapter 3 describes the experimental techniques used throughout this PhD thesis.

Chapter 4 is dedicated to the influence of Cu and Ti on the PV performances of single-crystalline Czochralski Si solar cells. Then in Chapter 5 the experimental studies are transposed to multicrystalline Si.

The last chapter (chapter 6) focuses on the role of phosphorus-rich layers during rapid annealing on carrier recombination and trapping in Cu-contaminated multicrystalline Si.

Introduction – Bibliography

1. International technology roadmap for photovoltaic (ITRPV). 5th edition, March (2014).
2. http://www.trinasolar.com/
3. D. Macdonald, and L.J. Geerligs, Recombination activity of interstitial iron and other transition metal point defects in p- and n-type crystalline silicon. Appl. Phys. Lett. 85, 18 (2004).
4. S. Dubois, Effects of the impurity-defect interactions on the photovoltaic and electrical properties of crystalline silicon solar cells. PhD Thesis. Paul Cezanne University, Marseille, France (2007).
5. O. Breitenstein, J. Bauer, K. Bothe, W. Kwapil, D. Lausch, U. Rau, J. Schmidt, M. Schneemann, M.C. Schubert, J.-M. Wagner, and W. Warta, Understanding junction breakdown in multicrystalline solar cells. J. Appl. Phys. 109, 071101 (2011).
6. D. Macdonald, A. Cuevas, A. Kinomura, Y. Nakano, Phosphorus gettering in multicrystalline silicon studied by neutron activation analysis. 29th Photovoltaic Specialists Conference Proceedings (IEEE), New Orleans, USA, 285-288 (2002).
7. T. Buonassisi, A.A. Istratov, M.D. Pickett, J.P. Rakotoniaina, O. Breitenstein, M.A. Marcus, S.M. Heald, and E.R. Weber, Transition metals in photovoltaic-grade ingot-cast multicrystalline silicon: Assessing the role of impurities in silicon nitride crucible lining material. J. Crystal Growth. 287 (2), 402-407 (2006).
8. K. Graff, Metal Impurities in Silicon-Device Fabrication. 2nd edition, Springer, Berlin (1999).
9. B.S. Xakalashe, and M. Tangstad, Silicon processing: from quartz to crystalline silicon solar cells. Chemical Technology. 32-37 (2012).
10. A.A. Istratov, C. Flink, H. Hieslmair, T. Heiser, and E.R. Weber, Influence of interstitial copper on diffusion length and lifetime of minority carriers in p-type silicon. Appl. Phys. Lett. 71, 2121 (1997).
11. B.B. Paudyal, K.R. McIntosh, and D.H. Macdonald, Temperature dependent carrier lifetime studies on Ti-doped multicrystalline silicon. J. Appl. Phys. 105, 124510 (2009).
12. G. Coletti, P.C.P. Bronsveld, G. Hahn, W. Warta, D. Macdonald, B. Ceccaroli, K. Wambach, N.L. Quang, and J.M. Fernandez, Impact of metal contaminations in silicon solar cells. Adv. Funct. Mater. 21, 879-890 (2011).

CHAPTER 1. DEFECTS IN CRYSTALLINE SILICON SOLAR CELLS

This thesis essentially focuses on the influence of Copper (Cu) and Titanium (Ti) on the photovoltaic (PV) performances of crystalline Silicon (Si) solar cells. However, even using initially ultra-pure Si feedstock, the deliberately contaminated samples will contain defects other than Cu and Ti, which could interfere with the conclusions drawn from our experimental studies, particularly via interactions with both studied elements. Therefore this chapter aims at presenting the physics of solar cells and the key physical parameters that can be affected by the presence of defects within the Si crystal. Secondly the main Si purification and crystallization processes are presented, with a particular attention paid to the evolution of the impurity contents all along these process flows. Eventually the main impurities usually found in crystalline Si are presented, and their extraction (external *gettering* effect) or electric neutralization throughout the solar cell fabrication process, discussed.

1.1 Physics of solar cells

This part focuses on the classical Si-based PV solar cells, with a *p*-*n* junction created by the association of both *p*- and *n*-type crystalline Si materials (homo-junction solar cells).

1.1.1. Doping of silicon, the p-n junction

Doping is a defect-engineering technique used to vary the density of electrons and holes in semiconductors. Doping creates *n*- (electron rich) or *p*-type (hole rich) materials and is therefore essential to form the *p*-*n* junction of solar cells. For the doping procedure, impurity atoms are introduced into an otherwise intrinsic semiconductor. These impurity atoms are classified as donor or acceptor elements.

Regarding Si, donor elements have more valence electrons than the substitutional Si atom they replace (Figure 1.1). Donor elements offer their extra valence electrons to the conduction band, making it *n*-type.

Acceptor elements have fewer valence electrons than the substitutional Si atom they replace (Figure 1.1). They provide excess holes that increase the hole carrier density of the semiconductor, making it *p*-type.

Si (element from the group IV of the periodic table) uses group V atoms as donors and group III atoms as acceptors. The Si wafers used by the PV industry are usually *p*-type, boron (B)-doped. The *n*-type region is usually created by the high T diffusion of phosphorus (P) atoms.

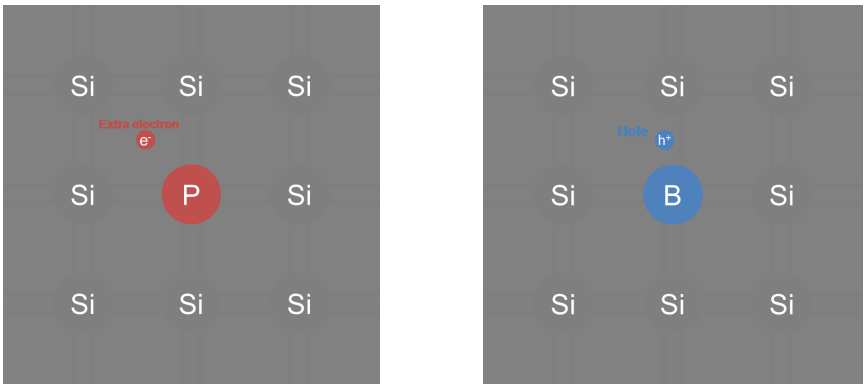

Figure 1.1 – Schematic of a silicon crystal lattice doped with P and B impurities to produce n-type (left) and p-type (right) semiconductor materials.

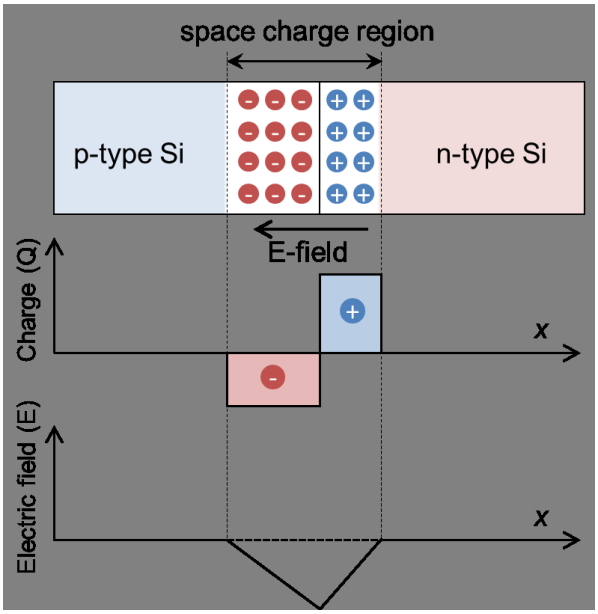

Figure 1.2 – Schematic variations of the charge density and the electric field across a p-n junction.

A *p*-*n* junction diode is formed by joining *n*-type and *p*-type semiconductor materials (Figure 1.2). When *n*- and *p*-type materials are set into contact, the electrons and holes move to the other side of the junction, leaving behind charges on dopant atom sites, which are fixed in the crystal lattice. Therefore, an electric field $\bar{E}$ is created by these fixed charges (positive ions in the *n*-type material and negative ions in the *p*-type material). This region is called the "space charge region" (*scr*).

1.1.2. Light absorption, carrier photogeneration and collection

A simple conventional solar cell structure is depicted in Figure 1.3. Sunlight is incident from the top, on the front of the solar cell. A metallic grid forms one of the electrical contacts of the diode and allows light to penetrate the semiconductor between the grid lines and thus be absorbed and converted into electrical energy. An antireflective layer between the grid lines increases the amount of light transmitted to the semiconductor. The diode's other electrical contact is formed by a metallic layer on the back of the solar cell [1].

All electromagnetic radiations, including sunlight, can be viewed as being composed of particles called photons which carry specific amounts of energy determined by the spectral properties of their source. Photons also exhibit a wavelike character with the wavelength (λ), being related to the photon energy ($E(\lambda)$) by

$$E(\lambda) = \frac{hc}{\lambda} \tag{1.1}$$

where h is Plank's constant and c is the speed of light.

If the photon is absorbed within the Si material, it has the possibility of exciting an electron from the valence band to the conduction band. A key factor in determining if a photon is absorbed or transmitted is the energy of the photon. Photons entering a semiconductor material can be divided into three groups based on their energy (E_{ph}) compared to that of the semiconductor band gap (E_G) [2]:

- $E_{ph} < E_G$ Such photons interact only weakly with the semiconductor, passing through it as if it were transparent.
- $E_{ph} > \approx E_G$ Such photons have enough energy to create an electron-hole pair and are efficiently absorbed.
- $E_{ph} >> E_G$ Such photons are strongly absorbed. However, for photovoltaic applications, the photon energy higher than the band gap is wasted as electrons quickly thermalize back down to the conduction band edges.

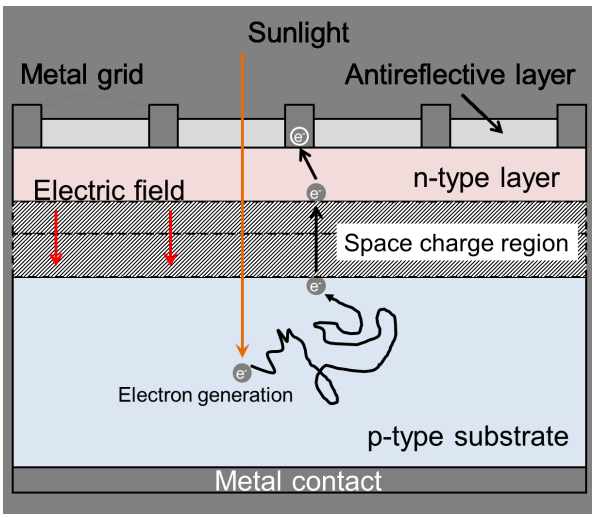

Figure 1.3 – Schematic of a simple conventional solar cell. Generation of electrons (e^-); diffusion of the minority carriers towards the junction; acceleration by the electric field and collection by the metal electrodes.

In Si, at room temperature, thermal energy is sufficient to instantaneously dissociate the photogenerated electron-hole pair (exciton). If the photon is absorbed within the *p*-type region of the cell, an excess minority carrier (electron) is created. This electron diffuses within the semiconductor material. If the electron reaches the *p-n* junction, the carrier is *accelerated* by the permanent electric field within the space charge region, and is collected by the metal electrodes. However, a number of pitfalls (*e.g.* recombination on impurity or structural defects) may prevent the photogenerated electron to reach the electrode, thus reducing the efficiency of the conversion process.

1.1.3. Charge carrier diffusion length, lifetime and mobility.

The minority carrier diffusion length (L) is the average distance a carrier can move from *the point* of generation until it recombines. Thus, L is a key parameter, which strongly governs the PV performances: the higher the L, the higher the PV conversion efficiency (η). L is defined by the following expression:

$$L = \sqrt{D\tau} \tag{1.2}$$

where τ is the charge carrier lifetime, which can be seen as the time interval between the photogeneration of a charge carrier, and its recombination. As evoked later in the manuscript (section 1.2.2), τ is a key parameter, which is usually strongly affected by the presence of impurities.

Diffusion coefficient or diffusivity (D) is related to the carrier mobility (μ) via the Einstein relation:

$$D = \frac{kT}{q}\mu \tag{1.3}$$

where kT/q the thermal voltage (k is the Boltzmann constant, T the temperature and q the elementary charge).

In standard Si materials, μ is mainly governed by the phonons and the substitutional dopants, structural defects are expected to play a minor role.

1.1.4. Forward I-V characteristics under illumination

The illuminated current-voltage (I-V) characteristic of a solar cell is given by the superposition of the dark I-V curve of the solar cell diode with the light-generated current. An example of illuminated I-V curve is shown in Figure 1.4, with the key PV parameters represented.

The short circuit current (I_{sc}) is the current delivered by the cell when the potential difference across the cell is zero. The I_{sc} depends on various factors which are described below:

- the area of the solar cell. In order to compare the performances of solar cells with difference areas, the short-circuit current density (J_{sc} in A/cm^2) is commonly presented, rather than the I_{sc};
- the number of incident photons (i.e., the power of the incident light source);
- the spectrum of the incident light. For most solar cell measurements, use is made of the standardized to the AM1.5 spectrum;
- the optical properties (absorption and reflection) of the solar cell;
- and last but not least, the collection probability of the solar cell, which depends chiefly on the surface passivation and the carrier lifetime or minority carrier diffusion length in the base (p-type region in Fig. 1.3) and the emitter (n-type region in Fig. 1.3). Therefore as τ and L are usually affected by the presence of metal impurities, high metal impurity contents are generally responsible for low I_{sc}.

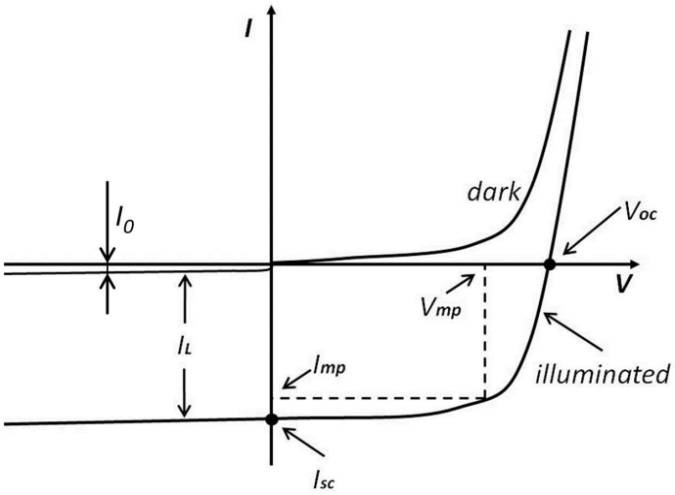

Figure 1.4 – I-V characteristics of a solar cell non-illuminated (dark) and illuminated [3]

The open-circuit voltage (V_{oc}) is the maximum voltage delivered by the cell, corresponding to a zero current. The V_{oc} can be estimated by the following equation:

$$V_{oc} = \frac{nkT}{q} \ln\left(\frac{I_L}{I_0} + 1\right) \tag{1.4}$$

The above equation shows that V_{oc} depends on the saturation current (I_0) of the solar cell and the light-generated current (I_L). I_0 is a parameter varying on orders of magnitude from one PV device to another. I_0 depends on carrier recombination in the solar cell (bulk and surface recombinations). Particularly, the lower the L, the higher the I_0. Therefore, V_{oc} can significantly be affected by large amounts of metal impurities.

The I_{sc} and the V_{oc} are the maximum current and voltage that a solar cell can deliver. However, at both of these operating points, the electric power from the solar cell is zero. The fill factor (FF) is a parameter which, in conjunction with V_{oc} and I_{sc}, determines the maximum electric power (P_{max}) that can be delivered by a solar cell. The FF is defined as the ratio of P_{max} to the $V_{oc} \times I_{sc}$ product:

$$FF = \frac{P_{\max}}{V_{oc} I_{sc}} = \frac{V_{mp} I_{mp}}{V_{oc} I_{sc}} \tag{1.5}$$

where V_{mp} and I_{mp} are the voltage and current respectively, associated with the point of maximum power.

FF is influenced by several mechanisms. Firstly the parasitic resistive losses and the shunt issues strongly affect *FF*. The shunt issues can be due to non-optimized metallization processes, but also to the presence of conductive precipitates (e.g. metal silicides) crossing the *p-n* junction. *FF* also depends on carrier recombination within the space charge region. Therefore the presence of high amounts of metal impurities within the space charge region can detrimentally affect the *FF*. Also high increases of the charge carrier lifetime with the excess carrier density can significantly decrease *FF*, as explained in [4]. Indeed, according to Macdonald *et al.* [4], the *FF* reveals how the voltage changes from open-circuit to maximum power in comparison to the 'ideal' case. In this ideal case the lifetime is assumed constant at all voltages, or in other words, injection-level independent. If the lifetime changes with injection-level, an altered fill factor will result.

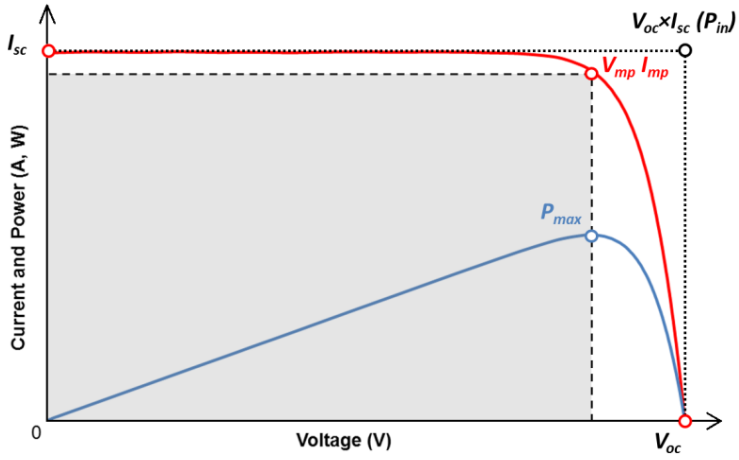

Figure 1.5 – Solar cell output current (red line) and power (blue line) versus the applied voltage. This figure presents also the key PV parameters: the V_{oc} and I_{sc} points, as well as the maximum power point (V_{mp}, I_{mp}).

The conversion efficiency (η) is the most commonly used parameter to compare the performances of different solar cells. η is determined as the fraction of incident power (P_{in}) which is converted to electricity and is defined by:

$$\eta = \frac{P_{\max}}{P_{in}} = \frac{V_{oc} I_{sc} FF}{P_{in}} \tag{1.6}$$

η depends on the spectrum and intensity of the incident sunlight and the temperature of the solar cell. Therefore, conditions under which η is measured must be carefully controlled in order to compare the performance of one device to another. Terrestrial solar cells are measured under AM1.5 conditions and at a temperature of 25 °C.

1.1.5. Reverse I-V characteristics, junction hard breakdown voltage

Another important parameter for solar cells is the absolute value of the junction hard breakdown voltage (V_{bd}). The junction hard breakdown is related to the part of the reverse *I–V* curve where the current suddenly sharply increases upon lowering the reverse bias. This breakdown type governs the global *I–V* curve at high reverse bias (in absolute values). V_{bd} is a crucial parameter since it governs the long-term performances of a solar module. Indeed when a cell within the module is shaded, it can be reversely biased and act as a receptor, inducing a loss of the global power of the panel. If the reverse bias is close to V_{bd}, large currents can locally flow through the cell leading to thermal damages. These issues can be mitigated by the presence of protection diodes [5]. However they are only efficient in standard modules (60 cells) provided that V_{bd} is higher than about 12 V. For the base doping levels usually used for the solar cell fabrication (lower than 10^{17} cm^{-3}), the junction hard breakdown is usually governed by the avalanche effect (impact ionization) [6]. Figure 1.6 presents the mechanism which leads to *avalanche breakdown*. In reversely-biased *p-n* junctions, large electric fields accelerate free carriers in the space charge region. When the electric field is sufficiently strong (of the order of 10^5 $V.cm^{-1}$, the kinetic energy gained by the carriers is high enough to knock valence electrons out of their state and lift them to the conduction band (impact ionization) when in turn they may be accelerated and participate in the multiplication process. When the breakdown is governed by the avalanche effect, the V_{bd} values increase as the T increases (for high T the accelerated free carriers within the *scr* lose part of their energy to optical phonons).

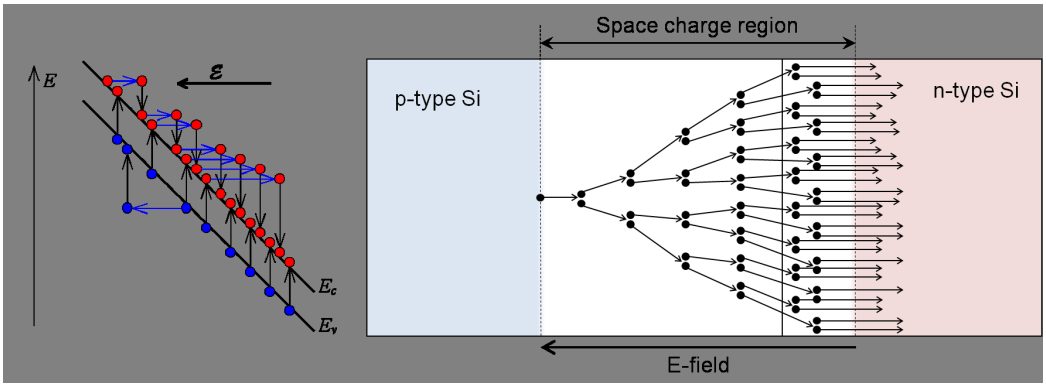

Figure 1.6 – Schematics of the avalanche breakdown process. Electrons in the conduction band are accelerated by the large electric field in the reversely-biased p-n junction. If the carrier kinetic energy is high enough, valence electrons can be transferred to the conduction band, taking part in the electron multiplication process.

An approximate empirical universal expression for V_{bd} calculation (in volts) can be given as follows, for abrupt junction [6]:

$$V_{bd} \cong 60\left(E_g/1.1\right)^{3/2}\left(N_B/10^{16}\right)^{-3/4} \tag{1.7}$$

where E_g is the band gap (eV), and N_B is the background doping density (cm^{-3}).

1.2 Charge carrier transport properties, recombination and trapping

1.2.1 Charge carrier mobility, silicon resistivity

μ determines the manner charge carriers move through a semiconductor under an external electric field (E). In a semiconductor, μ can be expressed as [7]:

$$\mu = \frac{v_d}{E} \tag{1.8}$$

where v_d is the drift velocity of the charge carrier (i.e., the average velocity increase of the carrier between two consecutive collisions caused by the electric field).

Electrons and holes in a semiconductor behave much like free particles of the same electronic charge with effective masses. Thus, they are subject to the classical processes of drift and diffusion. Drift is a charged particle's response to an applied electric field.

Different carrier scattering mechanisms influence μ in Si materials, e.g. lattice (phonon) scattering, defect scattering (extended crystal defects, ionized or neutral impurities), and carrier-carrier scattering. The overall carrier mobility (μ_{tot}) that takes into account all these different mechanisms can be approximated through Matthiessen's rule:

$$\frac{1}{\mu_{tot}} = \sum_{i-1}^{n} \frac{1}{\mu_i} \tag{1.9}$$

where μ_i is the mobility related to the i-th scattering mechanism. The balance between these mechanisms varies with temperature, and it has been shown that the dominant scattering

mechanisms in a non-compensated Si material at room temperature are ionized impurity scattering and lattice scattering. The scattering of charge carriers by phonons and ionized impurities is in principle well covered in classical μ models [8].

The bulk resistivity (ρ) of the Si wafers has strong influences on the performances of the PV device. For crystalline Si, the optimum bulk ρ has been empirically determined to be approximately 1 Ω.cm, a value which balances the requirements for carrier recombination, operating voltage of the solar cell and surface passivation [9]. The resistivity (ρ) is defined as the proportionality constant between the electric field and the current density.

For semiconductors with both electrons and holes as carriers, we obtain:

$$\rho = \frac{1}{\sigma} = \frac{1}{q(\mu_n n + \mu_p p)} \tag{1.10}$$

where σ is the material conductivity, μ_n and μ_p the electron and hole μ; and n and p the electron and hole densities, respectively.

Consequently for *n*-type Si: $\rho \cong \frac{1}{q\mu_n n}$ and for *p*-type Si: $\rho \cong \frac{1}{q\mu_p p}$ (1.11)

Notice that in a B-doped material, with a standard ρ equal to 1 Ω.cm, p is approximately equal to the B concentration ([B]). Consequently, from the ρ (usually determined by the four point probe method), the dopant density can be computed.

1.2.2 Carrier recombination and trapping

There are three fundamental recombination mechanisms in semiconductors which are necessarily present to some extent in any sample: radiative, Auger and multi-phonon recombination (known as Shockley-Read-Hall (SRH)), illustrated on Figure 1.7 [4, 6]. These mechanisms differ in the way the excess carrier energy is dispersed throughout the recombination process, being mediated by photons, carriers and phonons respectively.

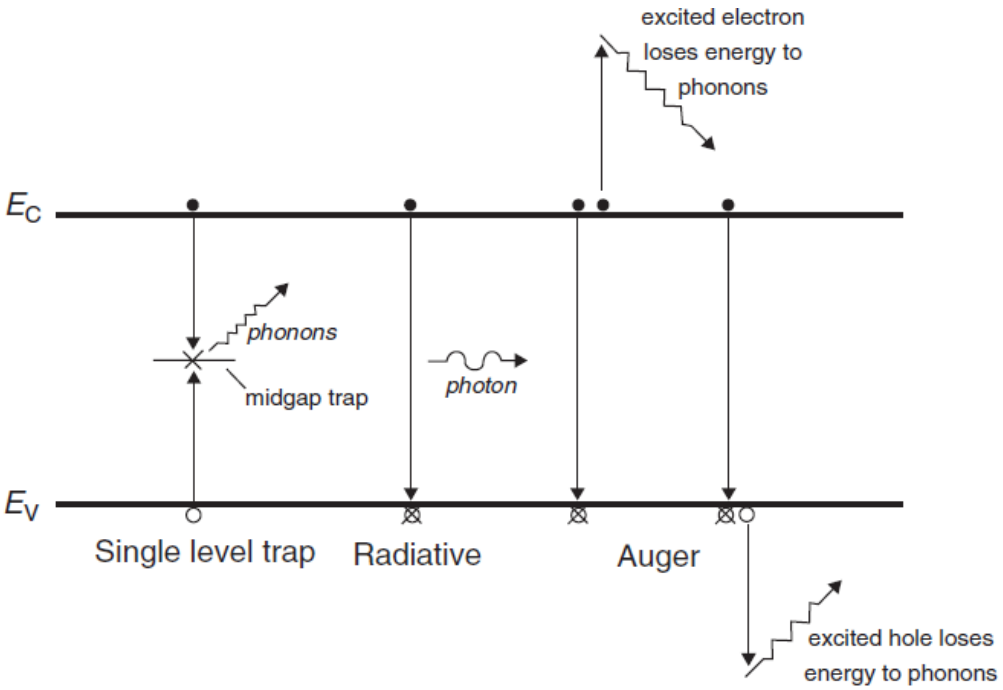

Figure 1.7 – Recombination processes in semiconductors [1]

Radiative recombination is simply the process of optical absorption occurring in reverse. Consequently, in radiative recombination, the excess energy is emitted as a photon as illustrated in Figure 1.7. The radiative recombination rate (U_{rad}) depends jointly on both the electron and hole concentrations, since one of each is required for the process to occur [7]. In *p*-type material this gives rise to the following expression:

$$U_{rad} = B\Delta n(p_0 + \Delta n) \tag{1.12}$$

where B is a constant equal to 1.0×10^{-14} $cm^3.s^{-1}$ for Si, p_0 the equilibrium hole density and Δn the excess carrier density. Hence, from equation 1.12 the radiative recombination lifetime τ_{rad} is given by:

$$\tau_{rad} = \frac{\Delta n}{U_{rad}} = \frac{1}{B(p_0 + \Delta n)} \tag{1.13}$$

Radiative recombination is typically the dominant recombination process in direct gap semiconductors such as GaAs. In indirect gap semiconductors such as Si, this recombination is negligible and can usually be safely ignored in the analysis of measured recombination lifetimes in Si solar cells.

In the *Auger recombination* process, the electron recombining with the hole gives the excess energy to a second electron in the conduction or valence band, instead of emitting light, as illustrated in Figure 1.7. Auger recombination is typically observed, when either the doping density (N) or the Δn are very high. Auger lifetimes for p-type Si can be approximated [10]:

$$\text{for high } \Delta n\text{: } \tau_{Auger,hi} = \frac{1}{C_a \Delta n^2}$$

$$\text{and for low } \Delta n\text{: } \tau_{Auger,li} = \frac{1}{C_p N^2} \tag{1.14}$$

where Δn is the excess carrier density, N is the net dopant concentration, and $C_a = 1.66\times10^{-30}$ $cm^6.s^{-1}$ and $C_p = 9.9\times10^{-32}$ $cm^6.s^{-1}$ are the Auger coefficients for Si.

Like radiative recombination, Auger processes are intrinsic, meaning that their presence do not depend on the specific techniques and/or feedstocks used for silicon crystal growth (apart from the impact of the dopant density on their low-injection magnitudes), and are in this sense unavoidable. Unlike radiative losses however, they often contribute significantly to the overall effective lifetime in silicon, particularly at high carrier densities. At lower carrier densities in Si, the lifetime is usually dominated by recombination through defects, as discussed below.

Recombination through defects. In SRH-recombination [11,12], electron and hole recombine through energy levels present in the Si band gap, introduced by defects (as illustrated in Figure 1.7). It is a two-step process, characterized by the recombination center density N_T, the energy level E_T in the band gap and the recombination center capture cross-sections σ_n and σ_p for electrons and holes, respectively. The energy liberated during recombination is dissipated by lattice vibrations. The SRH recombination lifetime is given by the simplified expression [4]:

$$\tau_{SRH} = \frac{\tau_{n0}\left(p_0 + p_1 + \Delta n\right) + \tau_{p0}\left(n_0 + n_1 + \Delta n\right)}{n_0 + p_0 + \Delta n} \tag{1.15}$$

Equation 1.15 further reduces for *p*-type Si, to:

$$\tau_{SRH} = \frac{\tau_{n0}\left(p_0 + p_1 + \Delta n\right) + \tau_{p0}\left(n_1 + \Delta n\right)}{p_0 + \Delta n} \tag{1.16}$$

where τ_{n0} and τ_{p0} are parameters defined below; and the statistical factors n_1 and p_1 are the electron and hole densities when the Fermi level coincides with the recombination centre energy E_T:

$$\tau_{p0} = \frac{1}{N_T v_{th} \sigma_p} \qquad \tau_{n0} = \frac{1}{N_T v_{th} \sigma_n} \tag{1.17}$$

$$n_1 = N_C exp\left(\frac{E_T - E_c}{kT}\right) \qquad p_1 = N_V exp\left(\frac{E_c - E_g - E_T}{kT}\right) \tag{1.18}$$

where v_{th} is the carrier thermal velocity, N_T is the density of recombination center, σ_n and σ_p are the capture cross-sections for electron and hole, N_C and N_V are the effective densities of states at the conduction and valence band edges, and E_c and E_g the conduction band and band-gap energies.

The expression 1.16 shows that the SRH lifetime can significantly vary with the excess carrier concentration.

SRH recombination takes place whenever there are impurities or defects in the semiconductor, and is particularly important for indirect band gap semiconductors such as Si. For mc-Si solar cells, this is the most important recombination process because of the high density of impurities and crystallographic defects. SRH recombination depends inversely on the density of recombination centers and capture cross sections, but does not depend directly on the energy level introduced by the defect. Recombination centers with E_T close to the mid band gap are usually the most effective recombination centers [13].

In most practical cases two or more of the bulk recombination mechanisms described above may be important in a given sample at a given excess carrier density. For independent processes, the net recombination rate is the sum of the individual rates, resulting in an

effective lifetime τ_{eff}. For example, when SRH, Auger and radiative recombination mechanisms are all expected to play a role, τ_{eff} is given by:

$$\frac{1}{\tau_{eff}} = \frac{1}{\tau_{rad}} + \frac{1}{\tau_{Auger}} + \frac{1}{\tau_{SRH}} \tag{1.19}$$

Surface recombination is a special case of SRH recombination in which the localized energy states occur at the surface. Unlike bulk SRH centers however, these states do not usually occupy a single energy level, but rather form a set of states distributed across the band-gap. Surface recombination analysis is performed in terms of surface recombination velocities (SRV) instead of lifetimes, however, the principles are identical to bulk SRH recombination. In the simpler case of a sample of thickness W, with a constant bulk lifetime (τ_b) and a small constant SRV (S) that is the same on each surface, the effective carrier lifetime is given by [4]:

$$\frac{1}{\tau_{eff}} = \frac{1}{\tau_b} + \frac{2S}{W} \tag{1.20}$$

The requirement that S be small arises from the assumption that the surface recombination rate is not limited by the diffusion of carriers to the surfaces. The accuracy of this expression for various sample thicknesses and values of S has been discussed by Sproul for carrier decay mode [14].

Carrier trapping. Minority carrier traps are often present in significant quantities in solar grade mc-Si [15]. Minority carrier traps are generally attributed to shallow energy levels in the Si band-gap, with strongly asymmetric capture cross sections. These defects ‘capture’ and ‘hold’ a minority carrier for a limited time, before ‘releasing’ the carrier back into the band from whence it came [15,16].

Trapping was first noticed and modeled in poor quality single crystal silicon by Hornbeck and Haynes [16]. Their models were able to extract the trap density (N_t), the trap/escape ratio (τ_t/τ_g), and the trap energy level in the band-gap ($E_C - E_T$). An assumption of this model is that τ_{eff} is constant and injection independent. This model was transposed to Quasi-steady-state photoconductance decay (QssPC) data affected by traps by Macdonald and Cuevas [15]. Two different types of defects in mc-Si are usually involved in trapping mechanisms: metal-boron pairs and dislocations [15]. The trapping centers induce unusual

behaviors of the photoconductance at low excess carrier density, equal to and below the trap density. An important consequence of such behavior is that any photoconductance based carrier lifetime technique cannot be relied upon to provide reasonable lifetime measurements at these injection levels, which are often of great interest in solar cell applications [15-17]. Carrier traps observation in mc-Si could be a good indicator of material quality [17]. A more thorough review of the physics behind trapping, and its effects on devices, can be found in the literature [15-17 and references therein].

1.3 Si production: from silica to virtually pure Si

As solar cells with high conversion efficiency require high carrier lifetimes, the metal impurity content has to be low, usually well below 10^{15} cm^{-3}. Therefore the Si materials have to be purified. The standard gaseous distillation process yields high purity electronic grade (EG) materials, but it is costly and based on the use of highly toxic chlorides. On the other hand, the promising Si refinement processes by metallurgical routes should offer low cost feedstock, produced by *eco-friendly* processes. However the metal impurity contents are expected to be higher than the concentrations usually found in standard EG Si. As this PhD thesis focuses on the effect of metal impurities, it is particularly important to present the main processes used for the Si purification, and to compare the impurity concentration levels associated with each technology.

1.3.1 Carbothermic reduction

Carbothermic reduction is a process used to produce metallurgical grade silicon (MG-Si, with a typical purity of 98-99 wt. %). MG-Si is produced in electric arc furnaces [1]. In principle, this process is much the same as it was at the beginning of the twentieth century, when it was first developed for ferrosilicon and other alloys. However, the operational execution has greatly improved, with larger furnaces, more efficient material handling and better control of the process. The furnace consists essentially of a crucible filled with quartz and carbon based materials. Silicon is freed by the carbothermic reduction of silica according to the overall reaction [1,18]:

$$SiO_2(s) + 2C(s) \rightarrow Si(l) + 2CO(g)$$

The major carbon sources are coal and coke while wood chips are used to add porosity to the reacting mass in order to allow escape of the product gases CO and SiO. Complex reactions take place between reactants and the SiC(s) and SiO(g) intermediates at temperatures that range up to 2300 K between adjacent electrodes. The manufactured MG-Si product contains about 1-2 wt. % impurities after it is gas refined with chlorine or oxygen. The main impurities are: iron (Fe), aluminum (Al), calcium (Ca), titanium (Ti), carbon (C) and oxygen (O). The other main impurities are metals, particularly transition elements (V, Cr, Mn, Co, Ni, Cu, Zr, Mo), boron and phosphorus. The composition of the contaminants depends on many factors, e.g on the raw silica, the components used for the silica reduction and the actual processes. A list of impurity concentration ranges is displayed in Table 1.1 [1].

Table 1.1 – Representative concentrations of the impurities in MG-Si.

Impurity	Fe	Al	Ca	Ti	C	O
Concentration (wt.%)	0.2-1	0.4-1	0.2-1	0.01-0.1	0.1-0.15	0.005-0.01
B and P	10-100 ppm wt each					
Transition elements: V, Cr, Mn, Co, Ni, Cu, Zr, Mo	10-100 ppm wt each					

1.3.2 Purification by chemical routes, the Siemens process

In the *Siemens process*, the metallurgical grade silicon is transferred into the gaseous phase by reaction with anhydrous hydrogen chloride in a fluidized bed reactor according to the simplified expression [1,18]:

$$Si(s) + 3HCl(g) \rightarrow SiHCl_3(g) + H_2(g)$$

After the reaction, most of the silicon is bound in trichlorosilane (TCS), with a small percentage forming chlorides such as $SiCl_4$. TCS can easily be purified by fractional distillation (making use of differences in boiling points of the other chlorides) as well as by passing it through several filters.

Afterwards, the gaseous TCS is directed towards pure monocrystalline silicon seed rods which are heated to temperatures above 1100 °C. At the silicon surface, the TCS is reduced by hydrogen following the reaction:

$$SiHCl_3(g) + H_2(g) \rightarrow Si(s) + 3HCl(g)$$

The resulting polysilicon rods are crushed and used as highly pure silicon feedstock, also called as electronic-grade feedstock. In general, the impurity content is lower than 0.001 ppb wt.

1.3.3 Purification by metallurgical routes: focus on the PHOTOSIL process

A few years ago, as the demand for high-quality solar grade Si (SoG-Si) feedstock exceeded few years ago supply and drove prices upwards, alternative purification cycles were developed to reduce the prices for SoG-Si. Particularly, the PHOTOSIL process, that relies on metallurgical purification steps (the material remains in the liquid and solid states) was developed in France [19-22]. This Si production route can be five times more energy efficient than the conventional Siemens process that uses an amount of energy by quantity of material produced higher than 200 kWh/kg [18]. A complete description of the PHOTOSIL process can be found in [19-22 and references therein].

A first important step, which takes place before the PHOTOSIL process itself, concerns the production of MG-Si. The liquid MG-Si is directly subjected to a segregation treatment which allows to remove metal impurities, but also P. The obtained, so called "Upgraded Metallurgical" (UMG-1) silicon is the starting material for the PHOTOSIL process.

As a first step of the PHOTOSIL process, the UMG-1 silicon is melted in an induction furnace and submitted to a second segregation process. At the end of the process the final part of the liquid silicon, into which elements with a small segregation coefficient have been rejected during the solidification, is separated by pouring it into a waste container.

The obtained solid UMG-2 silicon is then transferred to a plasma purification unit. An argon plasma gas that contains reactive species is created by induction and blown onto the surface of liquid silicon which is constantly renewed by electromagnetic stirring. During this critical step, reactive species based on oxygen and hydrogen form volatile particles with boron, decreasing the B concentration in the Si melt. At the end of the plasma treatment, the purified silicon is either rapidly cooled resulting in randomly solidified silicon, or preferentially solidified in a directionally way in order to lower again the total amount of impurities. Indeed, due to the oxygen introduced during the plasma treatment and to the graphite crucible used for the melting, the silicon bath is contaminated by oxygen and carbon. Therefore a controlled solidification helps to partially remove these elements. The purity of the PHOTOSIL Silicon was controlled and defined as presented in Table 2.2 [19,22].

Table 1.2 – Main impurities concentrations in PHOTOSIL silicon

Elements	B	P	Al	Fe	Cu	Ti
Concentration, ppm(w)	< 0.3	< 0.6	< 0.1	< 0.1	< 0.1	< 0.1

Recent results obtained in the frame of the PHOTOSIL project [21-23] demonstrated that *p*- and *n*-type Czochralski Si solar cells with PV conversion efficiencies exceeding 18 % could be fabricated using PHOTOSIL Si.

1.4 Crystallization of Silicon

The Si-based PV industry uses both multicrystalline (mc) and single-crystalline (sc) wafers. Thus both kinds of materials were investigated in the course of this thesis. The mc wafers are usually obtained by directional solidifications in crucibles (ingot casting). The sc wafers are generally produced by the Czochralski (Cz) method. Both processes are described below. As these processes are accompanied by segregation effects, the main theoretical background necessary to understand the problematic of segregation of impurities is presented.

1.4.1 Czochralski growth

Si is first molten in a SiO_2 crucible and maintained at a temperature just above the melting point. A rotating monocrystalline silicon seed with the targeted crystal orientation is then brought into contact with the surface of the Si melt. Then the crystal growth is initiated by pulling the seed from the melt and controlling the solidification velocity until the crystal has reached the desired diameter. The crucible can also be rotated, either in the same or in the opposite direction compared to that of the seed. When the process is properly executed, the obtained ingot is fully mono-crystalline and virtually free of dislocations.

Dopants, such as boron or phosphorus, are added to the feedstock before melting. By adjusting the temperature, the rotational speed and the pulling speed, the diameter of the ingot can be controlled. Typical industrial Cz-Si ingots have diameters ranging between 200 mm and 300 mm, with lengths up to 2 m. Since the melt and the crucible are kept at over 1400°C for a long time, oxygen is introduced into the Si melt because of the dissolution of the crucible, and is thus incorporated into the crystal. As a result, Czochralski-grown silicon contains high amounts of oxygen. Typical values for the interstitial oxygen (O_i) concentration [O_i] usually range between 5×10^{17} cm^{-3} and 1×10^{18} cm^{-3}.

1.4.2 Multicrystalline ingot casting

A more cost-effective way of crystallization is offered by the casting technique. Si is molten in a crucible and solidification is then induced through controlled cooling of the melt. As cooling takes place from below, the ingot grows from bottom to top. In the absence of a seed, the ingot is multicrystalline. The crucible is initially coated with an oxidized silicon nitride (Si_3N_4) layer which prevents the adhesion of the Si ingot with the SiO_2 crucible.

Generally mc-Si contains lower [O_i] (typically in the order of $1\text{-}5\times10^{17}$ cm^{-3}), than the values found for Cz-grown Si. On the other hand, mc-Si wafers contain significant amounts of metal impurities, mainly originating from the crucible and its coating. In addition, the solidified ingot consists of many crystallites or grains of different size and orientation (so-called grains). Apart from the many grain-boundaries, mc-Si also contains high amounts of dislocations and in particular dislocation clusters. Given such high concentrations of metal impurities and crystal defects, it is not surprising that the material quality of mc-Si is in general lower than that of Cz-Si.

1.4.3 Segregation of impurities

For both previously presented techniques for the production of Si ingots, the solidification is directional. This induces, due to the phenomenon of segregation, significant variations of the impurity contents along the solidification direction.

Segregation describes the re-distribution of dissolved impurities in a system that consists of two or more phases. The phases can either be different states of the same material (e.g., liquid, solid) or different material compositions, such as transition metal silicide and silicon.

Regarding the segregation of an impurity (*I*) between solid and liquid Si, the amplitude of this phenomenon depends on the segregation coefficient (*k*). At a given T, the equilibrium *k* is defined by the ratio of the solute concentration of the solidus curve ($C_S(T)$), to that of the *liquidus* curve ($C_L(T)$), concentrations extracted from the phase diagram of the Si-I system.

$$k = \frac{C_s(T)}{C_L(T)} \tag{1.21}$$

In purified Si, the impurity concentration is usually significantly lower than 10 %. In that case, the *solidus* and *liquidus* curves can be approximated by straight lines with slopes m_S and m_L, respectively. The equilibrium segregation coefficient k_0 can then be expressed as:

$$k_0 = \frac{m_L}{m_S} \tag{1.22}$$

From the segregation coefficient, the distribution of the impurity concentration ([I]) along the height of a directionally solidified crystal can generally be computed using the Scheil's equation [24]:

$$[I]_{f_S} = k_0 \times [I]_0 \times \left(1 - f_S\right)^{k_0 - 1} \tag{1.23}$$

$[I]_{fS}$ is the impurity concentration corresponding to the solidified fraction f_S. $[I]_0$ is the initial impurity concentration in the Si melt.

The previous equation is only valid in the case of a conservative system, in which there is no addition or loss of Si or impurity after the beginning of crystallization. In addition, this equation is only valid in the case of a perfectly mixed Si melt.

Figure 1.8 presents experimental values for the equilibrium segregation coefficients for most impurities in Si.

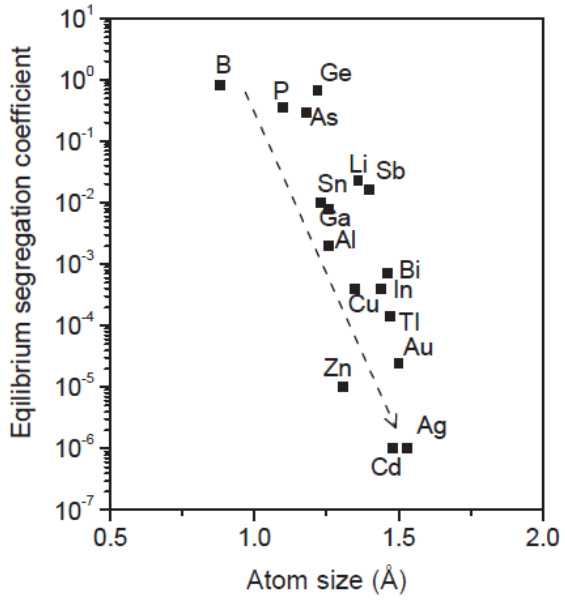

Figure 1.8 – Equilibrium segregation coefficient of various impurities in Si, as a function of the impurity atom size [25]

Regarding the growth of Cz ingots, although the bulk of the melt is effectively homogenized by thermal convection and by the rotation of the seed and/or crucible, the impurity concentration usually varies in the vicinity of the solid/liquid interface. To take this inhomogeneity into account, Burton *et al.* [26] considered the presence of a diffusion layer in the Si melt at the solid/liquid interface, with a thickness δ expressed as:

$$\delta = 1.6 \times D^{\frac{1}{3}} \times \nu^{\frac{1}{6}} \times \omega^{\frac{-1}{2}} \tag{1.24}$$

D is the diffusivity of the considered impurity in liquid Si. v is the kinematic viscosity of the Si melt, and ω the crystal rotation rate. They also showed that this imperfect mixing could be accounted for in the calculation of the impurity distribution, by simply using in Scheil's equation an effective segregation coefficient k_{eff}, defined by:

$$k_{eff} = \frac{k_0}{k_0 + (1 - k_0)\exp\left(-\frac{V\delta}{D}\right)} \tag{1.25}$$

V is the ingot pulling speed. This derivation of the effective segregation coefficient is commonly referred to as the BPS theory.

1.5 Main crystal defects – Impact on the PV performances

Crystal defects disturb the periodical array of the Si crystal lattice and can affect the charge carrier transport and recombination properties, consequently the PV performances of the fabricated solar cells. Crystal defects can be divided into several types:

- point defects which involve vacancies, self-interstitials and *dissolved* impurity atoms,
- 1-dimensional defects or line defects, mainly dislocations,
- 2-dimensional defects or planar defects, which include grain boundaries, stacking faults and surfaces,
- 3-dimensional defects or volume defects, like voids and precipitates.

1.5.1 Grain boundaries and dislocations

The main crystal defects in multicrystalline silicon are grain boundaries and dislocations (Figure 1.9). Concerning the efficiencies of solar cells, not only the concentration of these defects but also their electrical activity is considered as crucial. The grain sizes achieved with modern block-cast material are still large enough not to degrade solar cell efficiencies, provided that the electrical activity of the grain boundaries is low enough. Grain boundaries and dislocations, if electrically charged, effectively attract minority charge carriers and consequently represent highly active recombination centres for photo-generated charge carriers. The electrical activity of grain boundaries and dislocations is usually determined by their impurity decoration (specifically by transition metals) and strongly increases with impurity concentrations [13].

Dislocations are important because they can change the optical and electrical characteristics of a crystal. In addition, they also interact strongly with other defects and impurities and can lower the formation energy for precipitates. In Si, dislocations usually form at high temperatures (1000-1300 °C) during cooling of the solidified material. Local internal thermoelastic stresses during growth and subsequent cooling can cause dislocation formation and/or multiplication by a multiple cross slip process. In addition, dislocations can form in the vicinity of interfaces within the crystal, *e.g.* precipitate-bulk interfaces that can expand or contract differently due to; a) thermal gradients, b) change in composition or c) change in lattice structure. When the stresses reach a critical value, dislocations will form. Grain boundaries can also act as sources for dislocations.

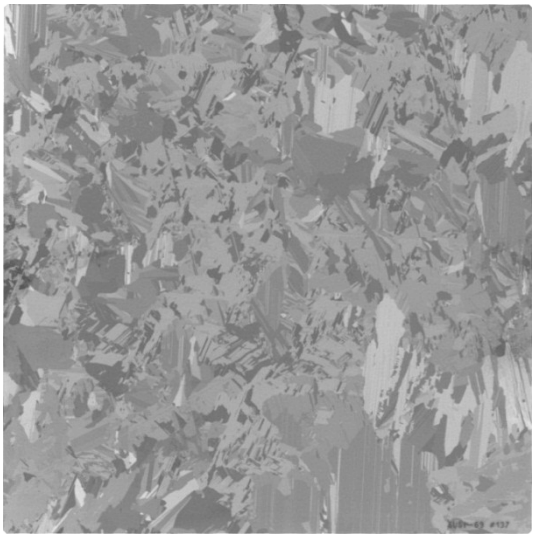

Figure 1.9 – Photograph of a typical 156×156 mm^2 mc-Si wafer.

Grain boundaries are the boundaries between grains of different orientations. Grain boundaries can be divided into three groups; Random angle grain boundaries, co-incidence site lattice (CSL) grain boundaries and low angle or sub-grain boundaries. When the misorientation between neighboring grains is below 10-15°, it is called a low angle grain boundary, which consists of an array of dislocations. For larger misorientations, reconstruction of the dangling bonds takes place and the boundary is continuous. Low angle grain boundaries are called tilt boundaries if they consist of edge dislocations, and twist boundaries if they consist of screw dislocations. Grain boundaries with very low misorientation angles of a few degrees are frequently called small angle grain boundaries [13].

It is well known that carrier recombination activity depends on grain boundary character and contamination. While grain boundaries in clean samples show very low recombination activity, almost independent of misorientation and temperature, the recombination activity increases with contamination level. Therefore the recombination activity of the grain boundaries varies within an ingot. Grain boundaries in the top and bottom of an ingot feature strongest recombination activity (compare to the grain boundaries located in the middle part of the ingot) due to the higher Fe contamination level [13].

Directionally solidified mc-Si ingots contain also different impurities, which can be present in the material as dissolved atoms, precipitates or clusters. According to their state, these impurities affect material properties to different degrees.

1.5.2 Light elements: C, N and O

Oxygen (O), Carbon (C) and Nitrogen (N) are the most common impurities in mc Si. O mainly comes from the silica crucible. N mainly comes from the crucible coating and C from the furnace graphite parts [13]. Both N and C form relatively large precipitates in the ~ μm range which are not very recombination active, but can cause shunting of the cell. Nitrogen-doped highly conductive SiC filaments were found to cause ohmic shunts. Both SiC and Si_3N_4 precipitates mainly form in the top part of the ingot and N has been found to enhance SiC formation. Nanoclusters of $FeSi_2$ and Cu_3Si have been observed on SiC inclusions. Also SiC filaments are often observed along grain boundaries and are aligned in the ingot growth direction.

Oxygen in interstitial position (O_i) is one of the most abundant defect in commercial silicon (Si) wafers. Although O_i is not directly harmful as such, it is the common precursor to

many defects that can govern the Si electronic and mechanical properties. Oxygen precipitates are known to have detrimental effects on the carrier lifetime and on the performances of the solar cells. In solar cell processing, they also develop detrimental internal gettering effects counterbalancing the external gettering effect created by the phosphorus (P) diffusion [27].

The formation of oxygen-based thermal donors (TD) can also modify the carrier transport properties. TD are oxygen-based nano-clusters which exhibit a double-donor behavior. They form within specific temperature ranges (i.e., around 450 °C). The formation rate of the thermal donors strongly depends on the O_i concentration. Recently, a promising method, based on the variation of the resistivity due to the TD formation, was recently proposed in our laboratory for determining and mapping the interstitial O concentration, whatever the thickness and the surface state of the studied sample [27,28].

Oxygen would also be involved in the defects activated under illumination at room T, responsible for the light-induced degradation (LID) of the PV performances of B-doped Si solar cells. The existing models for the formed complex, which would involve B and O, disagree on the nature of the B atoms (substitutional B_s [29] or interstitial B_i [30]) and O (interstitial O dimer O_{2i} [29] or monomer O_i [31]) and the complex formation mechanism (i.e., fast diffusion of the O_{2i} and capture by the B_s atoms [29] or activation of latent complexes [30,31]). These major difficulties in assessing the true nature of the B-O defects are mainly due to the fact that this complex is present at very low concentrations (the signature of the complex is not detectable by deep level transient spectroscopy), probably below 10^{11} cm^{-3}. Thus only the effects of the complex on τ (or any values influenced by τ) can be monitored. However the complex exhibits very high carrier capture cross sections (probably higher than 7×10^{-14} cm^2), and its effects on τ can be deleterious for the cell conversion efficiency. The LID of the carrier lifetime is an important drawback for crystalline silicon solar cells containing significant amounts of B and/or O. Most of the Si currently used by the PV industry is affected by this important issue, from the high efficiency solar cells prepared from Cz-Si (due to the large amount of O originating from the crucible), to the new low-cost SoG materials (because of the high amount of B).

1.5.3 Metal impurities in Si

The Si wafers used by the PV industry usually contain larger amounts of metal impurities than the values commonly found in the ultra-pure materials used by the Si-based integrated circuit industry. For instance Macdonald detected by neutron activation analysis

total iron (Fe) and chromium (Cr) bulk concentrations of 3×10^{14} cm^{-3} and 2×10^{15} cm^{-3} respectively in cast multicrystalline Si [4] whereas these concentrations are usually below 10^{11} cm^{-3} in Electronic-Grade Si (EG-Si). This higher presence of metal impurities has various origins. Firstly the refinement processes can be directly responsible for the high metal impurities contents, particularly when low-cost purification technologies by metallurgical routes are used. Secondly metal impurities can be introduced during the ingot growth from the crucibles and their coatings, or even during the ingot squaring and wafering steps (i.e., surface contamination from the wires and blades). Finally the solar cell fabrication process can contribute to these contamination issues, particularly during the chemical steps used for etching, cleaning or even rinsing the wafer surfaces, the unwanted elements diffusing into the Si bulk during the subsequent high temperature steps.

Metal impurities are known to introduce energy levels, usually deep, in the Si band gap. They generally feature high capture cross sections (between 10^{-17} and 10^{-12} cm^2). Consequently they act as virulent charge carrier recombination centers and even present at low concentration, drastically affect the charge carrier lifetime. For instance an interstitial iron (Fe_i) concentration ($[Fe_i]$) of 3×10^{12} cm^{-3} in low injection level conditions leads to a value of τ of about 2.5 µs whereas nowadays the cell producers expect τ higher than hundreds of microseconds for the fabrication of high efficiency solar cells. Consequently studying the effects of metal impurities on the performances of crystalline Si solar cells, goal of this PhD thesis, is of paramount importance.

In the literature numerous studies were dedicated to the physical properties (solubility, diffusivity) of the main metal impurities in crystalline Si (i.e., iron, copper) and their effects on the charge carrier recombination mechanisms. However the influences of such impurities on the PV performances of industrial-like crystalline Si solar cells were rarely studied, except in the pioneering works performed in the 1970's and 1980's by Westinghouse Corp [32], which reported the variation of the PV conversion efficiency with the impurity concentration for various common metal impurities. These important results are often used as references for defining specifications on the tolerable amount of impurities in Si feedstock. However these studies were based on a lab-scale solar cell fabrication process, with no hydrogen source (hydrogen being known for electrically passivating some metal impurities [33]) and no aluminum layer on the rear surface (aluminum being known for developing external gettering effects of metal impurities via the formation of a liquid alloy with Si for temperatures exceeding 577°C [34]). In addition, Westinghouse's studies were "only" dedicated to single-crystals deliberately contaminated (such data do not exist for mc materials). In

multicrystalline materials, metal impurities interact with extended defects (grain boundaries, dislocations) which can enhance their precipitation but can also be considered as impurity sources for the high temperature steps of the cell fabrication process. Thus there is a crucial need for updated and more detailed studies, particularly addressed to mc ingots grown by directional solidification and *p*-type Si solar cells fabricated via common industrial processes.

One of the most common and harmful impurities in mc-Si is Fe [32]. The main properties and effects of this element in Si are presented here because Fe is likely to interfere with some of the experimental results we obtained. Dissolved in the Si crystal, Fe is generally present as positively charged interstitial atoms (Fe_i). At room temperature Fe_i forms complexes with acceptors (negatively charged), typically with substitutional B (B_s) (Fe_iB_s pairs) [35,36]. Both types of defects, Fe_i and the Fe_iB_s-pairs, are strong recombination centers. The Fe_iB_s pairs can be dissociated by low T annealing steps (around 200° C) or by carrier injection (e.g., by illuminating the sample). As Fe_i and the Fe_iB_s-pairs have different energy levels and carrier capture cross sections, their recombination properties are different too. Particularly, at high injection levels, the carrier lifetime limited by the Fe_iB_s pairs is lower than the carrier lifetime limited by Fe_i. As a consequence, the dissociation of the Fe_iB_s pairs results in an increase in τ_{eff}. From the change in τ_{eff}, the dissolved Fe concentration can be extracted [37].

The influences of two other common and important impurities in Si-based PV, Ti and Cu (goal of this PhD thesis), are presented within a specific chapter (chapter 2).

1.6 Solar cell fabrication

This subsection focuses on the crystalline Si solar cells standard industrial fabrication process, as featured in our present study. This process consists in 7 main steps, as presented below:

1. Saw damage removal and texturization in a KOH solution;
2. P diffusion in order to form the n^+ emitter;
3. Deposition on the front surface of an hydrogenated Si-nitride (SiNx:H) layer used as antireflection coating (ARC) by plasma-enhanced chemical vapor deposition (PECVD)
4. Screen printing of silver front contact;
5. Screen printing of the Al contact;
6. Co-firing in an infrared light belt furnace;
7. Laser edge isolation.

With more or less minor modifications, this process is currently used by most of PV manufacturers [1]. The main virtues of this PV technology are easy automation, reliability, good usage of materials and high yield. Each step is briefly described below with illustrative purposes. Values of temperature, time, etc. are only indicative.

Texturization. KOH etching, leading to microscopic pyramids, is commonly employed for monocrystalline materials. To ensure complete texturing coverage and adequate pyramid size, the concentration, the temperature and the agitation of the solution and the time of presence within the bath must be controlled (in fact KOH at a higher concentration and at a higher temperature is commonly used as an isotropic etch for saw damage removal). Alcohol is added to improve homogeneity through an enhancement of the wettability of the silicon surface.

For this PhD thesis, anisotropic texture with alkaline solutions was also applied to multicrystalline wafers, but with much poorer results. Reflectance of the textured wafers is relatively high, because of randomly oriented grains. Another drawback is the existence of steps between grains, which may cause interruptions in the screen-printed metal contacts.

Phosphorus diffusion. Phosphorus is universally used as the *n*-type dopant for silicon in solar cells. The wafers to be diffused, loaded in quartz boats, are placed in a quartz tube with resistance heating and held at the processing temperature. The wafers enter and exit the furnace through one end, while gases are fed through the opposite one. The emitter is then formed using $POCl_3$ diffusion at temperatures in the range 820–870 °C and at reduced pressure to improve uniformity and throughput. Both surfaces and the edges of the wafer were diffused after this process.

ARC deposition. Hydrogen-rich silicon nitride films are largely used as antireflective coatings for industrial crystalline silicon solar cells. The films are deposited at 450 °C by a plasma-enhanced reaction of silane (SiH_4) and ammonia (NH_3) at reduced pressure on the front surface only. The SiNx:H film deposition process also induce surface and bulk passivation by hydrogen (as described in more details in a separate subsection). A subsequent thermal step is usually needed for the H diffusion into the Si bulk. An industrial process metal *firing* step generally fulfills this objective.

Front and back contacts print and dry. For the front surface, a silver grid electrode is printed. Regarding the back surface, an aluminum electrode is deposited on the full surface. Screen-printing is used for both electrodes (Ag and Al) deposition. The used metal-rich pastes are viscous liquids due to the solvents they contain. These solvents are usually evaporated in an in-line furnace at 200–250 °C. The dried paste is apt for subsequent processing.

Co-firing of metal contacts. A high-temperature step (few seconds at a T around 800 °C) is then needed: organic components of the paste must be burnt-off, the metallic grains must sinter together to form a good conductor, and they must form an intimate electric contact to the underlying silicon. An infrared (IR) light belt furnace is usually used for the wafers co-firing.

The front paste is deposited on an insulating layer (the ARC coating) and the Al contact on the parasitic *n*-type rear layer. Upon firing, the active component of the front paste locally dissolves the ARC coating to contact the n^+ emitter without shunting it.

The back Al paste must completely *perforate* the parasitic back emitter. The low eutectic temperature of the Al–Si system (577 °C) means that during the firing step, some silicon dissolves in the liquid Al and epitaxially recrystallizes upon cooling after the firing step, forming an Al-rich Si layer (the so-called BSF - for back-surface-field - layer).

1.7 External Gettering effect

Metal impurities and their complexes have detrimental impacts on the Si electrical properties and the solar cells performances, as discussed in the subsection 1.5.3. However, some metal impurities can be removed from the wafer's bulk by external gettering mechanisms [34,38]. There are several gettering technologies, which are widely used in the processing of silicon devices. These methods are based on the use of natural or deliberately introduced sinks for impurities within the bulk (internal gettering) or at the surface (external gettering) of the wafer. The goal is to concentrate impurities within areas of the material where their negative impact is minimized. Regarding solar cells, gettering steps occur coincidentally during other process steps. Particularly two steps develop external gettering effects, the P-diffusion step and the *firing* step (due to the formation of a liquid intermetallic Al-Si alloy). Phosphorus gettering is probably the most widely studied external gettering method for solar cell applications [34, 38-40]. Phosphorus gettering is even a vital step, improving the initially low carrier lifetimes of the typical mc-Si wafers. Phosphorus gettering works by creating a volume of silicon in which metallic impurities are more soluble than in the bulk of the wafer. At the high processing temperatures required for phosphorus to diffuse into silicon (typically > 800 °C), the higher solubility limit of metals in the n^+ layer, drives the randomly diffusing metal impurities towards the phosphorus doped silicon via a concentration gradient [38].

During the metal firing step, the presence of the liquid Al-Si alloy on the backside of the wafers, would also contribute to trap metal impurities, their solubility being higher within the liquid alloy.

1.8 Bulk Hydrogenation effects

It is well admitted that hydrogen plays an important role in improving the electrical properties of semiconductors [33,41]. It was soon established that atomic hydrogen in-diffusion in silicon passivates the electrical activity of both acceptor and donor dopants, as well as that of deep-level impurities. Hydrogen usually diffuses easily in silicon, especially via dislocations and passivates some of the energy levels associated to impurities and dislocations. In *p*-type material it would be in a positive charge state (H^+), while in *n*-type material it may be in a negative one (H^-). H^+ is a very fast diffuser (H would migrate on a length of 1.4 mm during a 80 min long annealing step at 450 °C) in lightly doped silicon where acceptor trapping is minimal. However its diffusivity is strongly reduced in imperfect or highly doped materials. Regarding the solar cell fabrication, H diffuses from the SiNx:H film into the Si bulk during the ARC deposition step and during the *firing* treatment During the *firing* treatment the H^+ diffusion would be enhanced by the ejection of vacancies due to the Al-Si alloy formation, these vacancies promoting the dissociation of slow-diffusing molecular H (H_2) [33,42].

The conventional processing steps used to fabricate solar cells from c-Si wafers improve the material quality, via both external gettering and passivation effects. Thus in-depth understanding of these effects could allow new adaptations of these processes in order to further improve the quality of the fabricated solar cells without additional technological steps.

Chapter 1 – Bibliography

1. A. Luque, and S.S. Hegedus, Handbook of photovoltaic science and engineering. 2nd edition, John Wiley & Sons Ltd (2011), and references therein.
2. S. Kasap, and P. Capper, Springer handbook of electronic and photonic materials. Springer science + Business media Inc (2006), and references therein.
3. P.S. Priambodo, N.R. Poespawati, D. Hartanto, Solar cells - silicon wafer-based technologies. Ch. 1. InTech (2011). DOI: 10.5772/1758. http://www.intechopen.com.
4. D.H. Macdonald, Recombination and trapping in multicrystalline silicon solar cells. PhD Thesis. The Australian National University (2001), and references therein.
5. V. Quaschning, and R. Hanitsch, Shading of Integrated Photovoltaic Systems in Buildings. Sol. Energy. 56, 513 (1996).
6. S.M. Sze, Physics of semiconductor devices. 2nd edition, John Wiley & Sons. New York (1981).
7. M.A. Green, Solar cells: Operating principles, technology and system application. The University of NSW. Kensigton (1992).
8. N.D. Arora, J.R. Hauser, D.J. Roulston, Electron and hole mobility in silicon as a function of concentration and temperature. 29th IEEE PVSC. 292 (1982).
9. L. Geerligs, D. Macdonald, Base doping and recombination activity of impurities in crystalline silicon solar cells. Prog. Photovolt: Res. Appl. 12, 309 (2004).
10. A. Richter, S.W. Glunz, F. Werner, J. Schmidt, and A. Cuevas, Improved quantitative description of Auger recombination in crystalline silicon. Phys. Rev. B. 86, 165202 (2012).
11. W. Shockley, and W.T. Read, Statistics of the recombinations of holes and electrons. Phys. Rev. 87, 835 (1952).
12. R.N. Hall, Electron-hole recombination in germanium. Phys. Rev. 87, 387 (1952).
13. H. Nordmark, Microstructure studies of silicon for solar cells: Defects, impurities and surface morphology. PhD Thesis. NTNU-Trondheim (2009), and references therein.
14. A.B. Sproul, Dimensionless solution of the equation describing the effect of surface recombination on carrier decay in semiconductors. J. Appl. Phys. 76, 2851 (1994).
15. D.H. Macdonald, and A. Cuevas, Trapping of minority carriers in multicrystalline silicon. Appl. Phys. Lett. 74, 1710 (1999).
16. J.A. Hornbeck, and J.R. Haynes, Trapping of minority carriers in silicon. I. p-type silicon. Phys. Rev. 97, 311 (1955).
17. J.T.H. Tan, Overcoming performance limitations of multi-crystalline silicon solar cells. PhD Thesis. The Australian National University (2007), and references therein.
18. W.C. O'Mara, R.B. Herring, L.P. Hunt, Handbook of semiconductor silicon technology. Noyes, New Jersey (1990), and references therein.
19. R. Einhaus, J. Kraiem, F. Cocco, Y. Caratini, D. Bernou, D. Sarti, G. Rey, R. Monna, C. Trassy, J. Degoulange, Y. Delannoy, S. Martinuzzi, I. Périchaud, M. C. Record, P. Rivat, PHOTOSIL – Simplified production of solar silicon from metallurgical silicon. 21st EU PVSEC. Dresden, 580 (2006).

20. J. Kraiem, R. Einhaus, S. Dubois, N. Enjalbert, B. Drevet, F. Servant, D. Camel, F. Lissalde, Innovative crystallisation of multi-crystalline silicon ingots from different types of silicon feedstock. 23rd EU PVSEC. Valencia, 1071 (2008).

21. J. Kraiem, B. Drevet, F. Cocco, N. Enjalbert, S. Dubois, D. Camel, D. Grosset-Bourbange, D. Pelletier, T. Margaria, R.Einhaus, High performance solar cells made from 100% UMG silicon obtained via the PHOTOSIL process. 35th IEEE PVSC. Honolulu, 001427 (2010).

22. F. Cocco, D. Grosset-Bourbange, P. Rivat, G. Quost, J. Degoulange, R. Einhaus, M. Forster, H. Colin, PHOTOSIL UMG Silicon: Industrial evaluation by multi-c p-type ingots and solar cells. 28th EU PVSEC. Paris (2013).

23. M. Forster, J. Degoulange, R. Einhaus, J. Veirman, N. Enjalbert, R. Cabal, F. Cocco, D. Grosset-Bourbange, P. Rivat, Y. Delannoy, G. Chichignoud, P-type and n-type Cz solar cells made with 100% PHOTOSIL silicon: Impact of boron concentration. 28th EU PVSEC. Paris (2013).

24. E. Scheil, Z. Metallkd. 34, 70-72 (1942).

25. G. Coletti, Impurities in silicon and their impact on solar cell performance. PhD Thesis. Utrecht University, (2011).

26. J.A. Burton, R.C. Prim and W.P. Slichter. The distribution of solute in crystals grown from the melt. Journal of Chemical Physics. 21, 1987 (1953).

27. J. Veirman, S. Dubois, N. Enjalbert, M. Lemiti, A fast and easily implemented method for interstitial oxygen concentration mapping through the activation of thermal donors in silicon. Energy Procedia. 8, 41 (2011).

28. F. Tanay, S. Dubois, J. Veirman, N. Enjalbert, J. Stendera, and I. Périchaud, Oxygen-related thermal donor formation in dopant-rich compensated Czochralski silicon. IEEE Trans. Electron. Devices. 61, 1241 (2014).

29. K. Bothe, and J. Schmidt, Electronically activated boron-oxygen-related recombination centers in crystalline silicon. J. Appl. Phys. 99, 013701 (2006).

30. V.V. Voronkov, and R. Falster, Latent complexes of interstitial boron and oxygen dimers as a reason for degradation of silicon-based solar cells. J. Appl. Phys. 107, 053509 (2010).

31. V.V. Voronkov and R. Falster, Light-induced boron-oxygen recombination centres in silicon: Understanding their formation and elimination. Solid State Phenomena. 3, 205 (2014).

32. J.R. Davis, A. Rohatgi, R.H. Hopkins, P.D. Blais, P. Rai-Choudhury, J.R. McCormick, H.C. Mollenkopf, Impurities in silicon solar cells. IEEE Trans. Electron. Devices. 27, 677 (1980).

33. S. Martinuzzi, I. Périchaud, F. Warchol, Hydrogen passivation of defects in multicrystalline silicon solar cells. Solar Energy Materials & Solar Cells. 80 (3), 343 (2003).

34. I. Périchaud, Gettering of impurities in solar silicon. Solar Energy Materials & Solar Cells. 72, 315 (2002).

35. D. Macdonald, T. Roth, P.N.K. Deenapanray, K. Bothe, P. Pohl, and J. Schmidt, Formation rates of iron-acceptor pairs in crystalline silicon. J. Appl. Phys. 98, 083509 (2005).

36. S. Dubois, O. Palais, M. Pasquinelli, S. Martinuzzi, C. Jaussaud, and N. Rondel, Influence of iron contamination on the performances of single-crystalline silicon solar cells: Computed and experimental results. J. Appl. Phys. 100, 024510 (2006).

37. F. Tanay, S. Dubois, N. Enjalbert, J. Veirman, and I. Périchaud, Quantification of the light-induced degradation effects in iron-rich silicon wafers via carrier lifetime measurements. 26th EU PVSEC. Hamburg, 1039 (2011).

38. S.M. Myers, M. Seibt, and W. Schroter, Mechanisms of transition-metal gettering in silicon. J. Appl. Phys. 88, 3795 (2000).

39. S. Dubois, N. Enjalbert, F.Warchol, S. Martinuzzi, Is impurity gettering or passivation by hydrogen the improvement key of mc-Si solar cells during processing steps?. Materials Science and Engineering B. 159, 239 (2009).

40. A. Peral, J.M. Míguez, R. Ordás, C. del Cañizo, Lifetime improvement after phosphorous diffusion gettering on upgraded metallurgical grade silicon. Solar Energy Materials & Solar Cells. 130, 686 (2014).

41. B.L. Sopori, X. Deng, J.P. Benner, A. Rohatgi, P. Sana, S.K. Estreicher, Y.K. Park, M.A. Roberson, Hydrogen in silicon: A discussion of diffusion and passivation mechanisms. Solar Energy Materials and Solar Cells. 41/42, 159 (1996).

42. S.K. Estreicher, J.L. Hastings, and P.A. Fedders, Hydrogen-defect interactions in Si. Materials Science and Engineering B. 58, 31 (1999).

CHAPTER 2. A COMPARATIVE REVIEW OF CU AND TI PROPERTIES IN P-TYPE SI

In this chapter the key properties of titanium (Ti) and copper (Cu) in *p*-type Si are presented and compared. Then the main previous studies regarding the influences of these elements on the performances of crystalline Si solar cells are mentioned and their results discussed.

As previously mentioned, the content of this PhD thesis focuses on both Cu and Ti, firstly because they are common metal impurities in Si for photovoltaic (PV) applications [1]. Secondly Cu and Ti are impurities with major differences regarding their physical properties (e.g., diffusivity, solubility, etc.) in Si. Therefore their spatial distribution (e.g., extent of precipitation) and their ability to be externally gettered are expected to be significantly different. Eventually, these elements have properties in Si representative of those of other impurities (e.g., cobalt and nickel for Cu, vanadium for Ti). Consequently, these elements can be considered as model impurities, our conclusions could be *a priori* transposed to a wide range of metal impurities found in Si.

2.1 Solubility and diffusivity

The most important properties that determine the behavior of transition metals in silicon and their impact on device performances are the solubility and the diffusivity. Indeed, these properties govern the spatial distribution of elements and their ability to be externally gettered.

2.1.1 Solubility

The solubility of an impurity is defined as the maximum concentration which can be dissolved in the crystal lattice at a given temperature. The temperature dependence of the solubility is generally expressed using an Arrhenius law:

$$S = 5 \cdot 10^{22} e^{\left(\frac{S_S}{k} - \frac{H_S}{kT}\right)} \quad (\text{cm}^{-3}) \ (\text{for } T < T_{eut}) \qquad (2.1)$$

where H_S is the solution enthalpy, S_S is the solution entropy, k the Boltzmann constant and T_{eut} is the eutectic temperature of the impurity-Si alloy.

Table 2.1 – Data for solubility and diffusivity calculations [1-3].

	S_S (k)	H_S (eV)	D_0 ($cm^2.s^{-1}$)	H_M (eV)
Cu	2.4	1.49	3×10^{-4}	0.18
Ti	4.22	3.05	1.45×10^{-2}	1.79

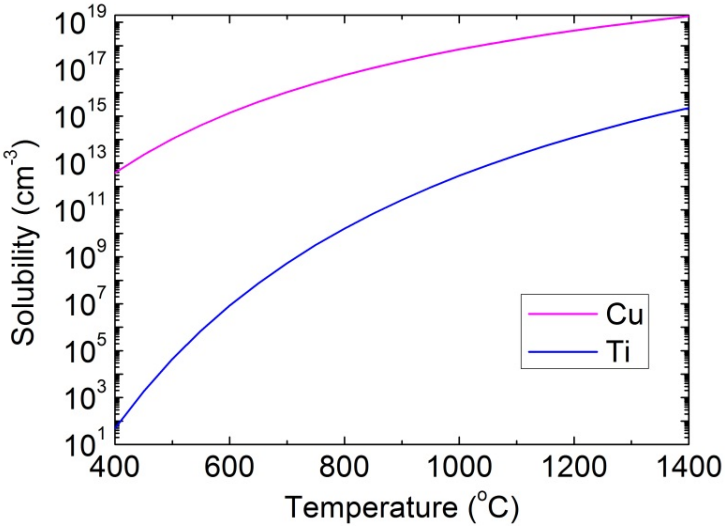

Figure 2.1 – Solubilities of Cu and Ti as a function of the temperature. Values calculated using equation (2.1) and data from Table 2.1.

2.1.2 Diffusivity

The diffusivity is also generally expressed, using an Arrhenius law:

$$D = D_0 e^{(-H_M/kT)} \qquad (cm^2.s^{-1}) \qquad (2.2)$$

where H_M is the migration enthalpy and D_0 is a temperature-independent pre-exponential factor.

However, if the diffusivity of Ti can directly be calculated using equation (2.2) whatever the boron concentration, regarding Cu, equation (2.2) is *stricto sensu* only valid for intrinsic Si *(i.e.* without any dopants). Indeed, it is often necessary to take into account the effect of Cu-B pairing due to electrostatic attractions between positively charged interstitial Cu (Cu_i^+) ions and negatively charged substitutional boron atoms (B_s^-). The consequence of this pairing is that only a fraction of the total Cu_i^+ concentration is mobile at any given moment, while the rest is temporarily trapped. In addition, a [B] dependence of the migration

enthalpy could be expected. In any case, the effective diffusivity (D_{eff}) of Cu in boron-doped silicon can be empirically expressed by the equation (2.3) when the boron concentration is below 10^{17} cm^{-3} [3].

$$D_{eff} = \frac{3 \cdot 10^{-4} e^{-2090/T}}{1 + 2.584 \cdot 10^{-20} e^{4990/T} N_A / T} \quad (cm^2.s^{-1}) \tag{2.3}$$

where T is the temperature in K and N_A the boron doping level in cm^{-3}.

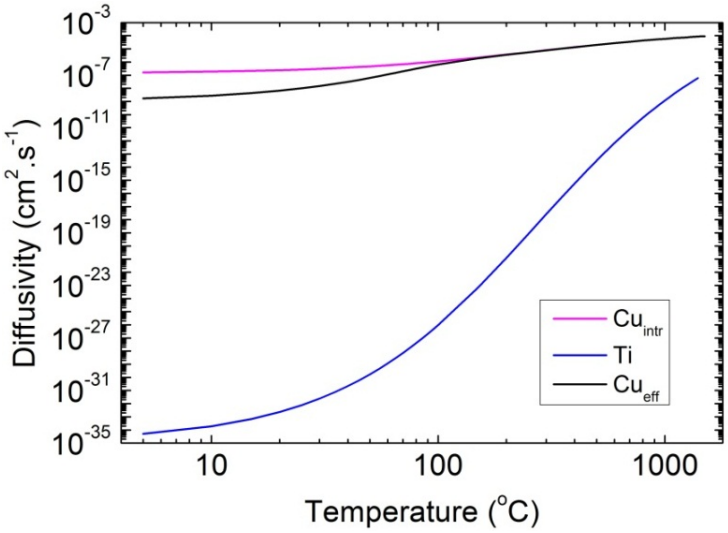

Figure 2.2 – Diffusivities of Cu and Ti as a function of the temperature. For Cu, are represented the values for intrinsic silicon ("Cuintr") and for boron-doped (N_A=1.6×10^{16} cm^{-3}) silicon ("Cu_{eff}"). Values were calculated using equations (2.2) and (2.3), and data from Table 2.1.

2.1.3 Precipitation mechanisms

The solubility decreases drastically towards room temperature. Therefore during cooling down processes (e.g., after ingot growth or emitter formation) the dissolved metal becomes increasingly supersaturated. To avoid supersaturation, impurities tend to form precipitates. However, for the precipitation to take place, both a sufficient impurity concentration excess and a sufficient diffusivity are required to form nuclei for both homogeneous and heterogeneous nucleations. Indeed, a given level of supersaturation is also necessary in the case of heterogeneous nucleation (e.g., in the presence of other precipitates or crystallographic defects) but it is generally much reduced. Once these nuclei are formed, an impurity should have sufficiently high mobility for the precipitate to grow.

At 840 C°, which is the typical temperature for phosphorus diffusion, the solubility of Ti is very low (around 5×10^{10} cm^{-3}). However its diffusivity does not allow enough mobility to reach the *n*-type layer or other precipitation sites. On the other hand, the Cu diffusivity is much higher, and this element can easily diffuse across the entire thickness of the wafer during the P-diffusion step. Slow diffusers like Ti and V are metal impurities for which, the presence/introduction into the silicon crystal should be avoided, since once they are incorporated in the ingot, they are very difficult to treat, being insensitive to any external gettering processes. Fast or relatively fast diffusers like Cu and Fe are usually presented as elements rather well tolerated since they can efficiently be extracted from the Si bulk by the external gettering effect developed by the P-diffusion step. Therefore their impacts on the material properties and the solar cell performances can considerably be reduced during solar cell manufacturing.

2.2 Effect on the carrier lifetime

Transition metals, dissolved and/or precipitated, are known to be harmful recombination centers in silicon [4-6]. They usually introduce energy levels within the Si band gap which can strongly reduce the charge carrier lifetime via SRH recombination [7] (see Chapter 1). The SRH recombination strength of a defect is determined by its density, the locations of its energy levels within the Si band gap (E_t), and their capture cross sections for both electrons (σ_n) and holes (σ_p).

2.1.1 Interstitial Ti

Ti is mainly present as interstitial atoms in the silicon lattice. Interstitial Ti (Ti_i) introduces three defect energy levels within the Si band gap: an acceptor (Ti_i-a) level, a donor (Ti_i-d) level, and a double donor (Ti_i-dd) level. These three levels can be involved in the carrier recombination. The electronic properties of the Ti defect levels in silicon were studied by several groups, essentially using deep-level transient spectroscopy (DLTS) analyses [1]. The defect energy levels were determined by DLTS to be $E_c-0.08$ eV, $E_c-0.27$ eV, and $E_v+0.28$ eV for the acceptor, donor, and double donor levels, respectively, where E_c and E_v represent the energy levels of the conduction and valence bands. These defect energy levels were identified from experiments carried out at low temperatures (T<200 K). However the location of the energy levels within the Si band gap is usually assumed to be T-independent.

DLTS analyses were also used in order to assess the σ_n for the acceptor and donor levels, and the σ_p for the double-donor level, each as a function of temperature [1]. Table 2.2 lists the main published data on the electronic properties of Ti_i in silicon.

Recently, in addition to DLTS, carrier lifetime spectroscopy was used to characterize the defect levels introduced within the Si band gap by interstitial Ti. Combinations of injection dependent and temperature dependent carrier lifetime spectroscopies (IDLS and TDLS) were used in several works to determine E_t, σ_n, σ_p and therefore the ratio of the capture cross sections σ_n/σ_p, also known as the symmetry factor k [8-10]. As shown in [8,10], the double-donor energy level (E_v+0.28 eV) would govern carrier recombination in *p*-type boron-doped Si. Roth *et al*. [9] also confirmed the location of the donor (Ti_i-d) level at E_c−(0.24±0.03) eV and showed that its k was equal to 7650.

Table 2.2 – Electrically active states and capture cross sections associated with interstitial Ti in silicon. Notice that some carrier capture cross section values were determined at T significantly lower than 300 K.

Defects	**E_t (eV)**	**σ_n (cm^2)**	**σ_p (cm^2)**	**k**	**Technique/ reference**
Ti_i-a	E_c−0.08	3.5×10^{-14}	-	-	DLTS/[1]
Ti_i-d	E_c−0.27	1.3×10^{-14}	-	-	DLTS/[1]
	E_c−0.271	$(2.99\pm0.26)\times10^{-14}$	$(1.35\pm0.04)\times10^{-15}$	22.16	DLTS/[11]
	E_c−(0.24±0.03)	-	-	7650	IDLS, TDLS/[9]
Ti_i-dd	E_v+(0.28±0.01)	-	1.9×10^{-16}	-	DLTS/[1]
	E_v+0.255	$(1.31\pm0.06)\times10^{-14}$	$(3.8\pm0.64)\times10^{-17}$	344.74	DLTS/[11]
	E_v+(0.289±0.005)	$(2.3\pm0.2)\times10^{-15}$	1.9×10^{-16}	12±0.7	N_{dop}-IDLS, TDLS/[1,8]
	E_v+0.255	1.5×10^{-15}	3.7×10^{-17}	40.4±4	IDLS, TDLS/[10,12]

The T-dependent trends in $\sigma_n(T)$ associated with various capture mechanisms were listed by Rein [8]. Among these mechanisms, only multiphonon emission (MPE) due to the deep centers yields an increase in σ_n with T. The electron capture cross section for Ti_i-dd associated with MPE can be expressed as [10]:

$$\sigma_n(T) = \sigma_\infty e^{\left(-E_\infty / kT\right)} \tag{2.4}$$

where σ_∞ is a T-independent prefactor and E_∞ an activation energy. $\sigma_\infty = 9.01\times10^{-14}$ cm^2 and E_∞ = 0.107±0.01 eV provide the best fit to the experimental data [10].

2.1.2 Interstitial Cu

Interstitial copper atoms (Cu_i) in *p*-type silicon have a low recombination activity compared to interstitial Ti atoms. The recombination activity is benign because interstitial copper atoms introduce a shallow energy level in the Si bandgap. Furthermore the introduced level has a small capture cross section for minority charge carriers (electrons). According to Istratov *et al*. [13,14] Cu_i introduces a donor level located at E_c-(0.15±0.01) eV (located via DLTS analyses).

A very important consequence of Istratov *et al*. [14] results, is that a Cu_i concentration ($[Cu_i]$) of 10^{13} cm^{-3} is compatible with electron diffusion length of the order of 1000 μm, a value significantly higher than the thickness of commercially available wafers (around 200 μm). Therefore Cu_i as such, should not significantly influence the photovoltaic performances of crystalline Si-based solar cells.

2.1.3 Copper pairs

Dissolved Cu atoms would also form Cu-Cu pairs in Si [15]. The most probable model for the Cu pairs, built from photoluminescence and DLTS analyses, is that of a pair involving both a substitutional and an interstitial copper atoms (Cu_s-Cu_i) [15-17]. Since Cu_s is expected to be a triple acceptor, and Cu_i is a donor, the most straightforward model for the Cu-pair related defect would be that of a donor-acceptor pair with a predominantly ionic bonding [15-17].

Copper-pairs in silicon introduce a donor level at E_v+(0.09±0.1) eV [1, 15,18]. The hole capture cross section is about 3×10^{-15} cm^2 [15]. Notice that the copper-pair concentration cannot easily be determined by DLTS analyses, essentially because iron-boron pairs have almost the same energy level and hole capture cross-section [18].

2.1.4 Copper precipitates

As written in section 2.1.2, Cu can easily precipitate in silicon. Among the various possible forms Cu can take in Si, the copper-silicide precipitates (Cu_3Si) tend to dominate the effect of Cu on the carrier lifetime [19-21].

One of the most important electronic features of Cu precipitates in general, is that they produce states in the forbidden gap which occupy a wide range of energy levels, as opposed to

discrete, single-energy states typically caused by interstitial metal atoms. This was particularly shown by modeling of DLTS spectra by Schröter *et al*., who identified a defect band within the Si band gap, located from E_c-0.2eV to E_c-0.5eV in Cu-contaminated Si samples [22]. They were also able to conclude that these states were "band-like" rather than "localized", meaning that they interact with one another directly through carrier hopping.

Recently Macdonald *et al*. [21] showed that the recombination activity of Cu precipitates in *p*-type crystalline silicon can be reasonably well described by the SRH statistics using a set of two effective energy levels and capture cross section ratios (see Table 2.3). These levels are located near the edges of the defect band known from DLTS studies. Therefore this study confirmed that in Cu-contaminated Si, the carrier lifetime is usually dominated by the Cu silicide precipitates.

Table 2.3 – Recombination parameters (Et, k) of Cu precipitates, determined by carrier lifetime spectroscopy, for various kind of Si materials and different ranges of Cu contamination [21].

Resistivity (Ω.cm)	Type	N_A or N_D (cm^{-3})	Fermi level E_C-E_F (eV)	Cu dose* (cm^{-3})	N_{SRH}** (relative)	E_C-0.2 eV level k-factor	E_C-0.58 eV level k-factor
250 FZ	*p*	5×10^{13}	0.78	3×10^{16}	95	0.015	10
250 FZ	*p*	5×10^{13}	0.78	1×10^{14}	1	0.015	10
12 Cz	*p*	1×10^{15}	0.86	2×10^{17}	140	0.015	10
1 FZ	*p*	1.5×10^{16}	0.93	3×10^{16}	35	0.015	10
20 FZ	*n*	2×10^{14}	0.31	1×10^{14}	2	0.015	10

**The Cu dose represents the amount of Cu introduced, which may be much greater than the final Cu density in the wafer bulk.*

***The relative recombination center density is the normalized density of these centers required to achieve a reasonable fit (the exact concentration of the centers being not known).*

The sizes of the Cu precipitates can be varied by changing the cooling rate following a high T treatment, as shown by Istratov *et al*. [23]. Copper diffusion in a vertical furnace was followed by a quench in silicone oil, ethylene glycol, or 10 % NaOH solution. The use of the vertical furnace enabled to obtain better defined cooling procedures than the horizontal furnace [23]. Also was showed that the DLTS spectrum and the minority carrier diffusion length depend on the size of the copper precipitates. Transmission electron microscopy (TEM) studies showed that the diameters of the copper precipitates were 30 nm, 70 nm and 240 nm, with densities of $4.3\cdot10^{12}$ cm^{-3}, $1.1\cdot10^{12}$ cm^{-3} and $1.4\cdot10^{9}$ cm^{-3} for estimated cooling rates of 2000 $K.s^{-1}$ (10 % NaOH), 1000 $K.s^{-1}$ (ethylene glycol) and 200 $K.s^{-1}$ (silicone oil), respectively (the annealing step was done at 850 °C, and the studied materials were *n*- and *p*-type single crystalline silicon wafers).

The precipitates were plate-shaped and mostly parallel to silicon (111) planes. The peak in the DLTS spectra was narrower for slower cooling rates. Istratov *et al.* [23] suggested that the high recombination activity of Cu precipitates is due to the attraction of charge carriers by space charge regions around the positively charged precipitates and the defect states close to the midgap.

2.1.5 Interactions with hydrogen

It is known that hydrogen can interact with defects (extended defects and point defects) in silicon. Particularly some harmful impurities in Si (e.g., iron, gold), can be passivated by forming electrically inactive complexes with H atoms.

However, the presence of hydrogen would not reduce the concentration of electrically active defects associated with Ti [24] in *p*-type Si. Indeed, in *p*-type Si, the Coulombic repulsion between H and Ti atoms would prevent the formation of Ti-H complexes [25]. On the other hand, regarding Cu, hydrogen can form H-Cu complexes. However these complexes would introduce recombinant energy levels in the Si band gap [26,27], affecting the charge carrier lifetime.

2.3 Effect on the PV performances

Ti and Cu introduce defect energy levels within the silicon band gap, which decrease the charge carrier lifetime. Therefore the presence of such elements within the Si substrate is likely to affect the PV performances of crystalline Si solar cells.

As previously mentioned, in the literature numerous studies were dedicated to the physical properties (solubility, diffusivity) of Ti and Cu in crystalline Si and their effects on the charge carrier recombination mechanisms. However the influences of such impurities on the PV performances of industrial-like crystalline Si solar cells were rarely studied, except in the pioneering works performed in the 1970's and 1980's by Westinghouse Corp [28], which reported the variation of the PV conversion efficiency with the impurity concentration for various common metal elements (Figure 2.3). For these groundbreaking studies, contaminants were added to the Si melt and small *n*-type and *p*-type Czochralski ingots were pulled. The "total" concentrations of impurities (dissolved and precipitated) in slices cut from the ingots were measured using neutron activation analysis and spark source mass spectrometry. Concentrations of electrically active defects were determined in some slices using DLTS.

Solar cells were fabricated (both n^+p and p^+n junctions) and the PV conversion efficiency measured. According to the Westinghouse study, the conversion efficiency of the *p*-type solar cells was strongly affected by Ti. Indeed, the normalized PV conversion efficiency (ratio between the efficiencies of the contaminated and non-contaminated cells) is equal to 0.8 for a Ti concentration as low as 10^{13} cm^{-3}. On the other hand Cu would be particularly well tolerated. Indeed, the Cu concentration should be higher than 10^{17} cm^{-3} in order to observe a significant decrease of the PV conversion efficiency.

These important results are often used as references for defining specifications on the tolerable amount of impurities in Si feedstocks. However these studies were based on a lab-scale solar cell fabrication process, with no hydrogen source (hydrogen being known for electrically passivating some metal impurities [29]) and no aluminum layer on the rear surface (aluminum being known for developing external gettering effects of metal impurities via the formation of a liquid alloy with Si for temperatures exceeding 577 °C [30]). In addition the Westinghouse studies were "only" dedicated to Czochralski-grown crystals deliberately contaminated ("cast" multicrystalline materials were not investigated). Thus there is a crucial need for updated and more detailed studies, particularly addressed to mc ingots grown by directional solidification and *p*-type Si solar cells fabricated via state of the art industrial processes.

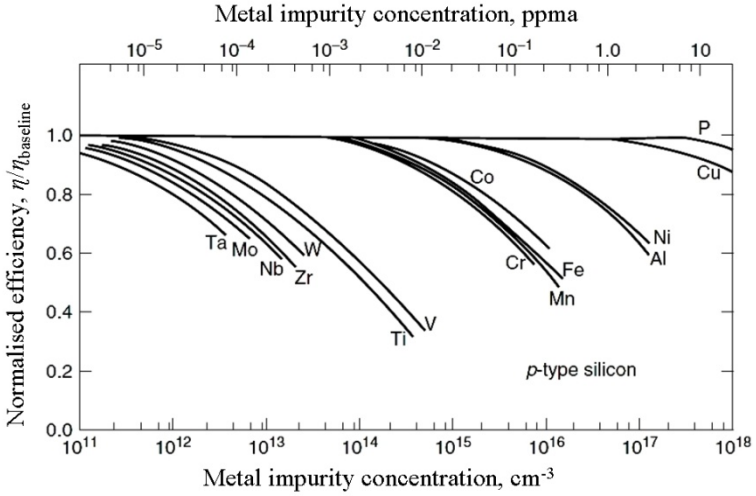

Figure 2.3 – Variation of the normalized efficiency with the wafer bulk metal impurity concentration (reprinted from [28]).

The impact of important transition metals, including titanium and copper, on the performances of "cast" multicrystalline Si solar cells was investigated more recently by Coletti at al. [31]. Each impurity was intentionally added to the silicon feedstock used to grow

p-type (B-doped with a targeted resistivity of 1 Ω.cm), directionally solidified, multicrystalline silicon ingots. In addition, the total ingot height was used for the evaluation of the effect of the studied elements. Therefore, each ingot provided a large range of impurity concentration levels. Furthermore, this allowed to relate the usable fraction of the ingot with the impurity content in order to obtain relevant insights into the tolerated contamination levels. Concerning the Ti and Cu contaminated ingots, 9.3 ppm wt of Ti and 97 ppm wt of Cu were respectively added in the corresponding feedstocks before crystallization [31]. In parallel to these contaminated ingots, reference uncontaminated ingots were grown and studied. All the ingots were cut into wafers and selections of wafers, regularly spaced along the ingots heights, were processed in solar cells. The solar cell fabrication process was a standard industrial process. Therefore the fabrication process included a P-diffusion step, the formation of an Al rear contact and the deposition of an hydrogenated SiNx antireflection coating layer.

In Figure 2.4, the PV conversion efficiencies of the reference, Cu contaminated and Ti contaminated solar cells are shown as a function of the initial location of the wafer along the ingot's height.

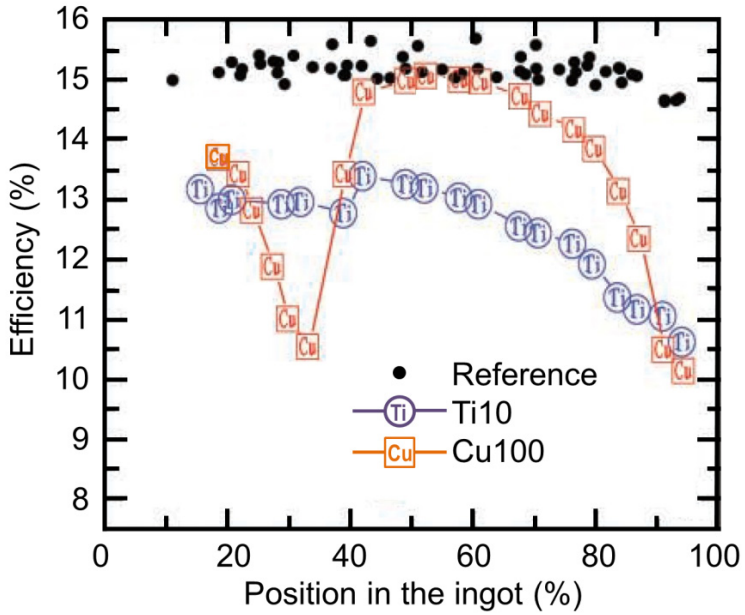

Figure 2.4 – PV conversion efficiencies of the reference, Cu contaminated and Ti contaminated solar cells as a function of the initial location of the wafer along the ingot's height [31].

The results from Coletti's study (Figure 2.4) showed that both Ti and Cu significantly affect the conversion efficiency. Particularly the efficiency of the Ti-contaminated cells monotonically decreases from the bottom to the top of the ingot. This is probably related to

the increase of the Ti concentration from the bottom to the top, due to segregation mechanisms. Regarding Cu, the cells performances would be significantly affected by the Cu contamination, essentially for initial ingot's fractions higher than 60 %, but the curve also presents an unexpected strong minimum around a solidified fraction of 30 %.

In order to understand the observed degradation, the spectral variation of the internal quantum efficiency (IQE) and fill factor (FF) of the solar cells were determined (Figure 2.5).

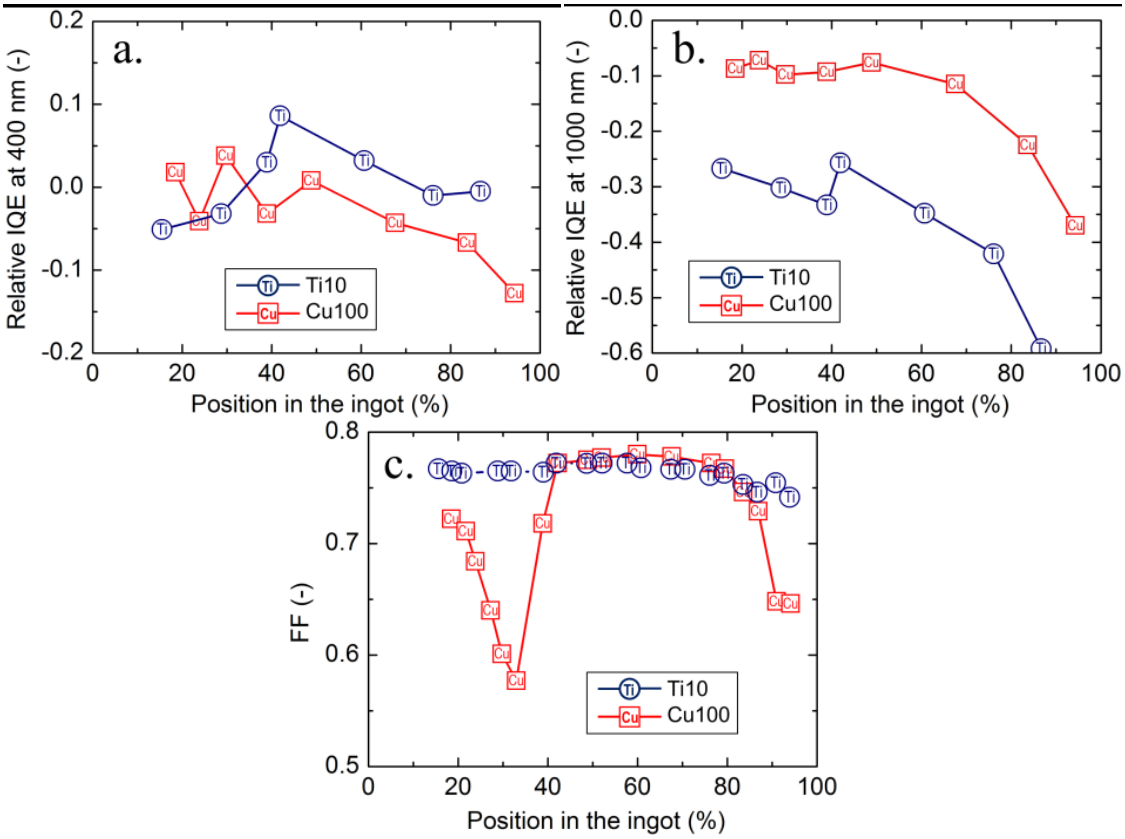

Figure 2.5 – Relative IQE versus the initial location of the wafer in the ingot (0 % corresponds to the bottom), presented for incident wavelengths of 400 nm (a) and 1000 nm (b). (c) Variations of the FF with the initial location of the wafers along the ingot's height (right) - data re-plotted from [31].

The IQE at 400 nm is essentially governed by carrier recombination in the emitter region while the IQE at 1000 nm mainly represents the recombination in the Si bulk and at the rear surface. Ti reduces the IQE at long wavelength (1000 nm) whereas Cu reduces the IQE at both long and short wavelengths. The different behavior for Cu can be explained by its fast diffusivity in silicon. Indeed, during the P-diffusion step, large amounts of Cu diffuse towards the emitter, and consequently affect its electrical properties (which explains the reduced IQE at short wavelengths). The carrier recombination in the base as well as in the emitter reasonably explains the degradation of the PV properties for the contaminated ingots.

The fill factor (FF) decrease is another mechanism that plays a role in the (further) decrease of the solar cell performances. Coletti showed that the solar cells fabricated from contaminated wafers from the bottom part of the ingots had low FF due to shunt issues (highlighted by lock-in thermography) [31]. Regarding Cu, it could also be explained by its high diffusivity. Indeed as a fast diffuser, Cu could easily out-diffuse during cooling steps, forming precipitates at the wafer surfaces. The presence of such precipitates in the emitter region could cause additional shunts that would explain the low FF. According to Coletti, the appearance of this phenomenon essentially at the bottom part of the ingot is not fully understood, and could be also due to the geometry of the small lab-scale furnace that was used to cast the ingots and the use of crucibles with a spherical bottom. Furthermore, SiN and SiC inclusions could also be responsible for the observed shunt issues [31].

From Coletti's studies it can clearly be concluded that Ti is significantly more detrimental than Cu. The addition of 10 ppm wt of Ti dramatically reduced the PV conversion efficiency along the entire ingot's height. However, Cu had the peculiarity of impacting both the base and emitter electrical properties. In addition large decreases of the FF of the Cu contaminated cells were highlighted, for which no fully satisfying explanation could be proposed.

2.4 Cu-related LID

In addition to the fact that Cu can affect the initial PV performances of the solar cells, several groups recently showed that Cu could be responsible for light-induced degradation (LID) effects of the carrier lifetime [32-35].

According to Belayachi *et al.* this degradation would be due to reactions within the wafer bulk or due to out-diffusion mechanisms of the Cu atoms at the surfaces [35]. Recently Savin *et al.* [36] studied the effects of copper, boron and oxygen on the LID via carrier lifetime measurements in various (Float Zone, Czochralski) single-crystalline Si materials. Savin *et al.* provided direct experimental evidences that the presence of neither boron nor oxygen is necessary for the observation of LID. Their results showed that the carrier lifetime degradation has a clear dependency on the copper concentration regardless of the silicon material, implying that LID can also occur solely due to copper (Figure 2.6). If Cu contaminated *p*-type silicon is exposed to light (e.g., sunlight or a halogen lamp), the carrier lifetime drastically decreases in the zones of the wafers contaminated by Cu, even at low global contamination levels ([Cu]~10^{13} cm^{-3}) [36].

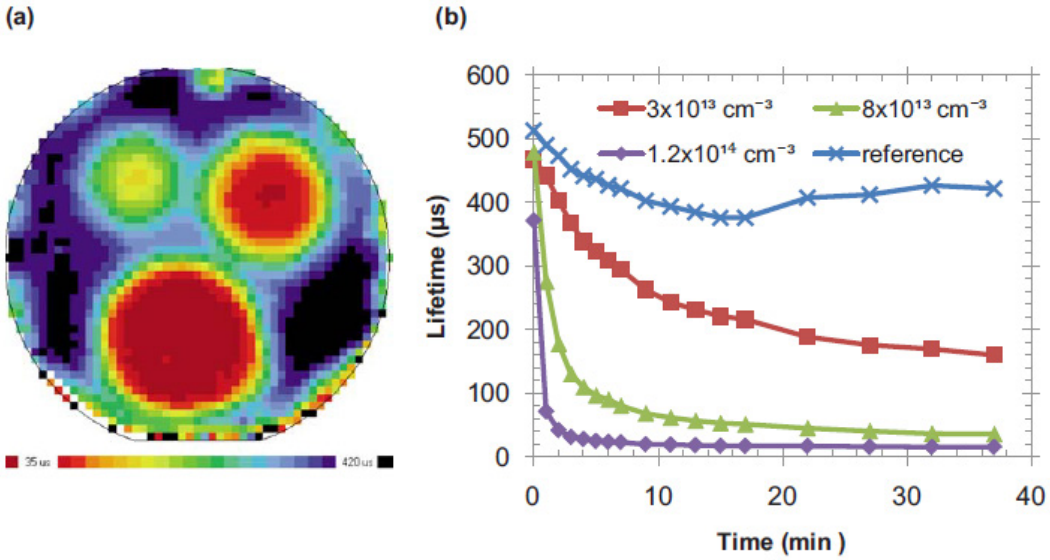

Figure 2.6 – (a) Carrier lifetime mapping obtained after 37 min of light illumination, for a p-type Cz silicon wafer with various copper global contamination levels: left upper spot [Cu]=3.0×10^{13} cm^{-3}, right upper spot [Cu]=8.0×10^{13} cm^{-3}, and lower spot [Cu]=1.2×10^{14} cm^{-3}. (b) For the same wafer, evolution under illumination of the carrier lifetime [36].

The LID observed in Cu contaminated silicon would be due to the fact that under illumination, the excess charge carriers would reduce the electrostatic repulsion between positively charged interstitial Cu ions (non-recombinant) and positively charged Cu precipitates (highly recombinant), this effect enhancing the Cu precipitation (e.g, [36]). Yli-Koski [37] modelled this room T precipitation effect of the Cu atoms under illumination (diffusion-limited precipitation theory). By comparing the computed results with experimental data (the precipitation time constant), Yli-Koski could estimate the size of the newly formed precipitates, responsible for the carrier lifetime decrease. Their calculated radii (a spherical shape is assumed) would be lower than 7 nm. To the best of our knowledge, the Cu precipitated formed via the illumination of the Si wafers have never been directly observed.

Recently, a method was proposed to minimize the Cu-related LID [38-41]. The method is based on the optimization of the surface charge of a silicon wafer. Depositing a large negative surface charge (around -11.1 µC/cm^2) enhances the diffusion of interstitial Cu from the sample bulk to the surfaces even at room T before illumination, reducing the interstitial Cu concentration within the Si bulk (see Figure 2.7). Thus, less Cu is able to precipitate in the bulk during illumination, and the amplitude of the LID is lower [38].

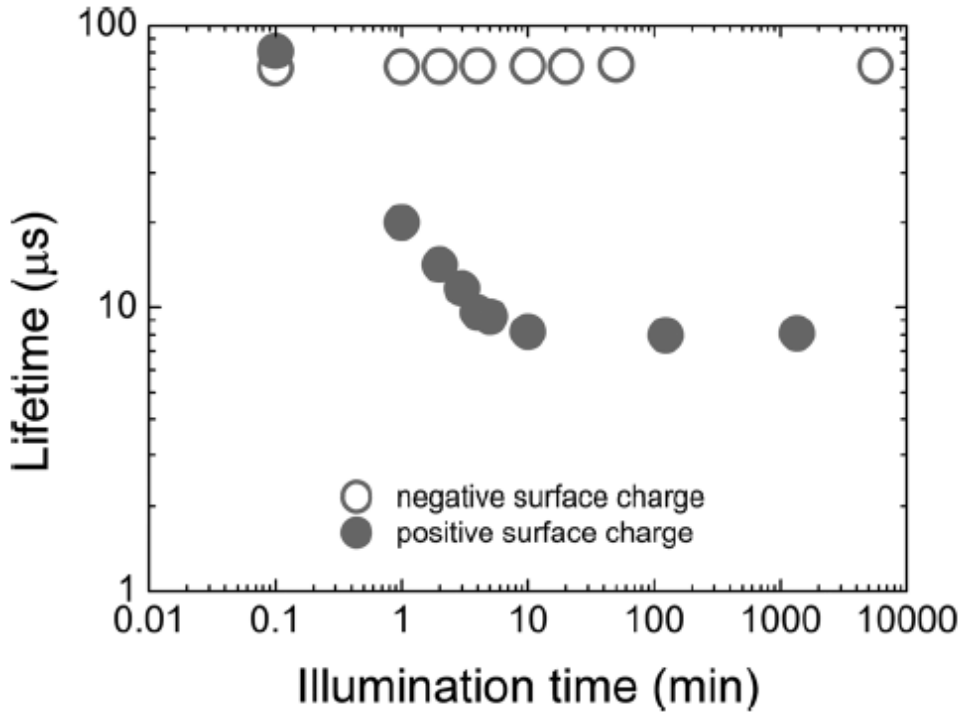

Figure 2.7 – Evolution under illumination of the carrier lifetime (high injection) with positive and negative surface corona charges. The studied Cz-Si B-doped sample has a resistivity in the range 18–24 Ω.cm and was contaminated with 8 ppm wt of copper solution [38] (the bulk Cu concentration is not known).

Boulfrad, *et al*. [39] recently brought experimental evidences that Cu ions accumulate near the wafer surface as a consequence of electrostatic attraction with the deposited negative surface charge. The evidence was twofold: (i) chemical analyses by means of total reflection X-ray fluorescence revealed the presence of Cu near the surface of a negatively charged Cu contaminated sample while no Cu signal was observed on the positively charged one, (ii) surface etching of the Cu-rich surface layer removed permanently the Cu related LID.

Finally, Lindroos *et al*. investigated the Cu-related LID in commercial multicrystalline silicon wafers, which were previously thermally oxidized [41]. For the wafers coming from the top part of the cast ingot, they highlighted important decreases of the carrier lifetime under illumination (for instance a decrease of the carrier lifetime from 141 μs to 7 μs was reported within a *good* grain). A relatively high interstitial copper concentration of 5×10^{12} cm^{-3} was identified as the cause for the strong degradation. The measured LID could be suppressed by the deposition of a large negative surface charge, either by external corona charging or via the atomic layer deposition of aluminum oxide layers. Interestingly, both negative charge deposition methods fully prevented the formation of recombination active copper precipitates during illumination, despite the differences in their charge densities and charge formation mechanisms.

Conclusion

To sum things up on these matters in relation with our present work, Coletti's studies [31] are particularly interesting since they addressed the influences of Cu and Ti on the PV performances of multicrystalline Si solar cells. However, in our opinion these studies should be updated and completed. Indeed the conversion efficiencies of the reference (uncontaminated) cells are around 15 % and do not reflect the performances associated with current "state of the art" industrial-like processes (giving efficiencies in the range 16 %-18 % with non-deliberately contaminated multicrystalline wafers). Furthermore these pioneering works could be extended with specific studies, evaluating the efficiencies of both the external gettering and hydrogen passivation effects. In addition, it would be important to consider also the reverse current-voltage (I-V) characteristics of the fabricated cells, since they can significantly govern the reliability and the outdoor performances of the solar panels. Eventually, it is of paramount important to assess the stability under illumination of the PV parameters, particularly for the Cu contaminated cells, since Cu was shown to be responsible for light-induced degradation (LID) effects of the carrier lifetime. All these points will be investigated in the frame of this PhD. Consequently our studies can be seen as strongly complementary from the previous works of the literature.

Chapter 2 – Bibliography

1. K. Graff, Metal impurities in silicon-device fabrication. 2nd edition, Springer. Berlin (1995) and references therein.
2. E.R. Weber, Transition Metals in Silicon. Appl. Phys. A. 30, 1 (1983).
3. A.A. Istratov, C. Flink, H. Hieslmair, E.R. Weber, and T. Heiser, Intrinsic diffusion coefficient of interstitial copper in silicon. Phys. Rev. Lett. 81, 1243 (1998).
4. S. Dubois, Effects of the impurity-defect interactions on the photovoltaic and electrical properties of crystalline silicon solar cells. PhD Thesis. Paul Cezanne University, Marseille, France (2007).
5. D. Macdonald, and L.J. Geerligs, Recombination activity of interstitial iron and other transition metal point defects in p- and n-type crystalline silicon. Appl. Phys. Lett. 85, 18 (2004).
6. A.R. Peaker, V.P. Markevich, B. Hamilton, G. Parada, A. Dudas, A. Pap, E. Don, B. Lim, J. Schmidt, L. Yu, Y. Yoon, and G. Rozgonyi, Recombination via point defects and their complexes in solar silicon. Phys. Status Solidi A. 209, 10 (2012).
7. W. Shockley, and W.T. Read, Statistics of the recombinations of holes and electrons. Phys. Rev. 87, 835 (1952).
8. S. Rein, Lifetime spectroscopy: A method of defect characterization in silicon for photovoltaic applications. Springer. Berlin (2005).
9. T. Roth, M. Rüdiger, W. Warta, and S.W. Glunz, Electronic properties of titanium in boron-doped silicon analyzed by temperature-dependent photoluminescence and injection-dependent photoconductance lifetime spectroscopy. J. Appl. Phys. 104, 074510 (2008).
10. B.B. Paudyal, K.R. McIntosh, and D.H. Macdonald, Temperature dependent carrier lifetime studies on Ti-doped multicrystalline silicon. J. Appl. Phys. 105, 124510 (2009).
11. A.C. Wang and C.T. Sah, Complete electrical characterization of recombination properties of titanium in silicon. J. Appl. Phys. 56, 1021 (1984).
12. A. Cuevas and D.H. Macdonald, N-type vs. p-type silicon: tackling impurity recombination in solar cells. nPV Workshop. Konstanz (2011).
13. A.A. Istratov, H. Hieslmair, C. Flink, T. Heiser, and E.R. Weber, Interstitial copper related center in n-type silicon. Appl. Phys. Lett. 71, 2349 (1997).
14. A.A. Istratov, C. Flink, H. Hieslmair, T. Heiser, and E.R. Weber, Influence of interstitial copper on diffusion length and lifetime of minority carriers in p-type silicon. Appl. Phys. Lett. 71, 2121 (1997).
15. A.A. Istratov, H. Hieslmair, T. Heiser, C. Flink, and E.R. Weber, The dissociation energy and the charge state of a copper-pair in silicon. Appl. Phys. Lett. 72, 474 (1998).
16. A.A. Istratov, E.R. Weber, Electrical properties and recombination activity of copper, nickel and cobalt in silicon. J. Appl. Phys. A. 66, 123 (1998) and references therein.
17. Carvalho, D.J. Backlund, and S.K. Estreicher, Four-copper complexes in Si and the Cu-photoluminescence defect: A first-principles study. Phys. Rev. B. 84, 155322 (2011).
18. S. Koveshnikov, Y. Pan, and H. Mollenkopf, Investigation of electronic states in copper doped p-type silicon. Electrochem. Soc. Proc. 96, 473 (1996).

19. R. Sachdeva, A.A. Istratov, E.R. Weber, Recombination activity of copper in silicon. Appl. Phys. Lett. 79, 2937 (2001).

20. A.A. Istratov, R. Sachdeva, C. Flink, S. Balasubramanian, E. R. Weber, Precipitation kinetics and recombination activity of Cu in Si in the presence of internal gettering sites. Solid State Phenomena. 82-84, 323 (2002).

21. D. Macdonald, A. Cuevas, S. Rein, P. Lichtner, S.W. Glunz, Temperature- and injection-dependent lifetime spectroscopy of copper-related defects in silicon. 3rd World Conference on Photovoltaic Energy Conversion. Osaka, Japan (2003).

22. W. Schröter, V. Kveder, M. Seibt, H. Ewe, H. Hedemann, F. Riedel, A. Sattler, Atomic structure and electronic states of nickel and copper silicides in silicon. Mat. Sci. Eng. B. 72, 80 (2000).

23. A.A. Istratov, H. Hedemann, M. Seibt, O.F. Vyvenko, W. Schröter, T. Heiser, C. Flink, H. Hieslmair, and E.R. Weber, Electrical and recombination properties of copper-silicide precipitates in silicon. J. Electrochem. Soc. 145, 3889 (1998).

24. R. Singh, S.J. Fonash, and A. Rohatgi, Interaction of low-energy implanted atomic H with slow and fast diffusing metallic impurities in Si. Appl. Phys. Lett. 49, 800 (1986).

25. W. Jost, and J. Weber, Titanium-hydrogen defects in silicon. Phys. Rev. B. 54, 16, 54 (1996).

26. S. Knack, J. Weber, H. Lemke, and H. Riemann, Copper-hydrogen complexes in silicon. Phys. Rev. B. 65, 165203 (2002).

27. N.A. Yarykin, and J. Weber, Identification of copper-copper and copper-hydrogen complexes in Silicon. Semiconductors. 47 (2), 275 (2013).

28. J.R. Davis, A. Rohatgi, R.H. Hopkins, P.D. Blais, P. Rai-Choudhury, J.R. McCormick, H.C. Mollenkopf, Impurities in Silicon Solar Cells. IEEE Trans. Electron. Devices. 27, 677 (1980), and reference therein.

29. S. Martinuzzi, I. Périchaud, F. Warchol, Hydrogen passivation of defects in multicrystalline silicon solar cells. Solar Energy Materials & Solar Cells. 80 (3), 343 (2003).

30. I. Périchaud, Gettering of impurities in solar silicon. Solar Energy Materials & Solar Cells. 72, 315 (2002).

31. G. Coletti, P.C.P. Bronsveld, G. Hahn, W. Warta, D. Macdonald, B. Ceccaroli, K. Wambach, N.L. Quang, and J.M. Fernandez, Impact of metal contaminations in silicon solar cells. Adv. Funct. Mater. 21, 879-890 (2011).

32. H. Väinölä, E. Saarnilehto, M. Yli-Koski, A. Haarahiltunen, J. Sinkkonen, G. Berenyi, and T. Pavelka, Quantitative copper measurement in oxidized p-type silicon wafers using microwave photoconductivity decay. Appl. Phys. Lett. 87, 032109 (2005).

33. H. Väinölä, M. Yli-Koski, A. Haarahiltunen, and J. Sinkkonen, Sensitive copper detection in p-type CZ silicon using μPCD. J. Electrochem. Soc. 150 (12), G790 (2003).

34. D.A. Ramappa, Surface photovoltage analysis of phase transformation of copper in p - type silicon. Appl. Phys. Lett. 76, 25, 19 (2000).

35. Belayachi, T. Heiser, J.P. Schunck, A. Kempf, Influence of light on interstitial copper in p-type silicon. Appl. Phys. A. 80, 201 (2005).

36. H. Savin, M. Yli-Koski, and A. Haarahiltunen, Role of copper in light induced minority-carrier lifetime degradation of silicon. Appl. Phys. Lett. 95, 152111 (2009).

37. M. Yli-Koski, Optical activation of copper in silicon studied by carrier lifetime measurements. PhD Thesis. Helsinki University of Technology, Electron Physics Laboratory (2004) and references therein.

38. J. Lindroos, M. Yli-Koski, A. Haarahiltunen, and H. Savin, Room-temperature method for minimizing light-induced degradation in crystalline silicon. Appl. Phys. Lett. 101, 232108 (2012).

39. Y. Boulfrad, J. Lindroos, M. Wagner, F. Wolny, M. Yli-Koski, and H. Savin, Experimental evidence on removing copper and light-induced degradation from silicon by negative charge. Appl. Phys. Lett. 105, 182108 (2014).

40. J. Lindroos, and H. Savin, Formation kinetics of copper-related light-induced degradation in crystalline silicon. J. Appl. Phys. 116, 234901 (2014).

41. J. Lindroos, Y. Boulfrad, M. Yli-Koski, and H. Savin, Preventing light-induced degradation in multicrystalline silicon. J. Appl. Phys. 115, 154902 (2014).

CHAPTER 3. STUDIED INGOTS - CHARACTERIZATION TECHNIQUES

This chapter presents the various ingots grown for this PhD thesis, and the different characterization techniques used, at both the wafers and solar cells levels.

3.1 Description of the studied ingots

Three single-crystalline (sc) Czochralski (Cz)-Si ingots and three multicrystalline (mc-Si) ingots were grown, with crystallization parameters and targeted compositional properties, presented below.

3.1.1 Czochralski ingots

Three Cz-Si ingots were grown using a standard Czochralski puller, by the company Siltronix. Ultra-pure Electronic-Grade Si (EG-Si) was used as a feedstock in an amount of 10 kg per ingot. The diameter of the ingots was about 4 inch. The crystals were pulled at a speed of 60 $mm.h^{-1}$, with a crucible rotation speed of 8 rpm and a seed rotation speed of 13 rpm. All ingots were Boron (B)-doped (0.145 ppm wt of B added to the feedstock) in order to obtain *p*-type Si wafers with a standard resistivity (ρ), around 1 Ω.cm.

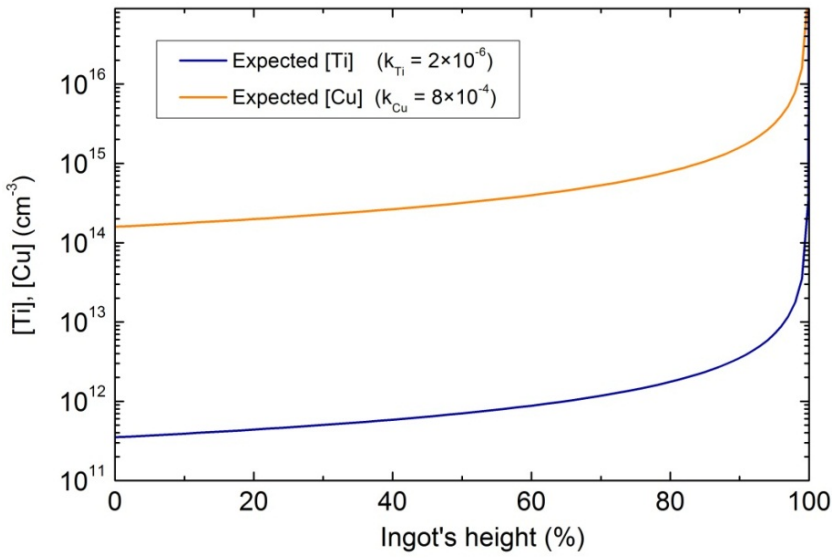

Figure 3.1 –Expected variations of [Cu] and [Ti] along the Cz-Si ingot's height calculated from Scheil's law.

The first ingot (Cz-Ref) was grown without intentional contamination. The feedstock used for the second ingot (Cz-Cu) was deliberately contaminated with 9 ppm wt, or equivalently 2×10^{17} cm^{-3}, of Cu. The third ingot (Cz-Ti) was deliberately contaminated with 6 ppm wt, or equivalently 1.8×10^{17} cm^{-3}, of Ti. The expected variations of the Ti and Cu concentrations, respectively [Ti] and [Cu], along the ingot's height were calculated from Scheil's law (Figure 3.1), using for the Ti and Cu effective segregation coefficients (k_{eff}), the values given in [1] (2×10^{-6} for Ti, and 8×10^{-4} for Cu, k_{Ti} and k_{Cu} respectively). We decided to use these k_{eff} values because they were experimentally determined for pulling conditions similar than those associated with the growth of our Cz ingots. With respect to the equilibrium partition coefficient given by Trumbore [2] for Cu, namely 4×10^{-4}, the somewhat higher value could possibly be due to incomplete mixing within the Si bulk, as discussed in chapter 1 (section 1.4.3).

3.1.2 Multicrystalline Si ingots

Three mc-Si ingots were grown by directional solidification from ultra-pure EG-Si feedstock (60 kg used per ingot) via semi-industrial furnaces installed at CEA-INES. The height of the ingots was about 180 mm, and the dimensions of the cross sections were about 380×380 mm^2. For a given ingot, a brick (cross section of about 156×156 mm^2) was extracted. All ingots were B-doped (0.145 ppm wt of B added in the feedstock) in order to obtain *p*-type Si wafers with a standard resistivity, around 1 Ω.cm.

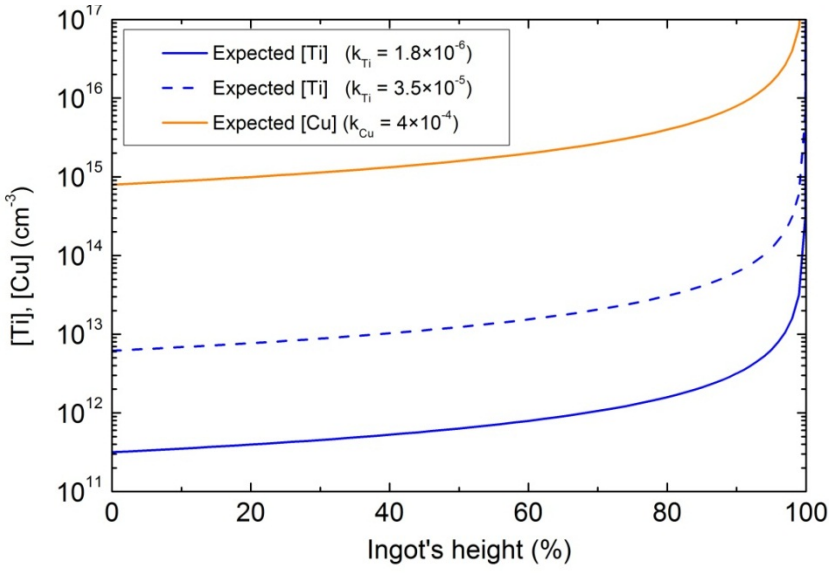

Figure 3.2 – Expected variations of [Cu] and [Ti] along the mc-Si ingot's height, calculated from Scheil's law.

The first ingot (mc-Ref) was grown without intentional contamination. The feedstock used for the second ingot (mc-Cu) was deliberately contaminated with 90 ppm wt, or equivalently 2×10^{18} cm^{-3}, of Cu. The third ingot (mc-Ti) was deliberately contaminated with 6 ppm wt, or equivalently 1.76×10^{17} cm^{-3}, of Ti. The expected variations of [Ti] along the ingot's height were calculated from Scheil's law (Figure 3.2), using for the k_{eff}, the values given in [3,4] (1.8×10^{-6} and 3.5×10^{-5}). We decided to use these k_{eff} values because they were experimentally determined for crystallization conditions similar than those associated with the growth of our mc ingots. The expected [Cu] also were calculated from Scheil's law, using for the segregation coefficient the value given in [2] ($k=4\times10^{-4}$), which corresponds to the Cu equilibrium segregation coefficient (k_{eq}). As for Ti, the two literature values are strongly different, one being slightly smaller than its Cz counterpart of the preceding paragraph, while the other is much larger. We are not in a position to criticize the value of 3.5×10^{-5} but it should be noted that it would require a virtually diffusive growth regime, which is quite unlikely.

3.2 Techniques for the evaluation of the compositional properties

3.2.1 Fourier-transform infrared spectroscopy (FTIR)

On wafers from the Cz-Si ingots and on vertical cuts from the mc-Si ingots, the interstitial oxygen (O_i) concentration ($[O_i]$) and the substitutional carbon (C_s) concentration ($[C_s]$) were determined by Fourier-Transform Infrared Spectroscopy (FTIR) along the ingot's height.

FTIR spectroscopy [5] is based on the principle of beam interference to yield an interferogram characteristic of the difference in path lengths between the two beams. This difference in path lengths information can be converted to a spatial frequency by means of a Fourier transformation and the results of the FTIR procedure are generally presented as absorbance versus wave number. The radiation emerging from the source is passed through an interferometer (usually a Michelson interferometer) to the sample before reaching a detector (Figure 3.3). Upon amplification of the signal, in which high-frequency contributions have been eliminated by a filter, the data are converted to digital form by an analog-to-digital converter and transferred to the computer for Fourier-transformation.

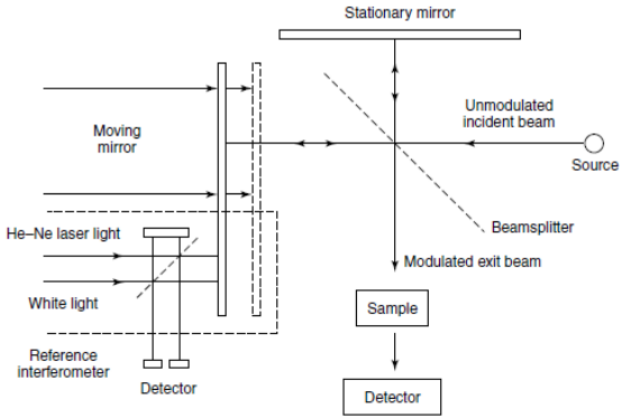

Figure 3.3 – Schematic diagram of a Michelson interferometer for FTIR [6].

Silicon atoms form bonds with the carbon atoms (Si-C) and oxygen atoms (Si-O-Si) in the lattice structure. Infrared spectrometry uses light of wavelengths (2-25 μm) to irradiate the sample. Silicon is transparent to these wavelengths, and as the light passes through the sample, chemical bonds in resonance with a wavelength can absorb a portion of the light. The amount of light absorbed is proportional to the concentration of atoms forming the bond, and thus is measured and used to quantify the concentration. In infrared spectroscopy, it is more convenient to represent the wavelengths as wavenumbers (units in cm^{-1}). With Si, the O_i absorption is centered at 1107 cm^{-1}, and the C_s absorption is centered at 605 cm^{-1}.

FTIR provides several advantages compared to other spectroscopic techniques: (1) simultaneous recording of spectra over a broad spectral range (4000-10 cm^{-1}) at resolutions 0.005-0.1 cm^{-1}; (2) high optical throughput because a circular aperture is used instead of a narrow slit as in conventional spectrometers and (3) very accurate optical calibration by the use of a frequency-stabilized reference laser for determination of the optical path-difference between the two light beams. Because of these advantages the use of FTIR for the determination of [O_i] and [C_s] levels in silicon is rapid, precise and non-destructive. On the other hand thick samples (thickness usually higher than 500 μm) have to be used and their surfaces have to be perfectly polished.

3.2.2 ICPMS, GDMS, SIMS

The concentrations of metal impurities in the studied ingots were determined by glow discharge mass spectroscopy (GDMS), inductively coupled plasma mass spectrometry (ICP-MS) and secondary ion mass spectrometry (SIMS). All these techniques indicate for a given impurity its total concentration, irrespective of its chemical state (dissolved, precipitated, ionized/neutral) within the Si bulk.

GDMS is accepted today as one of the most powerful and sensitive solid-state analysis methods for the trace and ultratrace analyses of solid samples and is routinely applied by companies and institutes producing different high-purity metals or alloys. The schematic of a glow discharge ion source is drawn in Figure 3.4 [7].

GDMS enables the elemental analysis of solid materials by sputtering a sample in a low-pressure DC argon discharge. The sputtered atoms are ionized in this plasma and extracted into the mass spectrometer for separation and detection. Because samples are analyzed in solid form, laborious and error prone dissolution procedures inherent to techniques as ICP-MS are avoided. Additionally, GDMS is free from the matrix dependence response.

The GDMS analyses that will be presented hereafter were subcontracted to the Shiva company. The uncertainties associated with the GDMS analyses were given to be about 20 %.

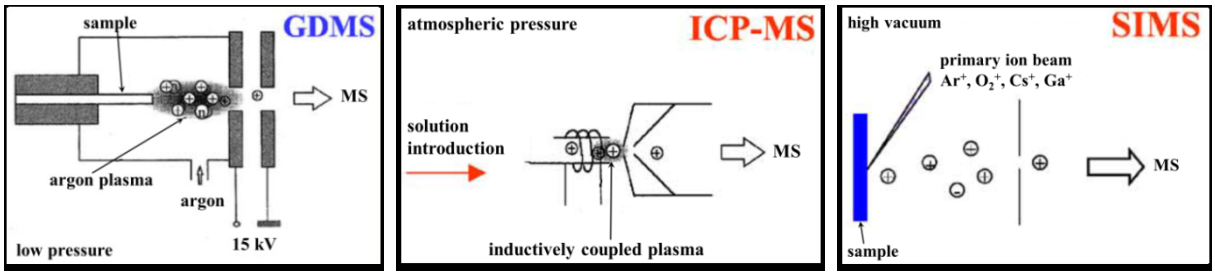

Figure 3.4 – Principles of GDMS, ICP-MS and SIMS analyses [7]

ICP-MS measures the masses of the element ions generated by the high temperature argon plasma. The ions created in the plasma are separated by their mass to charge ratios, enabling the identification and quantitation of unknown materials. ICP-MS offers very low detection limits for a wide range of elements [7,8].

Typically, ICP-MS analyses require the samples to be in a liquid form. Therefore, liquid samples require sample nebulization. The liquid sample is pumped from a vial, via a peristaltic pump, into the nebulizer. Liquid droplets are formed on the tip of a needle, where they become nebulized due to argon gas flowing through a second needle perpendicular to the sample needle. A small amount of aerosol created is swept into the torch.

The aerosol produced via nebulization enters the high temperature plasma, where it is first dried to a solid, and then heated to a gas, referred to as atomization. These atoms will continue to travel through the plasma, absorbing energy until they release an electron, becoming ionized. These newly formed ions then travel out of the torch and come to the mass

detector. The mass spectrometric separation of ion beams is realized in ICP-MS using both static and dynamic mass analyzers.

As ICP-MS requires samples in the liquid form, before such analyses, the Si wafers to be tested are dissolved (the so-called *digestion* step) by mixtures of acid solutions. The uncertainty regarding concentrations obtained with ICP-MS is given to be about ±10 %.

SIMS is based on the observation that charged particles (Secondary Ions) are ejected from a sample surface when bombarded by a primary beam of heavy particles [7,8].

In SIMS, the surface is bombarded by an energetic primary ion beam in vacuum. This desorbs surface species through a physical process called sputtering. Some of the sputtered fragments are ionized, and they are analyzed in a mass spectrometer. A basic SIMS instrument will, therefore, consist of: a primary beam source (usually O_2^+, O^-, Cs^+, Ar^+, Ga^+ or neutrals) to supply the bombarding species; a target or sample that must be solid and stable in a vacuum; a method of collecting the ejected secondary ions; a mass analyzer to isolate the ion of interest (quadrupole, magnetic sector, double focusing magnetic sector or time of flight); an ion detection system to record the magnitude of the secondary ion signal (photographic plate, Faraday cup, electron multiplier or a CCD camera and image plate).

Notice that the SIMS analysis allows obtaining both the impurity concentration and its depth distribution [7,8] with accuracy up to ±3 % [8].

3.2.3 DLTS

This technique is briefly described, since it was subcontracted by the SEMILAB company and was only used for the characterization of the Ti contaminated Cz wafers. Deep Level Transient Spectroscopy (DLTS) was developed in 1974 by D. V. Lang to investigate energetically "deep" charge trapping levels in semiconductor space charge structures, which may be either *p-n* or Schottky junctions [9]. It uses the fact that the *rf* capacitance of the sample depends on the charge state of deep levels in the space charge region (*scr*). Particularly the properties of the deep levels are investigated by determining the variation with the temperature of a transient capacitive signal, the analyzed capacitance being the space charge region of the tested junction.

The semiconductor is placed in a non-equilibrium state by an electric pulse. Particularly, by modifying the applied reverse voltage (to the junction), the occupation of the deep energy levels by the free carriers is changed.

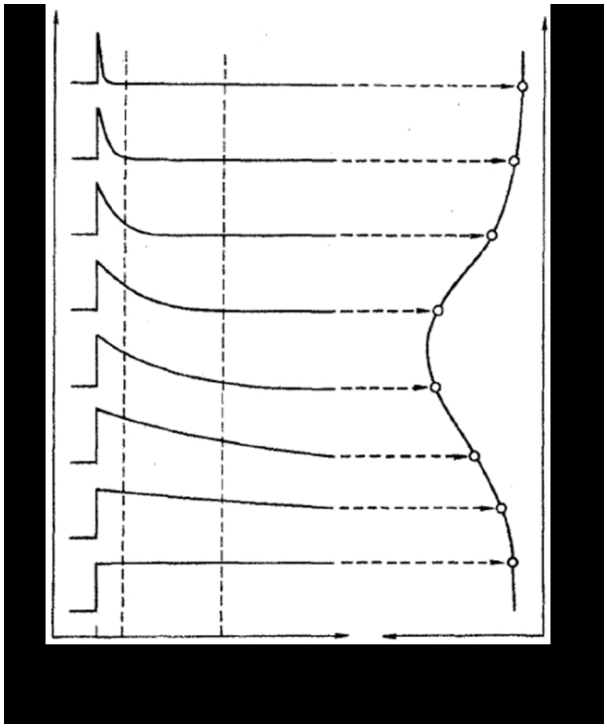

Figure 3.5 – Principle of the DLTS technique. The left-hand side shows capacitance transients at various temperatures, while the right-hand side shows the corresponding DLTS signal ($C(t_1)$-$C(t_2)$) as a function of the temperature [9].

Indeed, a momentary reduction of the reverse voltage allows the filling of the deep energy levels by free carriers. Carriers are then re-emitted towards the valence or conduction bands, this re-emission modifying the width of the space charge region, and therefore the capacitance of the tested structure.

The DLTS procedure consists in monitoring the transient of capacitance (following the electric pulse) as a function of the temperature. Particularly, the variation with the T of the parameter $\Delta C(T)=C(t_1)-C(t_2)$ is evaluated, $C(t_1)$ and $C(t_2)$ being the capacitance values determined at time t_1 and time t_2, respectively.

On the one hand, for low temperatures the carrier re-emission kinetics from the deep levels are particularly slow, therefore the corresponding ΔC are very low. On the other hand, for high temperatures the re-emission kinetics are so fast, that the associated ΔC are also very low. Consequently $\Delta C(T)$ features a maximum for intermediate T values, the so-called DLTS peak, corresponding to the temperature T_m.

T_m is relevant as such, since it can be seen as a signature of the present defect level. In addition, the amplitude of the DLTS peak is proportional to the associated trap density. Furthermore, the majority carrier capture cross section of the investigated energy level, and its

location within the semiconductor band gap, can be determined. Notice that the detection limit for the trap concentration is expected to be of the order $0.0001 \times p_0$, with p_0 the equilibrium majority charge carrier density.

3.3 Techniques for evaluating the electrical properties

3.3.1 Four-point probe technique for resistivity measurements

Resistivities (ρ) of studied samples were measured by the four-point probe technique. The four-point probe has four thin tungsten metal tips placed along a line with equal distance, s. The electric current is supplied through the two outer tips and the voltage is measured through the two inner tips. For a bulk material, ρ is given by the equation [10]:

$$\rho(\Omega \cdot cm) = dR_{\square} = d\frac{\pi U_v}{I_c \ln 2} \tag{3.1}$$

Where $R_{\square}$ is the measured sheet resistance, U_v is the measured voltage, I_c is the applied current and d is the thickness of the measured sample. The uncertainty regarding the obtained ρ is given to be about ±10 %.

3.3.2 Carrier lifetime measurement techniques (µW-PCD and QssPC)

Both, quasi-steady-state photoconductance (QssPC) and microwave detected photoconductivity decay (µW-PCD) techniques were used throughout this work to determine the effective carrier lifetime (τ_{eff}). In our present work, we were mostly interested in bulk (as opposed to surface) properties. Therefore, for these measurements, the surfaces of the studied samples were electrically passivated by hydrogenated Si nitride (SiNx:H) layers deposited by plasma-enhanced chemical vapour deposition.

The QssPC technique offers a fast and accurate means to determine τ_{eff} over a wide range of excess carrier density (Δn). This method was firstly published by Sinton and Cuevas in 1996 [11].

During a QssPC measurement, excess carriers are generated within the sample using a conventional xenon photo flash with a slow decay time, so that the sample can reach a "quasi-steady-state". The intensity of the flash is monitored as a function of time via a calibrated

solar cell. From the flash intensity, the carrier generation rate (G) can be estimated. The photoconductance ($\Delta\sigma$) of the sample is measured by inductive coupling via a coil placed below the sample, included in an *rf*-bridge circuit (Figure 3.6).

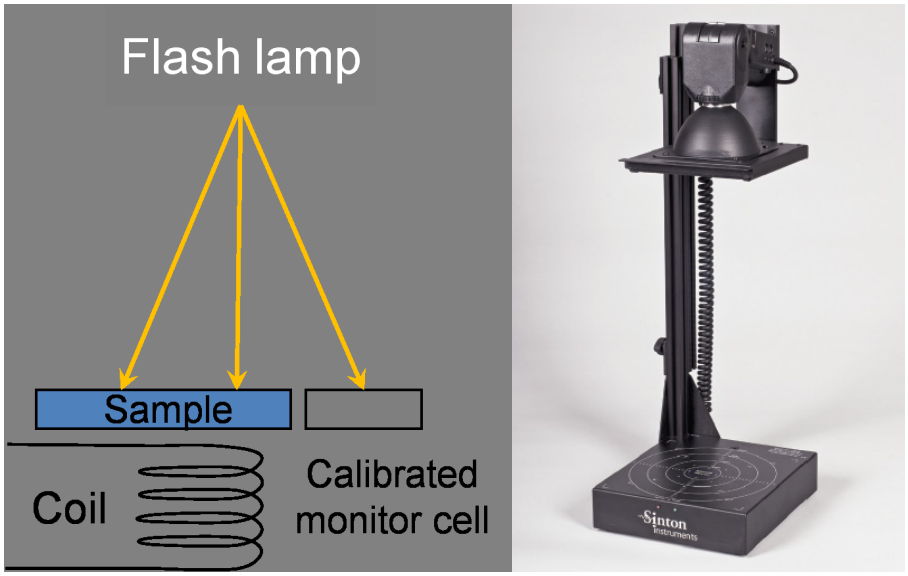

Figure 3.6 – Schematic (left) and picture (right) of the QssPC measurement system.

Δn is proportional to $\Delta\sigma(t)$:

$$\Delta\sigma(t) = q\Delta n\left(\mu_n + \mu_p\right) \tag{3.2}$$

q is the elementary charge, μ_n and μ_p are the electron and hole mobilities, respectively. This equation neglects the trapping of minority carriers and depletion region modulation effects.

Solving eq. (3.2) for Δn and using the independently monitored G, the τ_{eff} can be calculated using the expression:

$$\tau(\Delta n) = \frac{\Delta n}{G} \tag{3.3}$$

The QssPC is a contactless and fast measurement technique, which averages the measured conductivity signal over a measurement area of a few cm^2. The uncertainty regarding τ_{eff} is given to be about ±10 % [12].

µW-PCD allows spatially resolved carrier lifetime measurements. µW-PCD measurements were performed using a SEMILAB WT-2000 tool. The sample is placed under a microwave source and excess charge carriers are generated by a short laser pulse

(wavelength 904 nm, pulse length 200 ns, excited area 1 mm^2). Microwaves being reflected by free carriers in Si, the amplitude of the reflected microwave signal depends on Δn. The decay of the reflected microwave signal is monitored as a function of time [13]. This decay can usually be fitted by a single-exponential function, with a time constant assumed to be τ_{eff}. Notice that the reflected microwave power is in general a non-linear function of Δn. Therefore in this work, the τ_{eff} determined by μW-PCD are not associated with a Δn value.

3.4 Techniques for the characterizations of the photovoltaic properties of the solar cells

3.4.1 I-V characteristics

The illuminated current-voltage (I-V) characteristics were obtained by the "Variable Load" measurement method. The solar cell is placed on a temperature-controlled chuck at 25°C and is illuminated (AM1.5G spectrum under an intensity of 0.1 $W.cm^{-2}$). The test system presents a variable resistive load to the source under test. The variable load includes the short circuit and open circuit conditions and steps through many intermediate resistance values. It measures the voltage and current across the load at each value of load resistance. From the full I-V characteristic the main photovoltaic parameters (short-circuit current, open-circuit voltage, fill factor, conversion efficiency) are then extracted.

Dark reverse I-V characteristics were also obtained, in order to determine the hard breakdown voltage (V_{bd}) of Si solar cells. Hard breakdown refers to the ultimate breakdown mechanism, triggered by avalanche multiplication. V_{bd} is a key parameter that governs the long-term performances of PV modules. Throughout this work the V_{bd} was defined as the voltage at the maximum point of curvature of the reverse I-V curve.

3.4.2 LBIC analyses: determination of the minority carrier diffusion length

The Light Beam Induced Current (LBIC) technique consists in measuring the short circuit current delivered by an illuminated solar cell (or any *p-n* or Schottky junctions). Throughout this work, the LBIC analyses were conducted with a SEMILAB WT-2000 tool. In such a device, 4 different wavelengths (405 nm, 850 nm, 950 nm and 1015 nm) can be fed to the sample, allowing to probe the cell response at various penetration depths. The light beam size is about 100 μm. The localized beam sweeping the entire surface of the solar cell

(Figure 3.7), high resolution LBIC mappings can be obtained. Four different wavelength lasers can be used for this purpose.

From the LBIC values, mapping of the external quantum efficiency (EQE) can be obtained. The EQE is the ratio of the number of carriers delivered by the solar cell to the number of photons of a given energy incident on the solar cell.

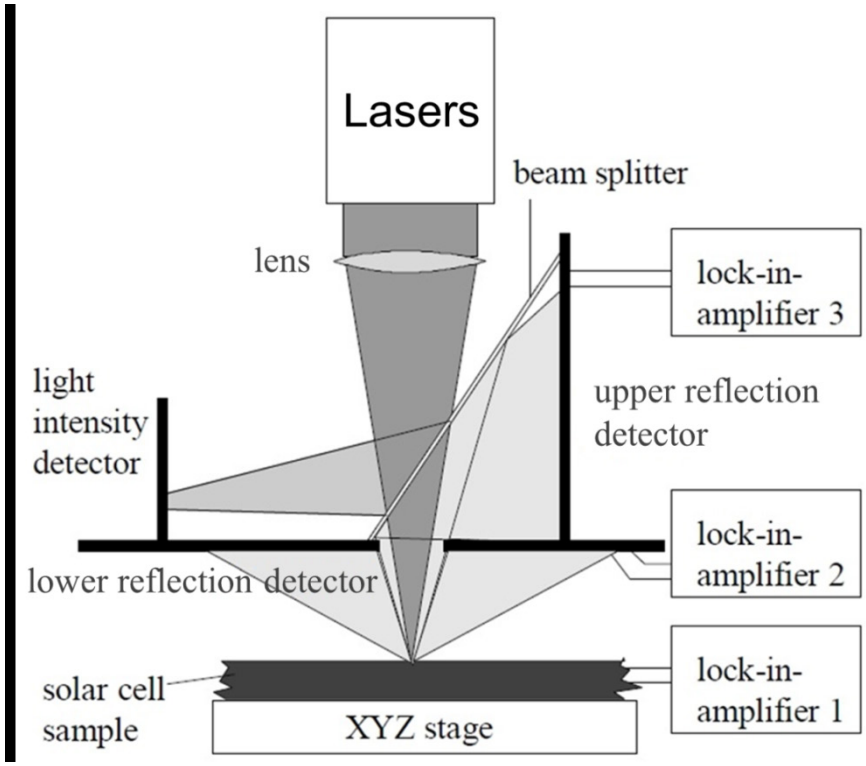

Figure 3.7 – Schematic drawing of an LBIC equipment [14]

In parallel to the LBIC measurements, the SEMILAB tool allows the realization of mappings of the solar cell reflectance (R). From the EQE and R values, for a given wavelength, the internal quantum efficiency (IQE) can be computed.

$$IQE(\lambda) = \frac{EQE\ (\lambda)}{1-R(\lambda)} \tag{3.4}$$

The IQE is the ratio of the number of charge carriers delivered by the solar cell to the number of photons of a given energy that penetrate within the silicon material.

An important fact is that the IQE depends on both the light penetration depth ($1/\alpha$) where α is the light absorption coefficient, and the minority carrier diffusion length (L_n). Thus knowing the IQE it is possible to estimate L_n (with a ± 10 % accuracy) via the equation (3.5):

$$\frac{1}{IQE(\lambda)} = \frac{1}{\alpha(\lambda) \times L_n} + 1 \quad (3.5)$$

Eq. 3.5 is valid if the following conditions are fulfilled:

- The thickness of the sample (*d*) is significantly higher than L_n.
- α and *d* obey the following expression: $\alpha(\lambda) \times d > 1$.
- The width of the space charge region and the emitter thickness, are significantly lower than *d*.
- The surface is polished (no deviation of the incident light).

3.4.3 Electroluminescence

Forward-biased electroluminescence relies on the same principle as a light emitting diode (LED). Current is fed into a solar cell and radiative recombination of carriers causes light emission. Due to the fact that Si is an indirect bandgap semiconductor, most of the recombinations occur via defects or Auger mechanisms. The amount of band-to-band recombination producing radiative emission is relatively low. However, the small amount of radiative recombination that takes place can be sensed using an infrared digital camera. The technique requires electrical contacts and so can only be used once the metallization has been applied and the cell is substantially complete. Electroluminescence (EL) provides important data about the uniformity of the PV performances of solar cells and modules. It is a qualitative technique, but has the advantage of being non-destructive and relatively fast with measurement durations of 1 s possible.

The emitted EL intensity is related to the densities of free carriers in the base layer, and therefore gives information on intrinsic and extrinsic cell parameters influencing them: bulk recombination, surface recombination, cracks, etc. Electroluminescence is also sensitive to resistance and shunts when driving current through the solar cell. So this technique can also show voids in metallization, higher resistance regions, shunts, and other device features. This is one of the most powerful techniques to rapidly assess the quality of both solar cells and modules and is getting much interest from the research point of view [15].

Reverse-biased electroluminescence (ReBEL) is used to identify locations in a photovoltaic device where junction breakdown occurs [16,17]. Indeed the breakdown of *p-n* junctions in silicon is usually accompanied by the emission of light. The light emission has been attributed to hot carrier interband recombination or relaxation and features a wide-band

spectrum including contributions in the visible range [18]. The exact origin of this luminescence is still under discussion.

3.4.4 Aging tests

Experimental studies on the evolution under illumination of the solar cell PV performances are of paramount importance, since the requirements of the PV industry regarding the stability of the cell efficiency are more and more aggressive. Particularly in the frame of this PhD such tests are essential. Indeed according to the literature Cu would be responsible for light-induced degradations of the charge carrier lifetime.

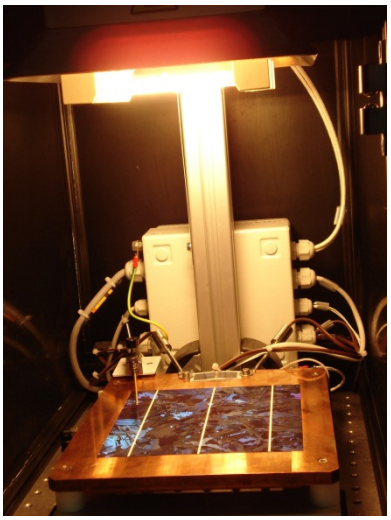

Figure 3.8 – Equipment for aging tests

For the aging tests solar cells were placed on a temperature (T) controlled chuck at 50°C and illuminated by a halogen lamp under a controlled and monitored intensity, equal to 0.05 $W.cm^{-2}$ (Figure 3.8). Under illumination, the V_{oc} was measured. T fluctuations (which were below 0.5 °C) were monitored and accounted for using standard correction procedures (dV_{oc}/dT values are around 2 $mV.K^{-1}$). When the V_{oc} reached stable values, the aging test was stopped.

Chapter 3 - Bibliography

1. J.R. Davis, A. Rohatgi, R.H. Hopkins, P.D. Blais, P. Rai-Choudhury, J.R. McCormick, H.C. Mollenkopf, Impurities in silicon solar cells. IEEE Trans. Electron. Devices. 27, 677 (1980).
2. F.A. Trumbore, Solid solubilities of impurity elements in germanium and silicon. The Bell System Technical Journal. 39, 205 (1960).
3. B.B. Paudyal, K.R. McIntosh, and D.H. Macdonald, Temperature dependent carrier lifetime studies on Ti-doped multicrystalline silicon. J. Appl. Phys. 105, 124510 (2009).
4. G. Coletti, P.C.P. Bronsveld, G. Hahn, W. Warta, D. Macdonald, B. Ceccaroli, K. Wambach, N.L. Quang, and J.M. Fernandez, Impact of metal contaminations in silicon solar cells. Adv. Funct. Mater. 21, 879-890 (2011).
5. P. R. Griffiths, J.A. De Haseth, Fourier Transform Infrared Spectrometry. 2nd edition, John Wiley & Sons Inc. (2007).
6. B. Stuart, Infrared spectroscopy: Fundamentals and applications. John Wiley & Sons Ltd (2000).
7. J.S. Becker, H.J. Dietze, State-of-the-art in inorganic mass spectrometry for analysis of high-purity materials. International Journal of Mass Spectrometry. 228, 127 (2003).
8. http://www.eag.com/
9. D.V. Lang, Deep-level transient spectroscopy: A new method to characterize traps in semiconductors. J. Appl. Phys. 45, 3023 (1974).
10. F.M. Smits, Measurement of sheet resistivities with the four-point probe. Bell System Technical Journal. 34, 711 (1958).
11. R.A. Sinton, and A. Cuevas, Contactless determination of current-voltage characteristics and minority-carrier lifetimes in semiconductors from quasi-steady-state photoconductance data. Appl. Phys. Lett. 69, 2510 (1996).
12. K.R. McIntosh, and R.A. Sinton, Uncertainty in photoconductance lifetime measurements that use an inductive-coil detector. 23rd EU PVSEC. Valencia, Spain (2008).
13. D.E. Kane, and R.M. Swanson, Measurement of the emitter saturation current by a contactless photoconductivity decay method (silicon solar cells). 18th IEEE PVSC. Las Vegas, USA, 578 (1985).
14. M. Rinio, H.J. Möller, and M. Werner, LBIC Investigations of the lifetime degradation by extended defects in multicrystalline solar silicon. Solid State Phenomena. 63, 115 (1998).
15. A. Petraglia, and V. Nardone, Electroluminescence in photovoltaic cell. Phys. Educ. 46, 511 (2011).
16. M. Lahbabi, A. Ahaitouf, M. Fliyou, E. Abarkan, J.-P. Charles, A. Bath, A. Hoffmann, S.E. Kerns, and D.V. Kerns, Analysis of electroluminescence spectra of silicon and gallium arsenide p-n junctions in avalanche breakdown. J. Appl. Phys. 95, 4 (2004).
17. K. Bothe, K. Ramspeck, D. Hinken, C. Schinke, J. Schmidt, S. Herlufsen, R. Brendel, J. Bauer, J.-M. Wagner, N. Zakharov, and O. Breitenstein, Luminescence emission from forward- and reverse-biased multicrystalline silicon solar cells. J. Appl. Phys. 106, 104510 (2009).
18. O. Breitenstein, J. Bauer, K. Bothe, W. Kwapil, D. Lausch, U. Rau, J. Schmidt, M. Schneemann, M.C. Schubert, J-M. Wagner and W. Warta, Understanding junction breakdown in multicrystalline solar cells. J. Appl. Phys. 109, 071101 (2011).

CHAPTER 4. INFLUENCES OF INTENTIONAL CU AND TI CONTAMINATIONS ON THE PROPERTIES OF CZ-SI WAFERS AND SOLAR CELLS

In this chapter the influence of intentional contaminations of the Si feedstock by titanium (Ti) and copper (Cu) on the properties of *p*-type single-crystalline Czochralski (Cz) Si wafers and solar cells were evaluated and compared. The characteristics of the three Cz ingots grown for this study - a reference ingot without intentional contaminations by metal impurities (Cz-Ref), a Cu contaminated ingot (Cz-Cu) and a Ti contaminated ingot (Cz-Ti) - were presented in the third chapter. These ingots were cut into wafers with a diameter equal to 100 mm for the Cz-Ref and Cz-Cu ingots, and equal to 75 mm for the Cz-Ti ingot. The initial thickness of all wafers was about 450 µm.

4.1 Compositional properties of the studied wafers

Three wafers from different positions (top, middle and bottom) along each Cz-Si ingot's height were collected for interstitial oxygen (O_i) concentration ([O_i]) determinations by Fourier-transform infrared spectroscopy (FTIR) (calibration coefficient of 3.14×10^{17} cm^{-2}). As shown in Figure 4.1, for a given solidified fraction, the extracted [O_i] values are very close for each ingot (Cz-Ref, Cz-Ti and Cz-Cu). For our present purposes, since O is known for strongly influencing the properties of Cz silicon wafers and cells, it is important to point out that the O content does not significantly vary from one ingot to another (for a given solidified fraction). Along the ingot's height, [O_i] are in the range 6.8×10^{17} cm^{-3} – 1.1×10^{18} cm^{-3}, which are typical values for Cz wafers. The substitutional carbon concentrations ([C_s]) were below the detection limit (DL) for FTIR analyses (DL about 10^{16} cm^{-3}).

The Cu concentrations ([Cu]) were determined by ICP-MS (inductively coupled mass spectroscopy) analyses. This technique gives for a given impurity its total concentration, irrespective of its chemical state (dissolved, precipitated, ionized/neutral) within the Si bulk. The uncertainties associated with the ICP-MS analyses were given to be about 10 %. The experimental [Cu] variation along the Cz-Cu ingot's height is shown in Figure 4.1. The experimental [Cu] are compared with the expected [Cu], calculated from Scheil's law, using for the effective segregation coefficient (k_{eff}) the value given in [1] ($k_{eff} = 8\times10^{-4}$). We decided

to use this k_{eff} value (the same remark applies for Ti below) because it was experimentally determined for pulling conditions similar to those concerning the growth of our Cz ingots.

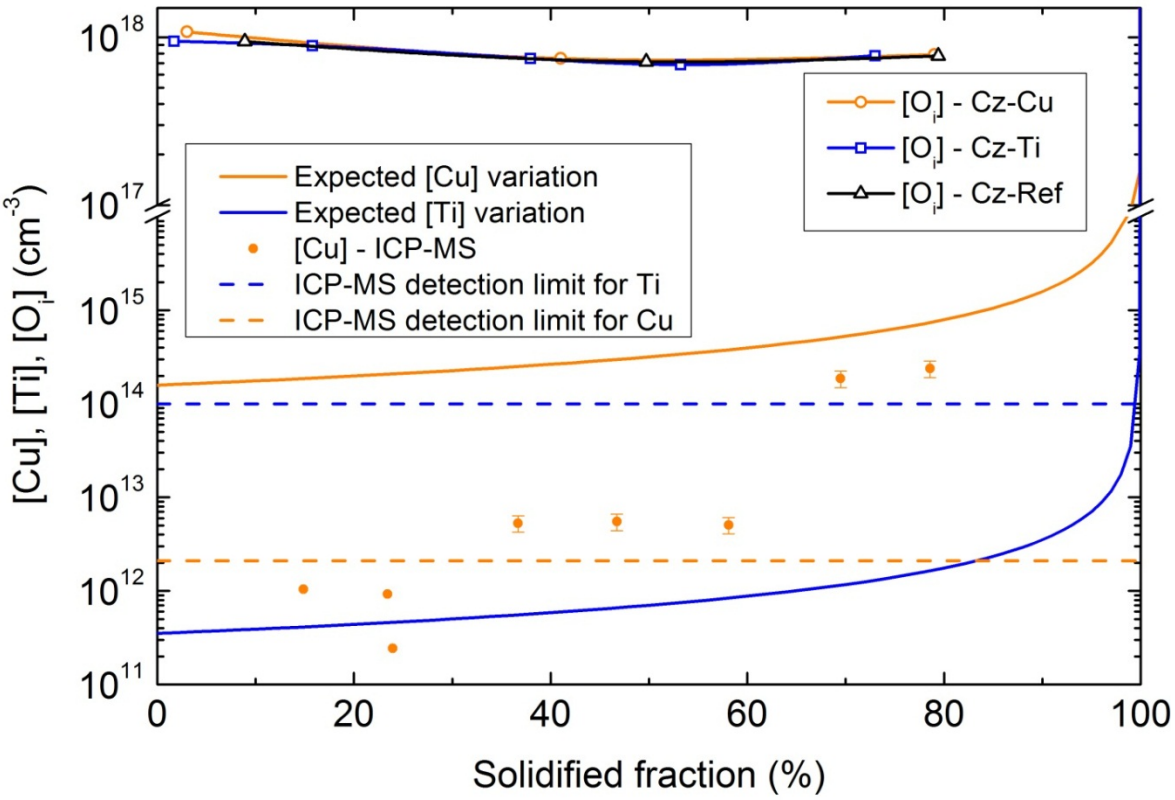

Figure 4.1 – [O_i], [Ti] and [Cu] variations versus the solidified fraction. The solid lines for [O_i] are only guides to the eyes. For Cu, both the expected and experimental [Cu] are represented. For Ti, only the expected [Ti] are represented. The detection limits (ICP-MS) for [Ti] and [Cu] are shown by dotted lines. Notice that the uncertainties for the [Cu] data points below the detection limit are not represented.

It should be noted, that the indicated (Figure 4.1) ICP-MS detection limit for Cu (2.1×10^{12} cm^{-3} corresponds to the quantification limit. Therefore, the relevance of the [Cu] data below this limit is highly questionable. The experimental [Cu] values are lower than the expected data. For instance, for a solidified fraction of 35 %, the experimental [Cu] are about 2 orders of magnitude lower than the computed values. Furthermore, the experimental [Cu] significantly vary along the ingot's height. For instance between the solidified fractions 20 % and 80 %, the experimental [Cu] increases by 2 orders of magnitude whereas the computed [Cu] only increases by 1 order of magnitude. It should be noted that the same conclusions would be drawn if we had used another partition coefficient, e.g. the equilibrium value k=4×10^{-4}. Two mechanisms can be invoked to account for these a priori surprising results: firstly, this could be due to Cu evaporation from the Si melt during the ingot's growth. Secondly, during the ingot's cooling, as Cu due to its high diffusivity is able to migrate on

few centimeters, Cu atoms could reach the periphery of the ingot and agglomerate at the surfaces (which are then removed) or even exo-diffuse. This mechanism is in good agreement with the fact that the difference between the experimental and computed [Cu] is significantly higher for the first solidified part of the ingot, the cooling for this region of the ingot being the slowest.

On the other hand the presence of Ti could not be detected by ICP-MS or secondary ion mass spectroscopy (SIMS) analyses. This is not altogether surprising, since the expected Ti concentrations ([Ti]), calculated from Scheil's law with a k_{eff} equal to 2×10^{-6} [1], are for the selected wafers, systematically below (Figure 4.1) the detection limits (DL) of both ICP-MS and SIMS analyses (respectively about 10^{14} cm^{-3} and 3×10^{13} cm^{-3})

To gain some insights into the issue of Ti incorporation, we conducted SIMS analyses of the surfaces of Ti-contaminated wafers which experienced a P-diffusion. Indeed the P-diffusion step is known for developing an external gettering effect of metal impurities, mainly via solid phase segregation mechanisms, the solubility of metal elements being higher within the P-rich layer. After the P-diffusion treatment, the gettered metal impurities are essentially agglomerated within the P-diffused layer (Figure 4.2), where their concentrations usually exceed the DL of the SIMS analyses (consequently they can be detected). Figure 4.3 presents [Ti] depth profiles obtained by SIMS for P-diffused samples. Notice that theses analyses were conducted on a Ti-contaminated Cz sample, but also on a Cu-contaminated Cz sample. Indeed, such analyses are usually affected by surface contamination issues. Thus, in order to take these potential artefacts into account, the Cu-contaminated sample, virtually Ti-free, acted as a reference sample. Firstly Figure 4.3 shows that the [Ti] agglomerated within the P-diffused layer (its thickness is about 0.35 nm) are significantly higher for the Ti-contaminated sample, despite the low diffusivity of Ti. This indirectly confirms that we succeeded in incorporating Ti atoms within the Si bulk. In a second step, the [Ti] determined for the Cu-contaminated sample were subtracted to the values found for the Ti-contaminated wafer (in order to take into account the surface contamination issues). Then we computed the total amount of Ti atoms trapped within the P-diffused layer. Using the standard diffusion formula $l = (D\times t)^{1/2}$, and a value of the Ti diffusion coefficient of 1.3×10^{-10} cm²/s, the length on which the Ti atoms diffuse during the P-diffusion step (L_P) was evaluated to be around 6 µm. Assuming that all the Ti atoms trapped within the P-diffused layer were initially (before the P-diffusion) homogeneously distributed over a length L_P, the initial bulk [Ti] could be estimated. Our computations showed that the initial bulk [Ti] should be about 10^{13} cm^{-3} for a solidified fraction of 76 %. Considering the uncertainties on the value of the diffusion and

partition coefficients, such a value can be considered in fair agreement with the expected [Ti] value from Scheil's law (around 2×10^{12} cm^{-3}).

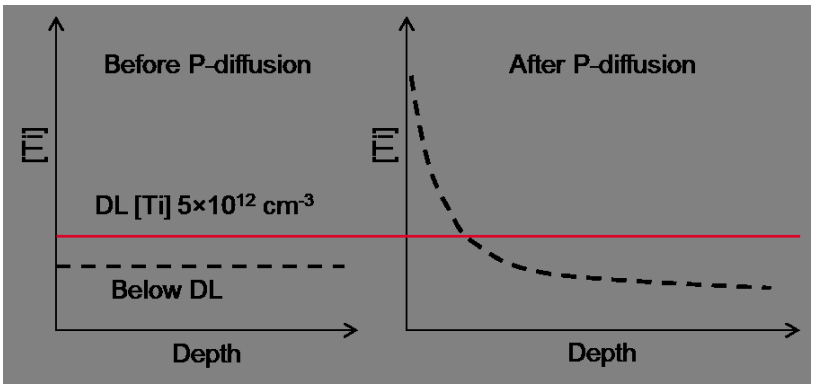

Figure 4.2 – Principles of the experimental protocol used to estimate the bulk [Ti]. Before the P-diffusion step, [Ti] (represented by the dotted lines) is below the SIMS detection limit (left) and cannot be detected. After the P-diffusion (right), due to segregation gettering effects, the [Ti] within the P-diffused layer can exceed the SIMS detection limit and the presence of Ti atoms can be detected.

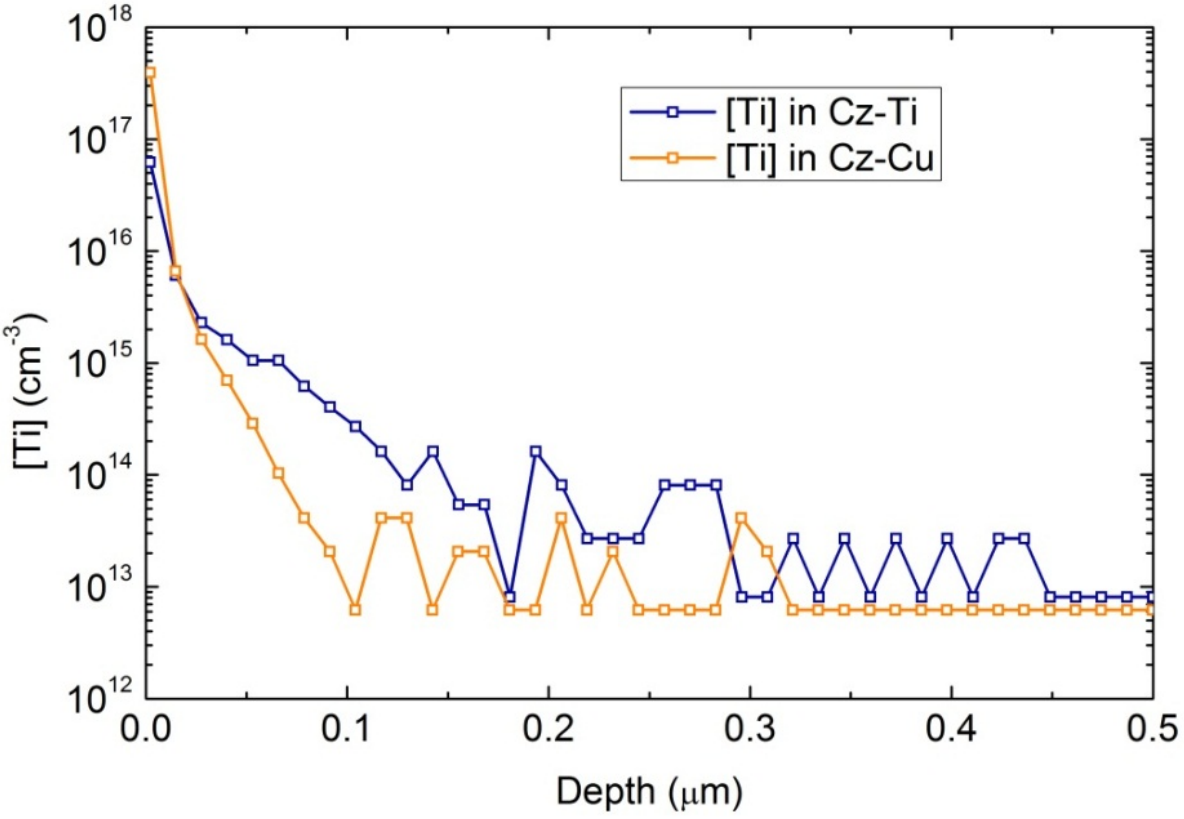

Figure 4.3 – SIMS depth profiles (variations of the Ti concentration) of P-diffused Cz wafers, Ti-contaminated and Cu-contaminated, associated with a solidified fraction of 76 %. The solid lines are only guides to the eyes.

In parallel, deep level transient spectroscopy (DLTS) analyses of a Ti-contaminated Cz wafer from the bottom part of the Cz-Ti ingot (solidified fraction of 70 %) were subcontracted

by SEMILAB. A DLTS peak, associated with a defect level located at 0.23 eV above the valence band (E_v) was detected which would correspond to the double-donor level introduced by interstitial Ti atoms (E_v+0.26 eV). The concentration of this defect is equal to 1.3×10^{13} cm^{-3}, therefore in very good agreement with the value estimated from the SIMS profiles conducted on the P-diffused layer.

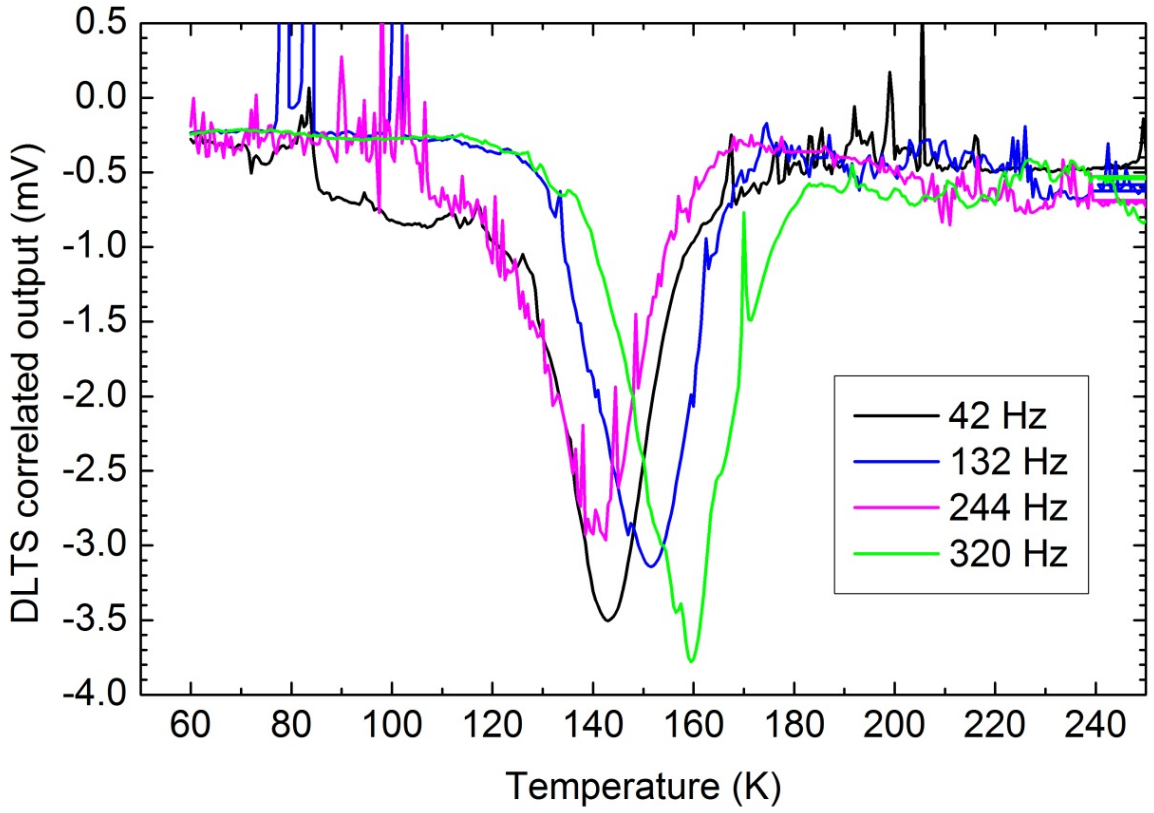

Figure 4.4 – Variations of the DLTS signal with the temperature. Measurements conducted at various frequencies: at 42 Hz, 132 Hz, 244 Hz, 320 Hz. Ti-contaminated Cz sample (solidified fraction equal to 70 %).

The fact that the experimental [Ti] are above (by a half order of magnitude) the expected [Ti] is not completely understood. It could be due to the use of an inappropriate k_{eff} for Ti.

4.2 Resistivity

Some wafers were collected at regular intervals along the ingots' height and the ρ were measured using a four-point probe setup and averaged over 25 positions across the wafer surface. The expected ρ variation was calculated using the B concentrations ([B]) and the corresponding mobility (μ) values. The [B] variation (and therefore the majority carrier

density variation) was calculated via the Scheil's law, with k_{eff} = 0.82, this value being computed using BPS equations (see Chapter 1) [2,3]. The Arora's model was used for the computation of the μ [4]. Calculated and experimental ρ variations along the ingots' height are shown in Figure 4.5.

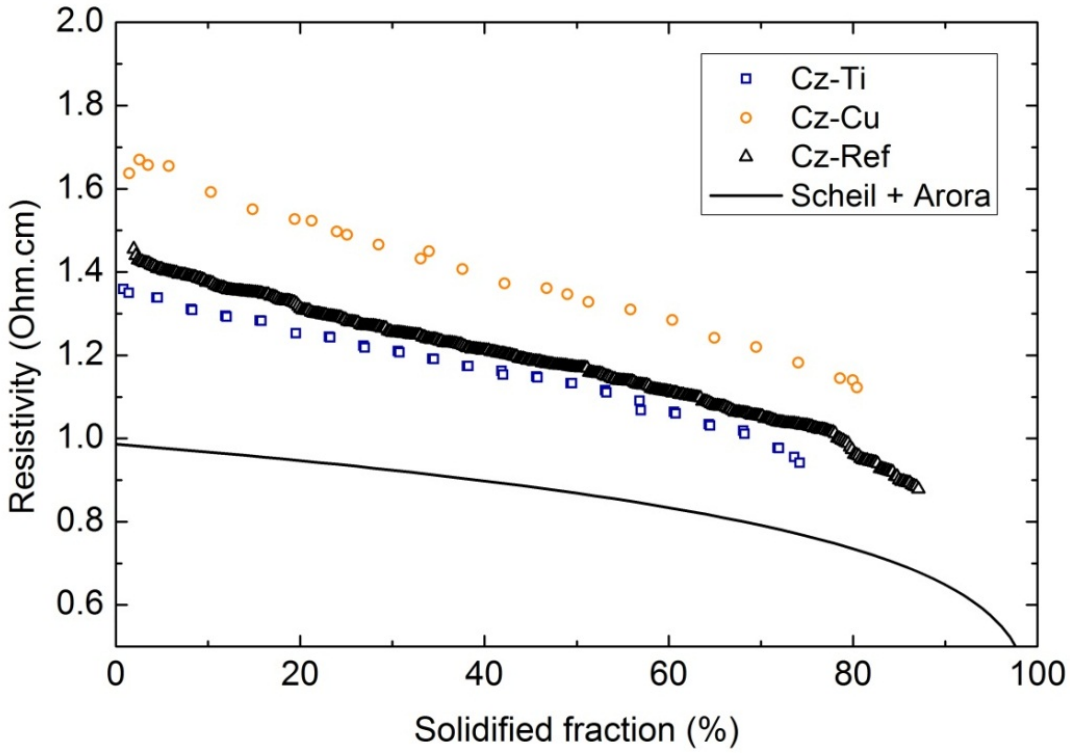

Figure 4.5 – Resistivity as a function of the ingots' height. The solid line corresponds to the computed values, via the combination of the Scheil's law (for determining the B content, and therefore the hole density) and the Arora's model (for computing the hole mobility).

The curves from the three ingots look very similar. This is particularly crucial regarding our study since the B content (and the corresponding hole majority carrier density) strongly influences the properties of the solar cells (e.g., the *p-n* junction barrier height). Therefore it was particularly important in order to assess the effect of an impurity, to be able to compare for a given solidified fraction, uncontaminated and contaminated wafers with the same B concentration. Regarding the slight discrepancy between the experimental ρ and the calculated values, our opinion is that it could be explained by the evaporation of B atoms from the Si melt. It should also be noted that at the low concentration levels of Ti and Cu involved, no impurity effect on carrier mobility should be expected.

4.3 Effect of the contaminations on the effective carrier lifetime – Influence of the P diffusion step

Effective carrier lifetime (τ_{eff}) measurements were done on as-received and P-diffused wafers. The wafers experienced chemical polishing steps (before the P diffusion in order to remove the surface region affected by the sawing step and then after the P diffusion in order to remove the n^+ emitter), and the surfaces were electrically passivated by hydrogenated Si nitride (SiNx:H) layers deposited by PECVD (plasma-enhanced chemical vapor deposition). Then τ_{eff} were measured by quasi-steady state photoconductance decay (QssPC) analyses and mapped via the micro-wave photoconductance decay (μW-PCD) technique.

The τ_{eff} variations with the solidified fractions are shown in Figure 4.6, for the Cz-ref ingot, the Cz-Ti ingot and the Cz-Cu ingot. Remarkably, for solidified fractions lower that 70 %, the τ_{eff} of the P-diffused wafers are not affected by the Cu-contamination. The highest τ_{eff} are even measured for Cu-contaminated samples, with values approaching 400 μs! These high τ_{eff} are probably explained by the fact that low Cu densities were incorporated into the ingot during the Cz growth. In addition, the τ_{eff} of the Cu-contaminated wafers were slightly improved by the P-diffusion. As a fast diffuser, Cu is well extracted from the Si bulk by the external gettering effect developed by the P-diffusion (during the P-diffusion step, Cu can migrate on lengths significantly higher than the thickness of the wafer). Thus the limited increase in lifetime upon P-diffusion also seems to point low Cu contents in the as-grown ingots. Nevertheless the better lifetime values as compared to the reference ingot for solidified fractions lower than 70 % remain surprising. This could be explained, as proposed in the literature, by the fact that during the cooling of the Cu-contaminated ingot, liquid Cu silicides could develop internal gettering effects [5], trapping other metal impurities (e.g., Fe, Cr, …). However, such a positive effect of the Cu contamination on the electrical properties of the Cz ingots should be confirmed on a larger number of ingots. For solidified fractions above 70 %, τ_{eff} could be affected by the Cu contamination (possibly due to higher Cu contents), however we shall see that this result was not confirmed at the solar cell level.

On the other hand, the Ti contamination, despite the low Ti concentrations, strongly affects the τ_{eff}. The τ_{eff} of the Ti-contaminated samples are below 55 μs, whatever the solidified fraction. This is probably explained by the fact that Ti is essentially present as interstitial atoms (as shown by the DLTS analyses), state for which Ti features harmful recombinant properties. The τ_{eff} of the Ti-contaminated samples decreases along the ingot's

height, which is probably related to increases in the [Ti], due to segregation effects. Eventually, the τ_{eff} of the Ti-contaminated samples is not improved by the P-diffusion. This is in good agreement with the low diffusivity of Ti. The majority of the Ti atoms cannot reach the n^+ region (external gettering site).

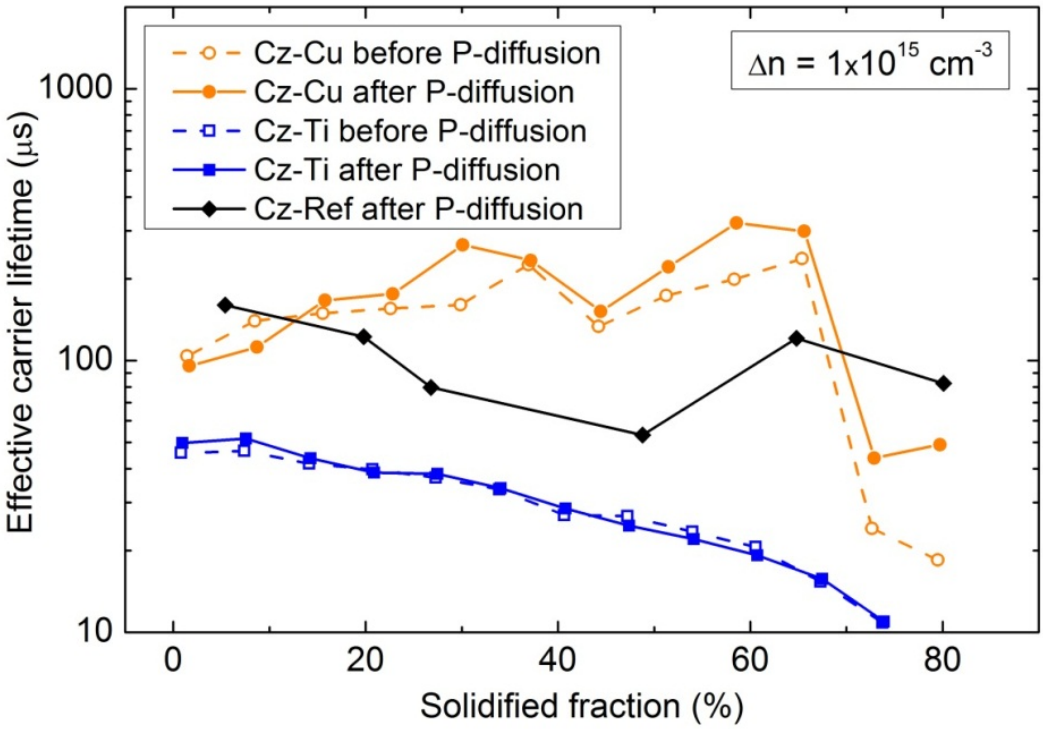

Figure 4.6 – Effective carrier lifetimes as a function of the ingots' height for Cz-Cu and Cz-Ti before and after the P diffusion step. The values are compared with those obtained for the reference (uncontaminated) Cz wafers which experienced the P-diffusion. The values were extracted for an excess carrier density equal to 10^{15} cm^{-3}. The solid and dash lines are only guides to the eyes.

It is particularly interesting to focus on the variations of τ_{eff} with the excess carrier density (Δn) of both Cu and Ti contaminated wafers, which experienced the P-diffusion step (Figure 4.7). Indeed, the τ_{eff} of the Cu-contaminated sample does not significantly vary with Δn, whereas the τ_{eff} of the Ti-contaminated wafer increases by one order of magnitude over the range of studied Δn. Such a behavior can strongly influence the performances of the Ti-contaminated cells. Indeed under standard illumination levels, open-circuit conditions are associated with Δn around 10^{15} cm^{-3}, whereas the short-circuit conditions are associated with Δn values around 10^{12}-10^{13} cm^{-3}. Therefore, as the lower the Δn the lower the τ_{eff}, very low τ_{eff} values (below 5 µs) are expected in short-circuit conditions. Consequently the Ti-contaminated cells should feature very low short-circuit current densities (J_{sc}).

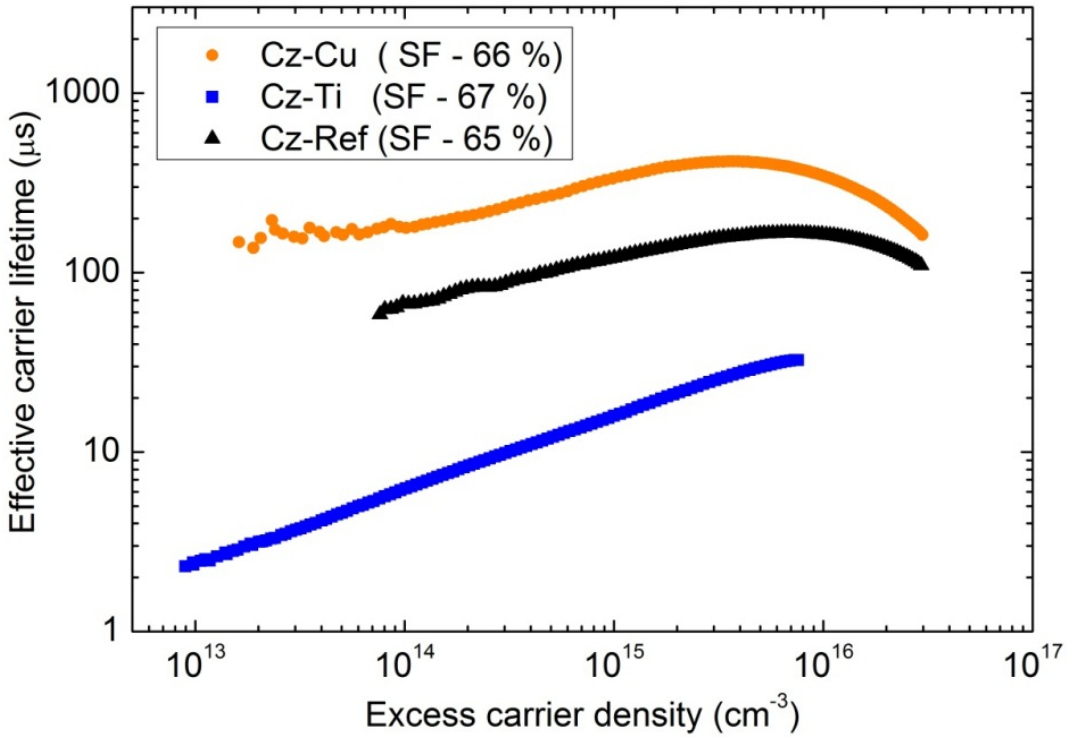

Figure 4.7 – Variations of the effective carrier lifetime with the excess carrier density. Cz-Ref, Cz-Cu and Cz-Ti wafers from similar solidified fractions (SF around 65 %). The wafers experienced a P-diffusion step.

The τ_{eff} were mapped by µW-PCD (Figure 4.8). The obtained τ_{eff} mappings (before and after the P-diffusion step), for Cu- and Ti-contaminated samples initially located in the middle part of the ingots, are shown in Figure 4.9 and Figure 4.10, respectively.

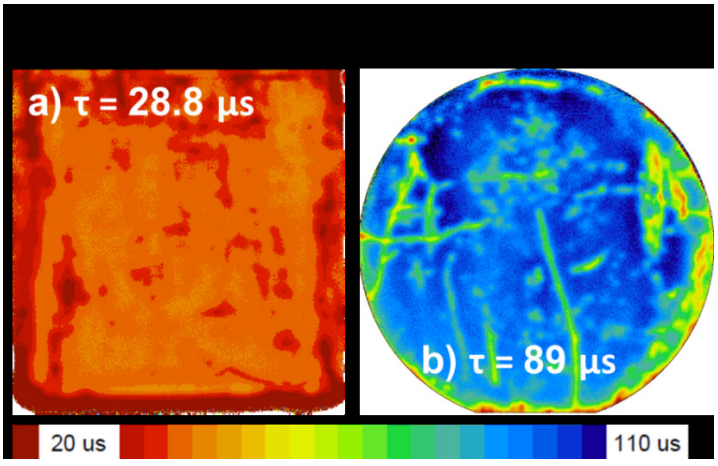

Figure 4.8 – τ_{eff} mapping obtained on P-diffused wafers from Cz-Ti (a) and Cz-Cu (b) ingots (SF=30 %).

The µW-PCD measurements confirm the QssPC data, particularly the fact that on the one hand the τ_{eff} of the Cu-contaminated samples are improved by the P diffusion step, whereas the τ_{eff} of the Ti-contaminated samples are not influenced by the P diffusion step. For

both, the Cu- and Ti-contaminated wafers, the τ_{eff} values are rather homogeneously distributed.

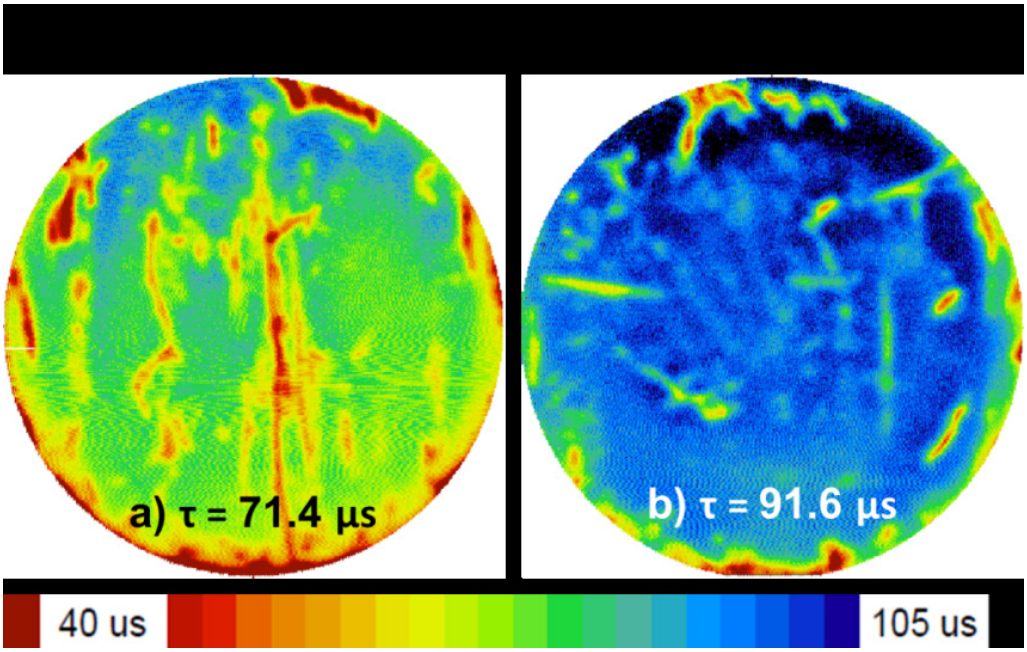

Figure 4.9 – τ_{eff} mappings obtained on as-received (a) and P-diffused (b) twin wafers from the Cz-Cu ingot (solidified fraction equal to 52 %). The presented values (respectively in black and white) correspond to the average τ_{eff}.

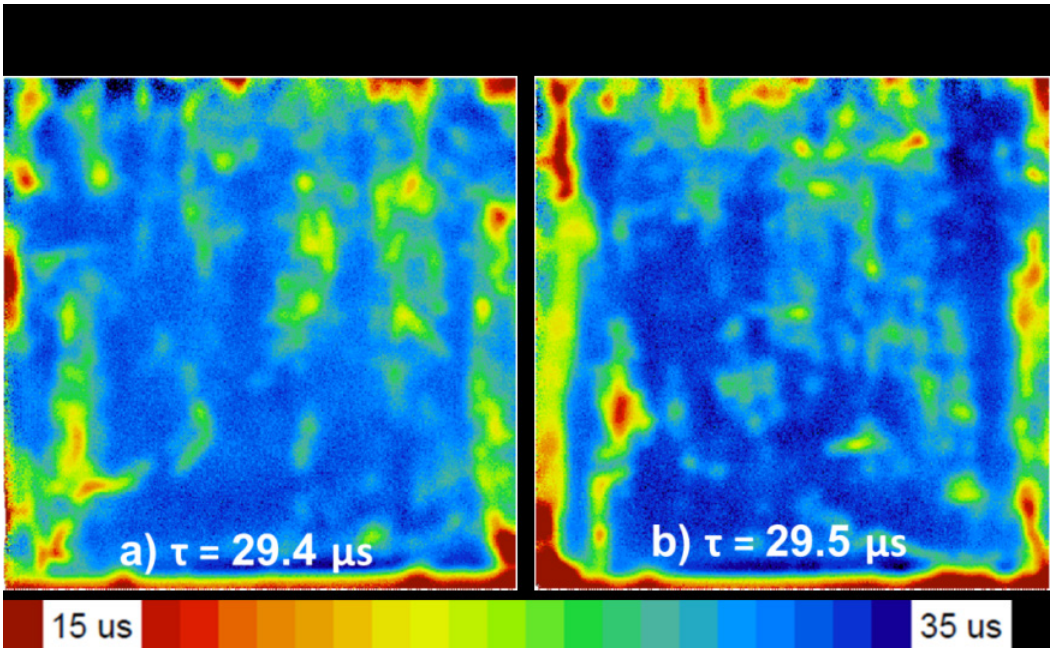

Figure 4.10 – τ_{eff} mappings obtained on as-received (a) and P-diffused (b) twin wafers from the Cz-Ti ingot (solidified fraction equal to 52 %). The presented values (respectively in black and white) correspond to the average τ_{eff}.

4.4 Effect of the Si hydrogenation on the electron diffusion length

It is known that hydrogen can interact with defects (extended defects and point defects) in silicon. Particularly some harmful impurities in Si (e.g., iron, gold), can be electrically passivated by H atoms. Therefore it is important to investigate the influences of the Si hydrogenation on the electrical properties of the Cu- and Ti-contaminated wafers, because a point to be recalled is that the hydrogenation effects occurring throughout the solar cell fabrication process are poorly understood, particularly when single-crystalline substrates are used. The source of hydrogen is provided by the anti-reflection coating layer of the cell (SiNx:H). Notice that it is crucial to investigate the possibility of passivating Ti with hydrogen since this impurity significantly affects the carrier lifetime.

For this experimental study, 6 wafers from each ingot were selected (2 adjacent wafers from the upper, middle and lower parts of the Cz-Cu, Cz-Ti and Cz-Ref ingots) and 20 wafers from the reference ingot were used for the optimization of the metallization firing step. Half of the wafers experienced a standard solar cell fabrication process with the SiNx:H layer and the others were fabricated without SiNx:H layer (therefore without source of H). The Current-Voltage (I-V) characteristics under illumination of the fabricated cells were measured. Due to their higher front surface reflectance, the solar cells without SiNx:H layers featured low PV conversion efficiencies. Nevertheless the goal of this study was not to obtain solar cells with good performances, but *simply* to fabricate functional solar cells without SiNx:H (fill factor higher than 65 %) in order to extract the effective electron diffusion lengths (L) via the combination of light beam induced current (LBIC) measurements and reflectance measurements done at various infra-red wavelengths. Indeed, the used screen-printed pastes, the metallization firing treatment, were developed for standard cells with the SiNx:H layer. Therefore the fabrication of cells without this layer is not so obvious. Then the efficiency of the hydrogen passivation could be evaluated by comparing the L for cells fabricated with wafers from the same solidified fraction, with and without SiNx:H layers. A point that should be stressed concerns the fact that the analytical method for determining the electron diffusion length assumes flat surfaces. Indeed, the textured surfaces deviating the incident light beam, the average depth at which the carriers are photo-generated cannot be precisely estimated. To overcome this issue, the determined L_{eff} is multiplied by a corrective factor defined by the equipment manufacturer for KOH texturation on (100)-oriented Si wafers, computed on the base of numerical simulation results.

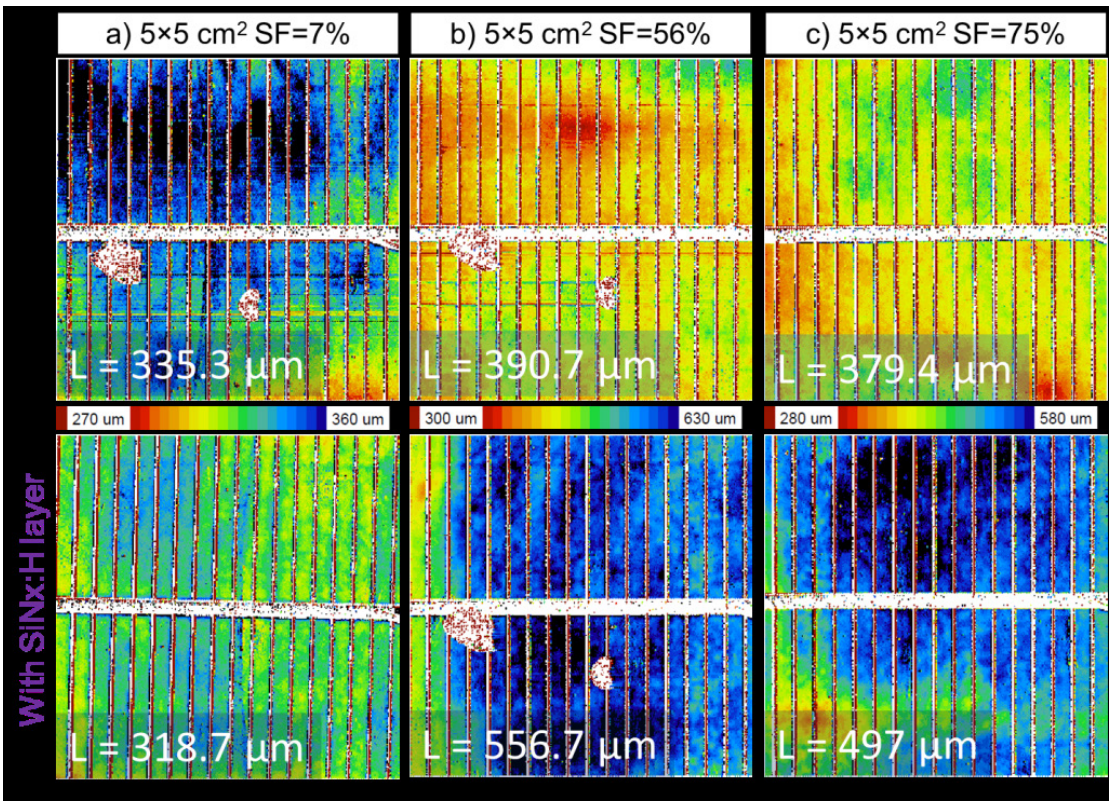

Figure 4.11 – Effective electron diffusion length mappings of the Cz-Ref solar cells with (bottom) and without (top) SiNx:H layer. The indicated L values (in white) correspond to the average values.

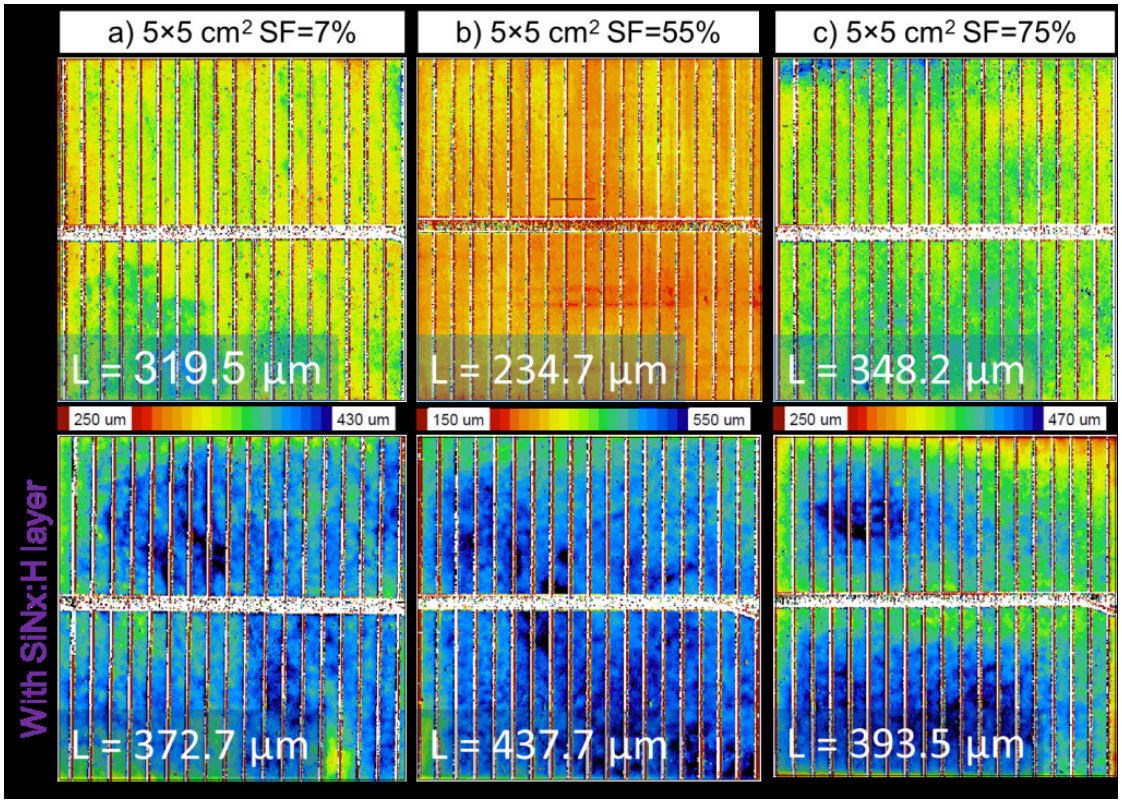

Figure 4.12 – Effective electron diffusion length mappings of the Cz-Cu solar cells with (bottom) and without (top) SiNx:H layer. The indicated L values (in white) correspond to the average values.

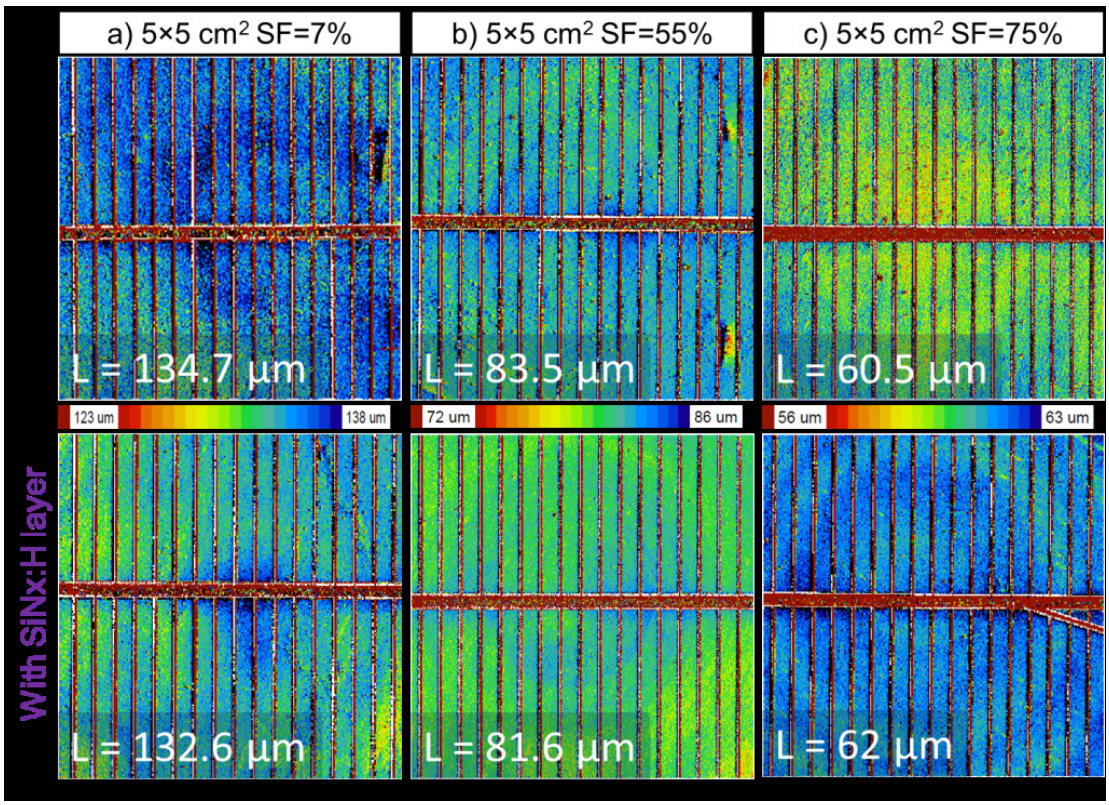

Figure 4.13 – Effective electron diffusion length mappings of the Cz-Ti solar cells with (bottom) and without (top) SiNx:H layer. The indicated L values (in white) correspond to the average values.

As shown by Figure 4.12 and Figure 4.13, the presence of the SiNx:H layer improved the L of the reference uncontaminated sample and the L of the Cu-contaminated sample. This could be taken as an indication that H electrically passivates defects present in the bulk of these Cz wafers. For Cu, this result was rather unexpected since H is expected to form recombinant complexes with Cu [6]. However the interpretation of this raw result requires some discussions. Indeed, first the extracted L for the reference and Cu-contaminated are in the range of the wafer's thickness. Therefore the validity of the extracted L is questionable (see chapter 3). Above all, for such high L the comparison of the data obtained with and without SiNx:H layers can be affected by parasitic contaminations occurring during the firing step. Indeed, this treatment is done in a metal-rich environment and the SiNx:H layer would act as a contamination barrier layer, protecting the quality of the Si bulk. Without this layer, the unintentional in-diffusion of impurities could be enhanced. These impurities, event present at low density, could affect the L of initially high quality samples, and therefore could alter the evaluation of the effects of the bulk hydrogenation only.

Regarding Ti, the obtained L are well below the thickness of the wafer and therefore the L comparisons are more relevant. However, the L of the cells with and without the SiNx:H layers are virtually the same. A first idea to account for this result is that it could be due to the

limited diffusion length of H in crystalline Si, and thus to a low density of H atoms introduced into the Cz material. Indeed, studies conducted in the lab a couple of years ago showed that in gold contaminated single-crystalline Si (gold concentration around 2×10^{13} cm^{-3}), the electrical neutralization of the substitutional gold atoms by H would be limited to few tens of micrometers below the surface, thus pointing towards a diffusion limited process [7]. On the other hand, recent studies about the involvement of H atoms into the permanent deactivation effect of the boron-oxygen related complexes showed that H would be after the firing step present in quantities high enough to passivate the B-O defects, along the entire thickness of single-crystalline wafers [8]. This apparent contradiction could be explained by the fact that a low H content (i.e., 10^{11}-10^{12} cm^{-3}) would be sufficient for the passivation of the B-O complexes which are likely to have a density lower than 10^{11} cm^{-3}, but would not be high enough to have an effect on metal elements with a density in the range 10^{12}-10^{13} cm^{-3}. But the lack of improvement associated to the presence of the SiNx:H layer could also be due to the fact that, according to the literature [9], unlike other metal elements (e.g. Fe, Au), Ti atoms would not be electrically passivated by forming complexes with H.

4.5 Illuminated forward I-V characteristics

Around 10 wafers were sampled at regular intervals along the ingots' height and transformed into solar cells following an industrial process. Both surfaces were texturized by the anisotropic chemical attack developed by the KOH solution. The n^+ emitter was formed by phosphorus diffusion. Then SiNx:H layers used as antireflection coating layers were deposited on the front surface by PECVD. The silver front and aluminium rear electrodes were deposited by screen printing before rapid annealing. Junction opening was performed by laser cutting. The fabricated solar cells were characterized by illuminated forward and dark reverse I-V measurements. For the forward I-V measurements, standard illumination and temperature were used (AM1.5G; 0.1 $W.cm^{-2}$; 25 °C). Notice that these measurements were performed without prior illumination. From these measurements the J_{sc}, the open-circuit voltage (V_{oc}), the fill factor (FF) and the PV conversion efficiency (η) were extracted.

Figure 4.14 presents the FF and the η of the produced solar cells, as a function of the solidified fraction of the corresponding wafer. It should be noted that the equipments and the processes used for the solar cells fabrication were not perfectly adapted to the morphology of our wafers due to their high thickness (450 µm instead of 200 µm for standard wafers) and their small surface area (5×5 cm^2 instead of 15.6×15.6 cm^2 for standard wafers). Particularly,

due to this non-standard geometry the firing treatment was not fully optimized which explains the moderate and scattered *FF* values (ranging between 71 % and 79 %). Nevertheless, the values obtains are relatively high, and as such they can be taken as a proof of the validity of the cell fabrication process and allow a meaningful discussion of the data.

Unexpectedly, in contradiction with the results presented in [10], the introduction of Cu in the feedstock did not affect the η. The average η for the reference and the Cu-contaminated solar cells were equal to 16.3 % and 16.4 %, respectively. The highest measured η, around 17.3 %, was even obtained for a Cu-contaminated cells.

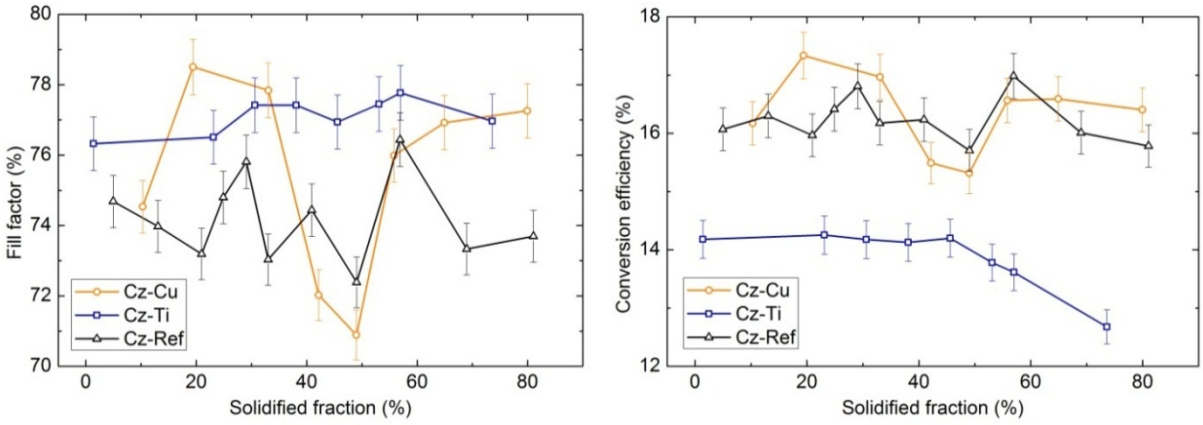

Figure 4.14 – Fill factor (FF) and Conversion efficiency (η) of the fabricated solar cells as a function of the solidified fraction of the corresponding wafers. The solid lines are only guides to the eyes.

Figure 4.15 presents the V_{oc} and the J_{sc} of the fabricated solar cells, as a function of the solidified fraction of the corresponding wafers. In good agreement with the fact that the τ_{eff} were not affected by the Cu-contamination, similar V_{oc} and J_{sc} were extracted for both the reference and the Cu-contaminated solar cells. On the other hand, as expected from the τ_{eff} measurements, the Ti-contaminated solar cells have lower V_{oc} and J_{sc} than the values found for the reference cells. For a solidified fraction of 40 %, the V_{oc} of the reference and Ti-contaminated cells are equal to 619 mV and 603 mV, respectively, and the J_{sc} values equal to 35.2 mA.cm^{-2} and 30.6 mA.cm^{-2}, respectively. The lowest J_{sc} and V_{oc} values for the Ti-contaminated cells are found for the cells fabricated with wafers from the last solidified fraction, in good agreement with the τ_{eff} measurements (the lowest τ_{eff} were measured for the samples from the last solidified fraction, due to the segregation of the Ti atoms during the growth of the ingot). Consequently the η of the Ti contaminated cells are significantly lower than the values found for the reference (uncontaminated) cells. For instance, for a solidified fraction of 40 %, the η of the reference and Ti-contaminated cells are equal to 16.2 % and

14.1 %, respectively. As discussed earlier, this strong effect of the Ti contamination is explained by the high recombination strength of interstitial Ti atoms, and to the fact that the interstitial Ti atoms are not neutralized by precipitation mechanisms or externally gettered due their low diffusivity. From an application oriented perspective, this is a very important result, since it demonstrates that Si feedstock which would feature Ti concentrations equal or higher than 6 ppm wt cannot be used for the fabrication of industrial solar cells.

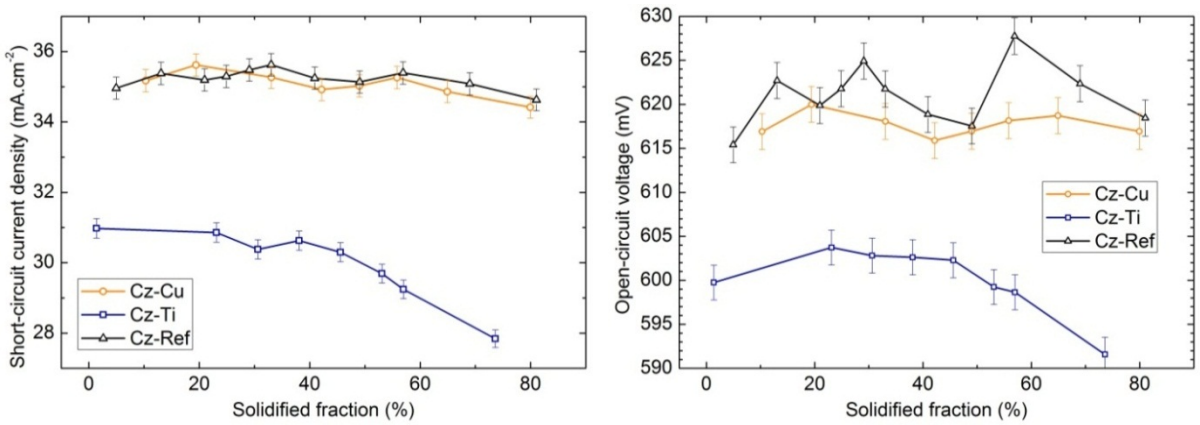

Figure 4.15 – Short-circuit current density (J_{sc}) and open-circuit voltage (V_{oc}) of the fabricated solar cells as a function of the solidified fraction of the corresponding wafers. The solid lines are only guides to the eyes.

4.6 Dark reverse J-V characteristics

The dark reverse J-V (current density – voltage) measurements of all solar cells (contaminated and non-contaminated), fabricated from wafers initially located in the bottom, middle and top parts of the ingots are shown in Figure 4.16. For the range of studied reverse voltages, the hard breakdown of the Cz-Si cells fabricated in the frame of this thesis could not be observed. Figure 4.16 shows also for comparison the dark reverse J-V characteristic of a highly doped multicrystalline Si solar cell ([B]=3×10^{17} cm^{-3}, [P]=2×10^{17} cm^{-3} [11]), which features a low (in absolute value) hard breakdown voltage (V_{bd}) of about 13 V. Our experimental results are consistent with the value computed from the approximate universal expression for V_{bd} presented in chapter 1, that for a [B] of 10^{16} cm^{-3}, would lead to V_{bd} = -68 V. The main result is that the Cz-Si cells fabricated in the frame of this thesis feature absolute V_{bd} values higher than 12 V. Therefore, despite the large intentional contaminations of the feedstock by Cu or Ti, they fulfil one of the main industrial requirements regarding the dark reverse I-V characteristics of the PV solar cells ($|V_{bd}|$>12 V).

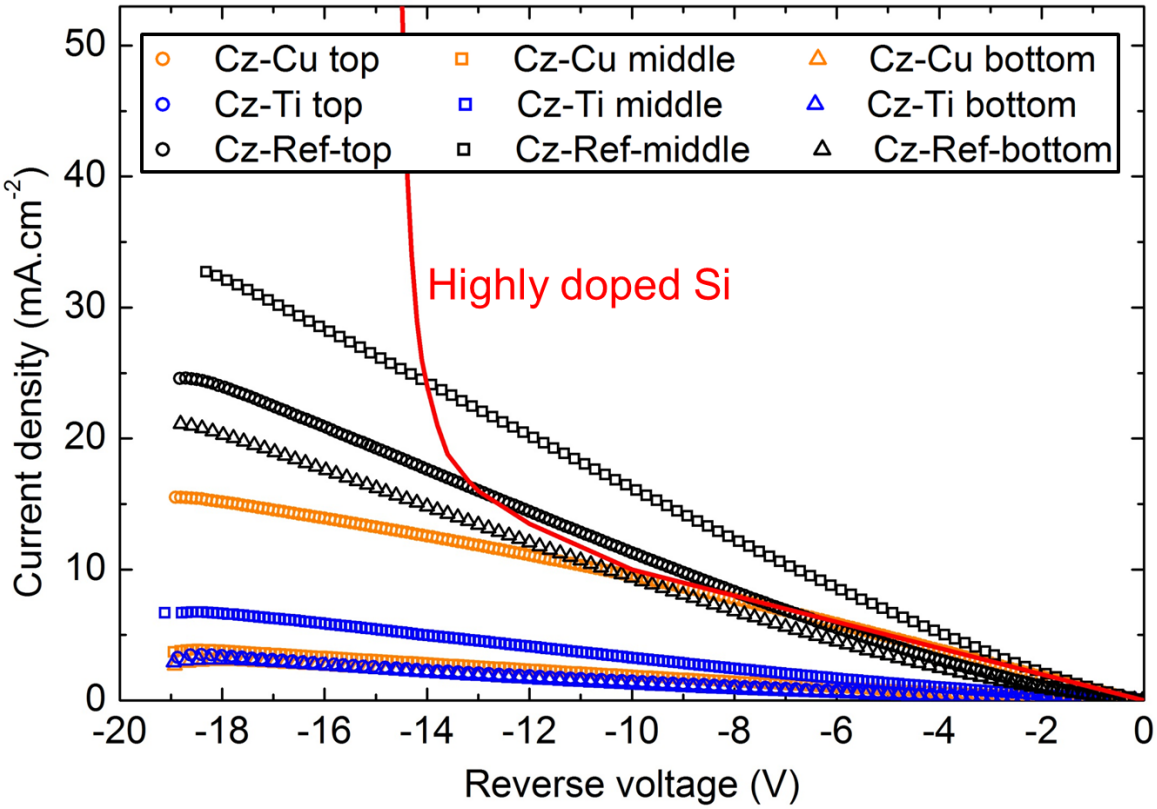

Figure 4.16 – Dark reverse J-V characteristics of the Cz-Cu, Cz-Ti and Cz-Ref solar cells and comparison with a standard multicrystalline Si solar cell fabricated from a highly doped (and compensated) silicon wafer.

Notice that for a given reverse voltage, large variations of the current density are observed for the studied cells, which are well correlated with the *FF* of the solar cells. Particularly we showed that the lower the *FF*, the higher the leakage current. Indeed, the low *FF* of the fabricated cells, due to the non-optimized solar cell fabrication process, where essentially due to shunt issues (probably located under the metal grid, because of *Ag* particles which would be present throughout the space charge region). These shunt issues under reverse bias increase the leakage current of the solar cells.

4.7 Evolution of the photovoltaic performances under illumination

Solar cells fabricated from wafers from the bottom parts (last solidified fractions, about 75 %) of the ingots were placed on a hot plate under a halogen spot with an illumination level of 0.05 W.cm^{-2} at 60 °C. The V_{oc} were monitored in order to evidence possible light-induced degradation (LID) effects (Figure 4.17). When the V_{oc} presented stable values, the illumination was stopped.

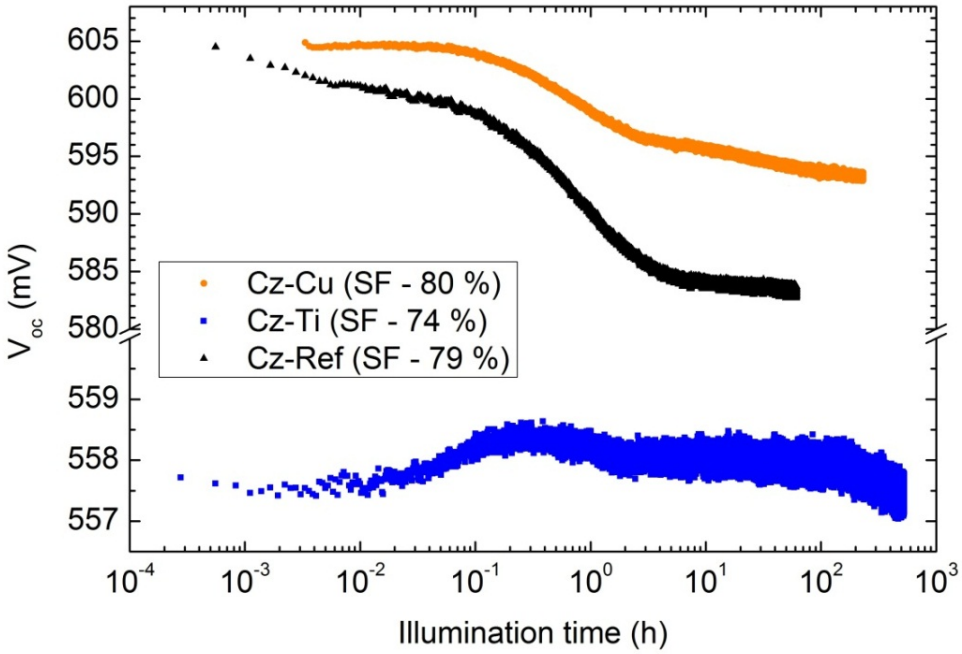

Figure 4.17 – Evolutions of the V_{oc} under illumination for Cz-Cu, Cz-Ti and Cz-Ref solar cells fabricated with wafers from the last solidified fractions of the Cz ingots.

We can notice first a strong decrease of the V_{oc} for the Cz-Cu and Cz-Ref solar cells, probably due to the activation of the B-O related complexes, commonly observed in B-doped samples. The associated efficiency losses for Cz-Cu, Cz-Ti and Cz-Ref solar cells after the aging tests, were equal to 4.8 %, 1.5 % and 9.4 %, respectively. For the Cz-Ref and Cz-Si samples, such strong degradations were expected since the $[O_i]$ for these samples was about 7.8×10^{17} cm^{-3}. From the empirical expression given by Bothe *et al*. [12], the τ dominated by the B-O related complexes (τ_{BO}) can be computed from the $[O_i]$ and [B] values.

$$\tau_{BO} = n \times 7.675 \times 10^{45}[B_s]^{-0.824}[O_i]^{-1.748} \quad (4.1)$$

The beneficial effect of a standard diffusion step on τ_{BO} is taken into account here by setting n to 2, as experimentally determined in [12]. Thus, for the studied samples, τ_{BO} is equal to 62 µs. For the Cz-Ref and Cz-Cu cells from the last solidified part of the ingots, the measured τ_{eff} (after the P-diffusion) are around 70 µs. Assuming that these τ_{eff} are equal to the initial bulk carrier lifetime (τ_{bi}), from the Matthiessen's law and the τ_{BO} value, it is possible to estimate the bulk carrier lifetime at the end of the degradation (τ_{bf}) which would be about 32 µs. Consequently, strong decreases of the bulk carrier lifetime are expected under illumination (from 70 µs to 32 µs), in good agreement with the significant decreases of the V_{oc} we

highlighted (the V_{oc} depending on τ_{eff}). The fact that the decrease of the V_{oc} is higher for the Cz-Ref is not understood since both samples (Cz-Ref and Cz-Cu) have virtually the same [O_i]. This is even more surprising since Cu is known from the literature to induce specific LID effects. However, again from an application oriented perspective, this is an important result which demonstrates that the presence of Cu has not a significant influence on the observed degradations.

Regarding the Cz-Ti cell, we did not observe degradations of the V_{oc}. The measured τ_{bi} was only about 10 µs, due to the strong negative impact of the Ti contamination on the carrier lifetime. Therefore the estimated τ_{bf} would be equal to 8.6 µs. τ_{bi} and τ_{bf} being similar, it can be stated that the activation/formation of the B-O related defects under illumination is not a dominant factor for the PV performances of the Ti-contaminated cells.

Conclusion

One of the main results of this chapter is related to the fact that the addition of 9 ppm wt of Cu into the Si feedstock does not affect the PV conversion efficiency of Czochralski Si solar cells. In addition, for these cells the breakdown voltage fulfills the widely accepted industrial requirement and we did not highlight additional effects of the Cu-contamination on the amplitude of the PV losses under illumination. This tolerance regarding the Cu contamination is mainly due to the fact that the incorporated Cu concentrations within the ingot were significantly below the expected values (this would be essentially due to the agglomeration/exo-diffusion of Cu at the surfaces of the ingot). Furthermore the carrier lifetime values of the Cu-contaminated samples were slightly improved by the external gettering effect developed by the P-diffusion.

On the other hand the addition of 6 ppm wt of Ti strongly affects the PV conversion efficiency of Czochralski Si solar cells. This is explained by the fact that due to its inability to precipitate (low diffusivity), Ti is essentially present as interstitial atoms, state for which Ti features harmful recombinant properties. Furthermore, again because of its low diffusivity, the carrier lifetime of the Ti-contaminated samples was not increased by the P-diffusion. In addition the electrical properties of the Ti contaminated samples were not improved by the hydrogenation treatment.

The hard breakdown voltages of both, Cu- and Ti-contaminated cells, systematically fulfilled the industrial requirement regarding this parameter.

Chapter 4 – Bibliography

1. J.R. Davis, A. Rohatgi, R.H. Hopkins, P.D. Blais, P. Rai-Choudhury, J.R. McCormick, H.C. Mollenkopf, Impurities in Silicon Solar Cells. IEEE Trans. Electron. Devices. 27, 677 (1980).
2. J.A. Burton, R.C. Prim, and W.P. Slichter, The distribution of solute in crystals grown from the melt. Journal of Chemical Physics. 21, 1987 (1953).
3. J.P. Garandet, New determinations of diffusion coefficients for various dopants in liquid silicon. International Journal of Thermophysics. 28, 4, 1285 (2007).
4. N.D. Arora, J.R. Hauser, D.J. Roulston, Electron and hole mobility in silicon as a function of concentration and temperature. 29th IEEE PVSC. 292 (1982).
5. T. Buonassisi, M. Heuer, A.A. Istratov, M.D. Pickett, M.A. Marcus, E.R. Weber, Internal gettering by metal alloy clusters. Patent Pub. No.: US 2006/0289091 A1 (2006).
6. S. Knack, J. Weber, H. Lemke, and H. Riemann, Copper-hydrogen complexes in silicon. Phys. Rev. B. 65, 165203 (2002).
7. S. Dubois, O. Palais, M. Pasquinelli, S. Martinuzzi, C. Jaussaud, Influence of substitutional metallic impurities on the performances of p-type crystalline silicon solar cells: The case of gold. J. Appl. Phys. 100, 123502 (2006).
8. S. Wilking, A. Herguth, G. Hahn, Influence of hydrogenated passivation layers on the regeneration of boron-oxygen related defects. Energy Procedia. 38, 642 (2013).
9. R. Singh, S.J. Fonash, and A. Rohatgi, Interaction of low-energy implanted atomic H with slow and fast diffusing metallic impurities in Si. Appl. Phys. Lett. 49, 800 (1986).
10. G. Coletti, P.C.P. Bronsveld, G. Hahn, W. Warta, D. Macdonald, B. Ceccaroli, K. Wambach, N.L. Quang, and J.M. Fernandez, Impact of metal contamination in silicon solar cells. Adv. Funct. Mater. 21, 879-890 (2011).
11. S. Dubois, J. Veirman, N. Enjalbert, F. Tanay, and G. Raymond, Studies on compensated and UMG material and solar cells. 21st Workshop on crystalline silicon solar cells & modules: Materials and processes (2011).
12. K. Bothe, R. Sinton, and J. Schmidt, Fundamental Boron–Oxygen-related carrier lifetime limit in mono- and multicrystalline silicon. Prog. Photovolt: Res. Appl. 13, 287 (2005).

CHAPTER 5. INFLUENCES OF INTENTIONAL CU AND TI CONTAMINATIONS ON THE PROPERTIES OF MC-SI WAFERS AND SOLAR CELLS

In this chapter the influences of intentional contaminations of the Si feedstock by titanium (Ti) and copper (Cu), on the properties of *p*-type multicrystalline Si (mc-Si) wafers and solar cells, were evaluated and compared. The three 60 kg, 'G2' size mc-Si ingots grown for this study - a reference ingot without intentional contaminations by metal impurities (mc-Ref), a Cu contaminated ingot (mc-Cu) and a Ti contaminated ingot (mc-Ti) - were presented in the third chapter. Notice, that in order to highlight possible effects of the Cu contamination on the photovoltaic (PV) properties, we decided for this study to introduce 90 ppm wt of Cu in the Si melt, as compared to only 9 ppm wt of Cu for the growth of the Cu-contaminated Cz ingot (presented in the previous chapter, for which no significant effects of the Cu contamination were observed). Bricks were extracted from these ingots, and were cut into wafers with a surface area equal to 156×156 mm^2 and a thickness of about 200 μm.

5.1 Compositional properties of the studied wafers

On vertical cuts from all ingots, the interstitial oxygen (O_i) concentration ([O_i]) and the substitutional carbon (C_s) concentration ([C_s]) were measured by Fourier Transform Infrared Spectroscopy (FTIR) along the ingots' height. The experimental [O_i] and [C_s] variations along the height of all ingots are shown in Figure 5.1.

We can notice (Figure 5.1) that on the one hand [C_s] and [O_i] were slightly higher for mc-Ref than for mc-Cu and mc-Ti. Similar crucibles and coatings were used for the solidification of all ingots. However, the mc-Ref ingot was grown in another furnace with a slightly different time-temperature profile which could contribute to the slight differences for [C_s] and [O_i]. On the other hand, [C_s] and [O_i] were almost identical for mc-Cu and mc-Ti.

The Cu concentrations ([Cu]) were determined by both glow discharge mass spectroscopy (GDMS) and inductively coupled plasma mass spectroscopy (ICP-MS) analyses. Let us recall that those techniques give for a given impurity its total concentration, irrespective of its chemical state (dissolved, precipitated, ionized/neutral) within the Si bulk. The relative uncertainties associated with the GDMS and ICP-MS analyses were given to be about 20 % and 10 %, respectively.

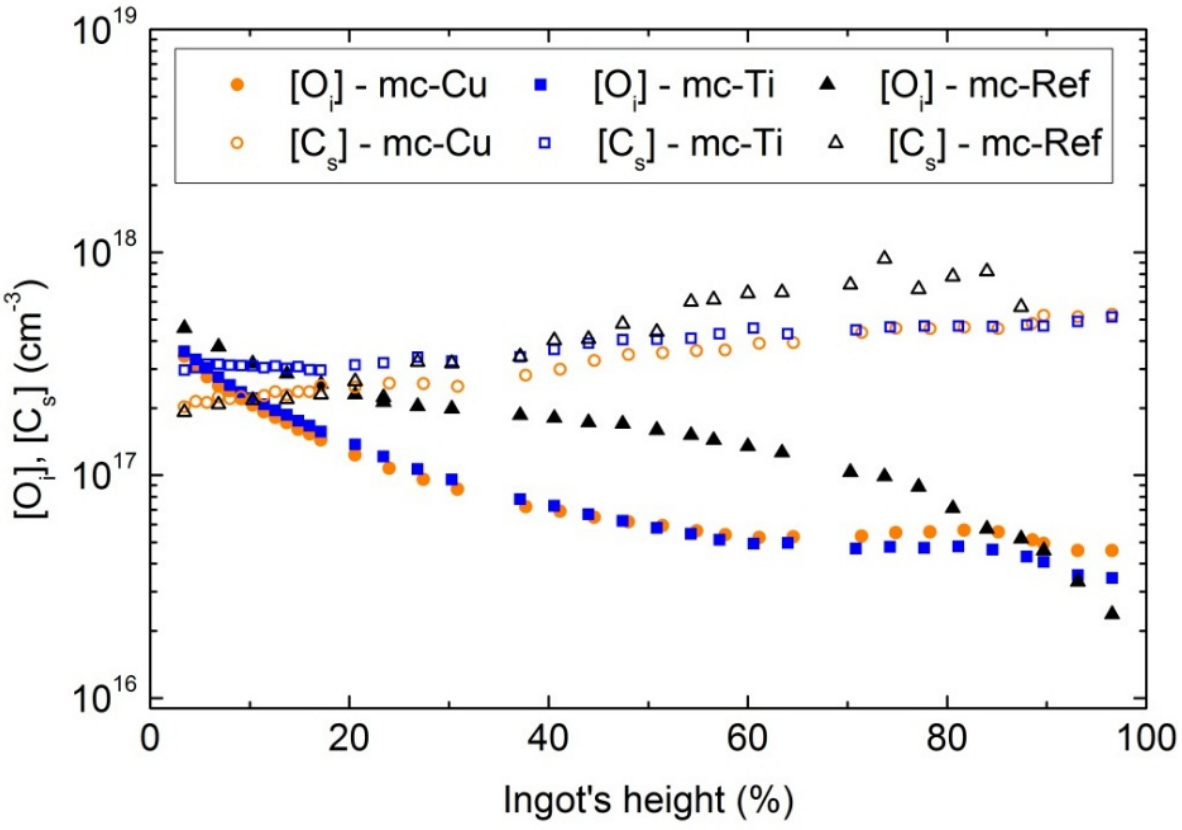

Figure 5.1 – [O_i] and [C_s] variations along the ingots' height.

Regarding Cu, we can notice that the [Cu] given by both the GDMS and ICP-MS analyses are in very good agreement (Figure 5.2). The experimental [Cu] were compared with the expected [Cu], calculated from Scheil's law, using for the segregation coefficient (k) the value given in [1] (k=4×10^{-4}), which corresponds to the Cu equilibrium segregation coefficient (k_{eq}). The experimental [Cu] values are slightly lower than the expected data. Furthermore, the experimental [Cu] do not significantly vary along the ingot's height (particularly between the middle and the top parts of the ingot). Indeed the [Cu] given by the GDMS analyses are similar for ingot's heights of 45 % and 85 %. This could be related to Cu evaporation from the melt and to the high Cu diffusivity in solid Si. Indeed during the ingot cooling, Cu is able to diffuse on few centimeters, which would contribute to the homogenization of the [Cu]. Interestingly, for the mc ingot the experimental and expected [Cu] values are in fair agreement whereas for the Czochralski (Cz) ingot they were significantly different. This could be due to the fact that during the cooling of the mc ingot, the exo-diffusion of Cu could be limited because of the presence of a coated crucible, and because of the larger length along which the Cu atoms have to migrate before reaching the ingot surface (about 90 mm from the center of the mc ingot to the free surface, against about 50 mm from the center of the Cz ingot to the surface). In addition [Cu] in mc-Ref were

measured by ICP-MS for different locations along the ingot's height (figure 5.2). The trend seems to follow Scheil's law, again with a small deviation towards lower values. Interestingly enough, Cu was also detected in mc-Ref but the [Cu] were significantly lower than the [Cu] in mc-Cu. The observed presence of Cu is probably associated with the use of a low purity silica crucible and its silicon nitride coating.

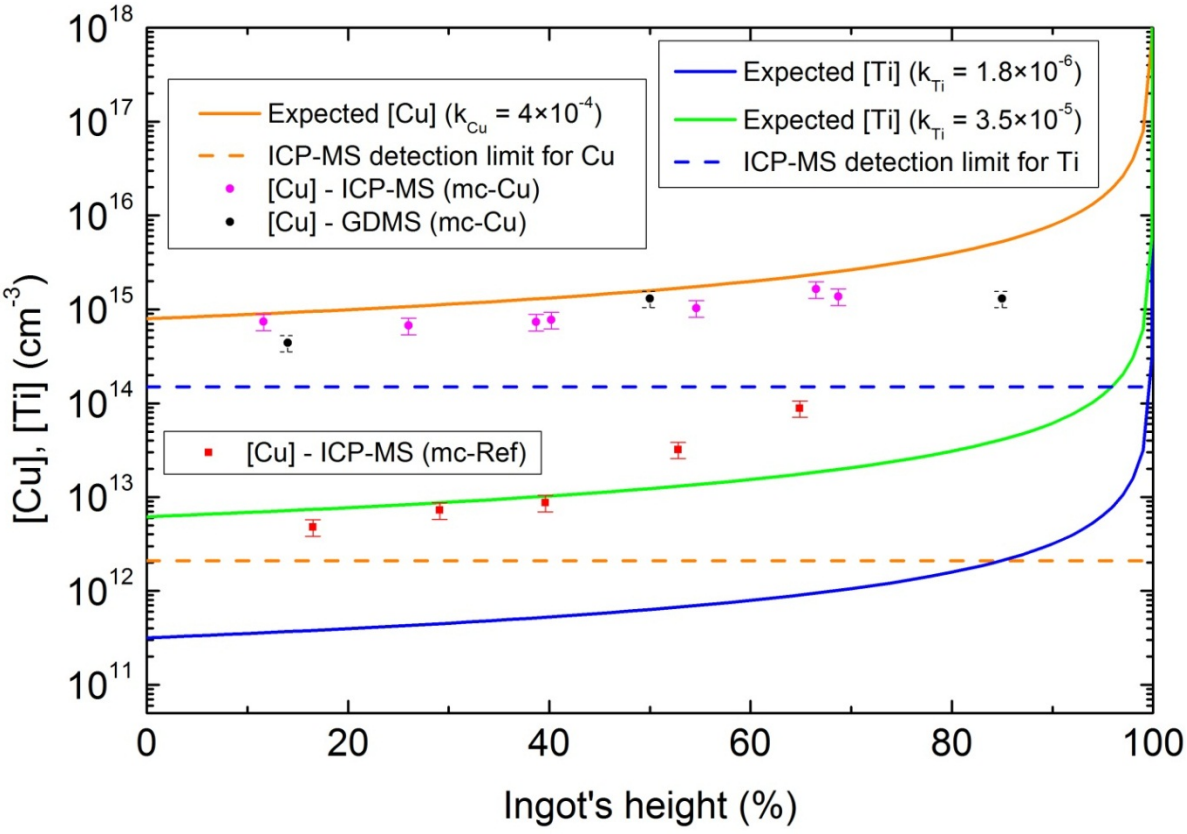

Figure 5.2 – [Cu] and [Ti] variations along the ingots' height. For Cu, both the expected and experimental [Cu] are represented. For Ti, only the expected [Ti] are represented.

On the other hand the presence of Ti could not be detected by ICP-MS or secondary ion mass spectroscopy (SIMS) analyses. This is in fair agreement with the expected Ti concentrations ([Ti]), calculated from Scheil's law with a k_{eff} equal to 1.8×10^{-6} [2] or with a k_{eff} equal to 3.5×10^{-5} [3]. Both k_{eff} values used for the calculation of the [Ti] were experimentally determined from analyses conducted on deliberately contaminated mc-Si ingots obtained by directional solidifications. For the selected wafers, the expected [Ti] should be systematically below (Figure 5.2) the detection limits (DL) of the ICP-MS analyses (DL about 10^{14} cm^{-3}).

5.2 Resistivity

Some wafers were collected at regular intervals along the ingots' height and the resistivity (ρ) were measured using a four-point probe setup and averaged over 25 positions across the wafer surface. The expected ρ variation was calculated using the B concentrations ([B]) and the corresponding mobility (μ) values. The [B] variation (and therefore the majority carrier density variation) was calculated via the Scheil's law, with k_{eff} = 0.8 (the k_{eff} value being here equal to the equilibrium segregation coefficient) [1]. The Arora's model was used for the computation of the μ [4]. Calculated and experimental ρ variations along the ingots' height are shown in Figure 5.3.

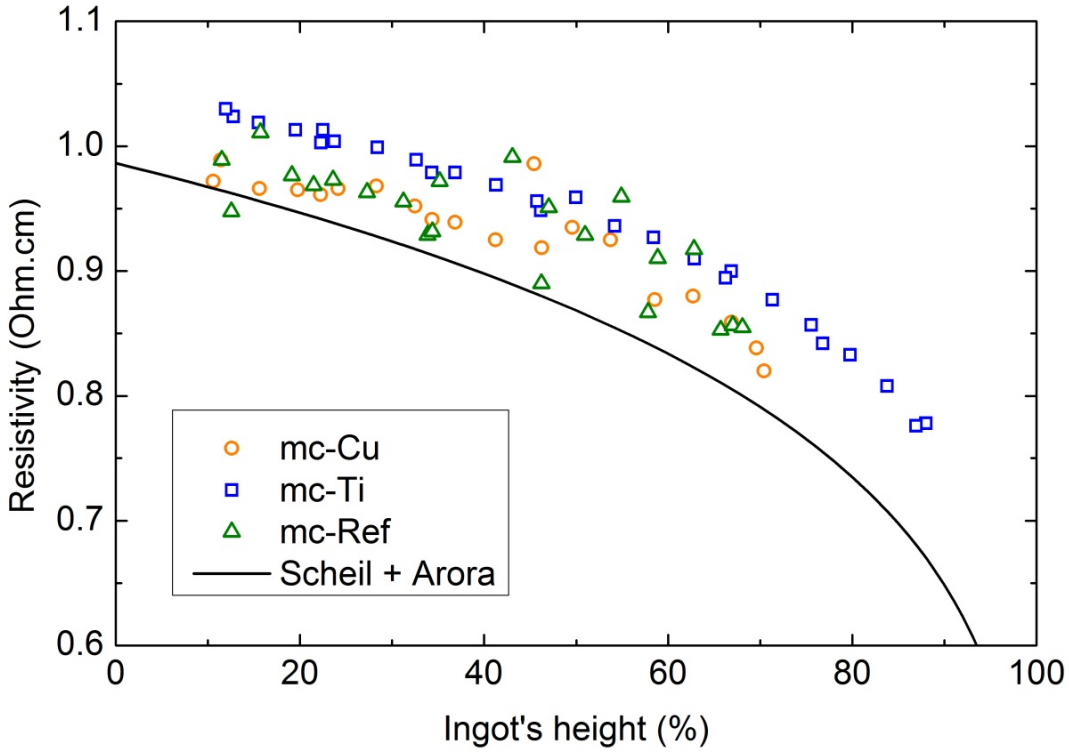

Figure 5.3 – Resistivity variations along the ingots' height. The solid line corresponds to the computed values, via the combination of the Scheil's law (for determining the B content, and therefore the hole density) and the Arora's model (for computing the hole mobility).

The experimental ρ values are for all three ingots in good agreement. This is particularly crucial regarding our study since the B content (and the corresponding hole majority carrier density) strongly influences the properties of the solar cells (e.g., the *p-n* junction barrier height). Therefore it was particularly important in order to assess the effect of an impurity, to be able to compare for a given solidified fraction, uncontaminated and

contaminated wafers with the same B concentration. Regarding the comparison with expected values, as already noticed in chapter 4, the slight discrepancy between the experimental ρ and the calculated values could be explained by a slight evaporation of B atoms from the Si melt during the growth of the ingots.

5.3 Effect of the contaminations on the effective carrier lifetime – Influence of the P diffusion step

Effective carrier lifetime (τ_{eff}) measurements were done on as-received and P-diffused wafers. The wafers experienced chemical polishing steps (before the P diffusion in order to remove the surface region affected by the sawing step and then after the P diffusion in order to remove the n^+ emitter), and the surfaces were electrically passivated by hydrogenated Si nitride (SiNx:H) layers deposited by PECVD (plasma-enhanced chemical vapor deposition). Then τ_{eff} were measured by quasi-steady state photoconductance decay (QssPC) analyses and mapped via the micro-wave photoconductance decay (μW-PCD) technique.

The τ_{eff} variations along the ingots' height are shown in Figure 5.4, for the mc-Ref ingot, the mc-Ti ingot and the mc-Cu ingot. In order to limit the influence of the minority carrier trapping on the QssPC analyses, which essentially occurs for low excess carrier densities (Δn) (i.e., for Δn lower than 3×10^{14} cm^{-3} for the studied samples), the τ_{eff} data presented in Figure 5.4 were extracted for a Δn equal to 3×10^{15} cm^{-3}.

Unexpectedly, the highest τ_{eff} are measured for the Cu-contaminated samples, despite the large Cu content introduced in the feedstock. The τ_{eff} of the Cu-contaminated wafers were improved by the P-diffusion, with values approaching 100 μs after the P-diffusion. The τ_{eff} of the Cu-contaminated samples, after the P-diffusion step, are rather uniform over the height of the ingot. Let us recall that an opposite conclusion had been drawn in chapter 4 for the case of single-crystalline wafers where the carrier lifetime improvement had been shown to be very limited. The difference could be due to the extraction of other fast diffusers, e.g. Fe [5], likely to be met in mc-Si materials. Such a hypothesis is supported by the results obtained on the reference wafers, that also exhibit a significant carrier lifetime increase, especially at solidified fractions above 40 %.

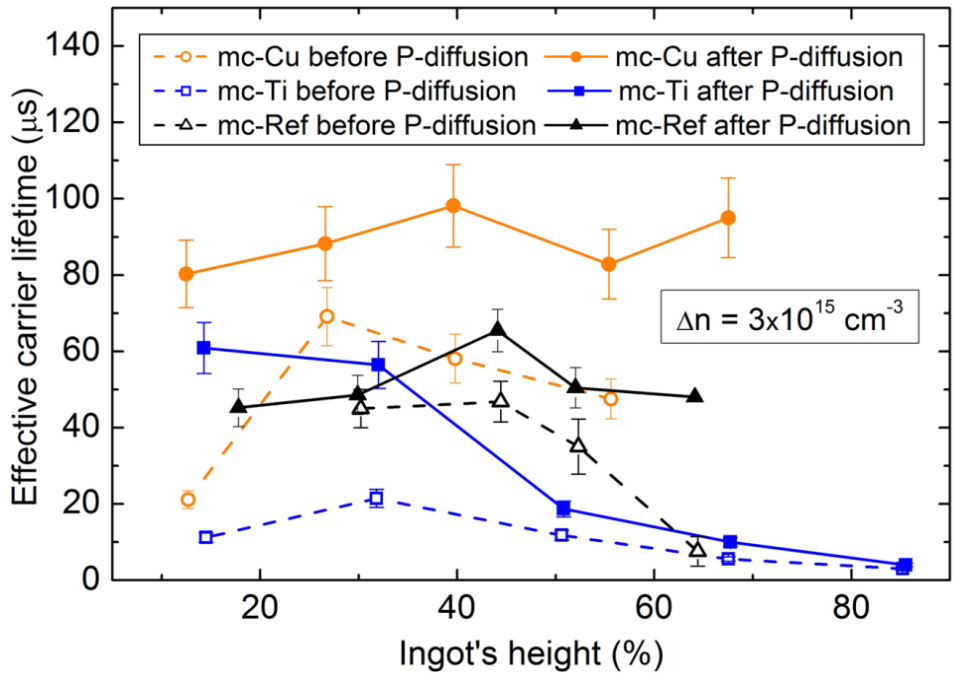

Figure 5.4 – Variations of the effective carrier lifetimes along the ingots' height for mc samples before and after the P-diffusion step. The values were extracted for an excess carrier density equal to 3×10^{15} cm^{-3}. The solid and dotted lines are only guides to the eyes.

The positive effect of the P diffusion in mc-wafers is also highlighted by µW-PCD measurements. Indeed the τ_{eff} measured on the P-diffused samples (τ_{diff}) and the as-received wafers (τ_{init}) were mapped. The obtained τ_{init} and τ_{diff} mappings, for mc-Ref and mc-Cu samples initially located in the middle part of the ingots, are shown in Figure 5.5 and Figure 5.6, respectively. For both, the reference samples and the Cu-contaminated samples, τ_{init} values were significantly improved by the P-diffusion, since they were multiplied by about 2.

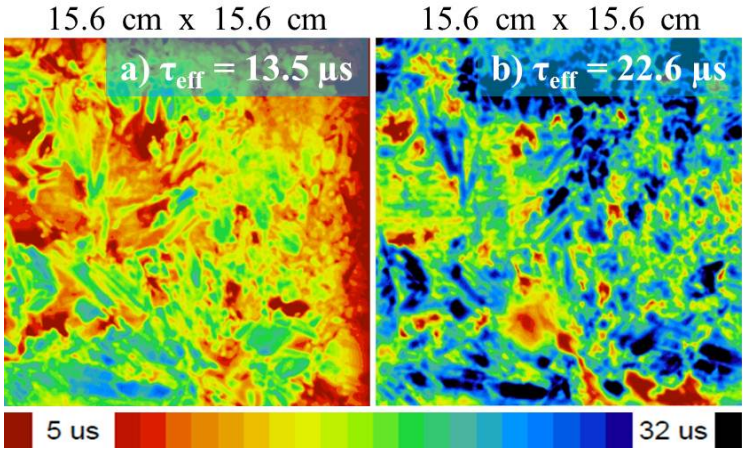

Figure 5.5 – τ_{eff} mapping obtained on as-received (a) and P-diffused (b) twin wafers from the mc-Ref ingot (52 % of the ingot's height). The indicated values (in white), are the average values.

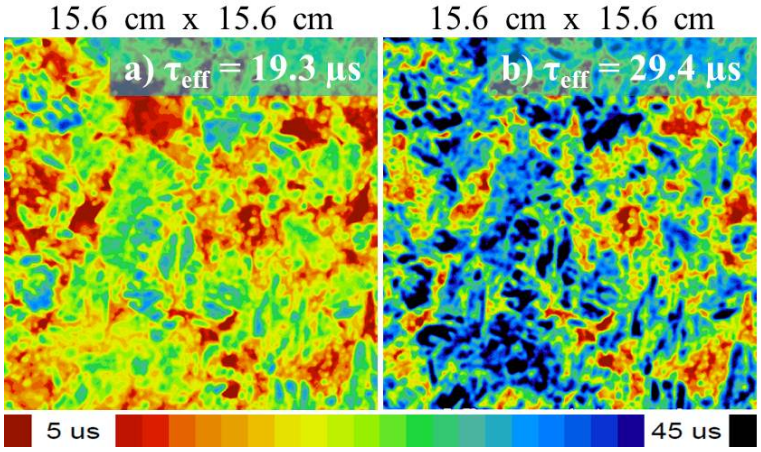

Figure 5.6 – τ_{eff} mapping obtained on as-received (a) and P-diffused (b) twin wafers from the mc-Cu ingot (52 % of the ingot's height). The indicated values (in white), are the average values.

In order to confirm the suggested extraction of the fast-diffusing metal impurities by the external gettering effect developed by the P diffusion step, *sister* wafers from the Cu contaminated ingot, without and with a P diffusion step, were analyzed by ICP-MS (Table 5.1). Notice that for the P-diffused wafer, the n^+ emitter was removed before the Si *digestion* procedure required for the ICP-MS analyses. After the P diffusion step, the [Cu] were below the detection limit. Similar results were obtained for Ni which is also a fast diffusing element in Si. On the other hand, the Ge content (slow diffusing element) was virtually unchanged. Therefore these complementary chemical analyses confirm the key role played by the P diffusion step, for the extraction of fast diffusing species atoms from the Si bulk.

The fact that the τ_{eff} values of the Cu-contaminated mc wafers were higher than the values found for the reference mc wafers is not fully understood. This could be explained, as proposed in the literature, by the fact that during the cooling of the Cu-contaminated ingot, liquid Cu silicides could develop internal gettering effects [6], trapping other metal impurities (e.g., Fe, Cr, …). However, such a positive effect of the Cu contamination on the electrical properties of multicrystalline ingots should be confirmed on a larger number of ingots.

Table 5.1 – Determined Cu, Ni and Ge concentrations (by ICP-MS) in sister Cu-contaminated mc wafers, without and with the P diffusion step. The values found for [Ge] are presented in order to highlight the reproducibility of the ICP-MS analyses, since Ge is an element that cannot be extracted by external gettering effects.

Ingot's height (%)	[Cu] (ppb wt)		[Ni] (ppb wt)		[Ge] (ppb wt)	
	without P-dif	with P-dif	without P-dif	with P-dif	without P-dif	with P-dif
39	33.43	<0.08	0.07	<0.08	10.21	11.56
67	74.27	<0.08	0.11	<0.08	14.09	13.85

On the other hand, the Ti contamination, despite the low expected Ti concentrations in the Si bulk (around 10^{12} cm^{-3}), strongly affects the τ_{eff}. The low τ_{eff} for the Ti contaminated sample are again probably explained by the fact that Ti would essentially be present as interstitial atoms, state for which Ti features harmful recombinant properties. Before the P-diffusion step, the τ_{eff} of the Ti-contaminated samples are below 25 µs along the entire height of the ingot. For the P diffused samples, the τ_{eff} of the Ti-contaminated samples decreases along the ingot's height, which is probably related to increases in the Ti concentration, due to segregation effects. As expected, due to the low Ti diffusivity, the τ_{eff} of the Ti-contaminated wafers from the middle and top part of the ingots, are not improved by the P diffusion. However, unexpectedly, we highlighted a significant increase of the τ_{eff} after the P diffusion step for the Ti-contaminated wafers from the bottom part of the ingot. For instance for an ingot's height of 32 %, the measured τ_{eff} before and after the P diffusion step are equal to 20 µs and 60 µs, respectively. Reasons for such an increase are not completely clear. Firstly, issues with the surface passivation of the non-diffused samples cannot be totally ruled out. Secondly, the bottom part of this ingot could be contaminated by high levels of fast diffusers (e.g. Fe, Cr, Co) externally gettered by the P diffusion step. Eventually, internal gettering effects (i.e., precipitation) of a low amount of Ti atoms along crystallographic defects or within intermetallic alloys during the P diffusion step could occur, which would allow increases of the τ_{eff} only for the parts of the ingot with the lowest Ti concentrations.

It is particularly interesting to focus on the variations of τ_{eff} with Δn (Figure 5.7). Indeed, unlike the data obtained with the single-crystalline samples, the QssPC data of some multicrystalline samples can be influenced by minority carrier trapping (strong increases of τ_{eff} at low Δn). This is particularly visible on Figure 5.7 for the *as-received* Cu contaminated wafer, whereas the QssPC data obtained for the reference sample are not significantly influenced by minority carrier trapping. Therefore large Cu concentrations in *p*-type mc Si do not affect the charge carrier lifetime, but can be responsible for electron trapping effects. Further studies regarding this Cu-related trapping effect will be presented within the 6th chapter of this manuscript.

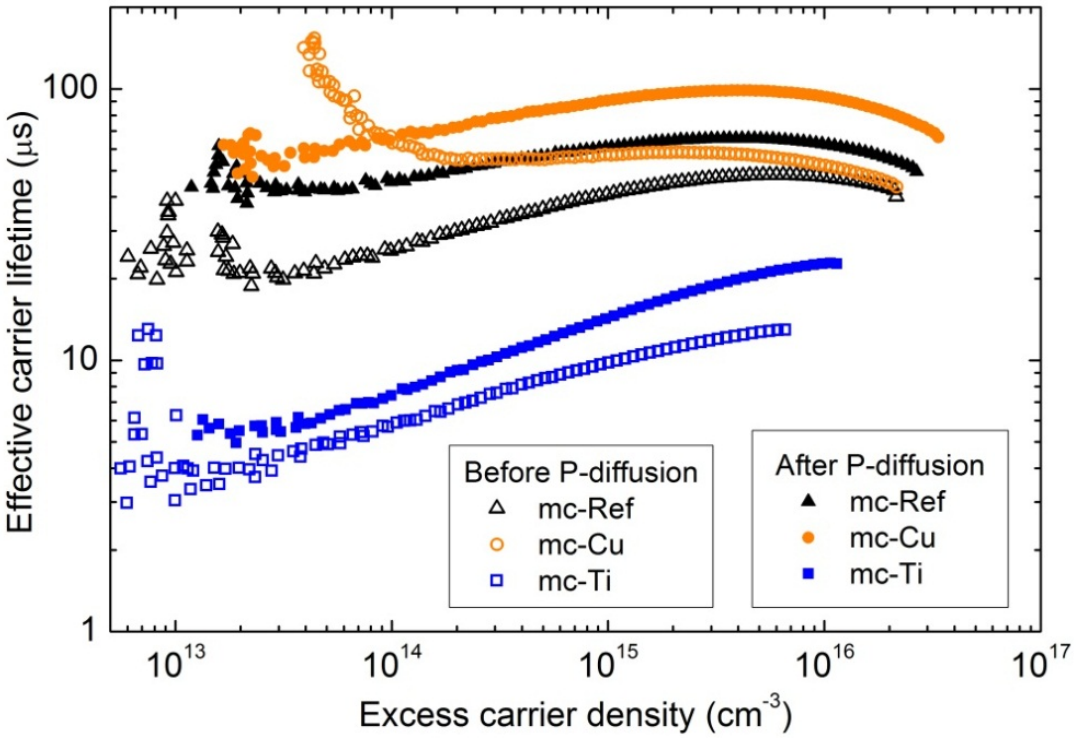

Figure 5.7 – Variations of the effective carrier lifetime with the excess carrier density. mc-Ref, mc-Cu and mc-Ti wafers from a similar ingot's height (~50 %), before and after a P-diffusion step.

Also, in good agreement with the data obtained for the Cz-Si wafers, the τ_{eff} of the reference and Cu-contaminated samples do not significantly vary with Δn, whereas the τ_{eff} of the Ti contaminated samples strongly depend on Δn. Indeed after the P diffusion step, from Δn=2×10^{13} cm^{-3} to Δn=10^{16} cm^{-3} τ_{eff} are only multiplied by 1.5 for the Cu contaminated sample, whereas τ_{eff} are multiplied by 4.2 for the Ti contaminated sample. The P-diffused Ti contaminated sample features very low τ_{eff} at low Δn (e.g., about 5 µs for a Δn equal to 2×10^{13} cm^{-3}, sample from the middle part of the ingot). Therefore, the Ti contaminated mc solar cells should have very low short-circuit current densities (J_{sc}), since this parameter is associated with low Δn, in the range 10^{12}-10^{13} cm^{-3}.

5.4 Effect of the Si hydrogenation on the electron diffusion length

It is known that hydrogen can interact with defects (extended and point defects) in silicon. Particularly some harmful impurities in Si (e.g., iron, gold), can be electrically passivated by H atoms. Therefore it is important to investigate the influences of the Si bulk hydrogenation on the electrical properties of the Cu- and Ti-contaminated mc wafers. The source of hydrogen is provided by the anti-reflection coating layer of the cell (SiNx:H). As

already mentioned in chapter 4, it is particularly important to investigate the possibility of passivating Ti with hydrogen since this impurity significantly affects the carrier lifetime.

For this experimental study, 6 wafers from each ingot were selected (2 adjacent wafers from the upper, middle and lower parts of the mc-Cu and mc-Ti ingots) and 20 wafers from the reference ingot were used for the optimization of the metallization firing step. Half of the wafers experienced a standard solar cell fabrication process with the SiNx:H layer and the others were fabricated without SiNx:H layer (therefore without source of H). The Current-Voltage (I-V) characteristics under illumination of the fabricated cells were measured. Similarly to what had been observed for the Cz samples in chapter 4, due to their higher front surface reflectance, the solar cells without SiNx:H layers featured low PV conversion efficiencies. Nevertheless the goal of this study was not to obtain solar cells with good performances, but *simply* to fabricate functional solar cells without SiNx:H (fill factor higher than 65 %) in order to extract the effective electron diffusion lengths (L_{eff}) via the combination of light beam induced current (LBIC) measurements and reflectance measurements done at various infra-red wavelengths. Indeed, the used screen-printed pastes, the metallization firing treatment, were developed for standard cells with the SiNx:H layer, therefore the fabrication of cells without these layers is not so obvious. Then the efficiency of the hydrogen passivation could be evaluated by comparing the L_{eff} for cells from the same location along the ingot's height, with and without SiNx:H layers.

Figures 5.8 and 5.9 present the L_{eff} values determined on mc-Cu and mc-Ti solar cells fabricated from twin wafers, with and without the presence of a SiNx:H layer. The ratio (r_H) between the L_{eff} measured on the cell with the SiNx:H layer and the L_{eff} measured on the cell without the SiNx:H layer was then computed and mapped. In parallel, is shown a reflectance mapping, revealing the grain structures of the studied samples (since an anisotropic KOH texturation step was used). A point that should be stressed concerns the fact that the analytical method for determining the electron diffusion length assumes flat surfaces. Indeed, the textured surfaces deviating the incident light beam, the average depth at which the carriers are photo-generated cannot be precisely estimated. To overcome this issue, the determined L_{eff} is multiplied by a corrective factor defined by the equipment manufacturer for KOH texturation on (100)-oriented Si wafers, computed on the base of numerical simulation results. However, for multicrystalline Si, the dependence of this corrective factor with the grain orientation is not taken into account, which affects the L_{eff} comparison from grain to grain. However, as for this specific study, we compare L_{eff} mappings for twin wafers (with and without the SiNx:H), which have exactly the same grain structure, relevant conclusions can be drawn.

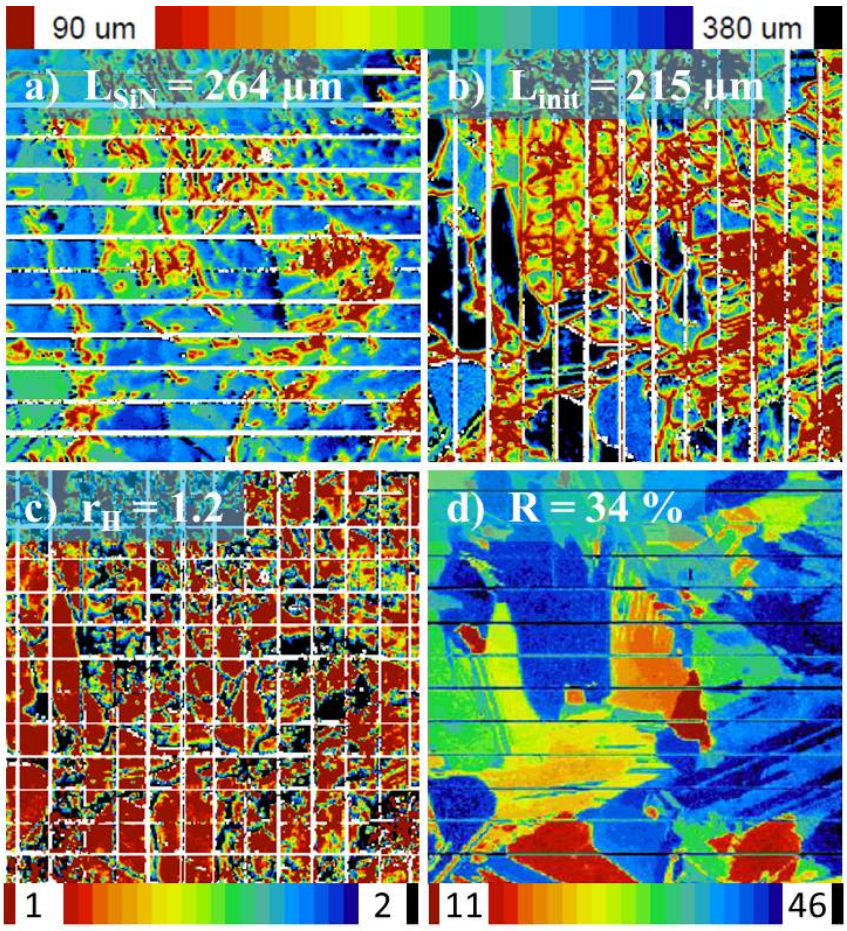

Figure 5.8 – L_{eff} mappings obtained on Cu-contaminated solar cells with (a) and without (b) the SiNx:H layer (wafers from the middle part of the ingot). c) Mapping of the ratio (r_H) between the L_{eff} measured on the samples with and without the SiNx:H layer. d) Reflectance mapping (unit in %) obtained with an incident monochromatic light with a wavelength equal to 406 nm. The indicated values (in white) are the average values, except the value given for r_H, which is simply the ratio between the average L_{SiN} and L_{init} values.

The raw results show (Figure 5.8 for the wafers from the middle part of the ingot) that the bulk hydrogenation improved the overall bulk electrical properties of the mc-Cu sample since the average L_{eff} was multiplied by about 1.2 via the presence of the SiNx:H layer (similar conclusions were obtained for the samples from the bottom and top parts of the ingot). On the one hand, the presence of an H source significantly enhanced the quality of the grain boundaries and the regions where dislocations clustered during the crystallization stage. This could be particularly due to the electrical passivation by H of the dangling bonds present along such extended crystallographic defects. On the other hand, interestingly, within the poorly dislocated grains, the introduction of H atoms slightly degraded L_{eff}. This result is not fully understood but could be due to the formation of H-Cu complexes, which are known for introducing recombinant energy levels in the Si band gap [7].

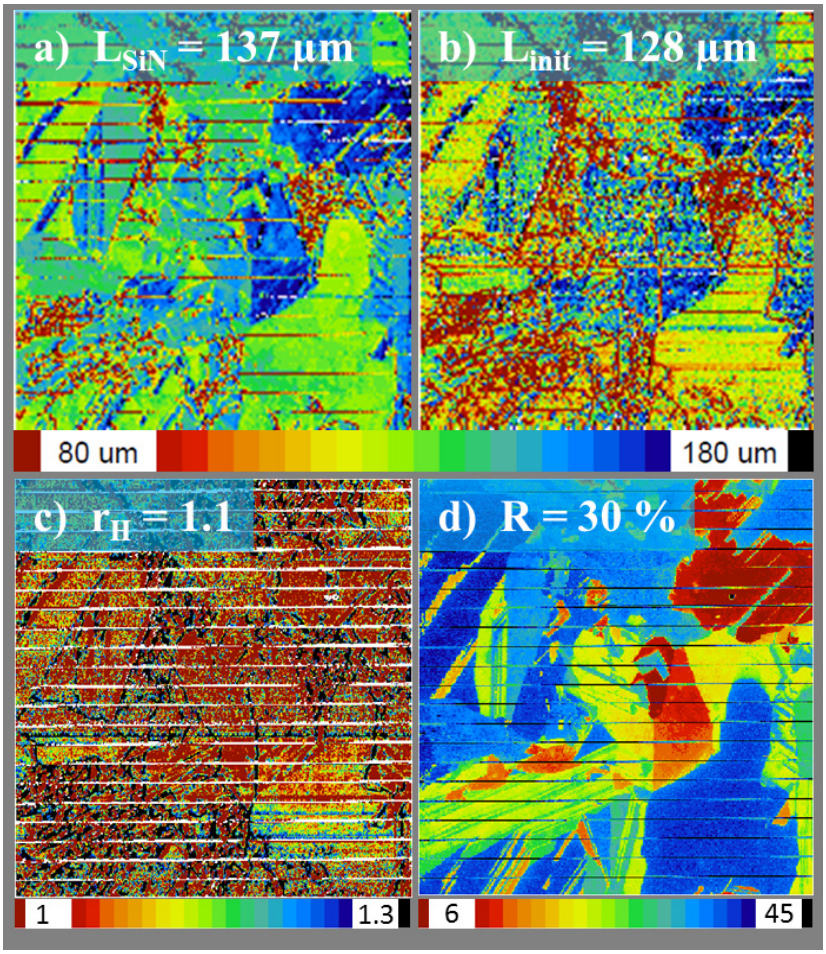

Figure 5.9 L_{eff} mappings obtained on Ti-contaminated solar cells with (a) and without (b) the SiNx:H layer (wafers from the middle part of the ingot). c) Mapping of the ratio (r_H) between the L_{eff} measured on the samples with and without the SiNx:H layer. d) Reflectance mapping (unit in %) obtained with an incident monochromatic light with a wavelength equal to 406 nm. The indicated values (in white) are the average values, except the value given for r_H, which is simply the ratio between the average L_{SiN} and L_{init} values.

As the dislocation-rich region are usually regions poorly sensitive to the main external gettering treatments, it confirms, as previously demonstrated [5], that the P-diffusion step and the bulk hydrogenation have complementary actions, which improve the overall Si bulk properties when the material is initially highly contaminated by fast diffusing metal impurities.

However this result has to be nuanced. Indeed, first the extracted L_{eff} for the Cu-contaminated cells are in the range of the wafer's thickness. Therefore the validity of the extracted L_{eff} is questionable (see chapter 4). In addition, as also mentioned in chapter 4, for such high L_{eff} the comparison of the data obtained with and without SiNx:H layers can be affected by parasitic contaminations occurring during the firing step. Indeed, this treatment is done in a metal-rich environment and the SiNx:H layer would act as a contamination barrier layer, protecting the quality of the Si bulk. Without this layer, the unintentional in-diffusion of

impurities could be enhanced. These impurities, event present at low density, could affect the L_{eff} of initially high quality samples, and therefore could alter the evaluation of the specific effects of the bulk hydrogenation.

Regarding Ti (Figure 5.9 for wafers from the middle part of the Ti contaminated ingot), the obtained L_{eff} are below the thickness of the wafer and therefore the L_{eff} comparisons are more relevant. Again, the presence of an H source improved the electrical quality of the grain boundaries and the regions where dislocations clustered during the crystallization stage. However, the L_{eff} of the cells with and without the SiNx:H layers are almost the same (similar conclusions were obtained for the samples from the bottom and top parts of the ingot). Eventually these results are in good agreement with previous studies from the literature [8], which argue that unlike other metal elements (e.g., Fe, Au), Ti atoms would not be electrically passivated by forming complexes with H. Let us mention that the other option discussed in chapter 4, namely that the diffusivity of H is limited in Cz wafers, cannot be invoked in the mc-samples discussed here.

5.5 Illuminated forward I-V characteristics

Around 10 wafers per ingot were sampled at regular intervals along the ingot's height and transformed into solar cells following an industrial process. Both surfaces were texturized by the anisotropic chemical attack developed by the KOH solution. The n^+ emitter was formed by phosphorus diffusion. Then SiNx:H layers used as antireflection coating layers were deposited on the front surfaces by PECVD. The silver front and aluminium rear electrodes were deposited by screen printing before rapid annealing. Junction opening was performed by laser cutting. The fabricated solar cells were characterized by illuminated forward and dark reverse I-V measurements. For the forward I-V measurements standard illumination and temperature were used (AM1.5G; 0.1 W.cm^{-2}; 25 °C). Notice that these measurements were performed without prior illumination. From these measurements the short circuit current (J_{sc}), the open-circuit voltage (V_{oc}), the fill factor (FF) and the PV conversion efficiency (η) were extracted.

Figure 5.10 presents the FF and the η of the fabricated solar cells, as a function of the initial location of the wafers along the ingots' height (i.e., solidified fraction). Firstly we can notice that for all ingots, the FF values, mainly governed by the quality of the solar cell fabrication process (e.g., emitter and metallization), were higher than 78.5 %. This means that

no major issues were met with the cell fabrication process and consequently, relevant comparisons can be made between the reference and the Cu- and Ti-contaminated samples.

The *FF* is essentially governed by the metallization technology, however it also depends on the electrical quality of the space charge region (*scr*), and therefore on the material quality. Particularly the lower the charge carrier lifetime within the *scr*, the higher the *p-n* junction recombination current density, and consequently the lower the *FF*. This is in good agreement with our experimental data. Indeed, for a given ingot's height, the lowest *FF* values are found for the Ti-contaminated cells, which feature the lowest carrier lifetime. Furthermore the *FF* of the Ti-contaminated cells slightly decrease over the ingot's height, in good agreement with the highlighted τ_{eff} decrease along the height of the Ti contaminated ingot.

Regarding the Cu contamination, the fact that the *FF* are not affected by the intentional large contamination is an important result. Indeed, as previously presented, Cu would essentially be present under the form of conductive Cu precipitates (silicides). Therefore as the *FF* is not affected by the presence of Cu, it means that the number of Cu precipitates throughout the *scr* (the width of the *scr* is estimated to be about 0.3 µm) should be very limited. Indeed, such precipitates, crossing the *scr*, would induce parasitic shunt effects, altering the *FF* values.

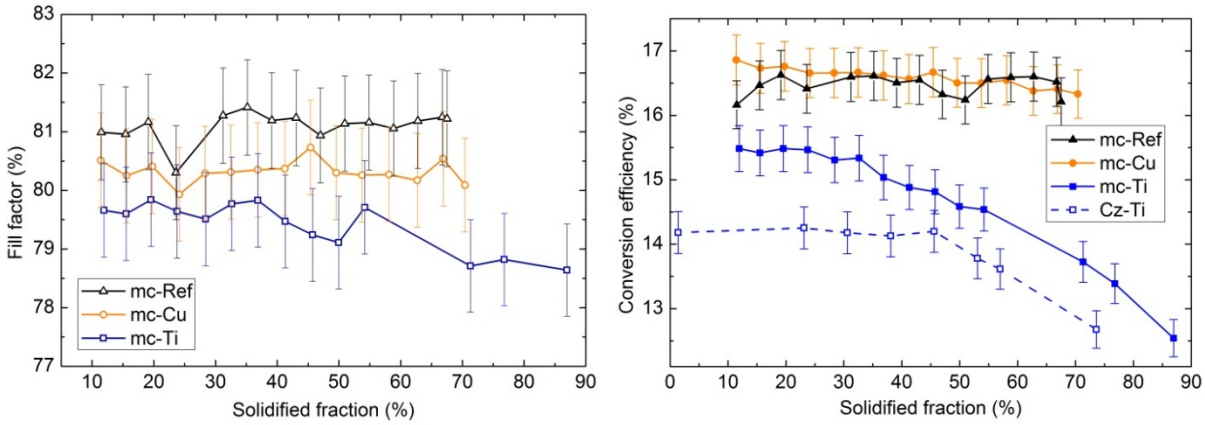

Figure 5.10 – Fill factor (FF) and conversion efficiency (η) of the fabricated solar cells as a function of the corresponding solidified fraction. The solid and dotted lines are only guides to the eyes.

Figure 5.11 presents the V_{oc} and the J_{sc} of the fabricated solar cells, as a function of the initial locations (solidified fraction) of the wafers along the ingots' height. In good agreement with the fact that the τ_{eff} were not affected by the Cu-contamination, similar V_{oc} and J_{sc} were extracted for both the reference and the Cu-contaminated solar cells. On the other hand, as expected from the τ_{eff} measurements, the Ti-contaminated solar cells had lower V_{oc} and J_{sc}

than the values found for the reference cells. For a solidified fraction of 50 %, the V_{oc} of the reference and Ti-contaminated cells are equal to 618 mV and 610 mV, respectively, and the J_{sc} values equal to 32.4 mA.cm^{-2} and 30.2 mA.cm^{-2}, respectively. The lowest J_{sc} and V_{oc} values for the Ti-contaminated cells are found for the cells fabricated with wafers from the last solidified fraction, in good agreement with the τ_{eff} measurements (the lowest τ_{eff} were measured for the samples from the last solidified fraction, due to the segregation of the Ti atoms during the growth of the ingot). Indeed the V_{oc} is essentially governed by two parameters, the *p-n* junction barrier height (which depends on the majority carrier density) and the charge carrier lifetime. Due to the high segregation coefficient of B, the majority carrier density can be considered as uniform along the studied height of the ingot. Therefore the V_{oc} variation is mainly dominated by the τ_{eff} variation, the lower the τ_{eff}, the lower the V_{oc}.

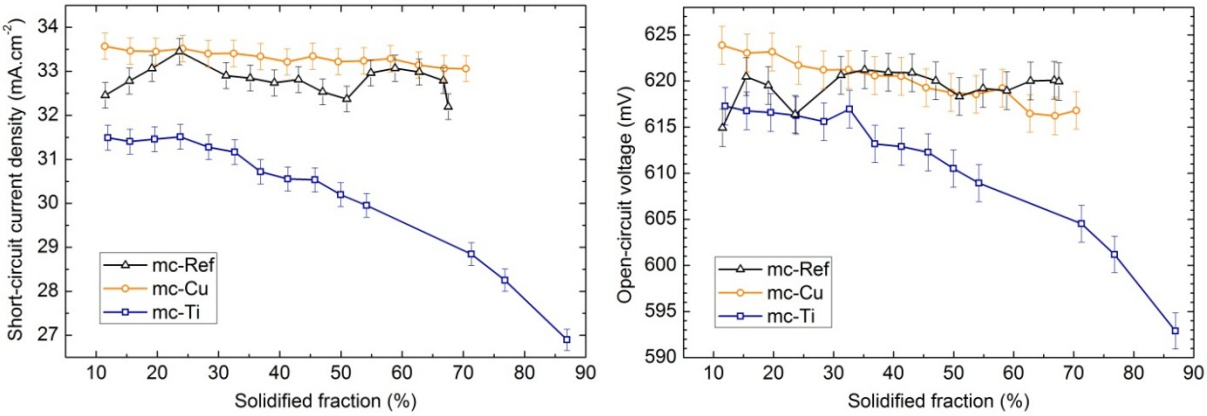

Figure 5.11 –Short-circuit current density (J_{sc}) and open-circuit voltage (V_{oc}) of the fabricated solar cells as a function of the corresponding solidified fraction. The solid lines are only guides to the eyes.

Regarding Cu, in contradiction with the results presented in [3], it is remarkable that the introduction of a very large amount of contamination (90 ppm wt) in the feedstock did not affect the η (Figure 5.9). The average η for the reference and the Cu-contaminated solar cells were equal to 16.5 % and 16.6 %, respectively. The highest measured η, around 16.8 % despite the KOH texturation not adapted to mc wafers, was even obtained for a Cu-contaminated cell.

On the other hand, essentially due to the low J_{sc} and V_{oc}, the η of the Ti contaminated cells are significantly lower than the values found for the reference (uncontaminated) and Cu-contaminated cells. For instance, for a solidified fraction of 50 %, the η of the reference and Ti-contaminated cells are equal to 16.2 % and 14.6 %, respectively. This is a very important result, since it demonstrates that Si feedstock which would feature Ti concentrations equal or

higher than 6 ppm wt cannot be used for the fabrication of industrial multicrystalline Si solar cells.

Regarding Ti, the comparison between the η of the Cz and mc cells is particularly interesting. Indeed, as shown in Figure 5.10, despite similar amounts of Ti introduced in the Si melt, the η of the the Ti-contaminated multicrystalline cells is significantly higher than the η of the Ti-contaminated Cz cells, despite a KOH texturation step which is not adapted for mc wafers. As an example, for an ingot's height of 20 %, the η of the mc and Cz Ti-contaminated cells are equal to 15.5 % and 14.2 %, respectively. This unexpected result is not fully understood, but it is supported by the fact that the τ_{eff} values of the Ti-contaminated wafers, which were higher for the mc samples (for a given solidified fraction and a given Δn). For instance, for a solidified fraction of 32 % and a Δn equal to 10^{15} cm^{-3}, the τ_{eff} of the mc and Cz Ti-contaminated wafers were equal to 43 µs and 34 µs, respectively. This important result could be explained firstly by the higher density of nucleation/precipitation centers in mc wafers (due to the large presence of extended crystallographic defects and other metal impurities acting as heterogeneous nucleation centers), which would contribute to a decrease of the concentration of harmful interstitial Ti atoms. Secondly the trapping of Ti atoms during the cooling of the mc ingot within intermetallic liquid silicides (formed due to the presence of metal impurities coming from the low cost silica crucible and its SiN coating), as proposed in [6], could contribute to this difference.

5.6 Dark reverse J-V characteristics

The dark reverse J-V (current density – voltage) measurements of mc solar cells (contaminated and non-contaminated), fabricated from wafers initially located in the last solidified parts of the ingot are shown in Figure 5.12. Notice that Figure 5.12 shows also for comparison the dark reverse J-V characteristic of a highly doped multicrystalline Si solar cell ([B]=3×10^{17} cm^{-3}, [P]=2×10^{17} cm^{-3} [9]), which features a low absolute value of the hard breakdown voltage (V_{bd}) (about 13 V), and the dark reverse J-V characteristics obtained for Ti- and Cu-contaminated Cz solar cells. We assumed here somewhat arbitrarily that the V_{bd} corresponds to the voltage for which the current density was equal to 20 $mA.cm^{-2}$. Indeed the studied range of voltages was not large enough, and the number of data points too limited, in order to safely apply, for determining the V_{bd}, the method based on the determination of the extremum value of the second derivative of the J(V) function,

From a practical standpoint, the main result is that the mc-Si cells feature absolute V_{bd} values higher than 12 V. Therefore, despite the large intentional contaminations of the feedstock by Cu or Ti, the fabricated cells fulfil one of the main industrial requirements regarding the dark reverse I-V characteristics of the PV solar cells ($|V_{bd}|>12$ V).

However, unlike what had been observed for the contaminated Cz solar cells, the hard breakdown of the mc cells was highlighted for the studied range of voltages, even for the reference mc solar cell. This comes as a surprise, since the empirical expression presented in chapter 1 would point to absolute V_{bd} values of the order of 60 V. The lower $|V_{bd}|$ found for the mc cells (in comparison with the Cz cells) could be explained by the mechanism recently highlighted by Bauer et a [10]. Indeed they showed that improved P diffusion along dislocations or grain boundaries in mc Si could locally modify the morphology of the *p-n* junction and enhance the junction breakdown [10].

However a point that should be stressed is the fact that the reference mc-Si cell features a rather low $|V_{bd}|$ (around 15 V). This result was unexpected because usually, the fabricated mc solar cells for similar B-doping levels, have higher $|V_{bd}|$. For comparison, Figure 5.12 presents also the dark reverse J-V characteristic of a B-doped, non-deliberately contaminated, mc solar cell, with a similar B concentration (mc-Si), but fabricated with a wafer from the last solidified part of another mc ingot. This solar cell features a more common $|V_{bd}|$, equal to 17 V. The FTIR analyses showed that for the middle and last parts of the studied ingots, the $[C_s]$ were higher for the mc-ref wafers (e.g., for an ingot's height of 60 % the $[C_s]$ for the mc-Ref is equal to 6.6×10^{17} cm^{-3}). The C solubility limit at 1400 °C is about 3×10^{17} cm^{-3} [11], below the determined $[C_s]$. Therefore SiC precipitates should be present in the studied mc solar cells. Particularly due to the higher $[C_s]$, the mc-Ref wafers could contain larger densities of SiC clusters/precipitates, which could enhance the junction breakdown, even if such precipitates are known in the literature for introducing ohmic hot spot rather than *p-n* junction breakdown sites [12].

The Ti-contaminated and Cu-contaminated wafers from the middle and last parts of the ingots exhibit higher $|V_{bd}|$ as compared to the mc-Si reference. The $|V_{bd}|$ of the Ti-contaminated and Cu-contaminated cells are equal to 17.8 V and 16.2 V, respectively. Therefore the Ti and Cu contamination would slightly enhance the *p-n* junction hard breakdown. Regarding the comparison with the reference cell, the higher $|V_{bd}|$ could be due to a lower carbon supersaturation (e.g., for an ingot's height of 60 % the $[C_s]$ for the mc-Ref and mc-Cu wafers are respectively equal to 6.6×10^{17} cm^{-3} and 3.9×10^{17} cm^{-3}).

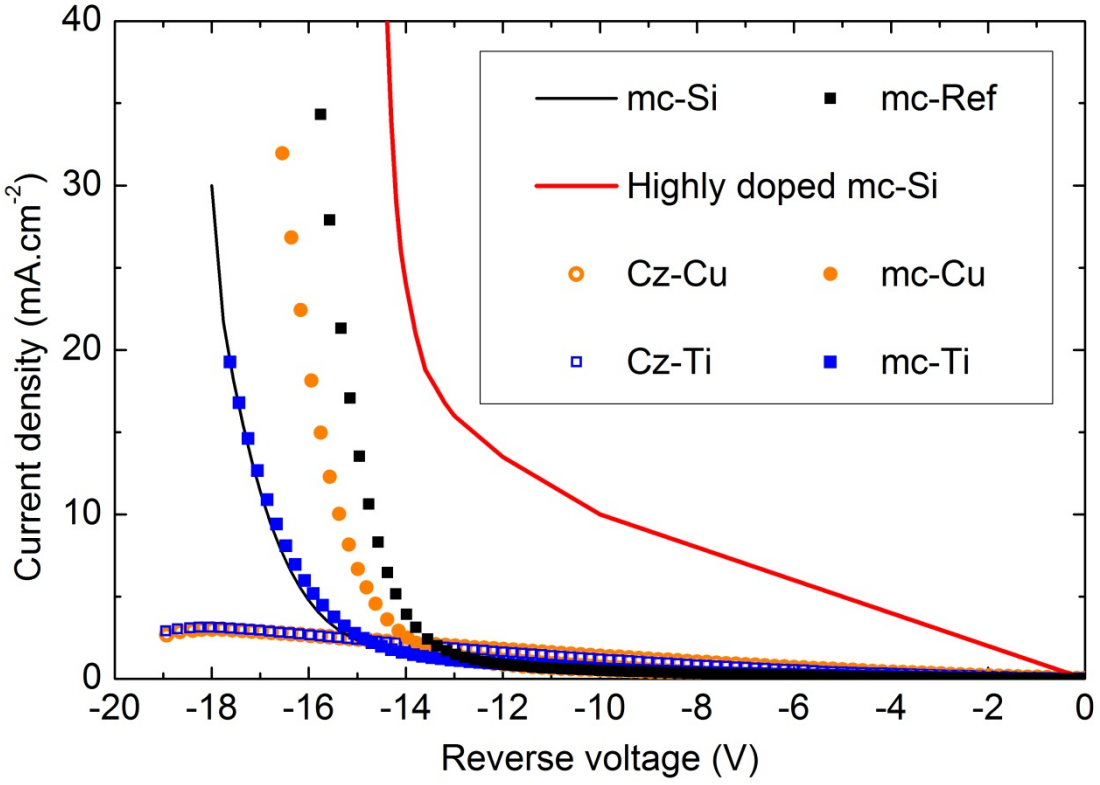

Figure 5.12 – Dark reverse J-V characteristics of mc-Si solar cells (reference, Cu-contaminated and Ti-contaminated) fabricated with wafers from the last solidified parts of the ingots. Comparison with the J-V characteristics obtained for contaminated Cz-Si cells, for a mc-Si solar cells fabricated from a strongly doped material, and for another reference mc-Si cell ("mc-Si" in the legend) featuring an expected V_{bd}.

To go further into the issue of the influence of Cu on junction breakdown, the dark reverse I-V measurements of three Cu-contaminated solar cells, fabricated from wafers initially located in the bottom, middle and top parts of the ingot are shown in Figure 5.13 a). Again, whatever the initial location of the Cu-contaminated wafers along the ingot's height, these cells feature $|V_{bd}|$ higher than 12 V.

However, we can notice that the higher the [Cu], the lower the $|V_{bd}|$. This would confirm the fact that Cu could have a slight negative influence on the *p-n* junction hard breakdown, even if the effect of the weak increase along the ingot's height of the majority charge carrier density on the *avalanche* breakdown cannot totally be ruled out. This influence of Cu on the V_{bd} could be due to the presence of Cu precipitates located within the *scr* or in the vicinity of the *p-n* junction [10], which could locally modify the energy band structures and therefore the behavior of the junction breakdown. Notice that such precipitates should not cross the *scr* since as mentioned previously, the FF was not affected by the Cu contamination. However further analyses should be conducted to validate this hypothesis.

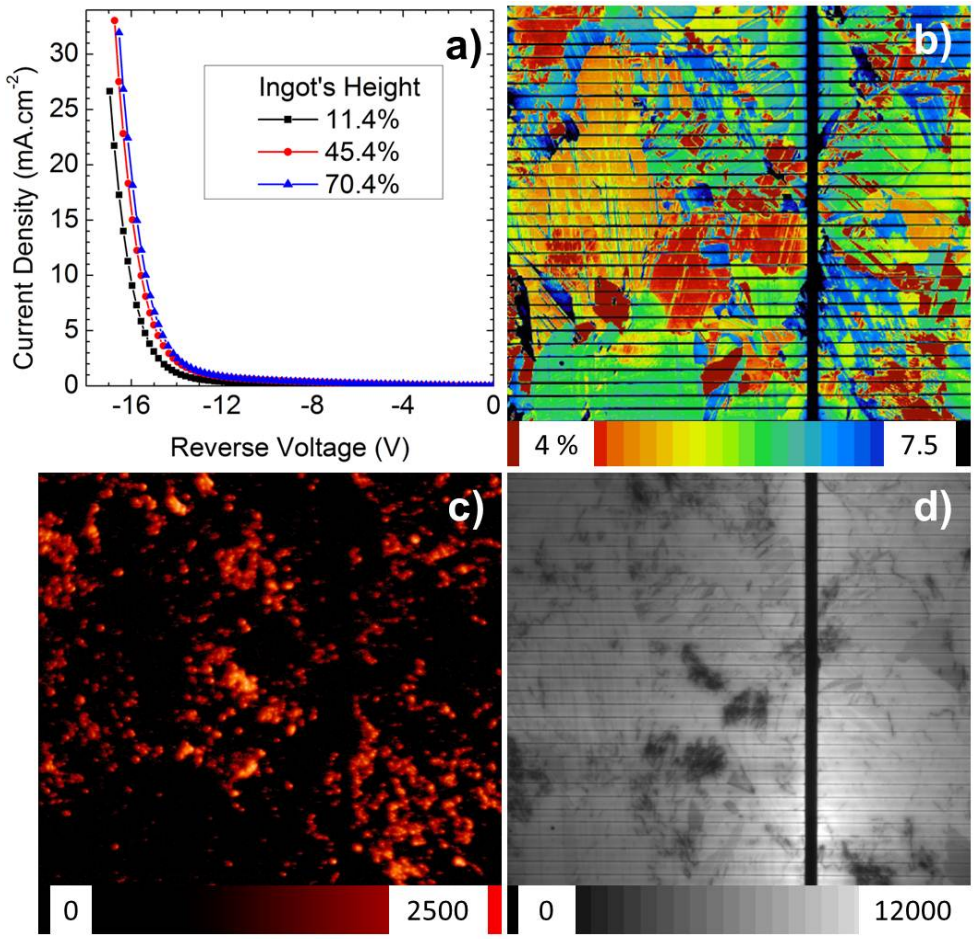

Figure 5.13 – (a) Dark reverse J-V measurements of Cu-contaminated solar cells fabricated from wafers initially located in the top, middle and bottom parts of the ingot. (b) Reflectance mapping (unit in %) obtained with an incident monochromatic light with a wavelength equal to 946 nm, revealing the grain structure; (c) reverse and (d) forward EL images (arbitrary units) of a solar cell fabricated from a wafer initially located in the middle part of the ingot.

Further analyses were conducted regarding the influence of Cu on the junction breakdown. It is particularly interesting to compare the ReBEL (reverse bias electroluminescence) analysis (Fig. 5.13 c)), which can be seen as an image of the breakdown sites, with the reflectance mapping (Fig. 5.13 b)), which is representative of the grain structure, and the forward electroluminescence analysis (Fig. 5.13 d)). We can notice that the junction breakdown mainly occurs along some grain boundaries and within regions rich in clusters of crystallographic defects, probably dislocations. As such defects could enhance the Cu precipitation it could reinforce the previous mentioned hypothesis (enhancement of the breakdown by the Cu precipitates). However, other mechanisms, independent of the Cu contamination, as an improved P diffusion along dislocations or grain boundaries which would locally modify the morphology of the *p-n* junction and enhance the breakdown [13] cannot totally be ruled out.

5.7 Evolution of the photovoltaic performances under illumination

Solar cells fabricated from wafers from the bottom and top parts of the mc ingots were placed on a hot plate (at 50 °C) under a halogen spot with an illumination level of 0.05 W.cm^{-2}. The V_{oc} were monitored in order to evidence possible light-induced degradation (LID) effects (Figures 5.14, 5.15). When the V_{oc} presented stable values, the illumination was stopped.

Figures 5.14 and 5.15 show that all studied cells were subjected to slight decreases of the V_{oc} during the aging tests. However the amplitude of the V_{oc} losses are very low. Particularly for the mc-Ref and mc-Cu cells, the V_{oc} losses are significantly lower that the V_{oc} losses measured with the corresponding Cz samples. For instance, for cells fabricated with wafers from the last solidified parts of the ingots, the V_{oc} losses for the mc-Ref and Cz-ref cells are equal to 4 mV and 20 mV, respectively. Regarding the Cu contaminated samples, the V_{oc} losses for the mc-Cu and Cz-Cu cells fabricated with wafers from the last solidified parts of the ingot, are equal to 5 mv and 12 mV, respectively. These differences regarding the V_{oc} losses of the mc and Cz cells are essentially explained by the differences in the [O_i]. Indeed, for the Cz samples, the LID effects are mainly dominated by the formation/activation of the boron-oxygen (B-O)-related complexes. For the samples from the last solidified fractions of the ingots, the computed (see equation 4.1, chapter 4) carrier lifetime limited by the B-O related complexes (τ_{BO}) are equal to 62 µs only for the Cz wafers due to the high [O_i], whereas τ_{BO} is as high as 3 ms for the mc samples (due to the lower [O_i]). Thus, as this value is significantly higher than the τ_{eff} measured after the P-diffusion step, the mc samples from the top part of the ingot should not be sensitive to the LID effect associated with the B-O related complexes formation.

The part of the mc ingots which is usually affected by LID effects due to the B-O related complexes formation is the bottom part of the ingot, because of the higher [O_i]. The computed τ_{BO} for the mc-Ref and mc-Cu samples from the bottom part (solidified fraction equal to 12 %) are equal to 198 µs and 667 µs, respectively. The difference is due to the fact that the [O_i] is higher for the mc-Ref sample ([O_i]=4×10^{17} cm^{-3}) than the value found for the mc-Cu sample ([O_i]=2×10^{17} cm^{-3}). These differences regarding the computed τ_{BO} could explain the fact that the V_{oc} losses for the samples from the bottom part of the ingot, are slightly higher for the mc-Ref sample (4 mV) than the values found for the mc-Cu sample (only 1 mV).

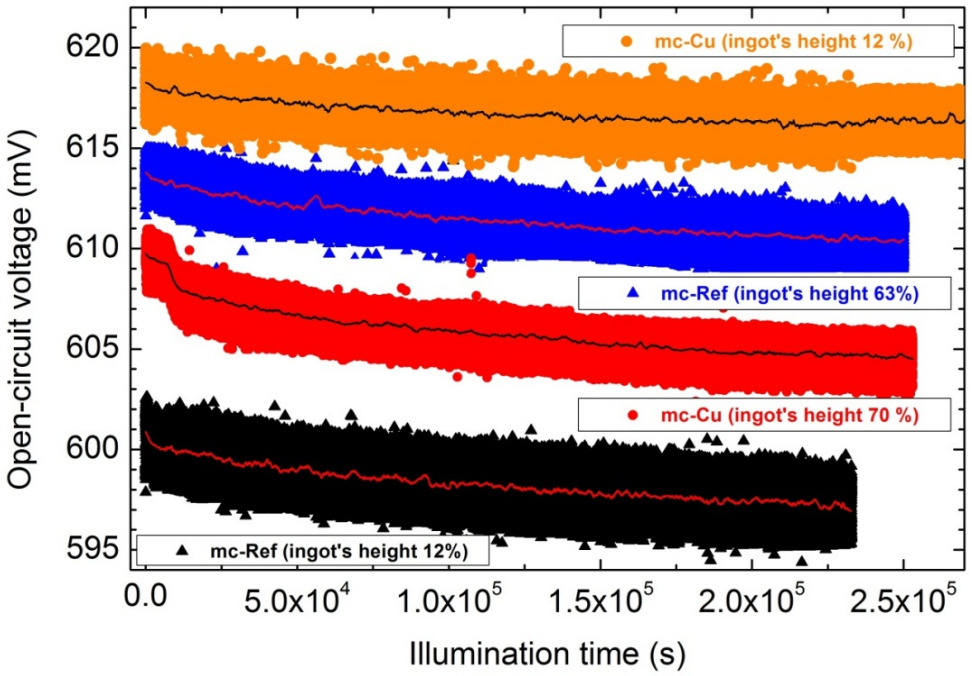

Figure 5.14 – Evolutions at 50 °C under illumination (halogen lamp, light intensity equal to 0.05 W.cm^{-2}) of the V_{oc} of mc-Ref and mc-Cu cells fabricated with wafers from the bottom (first solidified fraction) and top (last solidified fraction) parts of the mc ingots. The solid lines correspond to smoothing mathematical procedures applied to the experimental data.

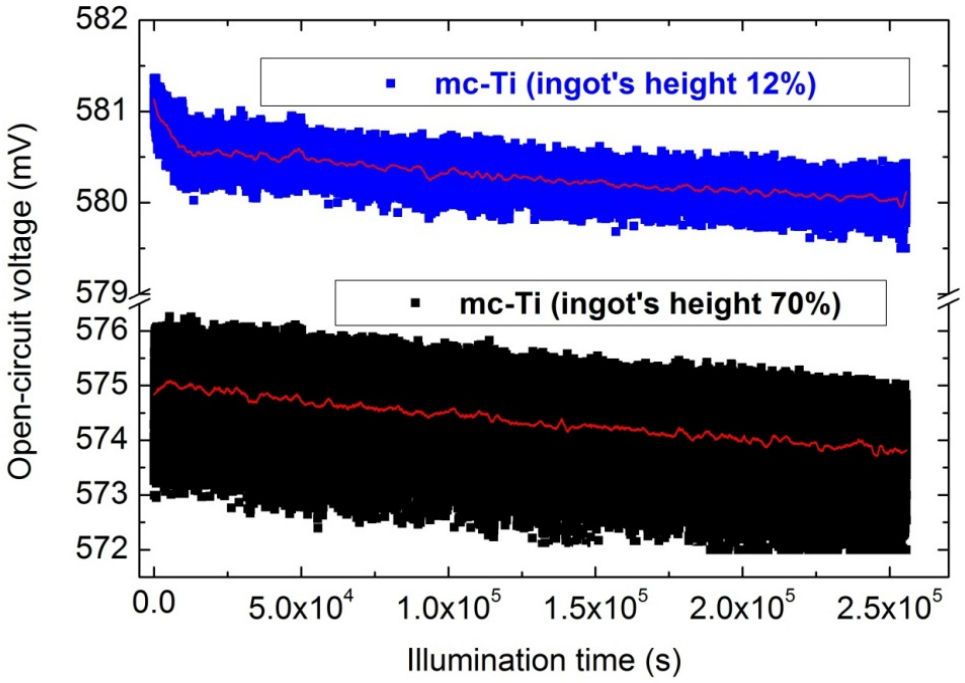

Figure 5.15 – Evolutions at 50 °C under illumination (halogen lamp, light intensity equal to 0.05 W.cm^{-2}) of the V_{oc} of mc-Ti cells fabricated with wafers from the bottom (first solidified fraction) and top (last solidified fraction) parts of the ingots. The solid lines correspond to smoothing mathematical procedures applied to the experimental data.

Regarding the Ti-contaminated cells, the V_{oc} losses are very low, around 1 mV. Notice that these losses are within the range of uncertainty of the measurement (the observed weak trends could simply be due to a slight decrease of the illumination level, because of an aging effect of the halogen lamp). Therefore it can be stated that the Ti-contaminated feature virtually stable performances.

As in general the V_{oc} losses of the mc Si cells were very low, close to the range of uncertainty of the measurement, the evolutions of the PV performances under illumination were also evaluated by illuminated I-V measurements before and after the aging test (the reproducibility of the I-V measurements was carefully controlled). The relative variations of the PV parameters were computed, and are presented in Table 5.2.

Table 5.2 – J_{sc}, V_{oc}, FF and η relative variations (negative values correspond to losses) after the aging tests.

Sample	Ingot' height (%)	Parameters variations (% rel)			
		J_{sc}	V_{oc}	FF	η
mc-Ref	12	-2.50	-0.29	0.13	-2.66
	63	-1.32	-0.48	-0.15	-1.93
mc-Cu	12	-1.25	-0.37	-0.02	-1.63
	63	-3.01	-0.45	0.38	-3.07
mc-Ti	12	-0.01	-0.45	0.20	-0.25
	70	-0.01	-0.33	0.25	-0.08

A first conclusion is that the values presented in Table 5.2 confirm that the Ti-contaminated cells feature virtually stable efficiency. This is due to the fact that the initial carrier lifetime of the Ti-contaminated samples, as dominated by the interstitial Ti atoms (around 15 µs for P-diffused wafers from an ingot's height of 70 %), is well below the computed τ_{BO} (about 3 ms at this ingot's height), the cell is thus not sensitive to the low density of B-O complexes activated under illumination.

As for the Cu contaminated cells, a first thing to be stated is that the sample from the ingot's height of 63 % should not be sensitive to the B-O related complexes activation under illumination. Indeed, the carrier lifetime after the P-diffusion step was about 80 µs, whereas the computed τ_{BO} is about 3 ms. Thus under illumination, the expected evolution of the carrier lifetime is benign, from 80 µs to 78 µs (according to the Matthiessen's law). However, the measured efficiency relative losses are significant (-3.1 %), stronger than the value obtained for the reference sample (-2.7 %) which contains a higher [O_i]. Therefore, and this is an

important result of this PhD thesis, the presence of Cu would induce strong LID losses (the industrial requirements regarding the efficiency losses under illumination are usually around -2 %, in relative).

Interestingly it is known in the literature that Cu can be responsible for specific LID effects of the carrier lifetime, even present at low concentrations ([Cu] ~ 10^{13} cm^{-3}) [14-16]. However these effects were poorly studied at the solar cell level. According to the previous studies of the literature (e.g, [14]), under illumination the excess charge carriers would reduce the electrostatic repulsion between positively charged interstitial Cu ions (non-recombinant) and positively charged Cu precipitates (highly recombinant), this effect enhancing the Cu precipitation and thus carrier lifetime degradation.

In order to bring further insights into these Cu-related LID mechanisms in mc samples, we conducted complementary studies on P-diffused Cu-contaminated Si wafers via carrier lifetime measurements under prolonged illumination, before and after the metallization firing step. The obtained results and the related discussions are presented in the next chapter (Chapter 6).

Conclusion

One of the main results of this chapter is related to the fact that the addition of 90 ppm wt of Cu into the Si feedstock, unexpectedly, did not affect the initial PV conversion efficiency of mc-Si solar cells. We showed that this was mainly due to the weak recombinant activity of the Cu atoms, combined with the external gettering effect developed by the P diffusion. The bulk hydrogenation only improved the electrical quality of the areas with large numbers of extended crystallographic defects. On the other hand, within the good grains, the hydrogenation slightly degraded the charge carrier lifetime (formation of recombinant Cu-H complexes). The initial performances were not affected by the contamination, nevertheless we highlighted a slight negative effect of Cu on the junction breakdown voltage. Above all, we showed that Cu was responsible for important LID effects. This is a crucial result. Indeed, let us recall that the efficiency targets of multicrystalline Si solar cells becoming higher and higher, their performances are more and more sensitive to LID effects of the carrier lifetime. As Cu is a common impurity in multicrystalline Si (Cu essentially comes from the silica crucible used for the directional solidification), a particular attention has to be paid to the Cu-related LID effect, and industrial solutions should be developed to suppress this issue.

On the other hand, the addition of 6 ppm wt of Ti to the feedstock strongly affected the PV conversion efficiency of mc-Si solar cells. As already stated in chapter 4, this is explained by the fact that Ti features harmful recombinant properties. In addition, because of the low Ti diffusivity, the carrier lifetime of the Ti-contaminated samples was not improved by the P-diffusion. Furthermore, the electrical properties of the Ti contaminated samples were not improved by the hydrogenation treatment. However, unexpectedly Ti is more tolerated in mc Si than in Cz Si. This could be due to the presence of extended crystallographic defects in mc Si, which would enhance the Ti precipitation. Therefore the density of harmful interstitial Ti atoms would be lower. We showed that the Ti contaminated solar cells featured absolute values of the junction breakdown voltage higher than 17 V, and virtually stable PV conversion efficiencies.

Chapter 5 – Bibliography

1. F.A. Trumbore, Solid solubilities of impurity elements in germanium and silicon. The Bell System Technical Journal. 39, 205 (1960).
2. B.B. Paudyal, K.R. McIntosh, and D.H. Macdonald, Temperature dependent carrier lifetime studies on Ti-doped multicrystalline silicon. J. Appl. Phys. 105, 124510 (2009).
3. G. Coletti, P.C.P. Bronsveld, G. Hahn, W. Warta, D. Macdonald, B. Ceccaroli, K. Wambach, N.L. Quang, and J.M. Fernandez, Impact of metal contaminations in silicon solar cells. Adv. Funct. Mater. 21, 879-890 (2011).
4. N.D. Arora, J.R. Hauser, D.J. Roulston, Electron and hole mobility in silicon as a function of concentration and temperature. 29th IEEE PVSC, 292 (1982).
5. S. Dubois, O. Palais, P.J. Ribeyron, N. Enjalbert, M. Pasquinelli, and S. Martinuzzi, Effect of intentional bulk contamination with iron on multicrystalline silicon solar cell properties. J. Appl. Phys. 102, 083525 (2007).
6. T. Buonassisi, M. Heuer, A.A. Istratov, M.D. Pickett, M.A. Marcus, E.R. Weber, Internal gettering by metal alloy clusters. Patent Pub. No.: US 2006/0289091 A1 (2006).
7. S. Knack, J. Weber, H. Lemke, and H. Riemann, Copper-hydrogen complexes in silicon. Phys. Rev. B. 65, 165203 (2002).
8. R. Singh, S.J. Fonash, and A. Rohatgi, Interaction of low-energy implanted atomic H with slow and fast diffusing metallic impurities in Si. Appl. Phys. Lett. 49, 800 (1986)
9. S. Dubois, J. Veirman, N. Enjalbert, F. Tanay, and G. Raymond, Studies on compensated and UMG material and solar cells. 21st Workshop on crystalline silicon solar cells & modules: Materials and processes (2011).
10. J. Bauer, D. Lausch, H. Blumtritt, N. Zakharov, and O. Breitenstein, Avalanche breakdown in multicrystalline solar cells due to preferred phosphorous diffusion at extended defects. Prog. Photovolt: Res. Appl. 21, 1444, (2013).
11. R. Hull, Properties of crystalline silicon. Ed. by R. Hull, INSPEC, IEE. London (1999).
12. O. Breitenstein, J. Bauer, K. Bothe, W. Kwapil, D. Lausch, U. Rau, J. Schmidt, M. Schneemann, M.C. Schubert, J.-M. Wagner and W. Warta, Understanding junction breakdown in multicrystalline solar cells. J. Appl. Phys. 109, 071101 (2011).
13. W. Kwapil, M. Kasemann, P. Gundel, M.C. Schubert, W. Warta, P. Bronsveld, and G. Coletti, Diode breakdown related to recombination active defects in block-cast multicrystalline silicon solar cells. J. Appl. Phys. 106, 063530 (2009).
14. H. Savin, M. Yli-Koski, and A. Haarahiltunen, Role of copper in light induced minority-carrier lifetime degradation of silicon. Appl. Phys. Lett. 95, 152111 (2009).
15. Belayachi, T. Heiser, J. P. Schunck, and A. Kempf, Influence of light on interstitial copper in p-type silicon. Appl. Phys. A. 80, 201 (2005).
16. J. Lindroos, M. Yli-Koski, A. Haarahiltunen, and H. Savin, Room-temperature method for minimizing light-induced degradation in crystalline silicon. Appl. Phys. Lett. 101, 232108 (2012).

CHAPTER 6. INFLUENCE OF PHOSPHORUS-RICH LAYERS DURING RAPID ANNEALING ON CARRIER RECOMBINATION AND TRAPPING IN COPPER CONTAMINATED MULTICRYSTALLINE SILICON

We have seen in chapter 5 that on the one hand Cu does not significantly affect the initial photovoltaic conversion efficiency of multicrystalline (mc) Si solar cells [1]. However, on the other hand we demonstrated that Cu is responsible for strong light-induced degradation effects [1]. To account for these observations, it was suggested that under illumination the excess charge carriers would reduce the electrostatic repulsion between positively charged interstitial Cu ions (non-recombinant) and positively charged Cu precipitates (highly recombinant), enhancing the Cu precipitation and therefore degrading the charge carrier lifetime (τ) [2].

The last high temperature (T) treatment of the solar cell fabrication process is generally a rapid thermal annealing (RTA) step, the so-called *firing*, essentially used for the sintering of the screen-printed metal electrodes. Due to the combined actions of the high T and the fast cooling, this step usually governs the final spatial distribution of metal impurities. Therefore, understanding its effects is crucial to limit the impact of metal impurities on the performances of solar cells. Recently, Tan *et al*. confirmed that *firing* steps degrade the τ of conventional mc-Si wafers, due to the dissolution of metal precipitates (particularly iron precipitates) [3]. They also showed that this degradation is weaker when P emitters are present during the annealing but proposed no explanation for such a finding. In these pioneering works [3], the presence and effects of Cu atoms were not evoked, and the carrier trapping not investigated. Our objective in this chapter is thus to examine the role of the P-rich layer during rapid annealing on the carrier recombination, the stability of the carrier lifetime under illumination and the electron trapping, in the deliberately Cu contaminated mc-Si wafers.

6.1 Experimental details

This study focuses only on the Cu-contaminated mc ingot. Adjacent s*ister* wafers were taken at an ingot's height of about 41 %. For these wafers, the corresponding [O_i] and [C_s] were equal to 7×10^{16} cm^{-3} and 3×10^{17} cm^{-3}, respectively. The wafers were acid etched and RCA cleaned before a 90 min double sided P diffusion resulting in a sheet resistance of ~ 70

Ω/□. Some wafers were then stripped of their n^+ emitters by acid etch. Notice that the total Cu concentrations ([Cu]) were determined on sacrificial samples by inductively-coupled plasma mass spectrometry before and after the P-diffusion (after the emitter etch). For the as-received sample, [Cu] was equal to 8×10^{14} cm^{-3}. For the P-diffused sample, [Cu] was below the measurement detection limit (around 2.1×10^{12} cm^{-3}), which confirms the fact that Cu atoms, due to their high diffusivity, are well extracted from the Si bulk by the external gettering effect developed by the P-diffusion [1]. All samples received a double sided plasma enhanced chemical vapor deposition (PECVD) hydrogenated Si nitride (SiN_x:H) coating. Then the samples were *fired* in a RTA infrared lamp furnace. More precisely, the annealing is made of two steps: the first at 550°C with a duration of 20 s, and the second at about 850°C during 3 s (the annealing conditions correspond to the solar cells metallization *firing* step). Samples were characterized before and after the RTA at 5 points across each sample, by inductively-coupled quasi-steady-state photoconductance decay (QssPC) measurements, giving the variation of the apparent effective τ (τ_{app}) with the apparent excess carrier density (Δn_{app}) [4]. For Δn_{app} higher than 7×10^{14} cm^{-3}, the QssPC data were not affected by minority carrier trapping. Therefore for such Δn, τ_{app} could be assumed to be equal to the effective carrier lifetime (τ_{eff}) and Δn_{app} to the excess carrier density (Δn). Just after the RTA, before any prolonged illuminations, the wafers were kept in the dark at 20°C and IC-QssPC measurements were done at various time intervals. Furthermore, the evolutions at 50°C of τ_{eff} under illumination (halogen lamp, intensity of 0.04 $W.cm^{-2}$) were monitored before and after the RTA.

6.2 Influences of phosphorus-rich layer during rapid annealing step on carrier recombination in mc-Cu

Figure 6.1 displays the τ_{eff} (associated with a Δn equal to 10^{15} cm^{-3}) of P-diffused wafers, before and just after the *firing* (RTA). Notice that before the *firing* step, τ_{eff} are lower for the samples with the n^+ layers, the P-diffused region increasing the surface recombination velocity (S), essentially due band-to-band related recombination mechanisms because of the high majority carrier density. Unexpectedly, τ_{eff} are improved by the *firing*, with and without n^+ layers. These results are *a priori* contradictory with those of Tan *et al*. [3], who highlighted increases of τ_{eff} after the *firing* step, for the samples with the n^+ layer only. Therefore for the Cu contaminated samples, the *firing* extracted, passivated or transformed pre-existing recombination centers, with and without n^+ layers. Even though both type of samples were

submitted to the same PECVD treatment, we considered that the S of the samples with and without n^+ layers could be different. In order to quantify the influence of the n^+ layer on the bulk quality improvements (we assume not effect of the RTA on S), we computed the value τ_{RTA} defined by $(\tau_{RTA})^{-1} = (\tau_P)^{-1} - (\tau_{P+RTA})^{-1}$. τ_P and τ_{P+RTA} are the τ_{eff} before and after the RTA, respectively. The averaged τ_{RTA} for the samples with and without n^+ layers are equal to 49.3 µs and 97.6 µs, respectively. Thus, the beneficial effects of the RTA on τ_{eff} are higher without n^+ layers.

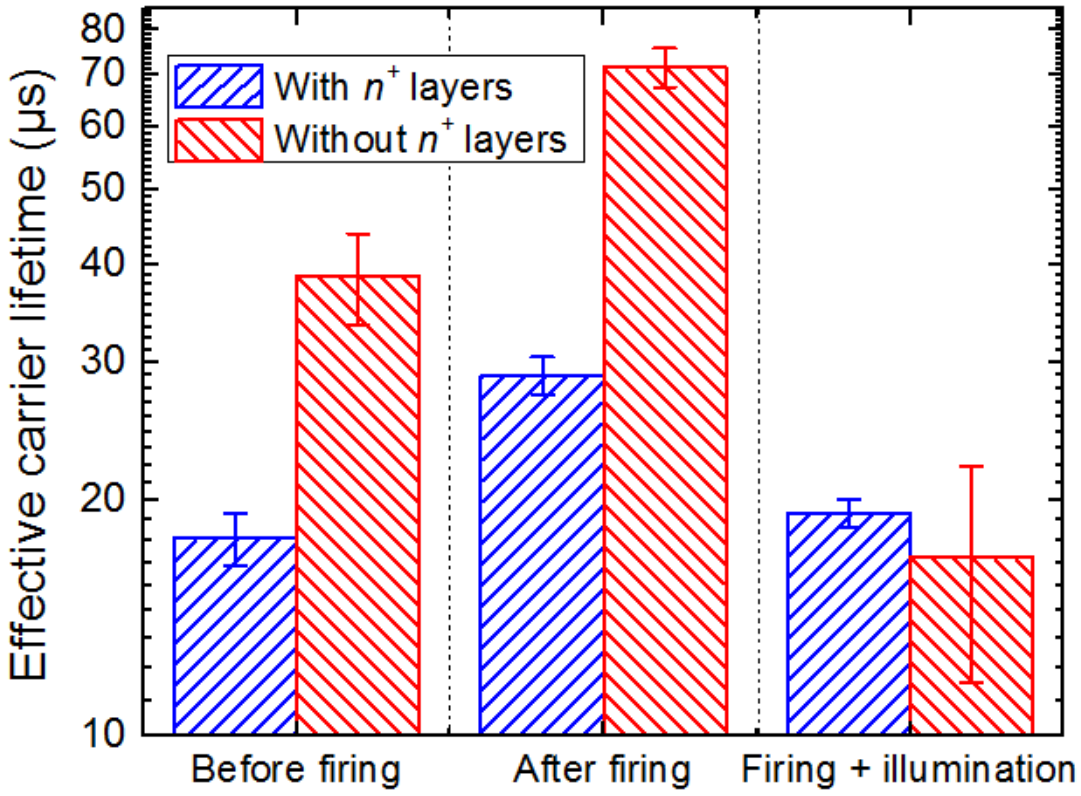

Figure 6.1 – Effective carrier lifetime of Cu-contaminated mc wafers which experienced a P diffusion step, with and without emitters (n^+ layers). The values were extracted at an excess carrier density of 10^{15} cm^{-3}. The measurements were done after the P-diffusion step (before firing), after the firing step before illuminating the samples (after firing), and after 30 hours at 50°C under permanent illumination (firing + illumination). The error bars represent the standard deviation of results.

These results can be explained by the fact that, as mentioned earlier, unlike interstitial iron, interstitial Cu (Cu_i) is a shallow donor with relatively benign electrical activity [5]. On the other hand, Cu precipitates are known to severely affect τ by forming bands of energy states within the Si bandgap, thereby providing very effective pathways for recombination [6]. Thus, as the Cu precipitates would dissolve during the *firing* treatment, the Cu precipitate

density and/or radius decrease, consequently τ_{eff} increases. These results bring new insights into the role of the n^+ layer. Indeed, as τ_{RTA} is lower with the n^+ layer, our contention is that the n^+ layer would prevent, or at least slow down, the dissolution of metal precipitates during *firing* treatments (and would not develop external gettering effects or enhance the passivation by hydrogen of dissolved metal elements, as discussed in [3]).

6.3 Influences of phosphorus-rich layer during rapid annealing step on carrier trapping in mc-Cu

Figure 6.2 shows the variation of τ_{app} with Δn_{app}, at various time intervals after the *firing* treatment for *sister* wafers *fired* with and without n^+ layers (between two measurements, the wafers were kept in the dark). Regarding the sample with n^+ layers, τ_{app} were perfectly stable (only the data concerning the measurements done just after the *firing* and 24 hours after the *firing* are presented in Figure 2). In addition, the QssPC data were not significantly affected by trapping (no abnormally high τ_{app} at low Δn_{app}). On the other hand, for the sample without n^+ layers, abnormally high τ_{app} at low Δn_{app} can be observed, which is very probably due to minority carrier trapping centers. For this sample, the experimental data at low Δn_{app} could successfully be fitted by the theoretical trapping model of Hornbeck and Haynes [7], nicely transposed to QssPC data by Macdonald and Cuevas [8], with the recombination lifetime assumed to be limited by band-to-band Auger recombination [9] and Shockley-Read-Hall recombinations [10] through a mid-gap energy level with asymmetric electron (σ_n) and hole (σ_p) carrier capture cross sections (σ_n/σ_p=65) and a shallow energy level (located at 0.2 eV above the valence band with σ_n/σ_p=0.1). Notice that we did not focus here on the nature of the defect levels dominating the recombination lifetime, which was only fitted in order to improve the extraction of the trapping parameters. The recombination lifetime is perfectly stable. However, a strong increase of the trapping density (N_t) is highlighted, from $N_t=6.0\times10^{13}$ cm^{-3} just after the *firing* to $N_t=7.5\times10^{14}$ cm^{-3} 24 hours after the *firing*. The trapping of minority carriers is not clearly observed for the sample fired with n^+ layers. As mentioned earlier, our contention is that this layer would prevent or slow down the dissolution of metal precipitates, the impurities causing trapping centers in the sample *fired* without the n^+ layer could be transition metals initially precipitated. Particularly as N_t increases after the annealing step, the trapping could be due, as suggested by Macdonald *et al*. [11], to boron-impurity pairs formed here at room temperature, pairs with a benign effect on carrier

recombination. However, the involvement of Cu in such trapping centers is rather unlikely, even if the formation of stable (at room temperature) Cu-B pairs was previously reported [12]. Firstly N_t is significantly higher than [Cu]. Secondly Reiss *et al*. determined the time constant (τ_{assoc}) of ion-pairing reactions in semiconductors involving mobile ions which are present in much lower concentrations than the fixed dopant ions [13]:

$$\tau_{assoc} = \frac{\varepsilon kT}{q^2[B]D_{Cu}} \tag{6.1}$$

ε is the Si dielectric constant, k the Boltzmann constant, [B] the boron concentration, q the elementary charge, and D_{Cu} the Cu diffusivity. Taking into account the B-dependent Cu diffusivity [14], if Cu-B were responsible for the observed trapping, τ_{assoc} should be about 1.6×10^{-3} s, therefore in strong disagreement with the time range corresponding to the experimental increase in N_t (several hours).

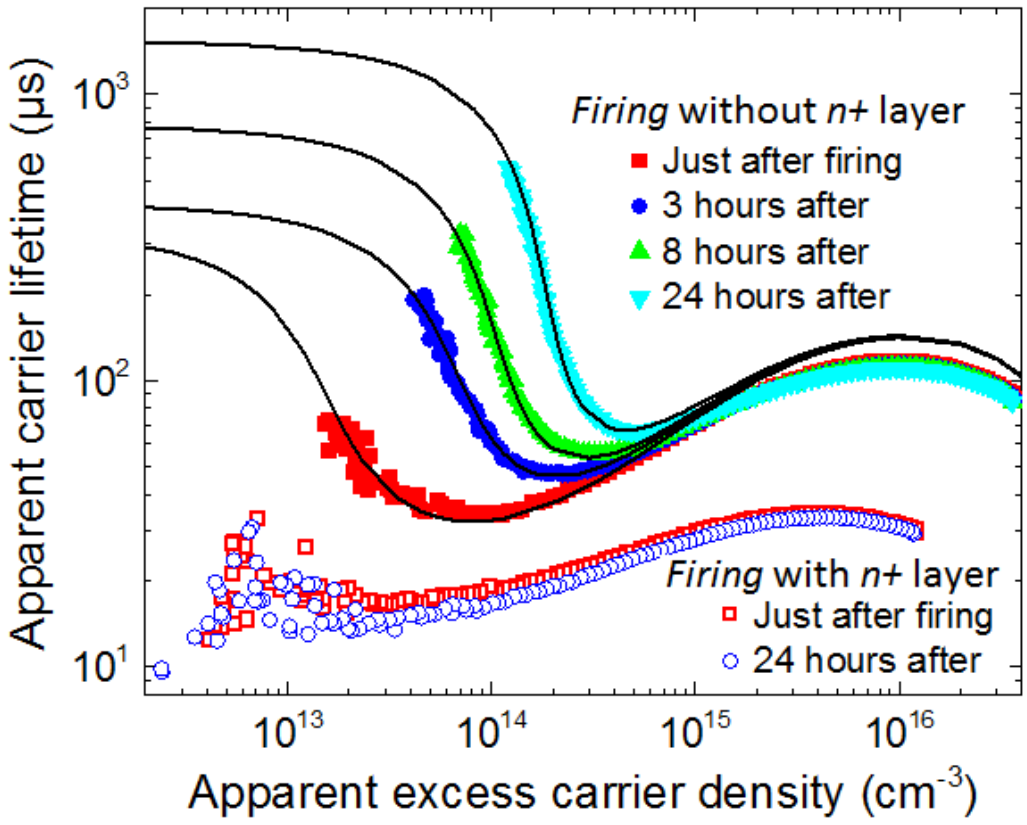

Figure 6.2 – Measured apparent carrier lifetime as a function of the apparent excess carrier concentration, at various time intervals after the firing step, for Cu-contaminated mc samples fired without and with the n^+ emitter. The lines show the fitted carrier trapping and recombination model.

Another mechanism, to the best of our knowledge not previously discussed in the literature, could be invoked to account for the N_t increase, namely the dissociation of the Cu-Cu pairs. Indeed in *p*-type Si, after a rapid annealing, some Cu-Cu pairs would be formed between a substitutional Cu atom and an interstitial Cu atom [15]. At room temperature the pairs would dissociate, and the concentration of single Cu_i atoms ($[Cu_i]$) would increase. As Cu_i introduces a shallow energy level (located at 0.15 eV below the conduction band) [16], whereas the Cu-Cu pairs introduce an energy level in the vicinity of the valence band [15], the higher $[Cu_i]$ due to the Cu-Cu pairs dissociation could be responsible for the increased minority carrier trapping. Istratov *et al*. [15] determined the dissociation time constant of the Cu-Cu pairs ($\tau_{Cu\text{-}Cu}$):

$$\tau_{Cu-Cu}(s) = 1.47 \times 10^{-10} \exp\left(\frac{1.02 \pm 0.07eV}{kT}\right) \quad (6.2)$$

Thus, at 298 K $\tau_{Cu\text{-}Cu}$ would be between 21 days and 14 years, therefore in disagreement with our data. In addition, the fact that the total Cu concentration is significantly lower than N_t weighs also against this hypothesis. Thus the true nature of the activated trapping centers remains unclear.

6.4 Influences of phosphorus-rich layer during rapid annealing step on the stability of carrier lifetime under illumination in mc-Cu

Figure 6.3 presents the averaged τ_{eff} (extracted for Δn=10^{15} cm^{-3}) evolution under illumination for samples with and without n^+ layers, before and after the *firing* step. Before the *firing* step, the τ_{eff} are stable under illumination. However after the *firing* step, the τ_{eff} decrease under illumination for both samples, moderately for the sample fired with a n^+ layer and very strongly for the sample fired without a n^+ layer. Due to the low $[O_i]$, this degradation cannot be due to the activation of the B-O related complexes. Indeed according to Bothe *et al*. [17], the τ limited by the B-O related complexes should be around 3.3 ms. Also the τ_{eff} decrease was observed for both low (Δn_{app} around 8×10^{13} cm^{-3}) and high (Δn_{app} around 2×10^{16} cm^{-3}) Δn_{app}, which means that the dissociation of the Fe-B pairs cannot be responsible for the observed τ_{eff} decrease (the Fe-B pairs dissociation inducing for the studied B concentration, an increase (resp. decrease) of τ_{eff} for Δn higher (resp. lower) than 2×10^{14} cm^{-3} [18]. Therefore the degradation is very probably related to interstitial Cu atoms, which would precipitate

under illumination, forming highly active recombination centers. This hypothesis is supported by the fact that the degradation is only observed after the *firing* step. Indeed, the cooling rate at the end of the P-diffusion step being low (about -0.05 $K.s^{-1}$), interstitial Cu atoms can easily find favorable sites (e.g. existing precipitates or extended defects) when the Cu concentration exceeds the solubility limit. Therefore $[Cu_i]$ is probably very low and negligible precipitation occurs under illumination. On the other hand, the cooling rate of the *firing* treatment being very high (about -21 $K.s^{-1}$), the $[Cu_i]$ is higher and low T Cu precipitation occurs under illumination. From the τ_{eff} determined before (τ_i) and after 30 hours under illumination (τ_f), the τ_{eff} limited by the defect activated or transformed under illumination (τ_{ill}) can be determined: $(\tau_{ill})^{-1} = (\tau_f)^{-1} - (\tau_i)^{-1}$. τ_{ill} are equal to 22.1 µs and 57.8 µs for the samples *fired* without and with n^+ layers, respectively. According to Väinölä *et al*. [19], after a high T step followed by a fast cooling, the higher the $[Cu_i]$, the lower τ_{ill}. Thus this confirms the fact that $[Cu_i]$ is higher for the sample *fired* without n^+ layers, and show that these results are eventually in very good agreement with the study of Tan *et al*. [3]: the presence of n^+ layers during a *firing* step limits the precipitates dissolution, and thus the density of dissolved transition metals due to the precipitates dissolution.

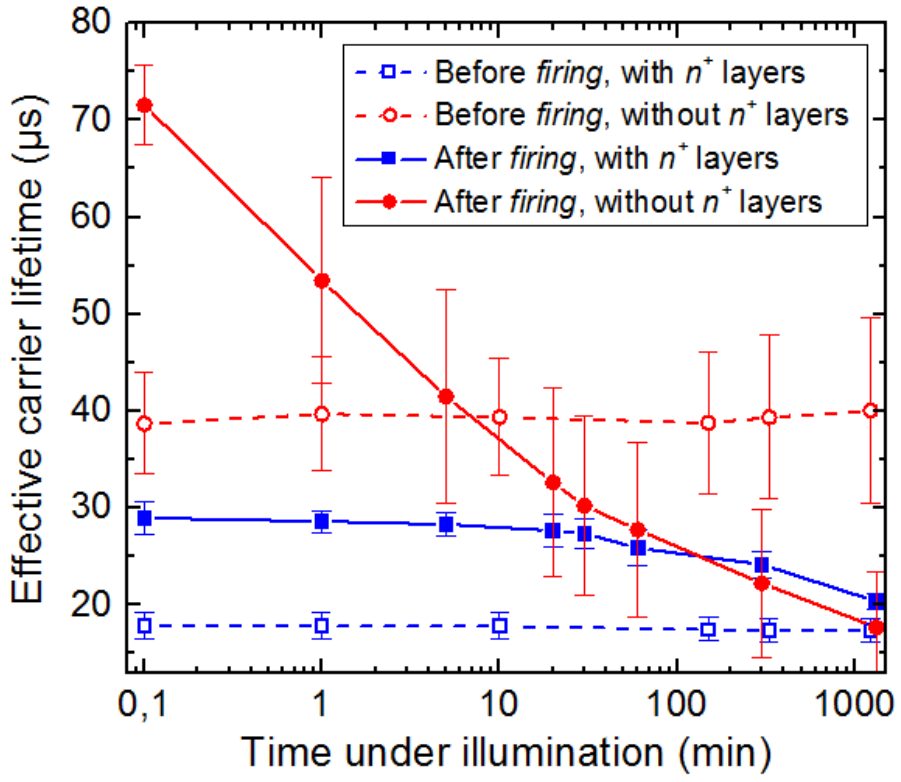

Figure 6.3 – Evolution under illumination of the effective carrier lifetime of P-diffused samples, with and without the n+ emitter, before and after the firing step. The values were extracted for an excess carrier density of 10^{15} cm^{-3}. The error bars represent the standard deviation of results. Lines are only a guide to the eye.

6.5 On the role of Si self-interstitials on the limitation of the metal precipitates dissolution

The mechanism by which the n^+ layer prevents the metal precipitates dissolution is not clearly understood.

Notice that in the study of Tan *et al*. [3], the possible role played by hydrogen atoms (released from the SiNx:H layer) was discussed and invalidated. The surface defects caused by the P diffusion could improve the dissolution of molecular H, and consequently the bulk formation of H-impurity complexes. In the light of our results, this hypothesis is eventually particularly interesting since the bulk hydrogenation develops opposite effects for Fe-rich Si (neutralization of interstitial Fe atoms) and Cu-rich Si (formation of recombinant H-Cu_i complexes), and therefore could explain the apparent contradiction between our results and those from Tan's study. However, as shown in the 5th chapter, even with Cu contaminated wafers, the average carrier lifetimes were slightly improved by bulk hydrogenation treatments. Thus, as the QssPC analyses give average τ_{eff}, this contradicts the proposed hypothesis, based on an enhancement via the $n+$ layer, of the bulk hydrogenation.

Another possible explanation we briefly investigated concerns the fact that the permanent electric field located at the *p-n* junction would act as a barrier preventing positively charged Cu_i ions to leave the cell base, much like the negative corona charges discussed in chapter 2 were seen to increase the extraction of Cu_i ions. The resulting high concentrations of Cu_i within the bulk would in turn limit the dissolution of Cu precipitates to the necessary amount to reach thermodynamic equilibrium at firing temperature. The quenched supersaturated ions would upon illumination reagglomerate, and enhance the growth of the Cu precipitates. However we did not investigate this hypothesis further particularly because the compatibility of this explanation with Tan's results is highly questionable. Indeed, due to their lower diffusivity, interstitial Fe atoms (being positively charged for T lower than typically 350 °C) could not interact with the electric field present at the junction.

We discuss here another possible explanation based on the involvement of Si self-interstitials (Si_I). The *firing* step induces a slight redistribution of the n^+ emitter (diffusion of P atoms). Indeed, we showed that the *firing* decreased the sheet resistance of the wafers with the n^+ emitter from 70.6 Ω/□ (before the firing) to 65.7 Ω/□. The P diffusion emits Si_I into the

Si bulk [20]. From the expression given by Tan and Gösele for the Si_I diffusivity in single-crystalline Si [21], during the *firing* step Si_I should diffuse on a length of about 15 µm only. However, in imperfect multicrystalline materials, the Si_I diffusivity could be higher and they could migrate on larger distances, the phenomenon is for instance well documented in the case of H diffusion from the SiNx PECVD layer [22]. Assuming that the volume change due to silicide formations is entirely accommodated by the emission or absorption of Si_I, the supersaturation of Si_I would limit the dissolution of α-$FeSi_2$ and $CrSi_2$ silicides [23], and could partly explain the results obtained by Tan *et al*. [3]. However on the other hand, the Si_I supersaturation would enhance the dissolution of Cu_3Si silicides [23], in strong disagreement with the results we obtained, which significantly affects the proposed hypothesis.

Conclusion

This investigation shows that the presence of phosphorus-rich layers during a *firing* step limits the dissolution of copper precipitates. Therefore, as copper precipitates are virulent recombination centers whereas the electrical activity of interstitial copper is benign, the samples *fired* without phosphorus emitters exhibit higher carrier lifetimes, but also a stronger sensitivity to the copper-related light-induced degradation. In addition, the samples *fired* without the phosphorus emitters are subjected to trapping effects, possibly involving metal elements initially precipitated.

Another important result of this chapter concerns the fact that the Cu-related LID effects are activated by the metallization *firing* step. Indeed, two main mechanisms can be responsible for the LID of mc Si solar cells: the formation of the boron-oxygen (B-O) related complexes, and the Cu precipitation. It is of paramount importance, if such LID effects are observed, to be able to identify the dominant LID mechanism. Using P-diffused wafers, if the B-O related LID effects are predominant, LID effects with similar amplitudes can be observed before and after the firing step. However, if the Cu-related LID effects are predominant, the LID effects can only be highlighted after the P-diffusion step. Therefore using P-diffused wafers, and by determining the evolution of the carrier lifetime under illumination before and after a firing step, we were able to show that the dominant mechanism involved in the LID effects is related to the copper contamination.

Chapter 6 – Bibliography

1. T. Turmagambetov, S. Dubois, J.-P. Garandet, B. Martel, N. Enjalbert, J. Veirman, and E. Pihan, Influence of copper contamination on the illuminated forward and dark reverse current-voltage characteristics of multicrystalline p-type silicon solar cells. Phys. Status Solidi C. 11, 1697 (2014).
2. H. Savin, M. Yli-Koski, and A. Haarahiltunen, Role of copper in light induced minority-carrier lifetime degradation of silicon. Appl. Phys. Lett. 95, 152111 (2009).
3. J. Tan, D. Macdonald, N. Bennett, D. Kong, A. Cuevas and I. Romijn, Dissolution of metal precipitates in multicrystalline silicon during annealing and the protective effect of phosphorus emitters. Appl. Phys. Lett. 91, 043505 (2007).
4. R. A. Sinton and A. Cuevas, Contactless determination of current–voltage characteristics and minority-carrier lifetimes in semiconductors from quasi-steady-state photoconductance data. Appl. Phys. Lett. 69, 2510 (1996).
5. A. Istratov, C. Flink, H. Hieslmair, T. Heiser, and E.R. Weber, Influence of interstitial copper on diffusion length and lifetime of minority carriers in p-type silicon. Appl. Phys. Lett. 71, 2121 (1997).
6. A. Istratov, H. Hedemann, M. Seibt, O.F. Vyvenko, W. Schröter, T. Heiser, C. Flink, H. Hieslmair, and E.R. Weber, Electrical and recombination properties of copper-silicide precipitates in silicon. J. Electrochem. Soc. 145, 3889 (1998).
7. J. A. Hornbeck and J. R. Haynes, Trapping of minority carriers in silicon. I. p-type silicon. Phys. Rev. 97, 311 (1955).
8. D. Macdonald and A. Cuevas, Trapping of minority carriers in multicrystalline silicon. Appl. Phys. Lett. 74, 1710 (1999).
9. A. Richter, S.W. Glunz, F. Werner, J. Schmidt, and A. Cuevas, Improved quantitative description of Auger recombination in crystalline silicon. Phys. Rev. B. 86, 165202 (2012).
10. W. Shockley, and W.T. Read, Statistics of the recombinations of holes and electrons. Phys. Rev. 87, 835 (1952).
11. D. Macdonald, M. Kerr, and A. Cuevas, Boron-related minority-carrier trapping centers in p-type silicon. Appl. Phys. Lett. 75, 1571 (1999).
12. M.O. Aboelfotoh, B.G. Svensson, Copper passivation of boron in silicon and boron reactivation kinetics. Phys. Rev. B. 44, 12742 (1991).
13. H. Reiss, C.S. Fuller and F.J. Morin, Chemical interactions among defects in Germanium and Silicon. Bell Syst. Tech. J. 35, 535 (1956).
14. A. Istratov, C. Flink, H. Hieslmair, E.R. Weber, and T. Heiser, Intrinsic diffusion coefficient of interstitial copper in silicon. Phys. Rev. Lett. 81, 1243 (1998).
15. A. Istratov, H. Hieslmair, T. Heiser, C. Flink, and E.R. Weber, The dissociation energy and the charge state of a copper-pair center in silicon. Appl. Phys. Lett. 72, 474 (1998).
16. A. Istratov, H. Hieslmair, C. Flink, T. Heiser, and E.R. Weber, Interstitial copper-related center in n -type silicon. Appl. Phys. Lett. 71, 2349 (1997).
17. K. Bothe, R. Sinton, and J. Schmidt, Fundamental boron–oxygen-related carrier lifetime limit in mono- and multicrystalline silicon. Prog. Photovolt: Res. Appl. 13, 287 (2005).

18. D. Macdonald, T. Roth, P.N.K. Deenapanray, T. Trupke, and R.A. Bardos, Doping dependence of the carrier lifetime crossover point upon dissociation of iron-boron pairs in crystalline silicon. Appl. Phys. Lett. 89, 142107 (2006).
19. H. Väinölä, E. Saarnilehto, M. Yli-Koski, A. Haarahiltunen, J. Sinkkonen, G. Berenyi, and T. Pavelka, Quantitative copper measurement in oxidized p-type silicon wafers using microwave photoconductivity decay. Appl. Phys. Lett. 87, 032109 (2005).
20. P. Fahey, R.W. Dutton, and S.M. Hu, Supersaturation of self-interstitials and undersaturation of vacancies during phosphorus diffusion in silicon. Appl. Phys. Lett. 44, 777 (1984).
21. T.Y. Tan, and U. Gösele, Point defects, diffusion, and swirl defect formation in silicon. Appl. Phys. A. 37, 1 (1985).
22. L. Sopori, K. Jones, and X.J. Deng, Observation of enhanced hydrogen diffusion in solar cell silicon. Appl. Phys. Lett. 61, 2560 (1992).
23. W. Schröter, V. Kveder, M. Seibt, A. Sattler, and E. Spiecker, Mechanisms and computer modelling of transition element gettering in silicon. Sol. Energy Mater. Sol. Cells. 72, 299 (2002).

SUMMARY AND OUTLOOK

Summary

This PhD thesis focused on the influences of Ti and Cu contaminations on the photovoltaic (PV) performances of both single-crystalline and multicrystalline Si solar cells.

The first chapter of this manuscript presented the mechanisms by which defects in crystalline Si influence the performances of PV solar cells. Particularly we showed that even using initially ultra-pure Si feedstock, deliberately contaminated with selected impurities at the ingots growth stage, the presence of defects other than the studied elements is unavoidable. These defects can particularly interact with the considered impurities and interfere with the conclusions drawn from the experimental results. Consequently the properties of the main defects usually found in crystalline Si were presented, and we then evoked the influence of the solar cell fabrication process (i.e., external gettering and hydrogenation effects) on their distribution and chemical state.

The second chapter summarized the main properties of Cu and Ti in Si. Interestingly these transition metals feature different behaviors in crystalline Si. Particularly the diffusivity of Cu is much higher than the diffusivity of Ti. As a matter of fact, Cu is essentially precipitated whereas Ti is mainly present as interstitial atoms. Their effects on the carrier lifetime are also significantly different. Indeed interstitial Cu has a benign electrical activity whereas interstitial Ti is an harmful recombination center. However Cu silicides introduce defect levels within the Si band gap which affect the carrier lifetime. In addition, Cu had been suspected to be responsible for light-induced degradation (LID) effects of the charge carrier lifetime, due to room temperature precipitation effects. Finally this chapter evoked the previous works dedicated to the influences of Cu and Ti on the performances of crystalline Si solar cells. We showed that there was a crucial need for updated studies, based on state of the art solar cell fabrication processes, assessing the effects of these elements on the initial PV performances, but also on the evolution of these performances under illumination, and on the junction breakdown voltage.

The third chapter presented the experimental protocols and the main characterization tools used throughout this PhD thesis. A particularity of our work consisted in studying the effects of Ti and Cu on the properties of both single-crystalline and multicrystalline Si solar cells. Our experimental studies were based on the growth of ingots, uncontaminated (acting as

references) and deliberately contaminated by Cu or Ti. The grown ingots were cut into wafers and their compositional and electrical properties were assessed. Then solar cells were made using industrial-like fabrication processes, and their illuminated forward and dark reverse current-voltage characteristics evaluated. A particular attention was also paid to the influence of both the external gettering and hydrogenation effects on the electrical properties of the contaminated wafers.

The fourth chapter was dedicated to the effects of Cu and Ti on the PV performances of Czochralski (Cz) single-crystalline Si solar cells. We unexpectedly showed that the introduction of important quantities of Cu in the Si melt during the ingot's growth (9 ppm wt) did not affect the solar cell performances. In addition, for these cells the breakdown voltage fulfills the widely accepted industrial requirement and we did not highlight additional effects of the Cu-contamination on the amplitude of the PV losses under illumination. We showed that this tolerance regarding the Cu contamination was firstly due to the fact that the incorporated Cu concentrations within the ingot were significantly below the expected values (this could be due to the agglomeration/exo-diffusion of Cu at the surfaces combined with the Cu evaporation from the Si melt). Secondly, we confirmed that Cu has a moderate effect on the carrier lifetime, carrier lifetime values slightly improved by the external gettering effect developed by the P-diffusion. On the other hand the addition of 6 ppm wt of Ti strongly affected the PV conversion efficiency of Czochralski-grown solar cells. This is explained by the fact that due to its low diffusivity, Ti is essentially present as interstitial atoms, state in which Ti features harmful recombinant properties. In addition, again because of its low diffusivity the carrier lifetime of the Ti-contaminated samples was not increased by the P-diffusion. Furthermore the electrical properties of the Ti contaminated samples were not improved by the Si bulk hydrogenation treatment. Nevertheless we showed that the Ti contaminated solar cells featured absolute values of the junction breakdown voltage higher than 20 mV, and stable PV conversion efficiencies.

In a second stage, these studies were transposed to multicrystalline Si. The obtained experimental results are presented within the fifth chapter of this manuscript. Regarding Ti, we showed once again that very low Ti concentrations are sufficient to strongly affect the PV performances. However, unexpectedly Ti was more tolerated in multicrystalline Si than in Czochralski Si. This could be due to the presence of extended crystallographic defects in multicrystalline Si, which would enhance the Ti precipitation. Therefore the density of harmful interstitial Ti atoms would be lower. We showed that The Ti contaminated solar cells featured absolute values of the junction breakdown voltage higher than 17 V, and stable PV

conversion efficiencies upon prolonged illumination. Regarding Cu, we decided to increase the amount of introduced Cu in the Si melt (from 9 ppm wt to 90 ppm wt). Despite the large contamination, the initial photovoltaic performances of the Cu contaminated solar cells were unexpectedly slightly higher than the performances of the reference (non-contaminated) cells! We showed that this was mainly due to the efficiency of the external gettering effect developed by the P diffusion. The bulk hydrogenation improved the electrical quality of the wafers only in the zones with a large number of extended crystallographic defects. Within the *good* grains, the hydrogenation slightly degraded the charge carrier lifetime (formation of recombinant Cu-H complexes). The initial PV performances were not affected by the contamination, nevertheless we highlighted a slight negative effect of the Cu addition on the junction breakdown voltage. Above all, we showed that Cu was responsible for important LID effects. This is an important result. Indeed, the efficiency targets of multicrystalline Si solar cells becoming higher and higher, the issue of LID effects on carrier lifetime becomes more and more crucial. As Cu is a common impurity in multicrystalline Si (Cu essentially comes from the silica crucible used for the directional solidification), a particular attention has to be paid to the Cu-related LID effect, and industrial solutions should be developed to address the problem.

The last chapter essentially focused on the *firing* step, used for the sintering of the screen-printed metal electrodes, since this step strongly influences the spatial distribution of the metal impurities within the finished PV device. Particularly we studied the influence of the n^+ (P-diffused layer) emitter on the carrier recombination and trapping of Cu contaminated wafers. We showed that the presence of phosphorus-rich layers during a firing step limits the dissolution of copper precipitates. Therefore, as copper precipitates are virulent recombination centers whereas the electrical activity of interstitial copper is benign, the samples *fired* without phosphorus emitters featured higher carrier lifetimes, but also a stronger sensitivity to the Cu-related LID. In addition, we showed that the samples *fired* without the phosphorus emitters are subjected to trapping effects, probably involving metal elements initially precipitated. The role of the n^+ layer on the limitation of the dissolution of the Cu precipitates is not clearly understood. We proposed and discussed in this manuscript an explanation based on the involvement of Si self-interstitials (Si_I), emitted by the diffusion of P atoms, which would interact with metal precipitates.

Outlook

Regarding the Cu contaminated Cz Si wafers, we showed that the experimental Cu concentrations were significantly lower than the expected values as computed using the Scheil's law. This difference being not clearly understood, it would be important to launch specific studies bringing dedicated experimental data in order to explain this important result. Particularly, as this result could be due to the exo-diffusion of Cu atoms from solid Si during the cooling of the ingot, it could be interesting to monitor the change in the bulk Cu concentrations of Cu contaminated Cz wafers, experiencing experimental conditions (temperature profile, atmosphere) representative of the cooling step of a Cz ingot.

We showed that small quantities of Ti have deleterious effects on the PV performances of crystalline Si solar cells. Consequently, it would be interesting to investigate industrial solutions limiting its effects. Particularly it has been shown in the literature that Cu would form liquid silicides during the cooling of the ingot, which could develop internal gettering effects of the slow diffusing metal impurities. Therefore the study of the properties of solar cells fabricated using wafers from an ingot intentionally contaminated by both Ti and Cu would be particularly interesting. Recently, such an ingot was grown in the lab. In the short-term, solar cells should be fabricated with the wafers from this ingot.

An important result of this PhD is the strong amplitude of the Cu-related LID effects towards the PV conversion efficiency of the multicrystalline Si solar cells. In the literature and throughout our studies, indirect evidences were brought concerning the mechanism responsible for these LID effects, which would be due to room temperature Cu precipitation. However, because of the size of the newly formed Cu precipitates / clusters, which would be around few nanometers, this precipitation mechanism has never been *directly* observed. Therefore, the *direct* observation of these precipitates, responsible for the Cu-related LID, via for instance the use of synchrotron radiations, would represent a fascinating scientific challenge.

Because of the importance of the Cu-related LID, it is of paramount importance to develop industrial solutions for the suppression of this effect. In the literature it was shown that the use of negatively charged dielectric layers deposited on the wafer surfaces efficiently suppressed the Cu-related LID via the trapping of interstitial Cu atoms at the surfaces. However to the best of our knowledge, this solution has never been investigated at the solar cell level. Thus such studies would be important in the future.

These studies were dedicated to Cz-Si and to *conventional* multicrystalline Si ingots grown by directional solidification in silica crucibles. Nowadays, new crystallization techniques are emerging which could be promising for the PV industry, among which the so-called “Mono-Like” technology and the “High Performance Multicrystalline” (HP mc) technology. The “Mono-like” technology is essentially a seed-assisted directional solidification of virtually single-crystalline Si ingots. The HP mc technology features the growth of multicrystalline ingots by directional solidification, but using specific coatings which enhance the nucleation mechanisms. This leads to mc wafers with small grain sizes, but with low and homogeneous densities of dislocations over the entire height of the ingot. Therefore, it would be important in the future to extend the conclusions of the studies carried out in the frame of this PhD to these new crystallization techniques.

LIST OF PUBLICATIONS

Journal papers

- T. Turmagambetov, S. Dubois, J. P. Garandet, B. Martel, N. Enjalbert, J. Veirman, E. Pihan. **Influence of copper contamination on the reverse and forward characteristics of multicrystalline p-type silicon solar cells.** Phys. Status Solidi (c). 11, No. 11–12, 1697–1702 (2014).
- T. Turmagambetov, S. Dubois, J. P. Garandet, H. Lignier and N. Enjalbert. **Influence of phosphorus-rich layers during rapid annealing on carrier recombination and trapping in copper contaminated multicrystalline silicon.** To be submitted to Appl. Phys. Lett. (2015)

Patent

- S. Dubois, T. Turmagambetov, J. P. Garandet, J. Veirman, B. Martel, E. Pihan. **Hydrogenated silicon substrate, process for hydrogenating a silicon substrate and passivizing metallic impurities contained in a silicon substrate.**

International conferences

- T. Turmagambetov, S. Dubois, J. P. Garandet, B. Martel, N. Enjalbert, J. Veirman, E. Pihan. **Influence of copper contamination on the illuminated forward and dark reverse I-V characteristics of p-type mc-Si solar cells.** E-MRS 2014 Spring Meeting, Lille, France, May 26-30 (2014)
- A. Betekbaev, B. Mukashev, Y. Pellegrin, K. Ounadjela, T. Turmagambetov, D. Kalygulov, A. Pavlov, D. Skakov and A. Serikkanov. **KazPV Project: Industrial development of a vertically integrated PV production in Kazakhstan based on SOG silicon.** 29th EU PVSEC 2014, The Netherlands, Amsterdam, September 22-26 (2014).

RÉSUMÉ ÉTENDU

De l'influence de contaminations par le cuivre et le titane sur les performances photovoltaïques de cellules solaires au silicium cristallin

Introduction, objectifs

L'industrie photovoltaïque (PV), en croissance monotone depuis plusieurs décades, est depuis longtemps largement dominée par la filière des cellules solaires PV au silicium (Si) cristallin. Cette croissance est accompagnée d'une baisse continue du prix des modules PV, avec un prix en 2014 voisin de 0.6 $/W.

Afin de maintenir la croissance du marché PV, il faut d'une part améliorer les rendements de conversion PV (η), et d'autre part diminuer le coût d'élaboration des modules PV. En 2014, 60 % et 40 % des cellules industrielles en Si cristallin sont respectivement fabriquées à partir de Si multicristallin (mc-Si) obtenu par solidification dirigée en creuset, et monocristallin (c-Si) issu de tirages Czochralski (Cz). Les prévisions de rendement pour ces deux filières, définies par la feuille de route internationale de l'industrie PV [1], sont ambitieuses puisqu'en 2018 des η respectifs de 20.0 % et 25.0 % sont attendus pour les cellules industrielles en silicium mc et Cz. De telles performances ne peuvent être obtenues que si les recombinaisons des porteurs de charge dans le volume et aux surfaces du dispositif sont limitées, et que la jonction *p*-*n* est d'excellente qualité (absence de recombinaisons dans la zone de charge d'espace et de courts-circuits parasites). Cela signifie que les teneurs en impuretés métalliques sont minimisées, ou du moins que ces éléments sont électriquement neutralisés. En effet les impuretés métalliques sont d'une part connues pour introduire des centres de recombinaison virulents qui affectent la durée de vie des porteurs de charge (τ). D'autre part, précipitées elles peuvent provoquer des courts-circuits localisés de la jonction *p*-*n*, délétères pour les performances globales du dispositif.

En parallèle, un levier fort de réduction du coût d'élaboration des modules PV serait de pouvoir utiliser un silicium de qualité solaire (SoG), purifié par voie métallurgique (SoG_M), à la place du silicium dit de qualité électronique (EG) purifié par voie chimique (procédé Siemens). En effet, les procédés de purification par voie métallurgique (le silicium ne passe

pas par une phase gazeuse) sont compatibles avec des coûts du silicium charge inférieurs à 15 €.kg^{-1}. Egalement, ces procédés de purification ont un faible impact sur l'environnement (absence notamment de produits chlorés, faible dépense énergétique comparée à celle du procédé Siemens). En contrepartie, les charges SoG_M contiennent en général des teneurs en impuretés métalliques supérieures à celles des charges EG.

Par conséquent, la présence d'impuretés métalliques dans le Si est une problématique centrale, que les deux défis clés de l'industrie PV sur Si (augmentation des performances, réduction des coûts) doivent surmonter. Dans ce contexte, l'objectif de cette thèse est le développement de connaissances nouvelles sur l'influence des impuretés métalliques sur les performances des cellules PV en silicium cristallin. Cette connaissance est essentielle notamment pour le développement de procédés d'ingénierie des défauts permettant la neutralisation électrique et/ou l'extraction des éléments les plus nocifs.

De nombreuses études se sont intéressées à l'effet du fer et du chrome sur les performances des cellules. De nos jours, l'influence de ces deux impuretés sur le η des cellules est plutôt bien connue [2]. Ainsi cette thèse s'intéresse à deux éléments métalliques dont les effets sur les performances des dispositifs PV ont été beaucoup moins étudiés : le cuivre (Cu) et le titane (Ti).

Le Cu a été choisi car il s'agit tout d'abord de l'un des éléments les plus abondants dans le mc-Si obtenu par solidification dirigée (des concentrations aussi élevées que 10^{13} cm^{-3} ont été détectées [3]). Le cuivre est essentiellement issu du creuset en silice utilisé pour la cristallisation, et de son revêtement anti-adhérent en nitrure de Si [4]. De plus le Cu a un coefficient de diffusion élevé qui favorise la contamination volumique du Si par cet élément. Enfin un élément nouveau est récemment apparu pour justifier encore notre choix du Cu, puisque les électrodes métalliques en argent utilisées pour la collecte des porteurs pourraient être remplacées à terme par des électrodes en Cu.

Le Ti a été sélectionné pour ce travail car il est également l'un des éléments les plus abondants dans le silicium métallurgique (issu de l'étape de carbothermie) [5]. Par conséquent, de fortes teneurs en Ti sont généralement détectées dans les charges SoG_M.

Il est important de préciser que ces deux éléments ont été aussi choisis car comme nous le verrons par la suite, d'une part leurs principales propriétés dans le Si sont bien connues (ce qui facilite le travail). D'autre part ces deux éléments ont des propriétés très différentes dans le Si. Enfin ils ont des caractéristiques semblables à celles d'autres contaminants métalliques, et peuvent donc être considérés comme des impuretés modèles, ce qui permettra de transposer les conclusions issues de ce travail de thèse à un nombre élargi d'autres métaux de transition.

A noter que depuis le début de ce travail de thèse, de nouvelles études se sont intéressées aux effets de ces éléments sur le η des cellules solaires au Si cristallin. Cependant, nos travaux se démarquent nettement de ces études puisque d'une part, nous travaillons conjointement sur le silicium monocristallin et multicristallin, pour faire la part des défauts de structure (cf. ci-dessous) et ce avec des procédés de fabrication des cellules PV équivalents aux procédés industriels actuels. Egalement, nos études s'intéressent aux effets de ces deux éléments sur le η « initial » des dispositifs, mais aussi sur la stabilité du rendement sous éclairement, ainsi que sur la tension de claquage de la jonction *p*-*n*, paramètre qui gouverne les performances des modules PV en conditions réelles de fonctionnement.

Chapitre 1. Principaux défauts dans le silicium cristallin, effets sur les performances photovoltaïques

Tout d'abord, ce chapitre présente le principe de fonctionnement de la cellule PV classique à base de silicium cristallin de type *p*. Egalement, il évoque les mécanismes par lesquels les défauts dans le silicium affectent les performances du dispositif PV. En particulier, la présence de défauts dans le silicium cristallin favorise les recombinaisons des porteurs de charge par un mécanisme de type Shockley-Read-Hall (SRH). Ces recombinaisons sont liées à la présence de niveaux en énergie introduits par les défauts dans la bande interdite du Si. Les défauts diminuent donc la durée de vie des porteurs de charge (τ) et par conséquent la longueur de diffusion des porteurs minoritaires (L). Or plus faibles sont ces paramètres, plus faibles sont le courant de court-circuit (J_{sc}), la tension de circuit ouvert (V_{oc}), et en raison des recombinaisons dans la zone de charge d'espace de la jonction *p*-*n*, le facteur de forme (*FF*) de la cellule. De plus, sous la forme de précipités conducteurs, les défauts peuvent en court-circuitant la jonction *p*-*n*, significativement altérer le *FF* et le V_{oc}.

Le silicium cristallin, même cristallisé à partir de charges ultra-pures, contient des défauts structuraux (joints de grains, dislocations…). Ces défauts, sont susceptibles d'interagir avec les éléments métalliques étudiés dans ce travail de thèse et de brouiller les conclusions extraites des données expérimentales. Ainsi, ce chapitre évoque également d'une part les techniques de cristallisation du Si utilisées dans ce travail de thèse (solidification dirigée en creuset pour l'obtention de lingots multicristallins et tirage Czochralski pour la croissance de lingots monocristallins). D'autre part sont présentés les principaux défauts présents dans le silicium cristallin et les effets de ces défauts sur les performances PV: les

défauts ponctuels intrinsèques (lacunes, auto-interstitiels), les défauts de structure étendus (joints de grains, dislocations, précipités), les impuretés métalliques (fer notamment) et les éléments légers (oxygène, carbone et azote).

Enfin, le procédé classique industriel de fabrication des cellules PV, utilisé dans le cadre de cette thèse, est détaillé. En particulier, les étapes technologiques qui influencent l'état et la distribution spatiale des impuretés métalliques sont présentées. Il s'agit tout d'abord de la diffusion phosphore, utilisée pour former l'émetteur n^+ de la cellule, qui développe un effet getter externe (extraction et piégeage) des impuretés métalliques. Egalement le dépôt PECVD (plasma enhanced chemical vapor deposition) de la couche anti-reflet de la cellule, qui est un nitrure de Si hydrogéné, a un rôle important, puisque l'hydrogène diffuse par la suite dans le volume du matériau pour électriquement passiver certains défauts cristallographiques et impuretés métalliques. Enfin, lors du recuit des électrodes métalliques, un alliage liquide entre le Si et l'aluminium (utilisé comme électrode pleine plaque face arrière) se forme, qui développerait un effet getter externe des éléments métalliques tout en favorisant la diffusion de l'hydrogène.

Chapitre 2. Etude comparative des propriétés du cuivre et du titane dans le silicium cristallin – Effets connus de ces impuretés sur les performances PV

Ce chapitre s'intéresse d'une part aux propriétés du Cu et du Ti dans le Si cristallin. Sont présentés les effets connus de ces deux éléments sur les propriétés de recombinaison des porteurs de charge, ainsi que sur les performances PV. Il est intéressant de constater que le Cu et le Ti ont des propriétés dans le Si, et des effets sur les propriétés électriques du matériau, très différents.

Tout d'abord le coefficient de diffusion du Cu est beaucoup plus élevé que celui du Ti. A titre d'exemple, à 800 °C, le coefficient du Ti est voisin de 10^{-10} $cm^2.s^{-1}$, alors qu'il est proche de 2×10^{-5} $cm^2.s^{-1}$ pour le Cu ! Ainsi à l'issue d'une étape à haute T, le Cu est essentiellement précipité, alors que les atomes de Ti, qui ne sont pas suffisamment mobiles pour atteindre les sites de précipitation, sont principalement en solution solide, en position interstitielle.

Egalement, l'effet de ces deux éléments sur la τ est bien différent. Le Ti, en position interstitiel, est un centre de recombinaison très virulent. Cela est lié au fait que le Ti introduit un niveau en énergie profond dans la bande interdite, situé à 0.28 eV au-dessus de la bande de

valence, et que ce niveau présente une section efficace de capture élevée pour les électrons (égale à 2×10^{-15} cm^2). En contrepartie, le Cu interstitiel a une activité électrique bénigne, principalement car ce défaut introduit un niveau plutôt superficiel dans la bande interdite, situé à 0.15 eV sous la bande de conduction. Par contre, les précipités de Cu présentent une activité recombinante plus importante. Ces défauts introduiraient une bande de niveaux en énergie dans la bande interdite, située entre 0.5 eV et 0.2 eV sous la bande de conduction. Enfin, la présence de Cu dans le Si entraîne des effets de dégradation sous éclairement (LID pour Light-Induced Degradation) de la τ. Cette dégradation serait liée à des mécanismes d'agglomération/précipitation du Cu à faible T sous éclairement. En effet, sous éclairement, les charges libres excédentaires permettraient au Cu interstitiel initialement positivement chargé de devenir neutre. Il pourrait alors migrer vers les précipités de Cu positivement chargés et la taille des amas/précipités de Cu augmenterait. A noter que des modélisations récentes indiquent que la taille des amas d'atomes de Cu responsables des effets de LID serait voisine de quelques nanomètres.

A propos de l'effet du Ti sur les performances des cellules solaires PV, les différentes études publiées convergent sur le fait que cet élément affecte fortement le rendement de conversion des cellules. Pour le Cu, les résultats de la littérature sont plus contradictoires. L'étude la plus récente [6] a montré qu'une contamination du Si charge (avant cristallisation) par une teneur en Cu de 90 ppm wt affecte fortement les propriétés électriques de l'émetteur et du volume des cellules mc.

Il est très important de noter que malgré ces précédentes études publiées dans la littérature, il est indispensable de lancer de nouvelles études sur l'effet du Ti et du Cu sur les propriétés des cellules PV. En effet, les procédés de fabrication utilisés pour ces études sont soit trop éloignés des procédés industriels actuels (absence d'hydrogénation du volume, absence de recuit rapide des électrodes métalliques), soit trop limités en termes de potentiels de rendements de conversion (ce qui peut masquer l'effet des éléments étudiés). De plus, ces précédentes études ne se sont pas intéressées à l'évolution sous éclairement des performances des cellules contaminées par le Cu. Enfin, ces études antérieures n'ont pas évalué l'effet du Ti et du Cu sur les tensions de claquage des jonctions, alors que ce paramètre gouverne les performances des modules PV en conditions réelles d'utilisation.

Chapitre 3. Cristallisation de lingots contaminés – Techniques expérimentales utilisées

Ce chapitre présente tout d'abord les différents lingots de type p dopés au bore, cristallisés pour ce travail de thèse. Concernant le silicium monocristallin, trois lingots d'environ 10 kg ont été obtenus par tirage Cz : un lingot de référence (non intentionnellement contaminé par des éléments métalliques), un lingot contaminé par le Cu (une concentration de 9 ppm wt de Cu a été ajoutée à la charge), et un lingot contaminé par le Ti (une teneur en Ti de 6 ppm wt a été ajoutée à la charge). Dans un second temps l'étude a été transposée au silicium multicristallin. Pour cela à nouveau trois lingots, cette fois d'environ 60 kg, ont été cristallisés par solidification dirigée en creuset dans un four semi-industriel : un lingot de référence (non intentionnellement contaminé par des éléments métalliques), un lingot contaminé par le Cu (une concentration cette fois de 90 ppm wt de Cu a été ajoutée à la charge), et un lingot contaminé par le Ti (une teneur en Ti de 6 ppm wt a été ajoutée à la charge).

Les différents lingots ont été ensuite découpés en plaquettes. L'une des originalités de notre étude concerne l'utilisation d'outils de caractérisation complémentaires, afin d'une part d'étudier à la fois les propriétés compositionnelles (analyses chimiques, spectroscopie infra-rouge à transformée de Fourier, « deep level transcient spectroscopy », « secondary ion mass spectroscopy »), et les propriétés électriques (mesures de résistivité, effet Hall, mesures de durée de vie des porteurs de charge) des plaquettes et d'autre part de caractériser l'effet des contaminations sur les performances PV des cellules (mesures courant-tension sous éclairement, cartographies en photo-courant, mesures courant-tension en polarisation inverse, acquisition d'images du signal électroluminescent, tests de vieillissement). Pour ces dernières caractérisations, des cellules solaires PV ont donc été fabriquées, via l'utilisation d'un procédé industriel de fabrication dont les principales étapes sont les suivantes:

- Texturation des surfaces par l'attaque anisotropique développée par une solution de KOH
- Diffusion phosphore en four à tube à partir de $POCl_3$ (formation de la jonction)
- Dépôt de la couche anti-reflet par PECVD : nitrure de silicium hydrogéné.
- Impression des électrodes métalliques par sérigraphie : grille en argent sur la face avant et couche d'aluminium pleine plaque sur la face arrière
- Recuit rapide de la cellule pour le frittage des pâtes de sérigraphie et la formation des contacts Si/métal

- Ouverture de la jonction (isolation électrique de la face avant et de la face arrière) par irradiation laser des bords de la cellule.

Chapitre 4. Effets du Ti et du Cu sur les propriétés des plaquettes et cellules solaires PV issues des lingots Czochralski

Ce chapitre s'intéresse donc aux propriétés des plaquettes et cellules issues des lingots monocristallins Cz de référence, et intentionnellement contaminés par le Ti et le Cu.

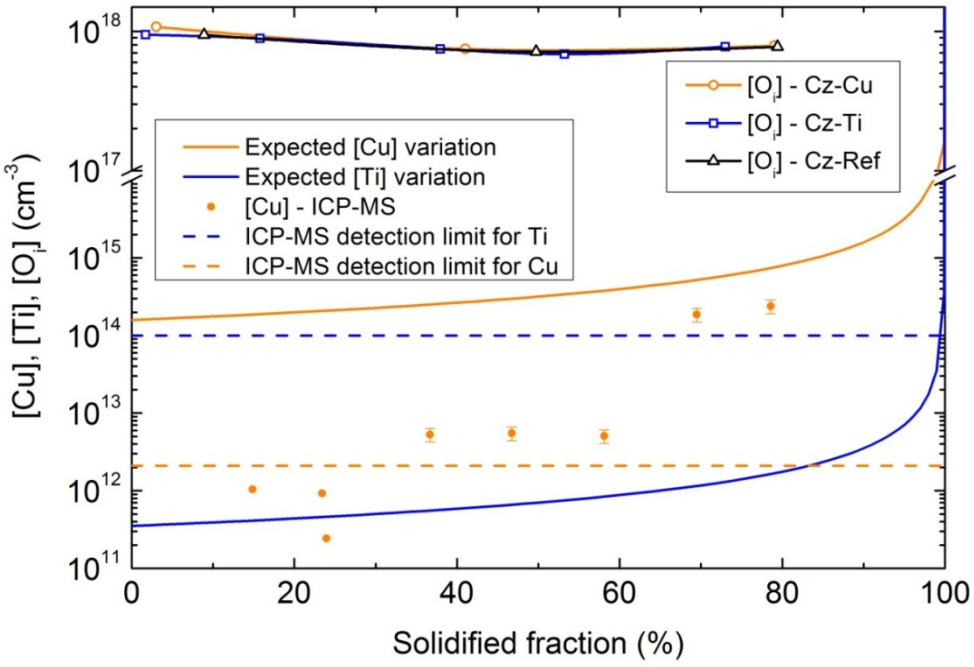

Figure 1. Lingots Cz. Variations des teneurs expérimentales en Cu, Ti et oxygène interstitiel (Oi) avec la fraction solidifiée. Variations des teneurs attendues (calculées) en Cu et Ti avec la fraction solidifiée.

Tout d'abord les propriétés compositionnelles des plaquettes ont été évaluées. Les teneurs totales en Cu ([Cu]) ont pu être déterminées par ICP-MS (inductively coupled mass spectroscopy). De façon inattendue (Figure 1), les [Cu] expérimentales étaient bien inférieures (de 2 décades pour une fraction solidifiée de 20 %) aux valeurs calculées à partir de la loi de Scheil. Cette différence n'est pas complètement expliquée. Elle pourrait être liée à la conjugaison de plusieurs effets : évaporation du Cu du silicium liquide au cours du tirage, diffusion en phase solide du Cu lors du refroidissement du lingot (en raison de son coefficient de diffusion élevé) et agglomération aux surfaces (qui sont par la suite rodées), voire exo-diffusion depuis la phase solide. A noter que la différence entre la teneur attendue en Cu et la teneur expérimentale diminue avec la fraction solidifiée. Ce résultat accrédite la thèse d'effets

d'agglomération aux surfaces/exo-diffusion, car le temps passé à haute température diminue avec la fraction solidifiée.

La présence du Ti au cœur des plaquettes n'a pas pu être mise directement en évidence par les analyses chimiques, mais elle a pu être quantifiée d'une part via des analyses par secondary ion mass spectroscopy (SIMS) effectuées sur la couche diffusée P (riche en impuretés), et d'autre part par des analyses DLTS (deep level transcient spectroscopy). Ces dernières nous ont permis de remonter à la teneur expérimentale en Ti interstitiel au cœur des plaquettes à la fraction solidifiée de 70 %, égale à $1{,}3\times10^{13}$ cm^{-3}. Cette valeur est dix fois plus élevée que la concentration calculée à partir de la loi de Scheil (environ 10^{12} cm^{-3}). La différence pourrait s'expliquer par un coefficient de ségrégation effectif utilisé dans la loi de Scheil qui ne correspond pas à la valeur expérimentale.

Les propriétés électriques ont ensuite été évaluées. Les résistivités sont en accord avec les valeurs attendues. La contamination par le Cu n'a pas eu d'effet important sur les τ des plaquettes issues des parties hautes (proches du germe) et centrales du lingot Cz. En effet des τ voisines de 300 µs ont été mesurées dans la partie centrale du lingot (similaires aux valeurs des plaquettes de référence). A noter cependant une chute significative de la τ dans la partie basse du lingot (fractions solidifiées supérieures à 70 %), avec des τ alors aussi faibles que 20 µs. Par contre, les τ des plaquettes contaminées par le Ti sont systématiquement bien inférieures aux valeurs obtenues sur les plaquettes de référence. A titre d'exemple, pour une fraction solidifiée de 40 %, la τ des plaquettes contaminées Ti est voisine de 30 µs !

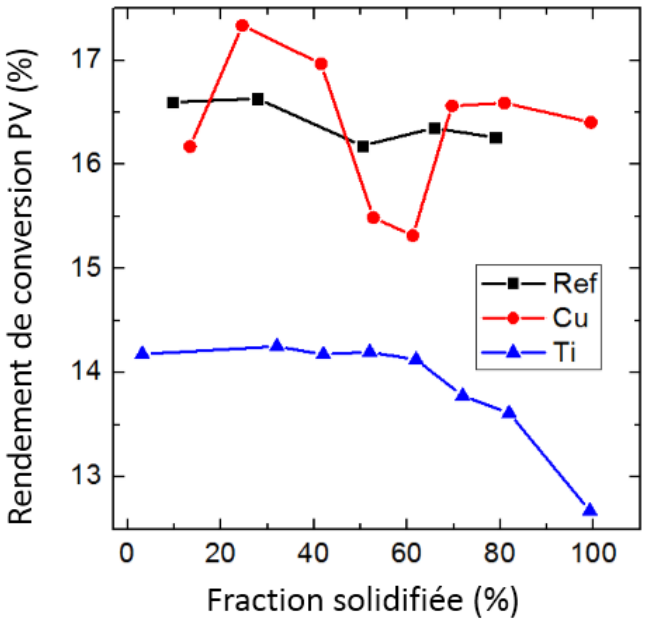

Figure 2. Variations avec la fraction solidifiée du rendement de conversion PV. Cas des cellules Cz de référence, des cellules Cz contaminées par le Cu, et des cellules Cz contaminées par le Ti.

Des cellules ont été fabriquées et leurs performances mesurées (Figure 2). La contamination par le Cu n'a pas affecté les performances des cellules solaires fabriquées, et ce pour les plaquettes issues de toute la hauteur du lingot ! En effet le rendement des cellules contaminées Cu est identique à celui des cellules de référence, proche de 17 % pour une fraction solidifiée de 40 %. En contrepartie, la présence de Ti a fortement altéré le rendement de conversion PV, puisque pour la même fraction solidifiée, la valeur de rendement mesurée ne dépasse pas 14.2 % !

En effectuant des mesures de τ avant et après l'étape de diffusion P, nous avons montré que la contamination par le Cu a peu d'effet sur les performances des cellules car d'une part comme précisé les τ des plaquettes contaminées sont initialement élevées, et d'autre part sont encore améliorées par la diffusion P. Par exemple, pour une fraction solidifiée de 52 %, la τ (évaluée par la technique de suivi par micro-ondes de la décroissance de photoconductivité) augmente de 71 µs à 92 µs via l'étape de diffusion P (Figure 3). Cela s'explique sans doute en raison du coefficient de diffusion élevé du Cu, qui favorise son extraction du volume par l'effet getter externe développé par la diffusion P. En contrepartie les τ avant diffusion des plaquettes contaminées par le Ti sont faibles, et elles ne sont pas améliorées par la diffusion P, le Ti ne diffusant pas suffisamment rapidement pour atteindre la zone de piégeage n^+.

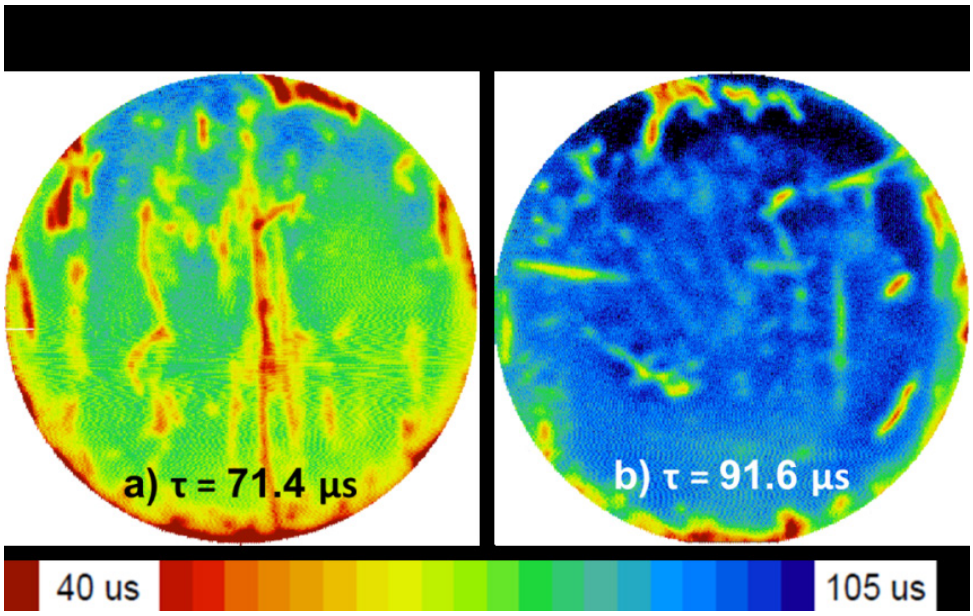

Figure 3. Cartographies de la durée de vie des porteurs de charges. Cas de plaquettes Cz contaminées par le Cu, initialement juxtaposées sur la hauteur du lingot (issues d'une fraction solidifiée de 52 %). Les surfaces sont électriquement passivées par des couches SiNx :H. (a) la plaquette n'a pas subi de diffusion P. (b) la plaquette a subi une étape de diffusion P, et l'émetteur a été chimiquement décapé. Les valeurs indiquées (en noir et blanc) sont les valeurs moyennes.

A noter que l'effet de l'hydrogénation sur les propriétés électriques du matériau a été étudié en fabricant des cellules avec et sans la couche de nitrure de Si hydrogéné (SiNx:H) et en estimant la longueur de diffusion des électrons (L) via des analyses LBIC (light beam induced current). Cependant, nous n'avons pas pu extraire de conclusions solides de cette étude, les L étant proches avec et sans couche SiNx :H. De plus pour les plaquettes contaminées Cu, les L étaient élevées. Nous étions donc dans une situation pour laquelle la méthode d'estimation des L n'est généralement pas fiable (L proche de l'épaisseur de l'échantillon). De plus, les L étaient si élevées qu'elles pouvaient être influencées par des contaminations parasites lors du recuit des contacts, favorisées par l'absence de la couche SiNx:H qui pourrait développer un effet barrière aux impuretés. Pour les cellules contaminées au Ti, nous n'avons pas observé d'amélioration associée à la présence d'une couche de SiNx :H, ce qui peut être dû soit au fait que le Ti n'est pas passivé par l'H, soit à des teneurs trop limitées en H dans le volume des cellules Cz.

Nous avons ensuite mesuré les caractéristiques I-V inverses de cellules solaires PV Cz contaminées par le titane et le cuivre. Les effets de claquage n'ont pas été observés sur la gamme de différence de potentiel étudiée (-20 V ; 0 V). Ainsi les tensions de claquage de ces cellules, qui sont en valeur absolue supérieures à 20 V satisfont la spécification industrielle pour ce paramètre, qui est de 12 V.

L'évolution sous éclairement des performances des cellules Cz de référence, contaminées Ti et contaminées Cu, a été également étudiée. Les cellules de référence et contaminées Cu se dégradent de façon conséquente (perte relative de rendement voisine de 5 % pour la cellule contaminée Cu). A noter par contre que la perte relative de rendement est plus forte pour la cellule de référence (proche de 9 %) que celle mesurée pour la cellule contaminée Cu. Cela indique que les effets de dégradation observés sont essentiellement gouvernés par l'activation/formation des complexes bore-oxygène [7] (le silicium Cz étant particulièrement sensible à ces effets de dégradation en raison des teneurs élevées en oxygène interstitiel, proches de 10^{18} cm^{-3}). Le rendement de la cellule contaminée par le Ti a peu varié sous éclairement (baisse relative de rendement inférieure à 2 %). Nous avons montré que ce résultat est lié au fait que la τ de ces plaquettes, gouvernée par le Ti interstitiel, est si faible, qu'elle n'est pas influencée par l'activation/formation des complexes B-O.

Chapitre 5. Effets du Ti et du Cu sur les performances des cellules solaires PV au silicium multicristallin obtenu par solidification dirigée

Ce chapitre s'intéresse aux propriétés des plaquettes et cellules issues des lingots en Si multicristallin de référence, et intentionnellement contaminés par le Ti et le Cu.

Tout d'abord les propriétés compositionnelles des plaquettes ont été évaluées. Les teneurs totales en Cu ([Cu]) ont pu être déterminées par ICP-MS et GDMS (« Glow Discharge Mass Spectroscopy »). La contamination volontaire par le Cu donne des résultats différents que la croissance soit faite par tirage Cz ou par solidification dirigée. En effet alors que pour le lingot Cz, pour la première fraction cristallisée, les [Cu] expérimentales sont 100 fois plus faibles que les valeurs attendues, pour le lingot mc, les [Cu] expérimentales sont similaires aux valeurs attendues. Les mécanismes physiques à l'origine de ces différences ne sont pas clairement identifiés. Cependant, des effets d'exodiffusion du cuivre, qui dépendraient de l'environnement à la surface du silicium solide (revêtement SiN pour le mc, surface à « nue » pour le Cz), de la distance entre le cœur du lingot et les surfaces (beaucoup plus élevée pour le lingot mc) et de profils de refroidissement différents pour chacune de ces techniques de croissance, pourraient être à l'origine de ces différences de comportement. A noter tout de même que pour le lingot mc, les [Cu] expérimentales sont légèrement plus faibles que les valeurs attendues (différence inférieure à la demi-décade). Egalement, les [Cu] expérimentales varient peu sur la hauteur du lingot. Ces résultats pourraient être expliqués par des mécanismes d'évaporation du Cu du bain de Si, et par le coefficient de diffusion élevé du Cu. En effet, durant le refroidissement du lingot, les atomes de Cu peuvent migrer sur plusieurs centimètres, ce qui contribuerait à l'homogénéisation des teneurs en Cu sur la hauteur du lingot mc.

Pour le titane, sa présence n'a pas été détectée, en particulier par GDMS. Il est donc présent à une concentration inférieure à la limite de détection de la GDMS pour cet élément, qui est égale à 2.9×10^{13} cm^{-3}. Cela est en bon accord avec les teneurs attendues qui devraient être sur la hauteur du lingot étudié inférieures à 3.0×10^{12} cm^{-3}.

Des cellules ont été fabriquées et leurs performances évaluées et comparées à celles de cellules fabriquées avec des plaquettes issues d'un lingot mc de référence (Figure 4). Tout d'abord, les résultats montrent, et ce de façon inattendue puisque contradictoire avec les résultats récents de la littérature [6], que la contamination par le Cu, malgré les 90 ppm wt introduits dans le Si liquide, n'affecte pas le rendement initial (avant éclairement prolongé)

des cellules. Au contraire, le rendement le plus élevé, proche de 17 % est obtenu pour une plaquette contaminée Cu ! C'est un résultat important, car il indique que de très fortes teneurs en Cu pourraient éventuellement être tolérées. Nous avons montré que ce résultat était essentiellement lié à l'effet getter développé par la diffusion P (efficace en raison du fort coefficient de diffusion du Cu), puisque la τ effective moyenne pour un échantillon initialement situé à 52 % de la hauteur totale du lingot, a été multipliée par 1.7.

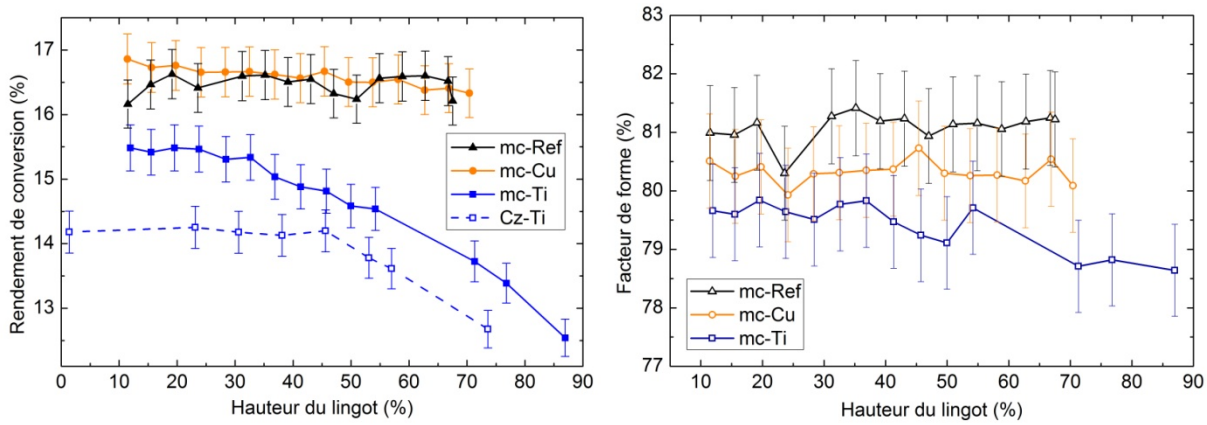

Figure 4. Variations sur la hauteur des lingots du rendement de conversion (à gauche) et du facteur de forme (à droite) des cellules mc de référence, contaminées par le Cu, et contaminées par le Ti. Comparaison avec les valeurs obtenues pour les cellules Cz contaminées par le Ti.

L'hydrogénation du volume des plaquettes contaminées par le Cu a permis d'améliorer légèrement la valeur moyenne de la L (les L de la cellule avec couche SiNx:H est 1.2 fois plus élevée que celle de la cellule sans couche SiNx:H, donc sans apport d'H). Ce faible effet de l'hydrogénation du volume sur les propriétés électriques des plaquettes a pu être expliqué. Nous avons en effet montré (Figure 5) que les propriétés électriques des zones proches des joints de grains ou des amas de dislocations étaient améliorées par l'apport d'H. Cela est vraisemblablement expliqué par l'effet connu de passivation par l'H des liaisons vacantes au niveau des défauts cristallographiques étendus. Par contre l'hydrogénation a affecté les propriétés électriques à l'intérieur des grains de bonne qualité structurale. Ce résultat, rarement observé avec le Si mc, est expliqué par le fait que l'H forme des complexes avec le Cu, complexes dont le pouvoir recombinant est supérieur à celui du Cu interstitiel [8].

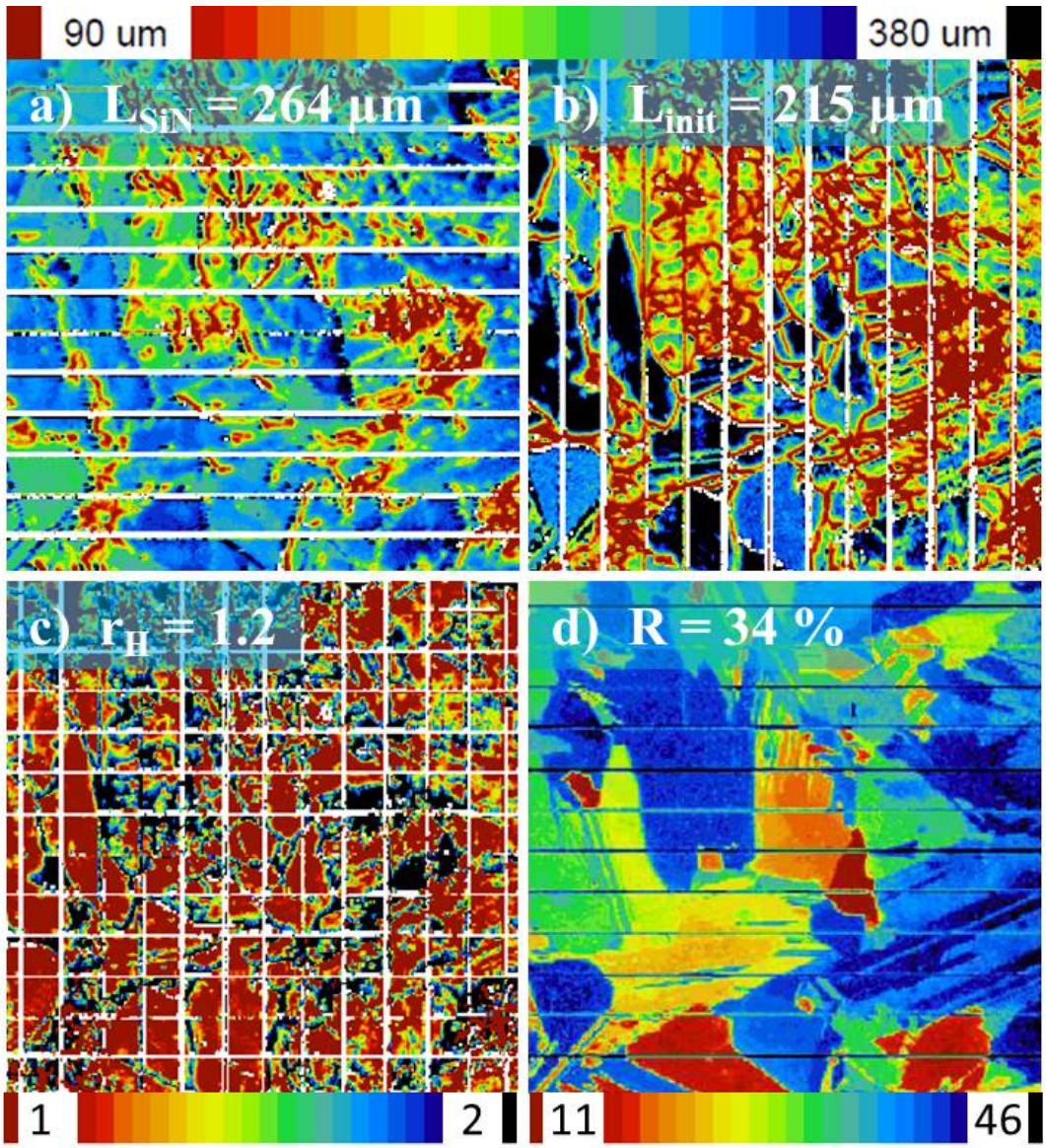

Figure 5. Cartographies en L de cellules contaminées par le Cu fabriquées avec (a) et sans (b) couche SiNx :H. Les plaquettes utilisées étaient initialement juxtaposées sur la hauteur du lingot. (c) cartographie du rapport entre les L de la cellule avec la couche SiNx:H et de la cellule sans la couche SiNx:H. (d) Cartographie en réflectivité pour révéler la structure de grain (la plaquette a été texturée KOH).

Une fois encore, la contamination par le Ti a fortement diminué les performances des cellules mc. En effet à 50 % de la hauteur du lingot, la contamination par le Ti entraîne une baisse du η de 2 % absolus. Cet effet délétère du Ti s'explique d'une part par le caractère très recombinant de cet élément (élément dont la précipitation est limitée du fait de son faible coefficient de diffusion, et qui en position interstitielle présente des sections efficaces de capture élevées pour les porteurs de charge), et d'autre part par son incapacité à être extrait du volume par l'effet getter externe développé par la diffusion P (à nouveau en raison de son faible coefficient de diffusion). Enfin, l'hydrogénation du volume n'a pas permis d'améliorer

la L des plaquettes contaminées par le Ti, cet élément ne formant pas de complexes électriquement inactifs (ou du moins peu actifs) avec l'H [9]. C'est un résultat crucial car il indique que si la teneur en Ti dans la charge est supérieure ou égale à 6 ppm wt, les rendements des cellules ne satisferont pas aux exigences industrielles (en général des rendements supérieurs à 16.5 % sur substrats mc sont attendus) et qu'il faut donc impérativement chercher à réduire les teneurs en cet élément.

Il est intéressant de comparer pour le Ti les résultats de cette étude avec ceux précédemment obtenus sur la contamination par cette impureté d'un lingot Cz (Figure 4). En effet, on constate que pour une contamination identique par le Ti de la charge de Si, le Ti est globalement mieux toléré dans le silicium mc que dans le silicium Cz. Malgré une texturation KOH peu adaptée pour le mc, à titre d'exemple pour la première partie solidifiée des lingots, les cellules mc contaminées Ti ont un rendement voisin de 15 % alors qu'il n'est que de 14 % pour les cellules Cz contaminées Ti ! On peut penser qu'à haute température, au cours du refroidissement des lingots, la plus forte densité de centres de nucléation hétérogènes dans le mc (défauts étendus notamment) a favorisé la précipitation du Ti et par conséquent la teneur en Ti dissous serait alors plus faible (c'est en solution solide que l'effet d'une impureté métallique comme le Ti est le plus marqué).

Les caractéristiques I-V inverses des cellules à l'obscurité ont ensuite été déterminées, en particulier pour extraire la tension de claquage (V_{bd}). Nous avons montré que la contamination par le Ti (pour les teneurs étudiées) n'a pas d'influence significative sur la caractéristique I-V inverse des cellules. Les cellules contaminées Ti ont également une tension de claquage bien supérieure (en valeur absolue) à la spécification industrielle de 12 V. Pour les cellules contaminées par le Cu, nous avons constaté que le claquage de la jonction intervient pour des tensions plus faibles en valeur absolue (voisines de 16 V) que ce qui est observé pour la cellule contaminée par le Ti (claquage autour de 18 V). Ainsi il semble que le Cu influence les mécanismes de claquage des jonctions *p-n*. Nous avons montré via des analyses du signal électroluminescent en polarisation inverse (Figure 6), que le claquage des cellules contaminées Cu prenait place de façon localisée au niveau de certains joints de grains et d'amas de dislocations. Cela pourrait être lié à une précipitation accentuée du Cu le long des défauts étendus, conduisant à la formation de siliciures de Cu conducteurs, qui pourraient alors au niveau de la jonction favoriser le claquage. Cependant, l'effet d'une diffusion accentuée du P le long de ces défauts étendus, qui entrainerait une courbure de la jonction *p-n* connue pour favoriser le claquage, ne peut pas être exclu.

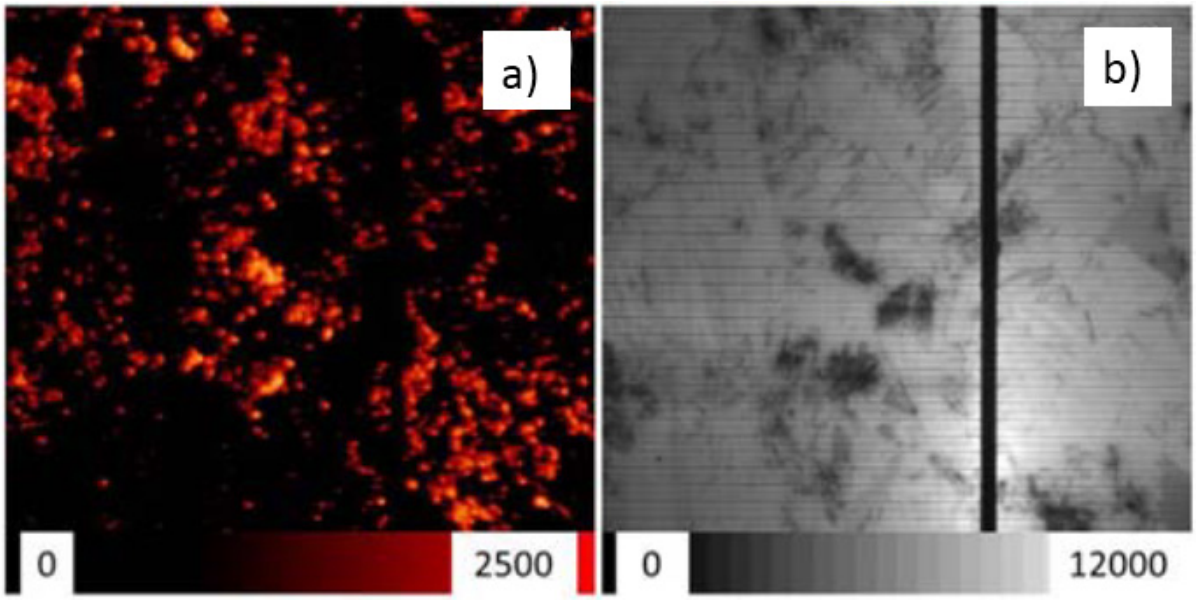

Figure 6. Images du signal électroluminescent d'une cellule mc contaminée Cu en polarisation inverse (a) et en polarisation directe (b).

L'évolution sous éclairement des performances des cellules mc de référence, contaminées Ti et contaminées Cu, a également été étudiée. Le rendement des cellules mc contaminées par le Ti était stable sous éclairement. A nouveau, cela est vraisemblablement lié au fait que la τ de ces plaquettes, gouvernée par le Ti interstitiel est si faible, qu'elle n'est pas influencée par l'activation/formation des complexes B-O ou l'activation d'autres centres de recombinaison sous éclairement. Par contre, et c'est l'un des résultats marquants de ce travail de thèse, les cellules mc contaminées par le Cu ont des performances qui se dégradent de façon très conséquente sous éclairement. En effet la baisse relative du rendement des cellules contaminées Cu issues de la partie médiane et haute du lingot est voisine de 3.2 % (les spécifications industrielles pour les baisses relatives de rendement des cellules mc sont en général inférieures à 2 %). Nous avons montré que ces baisses de rendement ne pouvaient pas être attribuées à la formation/activation de complexes B-O (faible teneur en oxygène interstitiel). Ainsi elles sont vraisemblablement liées à des effets de LID spécifiques au Cu. D'après la littérature, l'éclairement (via la photogénération de charges libres) atténuerait la répulsion électrostatique entre le Cu interstitiel (activité électrique faible) et les précipités/amas de Cu (activité électrique forte), les 2 défauts étant positivement chargés. L'éclairement favoriserait alors la précipitation/agglomération du Cu et augmenterait donc l'effet recombinant des précipités/amas. Il est nécessaire d'insister sur l'importance de ce résultat. En effet les exigences de l'industrie PV concernant les problèmes d'instabilité du rendement sous éclairement sont de plus en plus sévères. Or le Cu est l'une des principales

impuretés métalliques dans le mc Si, le Cu étant essentiellement introduit par l'utilisation du creuset en Si et son revêtement anti-adhérent. Il est donc indispensable lorsque des plaquettes de Si sont issues de solidifications dirigées, d'évaluer les éventuels effets de dégradation des propriétés électriques sous éclairement, en particulier pour les plaquettes issues de la partie haute des lingots, et de façon générale, de développer des procédés de fabrication des cellules permettant de s'affranchir des effets de LID liés au Cu.

Chapitre 6. Rôle de la couche n+ sur les propriétés de recombinaison et de piégeage des porteurs de charge à l'issue d'un recuit rapide. Cas des plaquettes contaminées par le cuivre

Comme nous venons de le voir, l'un des résultats marquants du chapitre 5 concerne l'importance des effets de LID des cellules multicristallines contaminées par le Cu. Afin de mieux appréhender cet effet, et de façon générale les propriétés de recombinaison et de piégeage des porteurs de charge dans les cellules contaminées par le Cu, ce chapitre s'intéresse à l'influence du recuit rapide (firing), utilisé pour le frittage des pâtes de sérigraphie, sur les propriétés électriques des plaquettes. En effet ce recuit rapide est la dernière étape à haute température du procédé de fabrication des cellules. Ainsi, cette étape a une influence forte sur la distribution spatiale et l'état chimique des impuretés métalliques dans le dispositif prêt à être intégré en module. D'après la littérature [10] cette étape entraîne, lorsqu'elle est effectuée sans la couche diffusée P (la couche n^+), une dégradation significative de la τ, qui serait liée à la dissolution de précipités métalliques (essentiellement de siliciures de fer). Cependant, toujours d'après la littérature, la présence de la couche n^+ permettrait de limiter cette dégradation volumique [10]. Cependant, l'influence dans ce cas positive de la couche n^+ n'est pas comprise. Ainsi, il est particulièrement intéressant d'étudier l'effet de l'étape de firing, et l'influence de la présence de la couche n^+ pendant ce recuit, sur les propriétés électriques des plaquettes contaminées par le Cu.

Pour cette étude des plaquettes multicristallines contaminées par le Cu initialement situées les unes à la suite des autres sur la hauteur du lingot ont été utilisées. Toutes les plaquettes ont subi une diffusion P, mais pour certaines, l'émetteur n^+ a été enlevé par attaque chimique, alors que pour les autres, il a été préservé. Des couches de nitrure de Si hydrogéné ont été déposées sur les 2 faces des plaquettes. Les plaquettes ont ensuite subi l'étape de firing. Des analyses QssPC (quasi-steady state photoconductance decay) ont été effectuées

avant et après l'étape de firing. Ces analyses permettent de connaître la variation de la τ apparente (τ_{app}) des porteurs de charge avec la densité apparente excédentaire des porteurs de charge (Δn_{app}). A noter que ces analyses ont été faites juste après le firing, et répétées à différents intervalles de temps successifs alors que les plaquettes étaient placées entre deux mesures à l'obscurité. Egalement, avant et après l'étape de firing, l'évolution de τ_{app} sous éclairement a été étudiée.

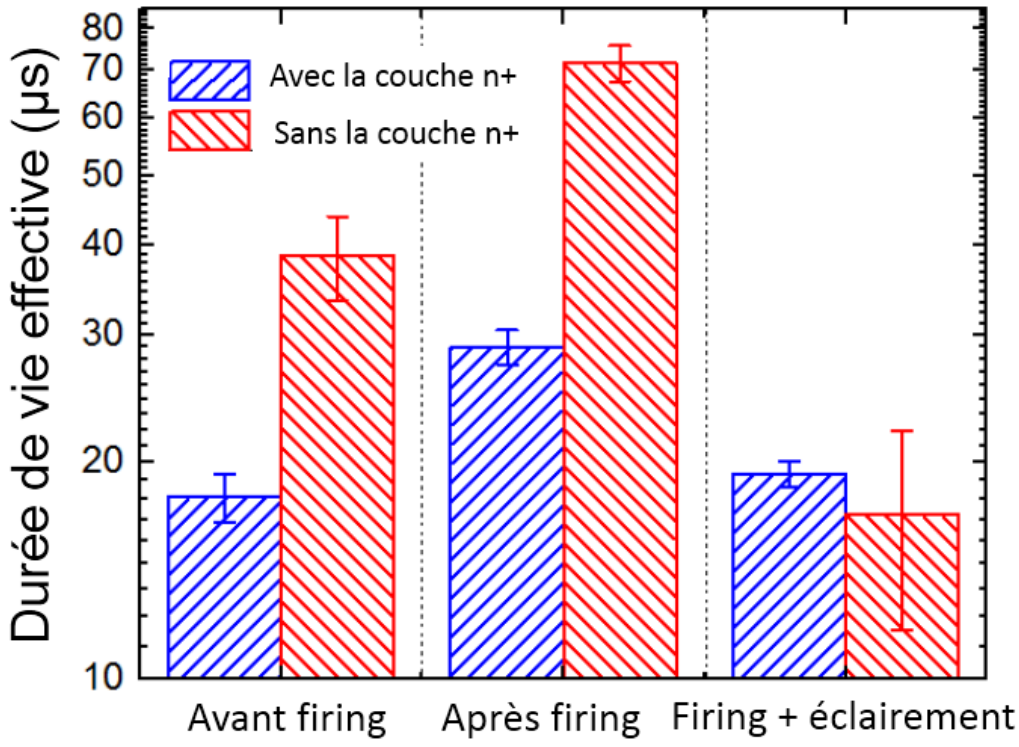

Figure 7. Durées de vie effectives d'échantillons contaminés par le Cu, diffusés P, avec et sans la couche n^+. Les valeurs ont été extraites pour une densité excédentaire des porteurs de charge de 10^{15} cm^{-3}. Les mesures ont été faites après l'étape de diffusion P (avant le firing), juste après le firing, ainsi qu'après le firing et un éclairement prolongé (30 heures à 50°C). Les barres d'erreurs représentent l'écart type des résultats obtenus (5 mesures effectuées par échantillons).

Tout d'abord nous nous sommes intéressés aux τ déterminées avant et après l'étape de firing (Figure 7). Nous avons montré pour les échantillons contaminés Cu, contrairement aux résultats publiés dans la littérature pour des échantillons mc non intentionnellement contaminés, que le firing s'accompagne d'une nette hausse de la durée de vie. Surtout, à nouveau en contradiction avec les résultats de la littérature, les densités et/ou la virulence des centres de recombinaison qui limitaient la τ avant le firing, diminuent plus fortement lorsque l'échantillon est recuit sans couche n^+ ! Ce résultat s'explique car le Cu, contrairement à la plupart des autres éléments métalliques (le fer notammen), est plus virulent précipité qu'en

solution solide. Or l'étape de firing, en raison du refroidissement rapide, empêche la re-précipitation du Cu remis en solution à haute température. Ainsi, les densités et/ou la taille des précipités de Cu à l'issue de l'étape de firing sont plus faibles, ce qui entraîne une hausse de la τ. Le fait que l'amplitude de la hausse de τ soit plus élevée sans couche n^+ lors du firing constitue un résultat nouveau et important, car il indique que la présence de la couche n^+ lors du firing, limite ou ralentit la dissolution des précipités métalliques.

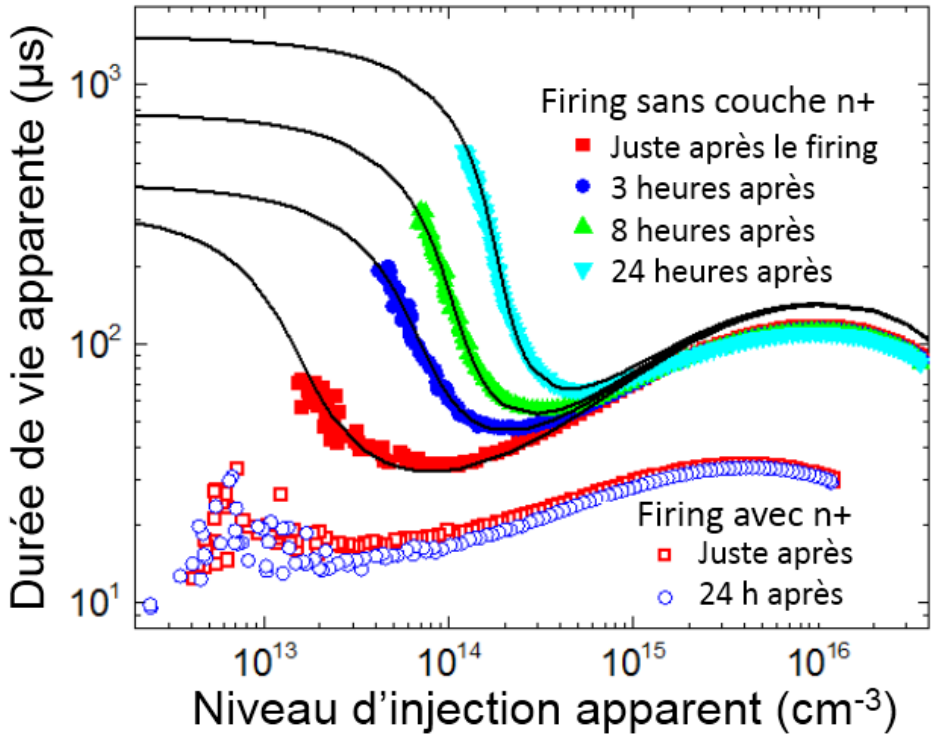

Figure 8. Variations de la durée de vie apparente des porteurs de charge avec la densité excédentaire apparente des porteurs de charge (niveau d'injection apparent). Les mesures ont été effectuées à différentes durées après l'étape de firing (entre 2 mesures les échantillons étaient placés à l'obscurité), pour des échantillons recuits avec et sans la couche n^+. Les lignes continues correspondent à des données calculées, ajustées sur les valeurs expérimentales, qui prennent en compte les recombinaisons SRH et Auger, et les mécanismes de piégeage des électrons via le modèle de Hornbeck and Haynes [11].

Après le firing, pour les plaquettes recuites avec une couche n^+, nous avons observé que les τ n'évoluaient pas lorsque les plaquettes étaient placées à l'obscurité entre 2 analyses QssPC. Pour les plaquettes recuites sans la couche n^+, nous avons mis en évidence une augmentation conséquente des effets de piégeage des électrons (capture et libération des électrons par un niveau en énergie généralement superficiel présent dans la bande interdite) lorsque les plaquettes après le firing sont à l'obscurité (Figure 8). Ainsi, en lien avec la conclusion du précédent paragraphe, cet effet de piégeage est très probablement lié à des

impuretés métalliques initialement précipitées. La nature exacte des centres pièges impliqués n'est pas connue. Nous avons discuté la possibilité que cette augmentation de la densité des centres pièges soit liée la dissociation des paires Cu-Cu [12]. En effet la paire Cu-Cu ne permettrait pas le piégeage des électrons, alors que le Cu interstitiel pourrait être un centre de piégeage efficace (introduction d'un niveau en énergie à proximité de la bande de conduction).

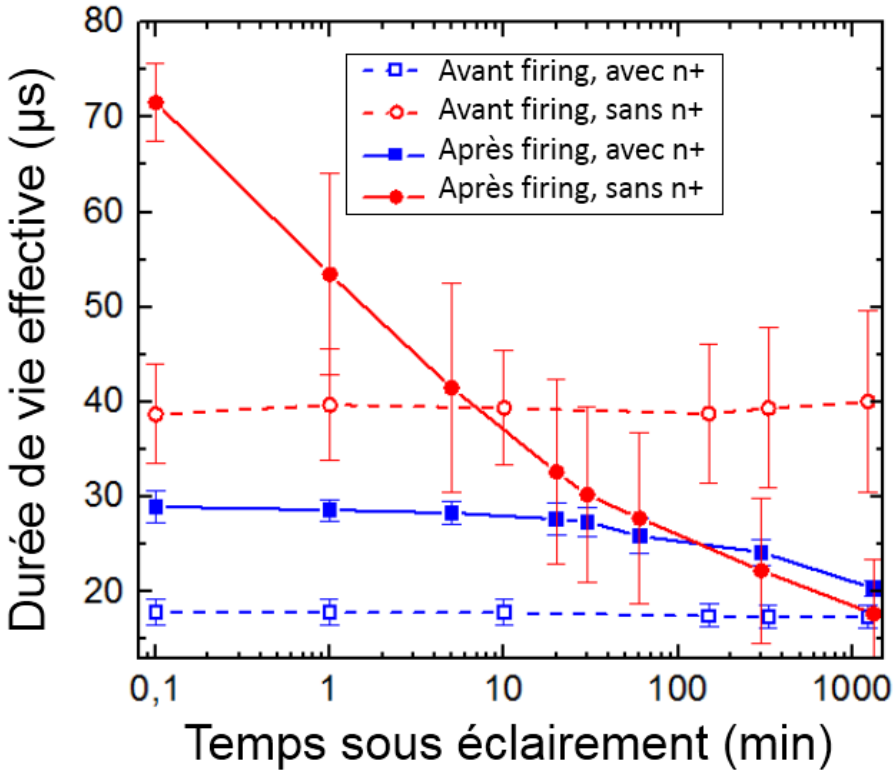

Figure 9. Evolutions sous éclairement de la durée de vie effective des porteurs de charge d'échantillons contaminés par le Cu diffuses P, avec et sans la couche n^+, et ce avant et après l'étape de firing. Les valeurs ont été extraites pour une densité excédentaire en porteurs de charge de 10^{15} cm^{-3}. Les barres d'erreurs représentent l'écart type des différents résultats (5 mesures par échantillon). Les lignes continues servent uniquement de guide à la lecture du graphique.

L'étude de l'évolution des τ sous éclairement après l'étape de firing était elle aussi particulièrement intéressante, car des diminutions conséquentes des τ sous éclairement ont été mises en évidence pour les plaquettes recuites sans couche n^+ (Figure 9). Cela s'explique car le refroidissement des plaquettes qui suit la diffusion P est suffisamment lent pour que le Cu puisse précipiter. Ainsi, la densité de Cu interstitiel est négligeable et par conséquent les effets de précipitation du Cu sous éclairement à basse T, qui entraînent une diminution de la τ, ne sont pas détectables. En contrepartie, le refroidissement associé à l'étape de firing est si

rapide, que le Cu serait essentiellement sous forme interstitielle à la suite de cette étape. Ainsi, sous éclairement des effets de précipitations/agglomérations prennent alors place qui diminuent la τ. L'amplitude justement de la diminution de τ sous éclairement est beaucoup moins conséquente pour l'échantillon recuit avec la couche n^+, ce qui confirme une fois encore que la présence de cette couche a limité ou ralenti la dissolution des précipités métalliques.

L'effet de la couche n^+ sur la limitation ou le ralentissement de la dissolution des précipités métalliques lors du firing n'est pas compris. Nous proposons et discutons dans le manuscrit une hypothèse basée sur l'injection lors du firing dans le volume des plaquettes d'auto-interstitiels depuis la couche n^+ [13]. La sursaturation de ces défauts ponctuels intrinsèques pourrait expliquer la stabilité des siliciures de fer (ce qui rendrait compte des résultats de la littérature), mais devrait par contre, en forte contradiction avec nos résultats, favoriser la dissolution des siliciures de Cu [14].

Un autre résultat marquant issu de ces études concerne le fait que les effets de LID liés au Cu sont « activés » par l'étape de firing. Cette particularité peut être utilisée pour identifier le mécanisme de LID dominant des cellules au Si multicristallin. En effet 2 principaux effets de LID sont susceptibles d'affecter les performances des cellules au mc Si : la formation des complexes B-O et la précipitation du Cu. Les effets de LID liés au B-O affectent la τ de façon semblable, avant et après l'étape de firing, alors que les effets de LID liés au Cu ne prennent place qu'après l'étape de firing. Ainsi, en étudiant l'évolution sous éclairement de la τ de plaquettes diffusées P avec des surfaces électriquement passivées, avant et après l'étape de firing, le mécanisme dominant de LID peut être identifié.

Conclusions

Ces travaux de thèse se sont intéressés à l'influence de contaminations volontaires du Si par le Cu et le Ti sur les performances des cellules solaires PV au Si monocristallin Cz et au Si multicristallin obtenu par solidification dirigée en creuset. Ces deux métaux de transition ont été sélectionnés car ce sont des éléments communs dans le Si utilisé pour la fabrication des cellules, et qu'ils ont également des propriétés dans le Si significativement différentes. De plus leurs caractéristiques dans le Si sont proches de celles d'autres contaminants métalliques, ce qui permet de les considérer comme des impuretés modèles. Nos travaux se démarquent clairement des précédentes études de la littérature, et ce pour différentes raisons. En

particulier nos travaux se sont intéressés aussi bien au Si monocristallin que multicristallin. D'autre part, ils se sont appuyés sur une large palette de techniques de caractérisation, nous permettant d'évaluer les propriétés compositionnelles, électriques et PV des matériaux étudiés. Enfin nos investigations ont abordé l'influence des contaminations volontaires sur le rendement initial des cellules, mais aussi sur la stabilité sous éclairement des performances PV ainsi que sur les caractéristiques I-V inverses des cellules.

Pour le Ti, nos travaux ont montré que cet élément a une influence délétère sur le rendement de conversion PV. En effet des concentrations en Ti dans les plaquettes aussi faibles que 10^{12}-10^{13} cm^{-3} entraînent des pertes de rendement de plusieurs pourcents absolus (par rapport aux rendements des cellules de référence non contaminées), et ce aussi bien pour les plaquettes mono- que multi-cristallines. Cela est lié à 2 principaux mécanismes. Tout d'abord le Ti est essentiellement en solution solide dans le matériau (son faible coefficient de diffusion limitant sa capacité à précipiter après mise en solution lors des étapes de procédé à haute température), état dans lequel son pouvoir recombinant est particulièrement élevé. D'autre part, à nouveau en raison de son faible coefficient de diffusion, cet élément n'est pas extrait en quantité suffisante du volume des plaquettes par l'effet getter externe développé par la diffusion P. De façon intéressante, le Ti est mieux toléré dans le Si multicristallin que monocristallin. Notre interprétation est que les défauts cristallographiques dans le Si multicristallin permettraient tout de même à une partie des atomes de Ti de précipiter. A noter enfin que la contamination par le Ti n'introduit pas d'instabilité sous éclairement des propriétés PV et ne favorise pas le claquage des jonctions, au moins pour les concentrations étudiées.

Pour le Cu, nos travaux ont montré de façon inattendue que le rendement des cellules n'a pas été affecté par la contamination par le Cu, et ce malgré les fortes teneurs en Cu introduites dans le Si liquide (90 ppm wt pour le mc Si) ! Cette tolérance s'explique par différentes raisons. Tout d'abord les teneurs en Cu dans les lingots cristallisés étaient systématiquement plus faibles que les valeurs attendues. Ces différences pourraient être liées à des effets d'évaporation du Cu du Si liquide et/ou à des effets d'exo-diffusion (voire une simple agglomération aux surfaces) du Cu au cours du refroidissement des lingots. Egalement, les τ des plaquettes contaminées Cu étaient améliorées par la diffusion P, cet élément en raison de son coefficient de diffusion élevé, étant efficacement extrait du volume par l'effet getter externe associé à cette étape. Par contre, si le Cu n'affecte pas le rendement initial (avant éclairement prolongé) des plaquettes, nous avons montré en contrepartie qu'il pouvait favoriser le claquage des jonctions. Surtout, les performances des cellules mc

contaminées par le Cu se dégradent de façon conséquente sous éclairement. Nous avons montré que ces effets de dégradation étaient « activés » par l'étape de firing. Cette étape de recuit, en raison du refroidissement rapide des plaquettes, « gèle » en position interstitielle des impuretés métalliques initialement précipitées et qui ont été remises en solution à haute température. Sous éclairement, le Cu en position interstitielle (état électriquement peu actif) migrerait et précipiterait (les précipités ont un fort pouvoir recombinant), ce qui s'accompagne d'une baisse importante de la τ. A noter que l'étude de l'évolution sous éclairement de la τ avant et après l'étape de firing, permet ainsi l'identification du mécanisme dominant de LID : formation des complexes B-O (LID présente avant et après le firing) ou précipitation du Cu (LID présente uniquement après le firing). Pour la suite, il serait important d'une part d'obtenir des informations expérimentales sur la nature des amas/précipités de Cu formés sous éclairement, et surtout de développer des procédés (ou d'évaluer des solutions a priori existantes à l'échelle des plaquettes), compatibles avec la fabrication industrielles des cellules solaires, pour éviter ces effets de dégradation sous éclairement.

Principales références

1. International Technology Roadmap for Photovoltaic (ITRPV), 5th Edition, March (2014).
2. S. Dubois, Effects of the impurity-defect interactions on the photovoltaic and electrical properties of crystalline silicon solar cells. PhD Thesis, Paul Cezanne University, Marseille, France (2007).
3. D. Macdonald, A. Cuevas, A. Kinomura, and Y. Nakano, Phosphorus gettering in multicrystalline silicon studied by neutron activation analysis. 29th Photovoltaic Specialists Conference Proceedings (IEEE), New Orleans, USA, 285-288 (2002).
4. T. Buonassisi, A.A. Istratov, M.D. Pickett, J.P. Rakotoniaina, O. Breitenstein, M.A. Marcus, S.M. Heald, and E.R. Weber, Transition metals in photovoltaic-grade ingot-cast multicrystalline silicon: Assessing the role of impurities in silicon nitride crucible lining material. J. Crystal Growth. 287 (2), 402-407 (2006).
5. B.S. Xakalashe, and M. Tangstad, Silicon processing: from quartz to crystalline silicon solar cells. Chemical Technology. 32-37 (2012).
6. G. Coletti, P.C.P. Bronsveld, G. Hahn, W. Warta, D. Macdonald, B. Ceccaroli, K. Wambach, N.L. Quang, and J.M. Fernandez, Impact of metal contaminations in silicon solar cells. Adv. Funct. Mater. 21, 879–890, (2011).
7. K. Bothe, R. Sinton, and J. Schmidt, Fundamental Boron–Oxygen-related carrier lifetime limit in mono- and multicrystalline silicon. Prog. Photovolt: Res. Appl. 13, 287 (2005).
8. S. Knack, J. Weber, H. Lemke, and H. Riemann, Copper-hydrogen complexes in silicon. Phys. Rev. B. 65, 165203 (2002).
9. R. Singh, S.J. Fonash, and A. Rohatgi, Interaction of low-energy implanted atomic H with slow and fast diffusing metallic impurities in Si. Appl. Phys. Lett. 49, 800 (1986)
10. J. Tan, D. Macdonald, N. Bennett, D. Kong, A. Cuevas, and I. Romijn, Dissolution of metal precipitates in multicrystalline silicon during annealing and the protective effect of phosphorus emitters. Appl. Phys. Lett. 91, 043505 (2007).
11. J.A. Hornbeck, and J.R. Haynes, Trapping of minority carriers in silicon. I. p-type silicon. Phys. Rev. 97, 311 (1955).
12. A.A. Istratov, H. Hieslmair, T. Heiser, C. Flink, and E.R. Weber, The dissociation energy and the charge state of a copper-pair center in silicon. Appl. Phys. Lett. 72, 474 (1998).
13. P. Fahey, R.W. Dutton, and S.M. Hu, Supersaturation of self-interstitials and undersaturation of vacancies during phosphorus diffusion in silicon. Appl. Phys. Lett. 44, 777 (1984).
14. W. Schröter, V. Kveder, M. Seibt, A. Sattler, and E. Spiecker, Mechanisms and computer modelling of transition element gettering in silicon. Sol. Energy Mater. Sol. Cells. 72, 299 (2002).

De l'influence de contaminations par le cuivre et le titane sur les performances photovoltaïques de cellules solaires au silicium cristallin

Résumé

Ce travail s'est intéressé aux influences du Cu et du Ti sur les performances des cellules solaires photovoltaiques (PV) au Si. Des lingots monocristallins et multicristallins (mc), volontairement contaminés, ont été cristallisés. Des cellules ont été fabriquées. Les effets du Cu et du Ti sur le rendement de conversion (η), sa stabilité, et la tension de claquage (V_{bd}) de la jonction, ont été évalués. Le Ti affecte fortement le η, en raison de son fort pouvoir recombinant et de son faible coefficient de diffusion, qui ne permet pas son extraction par effet getter externe. La contamination Ti cependant n'a pas d'influence significative sur la V_{bd} et la stabilité du η. Nous avons montré qu'une importante contamination Cu n'affecte pas le η des cellules mc, car le Cu diffuse suffisamment rapidement pour être extrait par effet getter externe. Par contre le η de ces cellules diminue sous éclairement, cette dégradation étant activée par le recuit rapide des métallisations.

Mots clés : silicium, photovoltaïque, impureté, cuivre, titane, recombinaison.

Influences of copper and titanium contaminations on the photovoltaic performances of crystalline silicon solar cells

Abstract

This thesis focuses on the influence of Cu and Ti on the photovoltaic (PV) performances of Si solar cells. Contaminated single-crystalline Czochralski and multicrystalline (mc) ingots were grown. Then wafers from these ingots were transformed into solar cells in order to assess the impact of Cu and Ti on the PV conversion efficiency (η), its stability, and the *p-n* junction breakdown voltage (V_{bd}). We showed that Ti strongly affects the η, because of the high recombination strength of slow-diffusing Ti atoms, which are not efficiently extracted by external gettering effects. However, Ti did not significantly influence the V_{bd} and the η stability. On the other hand, we unexpectedly showed that a strong Cu contamination did not affect the η. This is mainly due to the efficient extraction by external gettering effects of the fast-diffusing Cu atoms. Nevertheless, the Cu contaminated cells were affected by light-induced degradation (LID) effects, activated by the metallization firing step.

Keywords: silicon, photovoltaic, impurity, copper, titanium, recombination.